A QUADRUPOLE ION TRAP LASER MICROPROBE FOR THE MAPPING OF PHARMACEUTICAL COMPOUNDS IN INTACT TISSUE

By

FREDERICK J. TROENDLE

A DISSERTATION PRESENTED TO THE GRADUATE SCHOOL OF THE UNIVERSITY OF FLORIDA IN PARTIAL FULFILLMENT OF THE REQUIREMENTS FOR THE DEGREE OF DOCTOR OF PHILOSOPHY

UNIVERSITY OF FLORIDA

2000

ACKNOWLEDGMENTS

More than anyone else, I wish to express my thanks to my wife, Lorraine, without whom none of my accomplishments would have been possible or had any real meaning. More than anyone else, she has supported me and stuck by me as I pursued my wild dream of attaining a Ph.D. in chemistry. I have no idea what she sees in me, but I hope that in some small way I can come close to being who she believes I am.

I would also like to thank my parents, Gloria and Frank Troendle. They had seven children, yet I never felt that I was just one of the crowd. Despite the fact that I was the second born and the last in my family to achieve a college degree, they never treated me like the black sheep that I truly was. Their dedication to science, and more importantly to learning and understanding anything which was interesting, has always inspired me to seek out answers to things I did not know.

At the University of Florida, there are many to thank. First, I would like to thank Rick Yost, my research adviser, for taking a chance on a student who was nearly his own age with no real mass spectrometry experience. Rick gives as much guidance as requested and as much leeway as needed by

each student. His encouragement and guidance will be sought long after I have left the University of Florida.

Within the group of people I worked with at U.F., first, I wish to thank Christopher D. Reddick. Another Silver Spring, Maryland lad (like myself), Chris helped me get up to speed on Tubby so that I could do what was necessary to graduate. Of course, Chris also put together Tubby in its original incarnation, so everything I have done is simply a continuation of Chris's original work. I would also like to thank Joe Mulholland, who came into the group with me in 1996 and was always willing to debate (others call it argue) with me about any trivial point of science without taking it personally (which reminded me of my family). I also need to thank Brody Guckenberger for answering every question I had about mass spectrometry and for just being Brody. Joe McClellan deserves my thanks for his help with mass spectrometry and anything related to U.F. and graduate school. Former group members, Scott Quarmby, Jon P. DeGnore, and Steve Boue, all helped me during the first two years at U.F. and deserve my thanks. Current members (in addition to those mentioned above) who I wish to thank include James Murphy (for thinking that I knew enough about mass spectrometry to ask me questions) and Kevin McHale (for asking and answering questions and always being there and willing to help out).

I would like to thank Todd Prox of the machine shop for his endless patience and help in building a new, improved Tubby. I would never have

been able to do what I did without Todd's help. Also, I thank Joe Shalosky, the machine shop supervisor, who bailed me out of several situations which could have been disasters.

Finally, I wish to thank Bristol-Myers Squibb and the Florida Space Grant Consortium for their financial support. Of course, no dissertation would be complete without a thanks to Randy and the crew at Burrito Brothers for making lunch what it was.

TABLE OF CONTENTS

Abstract of Dissertation Presented to the Graduate School of the University of Florida in Partial Fulfillment of the Requirements for the Degree of Doctor of Philosophy

A QUADRUPOLE ION TRAP LASER MICROPROBE FOR THE MAPPING OF PHARMACEUTICAL COMPOUNDS IN INTACT TISSUE

By
Frederick J. Troendle

August, 2000

Chairman: Richard A. Yost
Major Department: Chemistry

Research was conducted on a custom built quadrupole ion trap laser microprobe instrument (constructed at the University of Florida). Initial studies with the instrument showed that it was capable of detection of pharmaceutical compounds in intact tissue masses at trace levels by use of matrix-assisted laser desorption ionization (MALDI); however, determining the exact spatial location of those compounds within the tissue mass was not possible by simple application of the MALDI matrix solution onto the surface of the tissue (the MALDI-drop method).

An X,Y-micro-manipulation stage was constructed so that spatial information about the location of drug compounds in intact tissue masses could be obtained. The studies showed that, within half the diameter of the probe tip (2 mm), all spatial information about the location of a drug compound was lost during the MALDI-drop method. In order to preserve the spatial

distribution of drug compounds in intact tissue samples, two alternative methods were investigated.

The first alternative method investigated to preserve the spatial distribution of the drug compounds within intact tissue samples was laser desorption coupled to chemical ionization (LD/CI). Studies demonstrated that the spatial distribution of drug compounds is maintained during LD/CI and that drug compounds could be detected at trace levels by LD/CI in intact tissue masses.

The second method investigated was the electrospraying of the MALDI matrix solution onto the surface of the tissue. An apparatus was constructed to perform the electrospraying of the MALDI matrix solution. Experiments showed that by electrospraying the matrix solution, the MALDI matrix solvent evaporated quickly enough to prevent significant migration of pharmaceutical compounds (within the resolution of the instrument—approximately 150 μm).

Samples of tissue with a distribution of a pharmaceutical compound were prepared and the ability of the instrument to map the location of a compound within intact tissue masses was demonstrated. The drug spiperone, at a level of 25 ng/mg of tissue, was mapped with a lateral resolution of 150 μm in a tissue sample by both LD/CI and the electrospray method. An experimental drug in animal tissue, at a level of 59 ng/mg, was mapped with a resolution of 150 μm in an intact tissue sample by both methods.

CHAPTER 1
INTRODUCTION

There are several chemical attributes that are important in pharmaceutical research and development when selecting a lead compound for development, including receptor/enzyme specificity, adequate potency, and lack of toxicity in the therapeutic range.[1] A significant, if not the most significant, factor however, is the availability of the agent at the site of action. Traditionally, in vitro cell-based assays have been used to determine the binding efficiency of a drug with a receptor site. These types of screens can give a good indication of a drug's activity, but they do not indicate whether or not the drug will be transported to the disease target. Conversely, metabolic profiling of bodily fluids using standard analytical techniques (chromatography,[2] nuclear magnetic resonance,[3] and mass spectrometry coupled with liquid chromatography[4]) can determine the systemic bioavailability of a specific drug compound, but provides limited information regarding the penetration of the drug into the tissues in either the intracellular and/or extracellular spaces. To determine whether a drug reaches its site of action and the chemical structure of the drug at that location requires microprobe techniques with high sensitivity and good spatial resolution. The combination of a microprobe instrument with high spatial resolution sampling

coupled with mass spectrometry for high sensitivity and selectivity makes a powerful investigative tool for pharmaceutical research and development.

Mass Spectrometry Microprobe Instruments

Mass spectrometry was a logical selection for application to microprobe or micro-sampling analysis. Mass spectrometry has the detection limits (typically in the low picogram range) necessary to keep the sample size, and therefore the spatial resolution, small. Mass spectrometry is also easily adaptable to micro-sampling techniques (as long as ions can be formed during or after sampling). Additionally, and perhaps most importantly, mass spectrometry yields a great deal of information about the chemical composition of the substance being studied in the form of elemental or molecular information.

One of the earliest examples of microprobe mass spectrometry was in 1963 when R. E. Honig and J. R. Woolston used a ruby rod laser to ablate approximately 150 μm by 125 μm craters in a variety of metals and semiconductor material.[5] At around the same time that the first laser microprobe instrument was being developed, the first ion beam microscope mass spectrometer was being created.[6] This new ionization technique blossomed in the 1980's with the advent of fast atom bombardment (FAB) and secondary ion mass spectrometry (SIMS). SIMS was able to bring the spatial resolution of microprobe instruments down below the 0.5 μm diameter range.

Since that time, microprobe mass spectrometers have undergone numerous and drastic changes.

As microprobe mass spectrometry has evolved, three different applications of the technique have emerged. One application is the field of chemical imaging. This field has grown significantly over the last several years. A quick search of papers published over the last five years (1994-1999) indicated over 260 papers were published using both mass spectrometry and imaging as keywords. For the purpose of this dissertation, imaging mass spectrometry is defined as the systematic movement of a sampling beam across a surface for the purpose of producing an image of the surface which is based on one or more chemical signatures. This definition is similar to the definition, given later, for mapping; however, the distinction between the two is drawn from the intended purpose of the investigation. Generally, one would image an object, while one would map the location of a compound within a larger matrix. There are times when one would map the location of a specific object (i.e. the location of a biologically important object which is mapped by looking at a particular chemical signature from the object), but generally mapping is done to plot the location of some chemical in a larger matrix and imaging is done to produce an image of an object.

One of the reasons for the explosion of imaging mass spectrometry has been the increase in computer technology and computing power. Bigger, faster, and more powerful computers have allowed for computer control of the

sampling beam, which has created more accurate and more reproducible scanning of the surface. The new, more powerful, computers have also provided the storage space necessary to handle the enormous amount of data that results from the imaging of a surface. Examples of imaging of surfaces include producing an image of a cell based on its chemical composition,[7] the imaging of the surface between two polymer layers,[8] the imaging of a metal screw head to characterize the ability of the instrument,[9] and many more.

The second field of microprobe mass spectrometry is mapping. Mapping can be defined as the systematic sampling of a surface for the purpose of plotting the location of a specific compound (or compounds) within a larger sample matrix. The mapping of surfaces by microprobe mass spectrometry include plotting the location of compounds separated by thin layer chromatography,[10] the location of phosphocholine in animal tissue,[11] and the mapping of proteins separated by gel electrophoresis.[12] The main purpose of this dissertation research was to develop a instrument which was capable of mapping the location of pharmaceutical compounds in intact tissue masses.

The third application of microprobe mass spectrometry is micro-sampling. While spatial resolution would not seem to be an issue with micro-sampling (simply stated as sampling a micro-volume of a substance), that is not always the case. When examining particles in an aerosol, the ability to ionize and analyze a single micrometer-sized particle can be of great

importance. A surface might be analyzed to determine its chemical heterogeneity without the need to map or image the surface. There are times when a thin layer of a substance needs to be analyzed without destroying the entire sample. In biological systems there are micrometer or smaller sized structures which may need to be interrogated to determine the presence of particular compound or element. The simple sampling of a substance (without mapping or imaging) at the micro-volume level is still an important application of microprobe instruments. Some examples of micro-sampling mass spectrometry include the sampling of micrometer-size glycerol droplets containing dissolved inorganic salts,[13] the sampling of rat hippocampal neurons to determine the concentration of aluminum,[14] and the characterization of pigments in the fruiting bodies of microlichen.[15]

Another distinguishing difference between applications of microprobe mass spectrometry today is whether the technique is applied to trace or major components within a sample. A certain trade-off is necessary when investigating trace components. If we assume that 10 picograms of analyte must be ablated from the matrix for adequate detection of the compound, and the compound is only present in the matrix at a concentration of 20 ppm, then 500 ng of matrix must be ablated for analytical detection. If on the other hand, the substance under investigation is a major component of the matrix (assume that it is 10%) then only 100 picograms of matrix must be ablated for analytical detection. Additionally, matrix interferences are more of a concern when

performing trace analysis. When looking for a major constituent in a matrix, the ion of interest will typically be discernable above the background noise caused by other matrix components and can be easily identified. However, when the compound under investigation is only a trace component in the matrix, the signal of the ion under investigation is typically buried in the background noise. One way around this problem would be to select a matrix which does not produce ions in the same m/z range as the ion of interest, but that is not very realistic except when dealing with specially designed experiments to test the sensitivity of the instrument. Of course, even when investigating major components of a matrix, interference ions from the matrix must be considered when performing quantitative analysis. This trade-off between trace or major components in a sample can impact the size of the spot used in sampling for microprobe analysis as well. If a greater volume of matrix must be ablated for analytical detection, then either the spot size used for sampling must be increased or the depth of penetration into the sample must be increased (possibly by multiple sampling of the same location).

This issue of spot size has an impact on the maximum resolution attainable with a microprobe instrument. Resolution is defined as the minimum distance between two objects at which the two objects can still be identified as separate. If the distance between each location sampled on a surface is greater than the diameter of the spot used during sampling, then the resolution of the instrument is defined as the distance between each sampling

location. This would be the minimum distance at which two objects (one having the analyte under investigation present and the other not having the analyte under investigation present) could be determined. On the other hand, if the distance between each sampling location is equal to or less than the diameter of the spot used for sampling, then the maximum attainable resolution of the instrument would be defined as the diameter of the spot used at each sampling location. For this reason, the distance between each sampling location on a surface is typically greater than or equal to the diameter of the spot used during sampling of the surface. It is obvious then that the maximum resolution possible by a microprobe instrument is determined by the diameter of the spot used during sampling.

For microprobe instruments using SIMS as a sampling and ionization source, the spot size used to image organic samples is generally in the 1 to 10 μm diameter range. In a typical mapping or imaging experiment, the primary ion beam is rastered across the sample surface in a line by line fashion (each line composed of several hundred individual spots, side by side).[16] At each spot a mass spectrum is collected. The intensity of the ion (or ions) corresponding to the analyte of interest is determined for each spot and then used to map or image the location of the analyte in the sample (using the intensity of ion signal versus position of the sampling beam). Recently, a SIMS microprobe instrument was used to produce an image of liposomes based on the intensity of the ion at m/z 166, which corresponds to the

phosphocholine headgroup minus H_2O.[17] The diameter of the spot used during sampling and the distance between each sample spot was 200 nm (well below the typical spot size used). To preserve the location of the phospholipids in the membrane of the liposomes, a preparation of hydrated liposomes (from lipids dissolved in an organic solvent, evaporated to dryness, and then re-hydrated) was placed between two silicon wafers and quick frozen by plunging the wafers into liquid propane. The frozen sample was then fractured while under vacuum to prevent the deposition of atmospheric water onto the exposed surface of the sample (SIMS penetrates only the uppermost monolayer of the sample). The surface exposed by the fracturing of the silicon wafers was then analyzed by a SIMS time-of-flight instrument (TOF).

With a laser microprobe instrument, the spot used during sampling is generally in the 25 to 50 μm diameter range. The larger diameter spot used for sampling in laser microprobe instruments is the result of the physical limitations of the light optics used to focus the laser beam. As is done with SIMS mapping or imaging, the laser beam is rastered across the surface of the sample and a mass spectrum is collected at each location analyzed (each spot sampled across the surface). The intensity of the ion (or ions) which correspond to the analyte of interest, along with the location on the surface where that mass spectrum was collected, is used to map or image the location of the analyte in the sample. Recently, a MALDI-TOF instrument was used to

image a copyright symbol (©) composed of coomassie blue dye which had been stamped onto a cationic cellulose membrane target.[18] The copyright symbol was 1000 μm in diameter. After stamping the symbol, the membrane surface was electrosprayed with a MALDI matrix solution containing α-cyano-4-hydroxycinnamic acid. The surface of the membrane was sampled by a nitrogen laser (337 nm) with a beam diameter of approximately 25 μm. The sample (which was attached to a moveable stage) was moved in the X and Y direction in increments of 25 μm. The final image produced was composed of approximately 1600 pixels (sampling spots), which corresponded roughly to a 40 x 40 array. The image was visualized by two different methods. The first method was simply the plotting of spots at 25 μm intervals in the X and Y directions. A spot was colored solid black if the signal/noise (S/N ratio) for the $[M+H]^+$ ion of coomassie blue (mw=831) was greater than 2 at the sampled location. If the S/N at the sampled location was less than 2, the spot plotted was an open circle. The second method of visualization used was similar to that used in the SIMS example given above, but when the S/N for the ion at m/z 832 (the $[M+H]^+$ ion of coomassie blue) was greater than 2, the intensity of the ion was plotted in the Z direction (with the location of that spot plotted in the X and Y direction). When the S/N of the ion at m/z 832 was less than 2, nothing was plotted. The image produced by MALDI-TOF was comparable to a photomicrograph of the stamped image.

While the above examples are only a small fraction of the current microprobe mass spectrometry work being preformed, they can be taken as typical examples of the current state of the discipline.

Laser Microprobe Mass Spectrometry

The use of a laser beam to desorb or ablate target compounds in a microprobe instrument was a logical selection. Lasers allow for a wide variety of spot sizes to be used (from greater than 1 cm to smaller than 1 μm in diameter depending on the laser) and a wide variety of power densities (usually in the 10^6 to 10^{11} W/cm^2 range) capable of producing a large number of gas-phase neutrals and ions from many thermally labile and nonvolatile compounds. The first laser microprobe mass spectrometry instruments were used primarily for mapping surfaces to determine elemental composition.[19-21] Since then, the laser microprobe mass spectrometer has been utilized on more diverse samples, ranging from geological specimens to human teeth.[22-26]

The early laser microprobe devices almost exclusively employed time-of-flight mass analyzers (TOF). TOF mass analyzers have experienced a re-emergence in the last several years with the growing popularity of both laser desorption and ionization (LDI) mass spectrometry and matrix-assisted laser desorption and ionization (MALDI) techniques.[27] The resurgence of TOF was also carried along by advances in micro-computing which allowed for faster electronics and more powerful storage of the large information gathered during

a TOF event. The time-of-flight mass analyzer determines the m/z of an ion, accelerated in the ion source, by the time required to drift through the field-free drift region and strike the detector. One of the first commercial laser microprobe instruments was the LAser Microprobe Mass Analyzer (LAMMA).[28] The LAMMA-500 (Leybold-Hereaus, Köln, Germany) instrument was based on a TOF mass analyzer using a Q-switched Nd:YAG laser which was capable of being focused to a 0.5 μm diameter spot size (the actual ablated area was usually around 1.0 μm depending on the selected power).[29] A He:Ne laser was used to mark the position of the ablation laser on the sample while viewed though a standard quartz microscope slide which served as the vacuum seal for the instrument. The sample was usually deposited on a copper grid mounted on the vacuum side of the microscope cover slide. The entire stage (cover slide and grid) was positioned for analysis by a x-y moveable stage. The sample could be viewed by a standard optical microscope with high resolving power and magnification up to 1200.[29] The LAMMA-500 was originally designed for the investigation of thin biological sections but was quickly found to be useful for a wide range of organic and inorganic applications.[30] Recently the LAMMA-500 has been used to determine chromium oxides clusters at a steelworks factory,[31] the metal binding properties of the algae *Stichococcus bacillaris*, [32] and for investigations into nucleosides and nucleotides.[33]

Since the laser in the LAMMA-500 impinged on the sample from the backside (the laser beam struck the side of the sample facing away from the extraction lens of the mass analyzer), it was limited to thin samples which could be easily penetrated by the laser beam. Because of this limitation, a second LAMMA instrument was introduced. The LAMMA-1000 (Leybold-Hereaus, Köln, Germany) brought the laser beam to the surface of the sample facing the extraction lenses at approximately a 30° angle.[34] The new design of the instrument allowed the sampling of thicker and more diverse samples such as thin layer chromatography plates, [35-37] organic compounds deposited on nitrocellulose,[38] and polymers.[39-40]

Since the introduction of the technique of using a laser beam for micro-sampling, the laser microprobe has been coupled to every type of mass analyzer including sector instruments,[41] quadrupole mass filter instruments,[42] Fourier transform ion cyclotron resonance ion traps,[43] and quadrupole ion traps.[44]

Quadrupole Ion Traps

History

Since the use and abilities of the quadrupole ion trap were critical to the research described in this dissertation, a brief history and a quick review of the theory behind the operation of the ion trap is in order.

The quadrupole ion trap was first introduced by physicists Wolfgang Paul and Helmut Steinwedel in 1953 as one type of electrode arrangement out of many possible (Figure1-1).[45] The quadrupole mass filter arrangement of four rods was another arrangement that Paul and Steinwedel also proposed. The quadrupole ion trap consists of a hyperboloid ring electrode with two hyperboloid end-cap electrodes (bottom two drawings in Figure 1.1). A radiofrequency (RF) voltage is applied to the ring electrode along with a direct current (DC) voltage applied between the end-caps and the ring electrode. The quadrupolar electric field produced by the applied voltages traps the ions. The trapped ions assume stable trajectories within the trap.

One of the earliest uses of the ion trap was to visualize the effects of the electric fields on charged micro-particles to compare the theoretically predicted trajectories to observed trajectories. Workers at the Ramo-Wooldridge Research Laboratory in Los Angeles constructed an ion trap for the purpose of viewing an ionized aluminum particle trapped in an ion trap to experimentally measure the frequency of motion.[46] The predicted trajectory for the particle was that of a 2:1 Lissajous figure where the major motion of the ion (in the z and r directions) would have a frequency of less than one half the frequency of the applied RF voltage (Figure 1.2). In addition to the major motion of the ion, a second "micromotion" was impressed on the ion which was taken to be the result of the applied RF (the micromotion is actually the applied RF frequency ± the secular frequency of the ion).

June 7, 1960 W. PAUL ET AL 2,939,952
APPARATUS FOR SEPARATING CHARGED PARTICLES
OF DIFFERENT SPECIFIC CHARGES
Filed Dec. 21, 1954 4 Sheets-Sheet 4

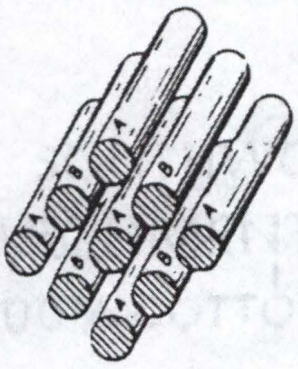

Fig.10.

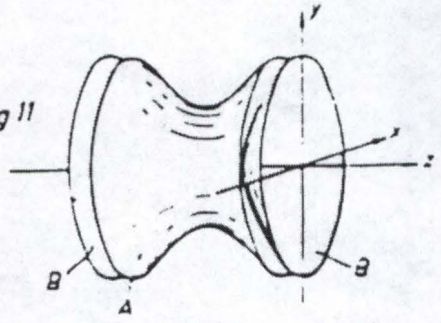

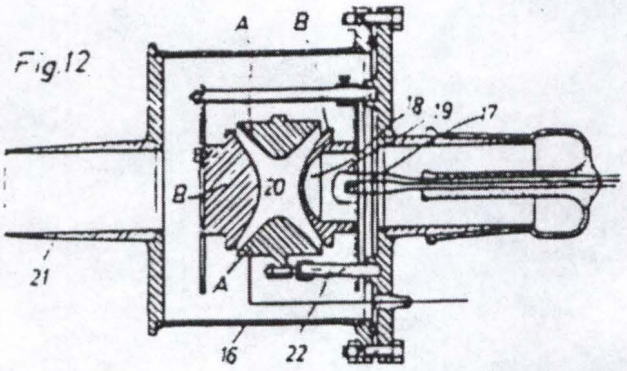

INVENTORS
WOLFGANG PAUL
HELMUT STEINWEDEL
By
ATTORNEYS

Figure 1.1. Sketches of electrode arrangements by physicists Wolfgang Paul and Helmut Steinwedel in original patent.[45]

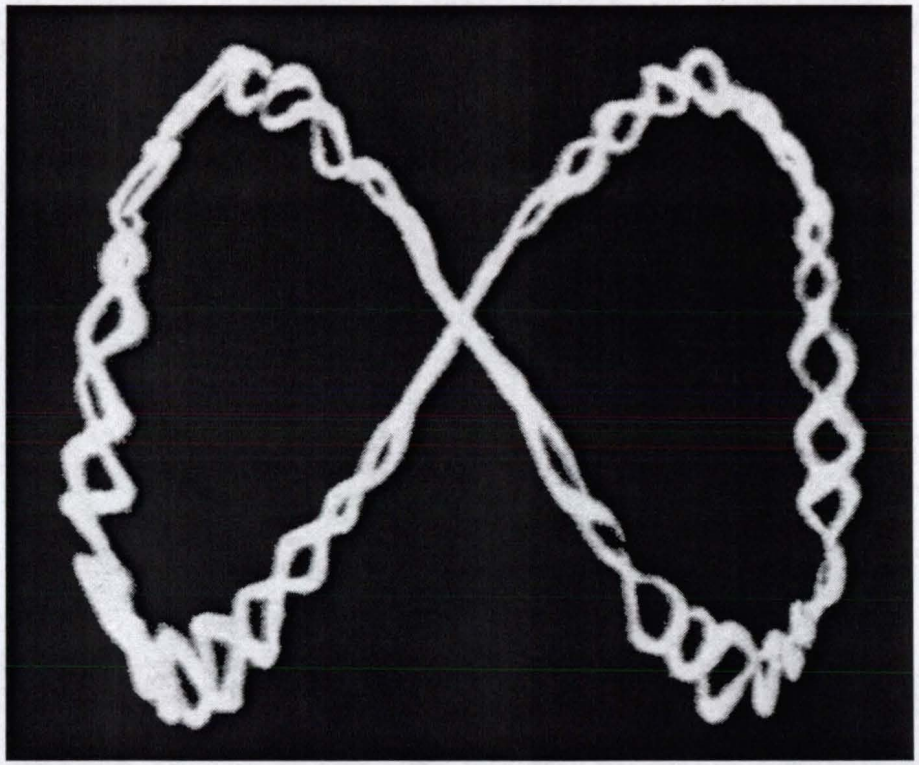

Figure 1.2. Retouched photograph of a singly charged aluminum dust particle (around 20 μm diameter) in an ion trap. The operating conditions were: RF = 500 V_{rms} at 150 Hz, DC = O V. The motion is that of a 2:1 Lissajous figure.[46]

Early use of the ion trap as a mass spectrometer determined the mass-to-charge ratio (m/z) of an ion by mass-selective detection which measured the resonant absorption of a 150 kilohertz (kHz) voltage applied across the end-caps of the ion trap.[47] Ions were continuously formed within the ion trap by the introduction of electrons through a hole in one of the end-cap electrodes. Ions which came into resonance with the voltage applied across the end-caps absorbed a portion of the power applied and caused a deflection on an oscilloscope. This method could be used to differentiate the m/z of an ion because in the presence of a uniform electric field an ion experiences a force which is converted into translational frequency of motion which is determined by the ion's m/z. Thus by slowly increasing the amplitude of the DC voltage, ions of increasing m/z came into resonance with the 150 kHz applied voltage.

Some years later, Rettinghaus developed an alternate means of mass-selective detection.[48] The detection method employed by Rettinghaus was similar to that used today for the detection of ions in an ion cyclotron resonance (ICR) mass analyzer. The RF voltage on the ring electrode was slowly increased (with no applied DC voltage) while a special circuit detected the induced current on the end-caps at a frequency of 410 kHz. As ions of increasing m/z came into resonance with the detection circuit, a current was induced on the end-caps due to the motion of the charged particles (ions) in the ion trap and were detected by the special circuit. Both of the detection

methods involved complex detection circuits and had very limited mass ranges over which detection could occur.

In 1967 P. H. Dawson and N. R. Whetten of the General Electric Research and Development Center demonstrated the use of the ion trap as a mass-selective storage device.[49] The trap design included holes drilled in one of the end-caps which allowed the stored ions to be drawn out of the device by application of a negative (for positive ions) DC voltage pulse (1-10μs in duration) to the end-cap (Figure 1.3). The ions were then detected by striking a Ag-Mg electron multiplier located just outside of the exit end-cap. This detection method was both simpler and cheaper than previous detection methods (electron multipliers were already being used for ion detection on quadrupole mass filter devices). In addition, a grid placed in front of a hole drilled into the ring electrode (for the introduction of electrons to produce ions) could be pulsed negative just prior to the detection pulse so that ions would not be continuously produced and only those ions in the trap with stable trajectories would be stored. By holding the ratio of the applied RF and DC potentials constant, only ions of a particular m/z would have stable trajectories within the trap and so be detected during the end-cap DC pulse-out event. This mass-selective storage operation of the ion trap is similar to the mass-selective stability operation of the quadrupole mass filter. The advantage demonstrated by the mass-selective storage of ions was a reduction of the space-charge effect since only ions of a given m/z were stored in the device

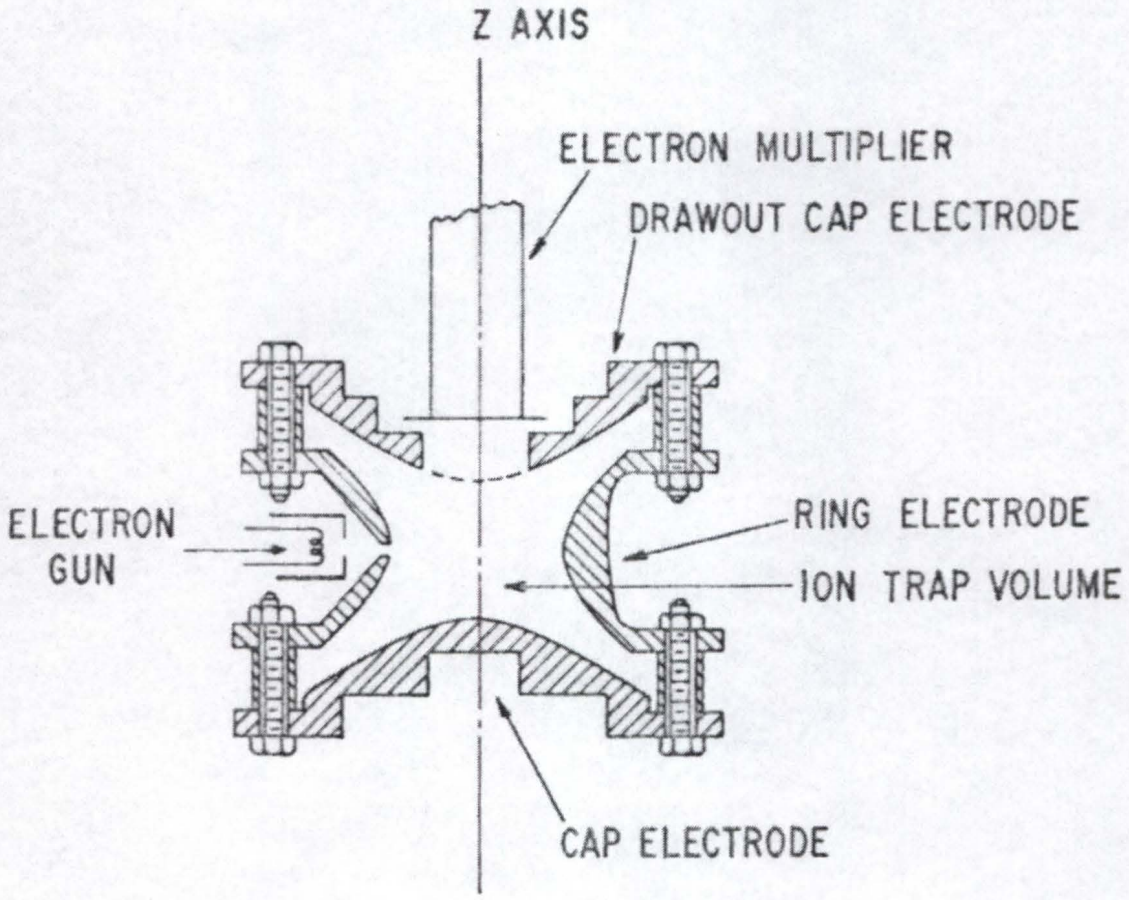

Figure 1.3. Ion trap used to test mass-selective storage of ions. Ions were formed in the trap by the introduction of electrons through the ring electrode. Ions of specified m/z were ejected through drawout end-cap electrode by application of DC voltage.[49]

prior to detection. Additionally, ion-molecule reaction products would have unstable trajectories under mass-selective storage and so not complicate the mass spectrum produced. The operation of the ion trap in mass-selective storage mode was able to store ions in the trap for a period of days, although there was demonstrated a loss of ion intensity due to ion scattering after a period of about 16 hours. The major drawback to this detection method was that only a single m/z could be detected for a given set of applied voltages. That meant that a different set of voltages had to be applied to the ion trap (and held stable long enough to pulse out the packet of ions) for each m/z detected.

While mass-selective storage represented a step forward in the operation of the ion trap, the ion trap remained mostly a device used for the investigation of gas-phase properties of molecules and was not widely viewed as a 'mainstream' analytical mass spectrometry device.

That changed with the introduction of a new operational mode for the ion trap called the mass-selective instability mode.[50] In mass-selective instability mode, the RF voltage applied to the ring electrode is increased from low amplitude to high amplitude. Ions stored within the ion trap assume frequencies of motion which are related to their m/z and the amplitude of the applied RF voltage. As the RF voltage increases, ions of increasing m/z become unstable in the z-direction (the direction of the end-cap electrodes) and are ejected from the trap. With holes drilled in one of the end-caps and an

electron multiplier placed outside the end-cap (similar to the design of Dawson and Whetten), ions which exit the ion trap through the holes drilled in the end-cap would strike the electron multiplier and be detected. It was also found that a slight background pressure of helium gas (approximately $1x10^{-3}$ torr) increased the resolution of the resulting mass spectrum by collisionally damping the ions in the trap, thus cooling the ions to the center of the trap so that they were ejected in a tighter packet. This mode of operation of the ion trap offered the increased benefits of a simpler operation (no need to apply a DC voltage for pulsing out the ions), a greater scan speed (the entire m/z range from 10 to 650 Daltons could be gathered in approximately 10 ms), an increased m/z range (with no DC voltage applied to the end caps, the greatest range of m/z's could be stored in the trap), and a reduction in the space-charge effect (by operating the ion trap with no DC voltage applied during scan-out).

Since the introduction of a commercial ion trap using mass-selective instability mode,[51] there have been several advances in the specific operation of the ion trap which have expanded its capabilities as a mass spectrometer.

One of the most powerful abilities of the quadrupole ion trap is its ability to selectively fragment ions to produce a characteristic 'daughter' ion spectrum, called MS/MS. The produced daughter ion spectrum can be used to unambiguously identify a compound even when the parent ion peak is indistinguishable from peaks produced by other compounds only one or a few

m/z units away. This ability is accomplished by the application of an alternating current (AC) voltage to the end-cap electrodes and is called collisionally activated dissociation (CAD).[52] In much the same way as the earliest detection method used with the ion trap (mass-selective detection), in CAD a voltage is applied to the end-cap electrodes of the ion trap at a selected frequency. Ions within the trap which have a secular frequency equal to the applied voltage will gain kinetic energy through resonant absorption. The gain in energy will result in increased translational motion along the axis of the applied voltage. Since in normal operation of the ion trap there is a background pressure of a light buffer gas (generally helium at a pressure of $1x10^{-3}$ torr), the increase in translational motion results in increased and more energetic collisions between the selected ion and the buffer gas. These collisions deposit energy in the ion and increase its internal energy. If the collisions are of sufficient energy for a sufficient amount of time, the internal energy of the ion is increased to the point that bonds within the ion are broken. Since the mass spectrometer detects ions, only those fragments of the ion which retain the charge are detected.

To be able to distinguish the daughter ion spectrum produced by CAD from the normal background ions present in most samples, it is necessary to first isolated the parent ion so that the daughter ions (of lower m/z than the parent) are easily discernible. To accomplish this, there have been several methods employed. Among the proposed, and used, methods for the isolation

of the parent ion are: (1) the two-step isolation method,[53] where two separate sets of RF and DC voltages are applied to the ring electrode in sequential fashion to first remove the ions of lower m/z than the parent ion and then to remove the ions of higher m/z than the parent ion; (2) the apex isolation method,[54] where the RF and DC voltages are selected such that the desired m/z of the parent ion is moved to the apex region of the stability diagram where ions of both higher and lower m/z than the selected parent ion become unstable (and so are ejected from the trap) at the same time; (3) the forward-reverse isolation method,[55] where an appropriate RF voltage is applied to the end-cap electrodes so that ramping the RF drive amplitude first up and then down causes the ejection of first the ions of lower m/z than the selected m/z and then the ions of higher m/z than the selected m/z; and the stored waveform inverse Fourier transform (SWIFT) isolation method,[56] where a broadband waveform with a missing notch of selected frequencies is produced by SWIFT and applied to the end-caps electrodes such that all ions except those within the frequencies of the notch are excited by the applied voltage and are ejected from the trap. Each of these methods has advantages and disadvantages related to their ability to effectively isolated the selected m/z with minimum loss. For most of the studies presented in this dissertation, the SWIFT isolation method was found to be the preferred method since it produced the best isolation with a minimum loss of parent ion signal intensity.

Ion Trap Theory

A quadrupolar ion traps consist of a three-electrode arrangement consisting of two end-cap electrodes and a ring electrode (Figure 1.4). In the mode of operation most commonly used an RF and DC potential is applied to the ring electrode while the end-caps are grounded. In this mode of operation, the applied potential produces a time dependent quadrupolar electric field in the ion trap. The potential ϕ at any point within the ion trap can be described by the equation:

$$\phi = \frac{\phi_o}{\left(r_o^2 + 2z_o^2\right)}\left(r^2 - 2z^2\right) + \frac{\phi_o}{2} \qquad 1.1$$

where ϕ_o is the potential applied to the ring electrode, r_o is the inside radius of the ring electrode, and z_o is one half the distance between the end-cap electrodes. The factor of two applied to the z_o^2 term is the result of the historical physical shape of commercial ion traps where $r_o^2 = 2z_o^2$.

The potential applied to the ring electrode can be a combination of RF potential (V) and direct current (DC) potential (U) such that:

$$\phi_o = U - V\cos\Omega t \qquad 1.2$$

where Ω is the angular frequency of the RF potential in radians s^{-1} and t is the time in seconds. The field is uncoupled so that the force experienced in one direction is independent of the force experienced in the other perpendicular

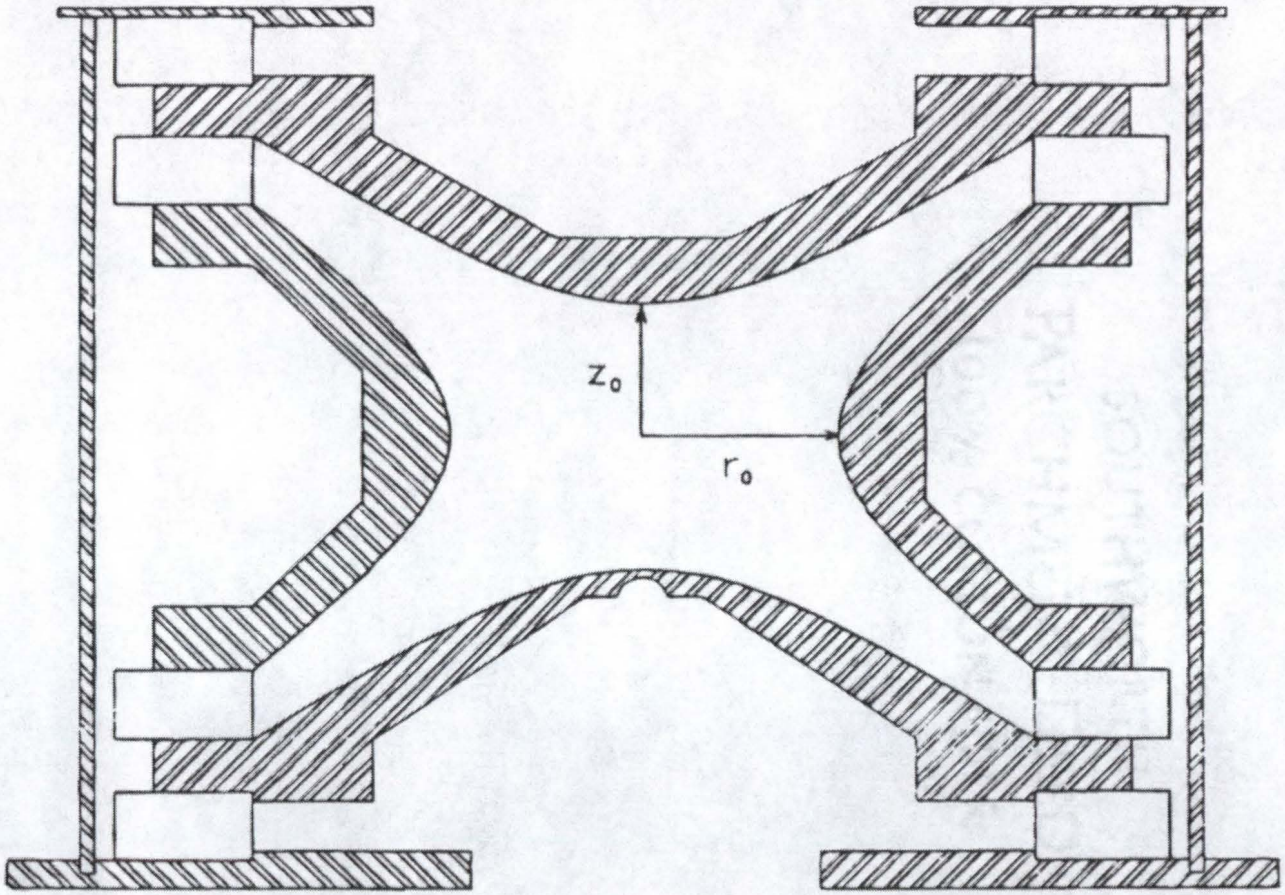

Figure 1.4. Schematic diagram of a three-dimensional quadrupole ion trap.[57]

direction. The force impressed on the ions by the electric field is described by applying Newton's equation of force ($F = ma$) in the form:

$$m\frac{d^2u}{dt^2} = -e\frac{\partial\phi}{\partial u} \qquad 1.3$$

where u can be either r or z, m is the mass of the ion, and e is the charge on the ion (in coulombs). Combining equation 1.1 and equation 1.2 into equation 1.3 for ϕ, then differentiating with respect to the individual axes and rearranging, the equations for the motion of ions within the quadrupolar field become:

$$\frac{d^2r}{dt^2} + \frac{2e}{m\left(r_o^2 + 2z_o^2\right)}\left(U - V\cos\Omega t\right)r = 0 \qquad 1.4$$

$$\frac{d^2z}{dt^2} - \frac{4e}{m\left(r_o^2 + 2z_o^2\right)}\left(U - V\cos\Omega t\right)z = 0 \qquad 1.5$$

Notice that equations 1.4 and 1.5 do not have cross terms, indicating that the ion motion along one axis is independent of the motion along the other.

These equations can be put into the form of a known second-order linear differential equation called the Mathieu equation with the following substitutions:

$$a_z = -2a_r = \frac{-16eU}{m\left(r_o^2 + 2z_o^2\right)\Omega^2} \qquad 1.6$$

$$q_z = -2q_r = \frac{-8eV}{m\left(r_o^2 + 2z_o^2\right)\Omega^2} \qquad 1.7$$

$$\xi = \frac{\Omega t}{2} \qquad 1.8$$

Substituting equations 1.6, 1.7, and 1.8 into expressions 1.4 and 1.5 transforms both expressions into a Mathieu equation with the form:

$$\frac{d^2u}{d\xi^2} + (a_u - 2q_u \cos 2\xi)u = 0 \qquad 1.9$$

Stable trajectories for ions along both the r and z axis are obtained only at certain a_u and q_u values. It is easy to see from equations 1.6 and 1.7 that all parameters other than U and V are constant for an ion of a certain charge and mass. Because of this, $a_u \approx \frac{Ue}{m}$ and $q_u \approx \frac{Ve}{m}$ (rather than m/e, traditionally mass spectrometrists have used m/z to indicate the mass to charge ratio of an ion where m represents the mass of the ions and z represents the number of fundamental charges on the ion). The values of a_u and q_u which result in stable trajectories along both the r and z coordinates can be plotted to produce a diagram which shows stable and unstable regions in a_u and q_u space. This type of diagram is called a stability diagram and provides a convenient method of visualizing ion trajectories within the ion trap (Figure 1.5).

The lines which crisscross the region of stable trajectories in both the r and z direction are iso-β lines and indicate a, q values that produce identical secular frequency of motion for ions of a given m/z. Current ion traps operate with no DC potential applied between the ring and end-cap electrodes. For this mode of operation, the ions line up along the $a_z = 0$ line in the stability

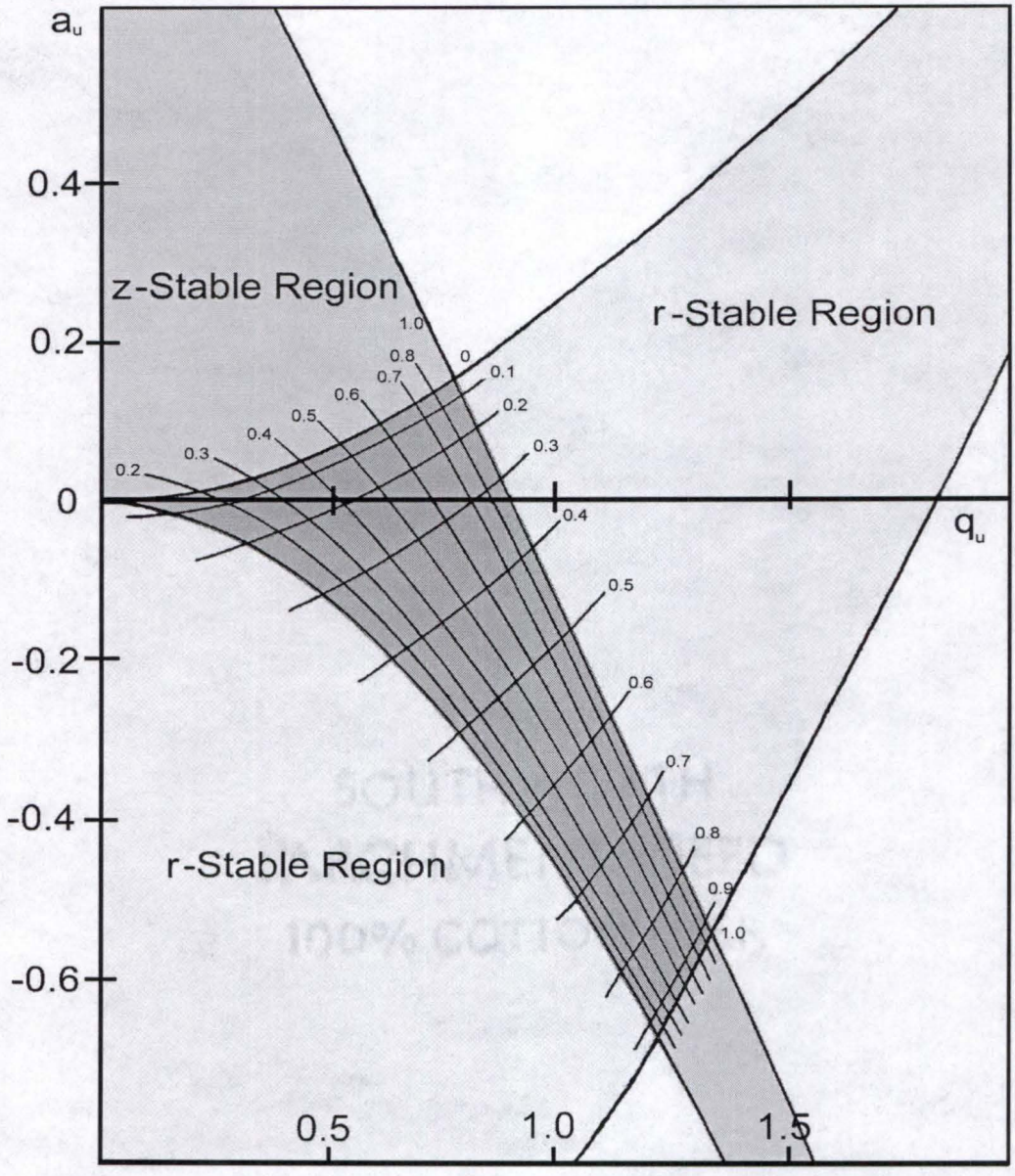

Figure 1.5. A stability diagram indicating the a_z and q_z values which produce stable trajectories for ions held within the ion trap. The lines which crisscross the region in which ions are stable in both the r and z directions are iso-β lines. These lines indicate values that produce identical secular frequency of ion motion.

diagram. Since q_z is inversely proportional to the m/z of an ion, the ions line up from left to right along the $a_z = 0$ line in order of decreasing m/z. Also, as indicated by equations 1.4 and 1.5, the time-dependent motion (or secular frequency) of the ions is inversely related to the m/z of the ion, such that, at a given RF potential (V) ions of lower m/z values will have higher secular frequencies. When the RF potential is increased to the point that an ion has a secular frequency greater than β=1 along the z coordinate (the right hand edge of the stability diagram), the ion becomes unstable in the z direction (along the end-cap axis) and is ejected from the trap out one or the other of the end-caps (when holes in the end-caps are present). Note that at this point the ion will still be stable in the r direction as indicated in the stability diagram. This is the theoretical basis of the mass-selective instability mode of operation of the ion trap which is used today for most commercial ion trap instruments.[50]

The equations given to describe the motion of ions in a quadrupolar electric field (equations 1.4 and 1.5) are strictly defined as applying only to a single ion. When several ions are present, the resulting interaction of the ions' electric field with the applied electric field causes the trajectories of the ions to be disturbed. This perturbation of the applied electric field is called the 'space charge' effect.[47] The result of the space charge effect is that some of the ions are shielded from the applied electric field. This shielding results in the secular frequencies of the ions being reduced and broadened.[58] The resulting

mass spectrum peaks are also broadened (a loss of resolution) and shifted so that they appear at higher m/z's (loss of mass accuracy).

Several methods have been developed to reduce the space charge effect on the resulting mass spectrum. One such method (which is currently employed on commercial ion traps) is to apply a supplementary AC potential to the end-caps (180° out of phase) at a frequency close to the secular frequency of the ions at $\beta_z = 1$ (the right-hand edge of the stability diagram).[59] This application of a supplementary potential is called resonant ejection. Resonant ejection of the ions has been found to reduce the broadening of the ion peaks and reduce the mass shifts associated with the space charge effect.

Another method (which can be used in conjunction with resonant ejection) is automatic gain control (AGC), which controls the number of ions injected into the trap and so reduces the space charge effect.[60] AGC is a simple process. Immediately prior to the analytical scan of the ion trap, ions are injected into, or formed inside of, the ion trap for a set period of time. The ions formed during this set period of time are quickly scanned out of the ion trap and detected. The total ion current produced by the ions is measured. Based on the amount of total ion current measured in this pre-analytical scan, the ion formation time used for the analytical scan is set so that the total ion current (which is related to the total number of ions present in the trap) is such that the space charge effect is reduced. Both resonant ejection and AGC, in conjunction with the mass-selective instability mode of operation, have

improved the analytical capabilities of the ion trap such that it rivals or exceeds other forms of mass analyzers.

One result of the application of a supplementary AC voltage for resonant ejection of ions from the ion trap is the ability to extend the m/z range of the trap. The quadrupole ion trap has a theoretically unlimited m/z range only if the RF potential can be increased to infinity (this assumes that the size of the trap and the frequency of the RF remains constant during scan-out, both of which are good assumptions). However, the RF potential can only be increased to a certain point before the voltage will begin to arc across the spacers between the ring and end-cap electrodes, or through the gas present in the trap, to ground. This maximum allowable voltage sets the upper mass limit during the normal operation of the ion trap. Using the values in Table 1.1 for the ITS-40 ion trap (which was used in all of the research performed in this dissertation) and equation 1.7, the m/z range is restricted to a maximum of approximately 650 Daltons. The q_{eject} value of 0.908 comes from the stability diagram and coincides with β=1 along the a_z = 0 line (the point at which the ion's trajectory becomes unstable and the ion is ejected from the trap). This restriction on the maximum m/z is one of the most serious drawbacks to the quadrupole ion trap. However, that restriction on the maximum m/z is only applicable when the q_{eject} used is at, or near, a value of 0.908. Since the application of a supplementary AC potential to the end-caps of the trap will cause ions of the correct secular frequency to gain translation motion in the

Table 1.1 Operating Parameters for the ITS-40 Ion Trap

f	1.0485 x10^6 Hz
Ω ($f2\pi$)	6.5879 x10^6 radians sec^{-1}
r_o	0.01 m
z_o	0.007811 m
V_{o-p}	7500 V
q_{eject}	0.908
mass	= Daltons * (kg/6.022x10^{26})

direction of the applied potential (along the z axis-toward the end-cap electrodes), by reducing the frequency of the applied potential, ions of larger m/z values can be ejected from the trap at a lower RF potential. The RF is increased normally during the scan-out event, yet ions are ejected from the trap at a lower q_{eject} which is related to the frequency of the supplementary applied AC potential. This method of extending the mass range of the ion trap is referred to as being extended by use of axial modulation.[61] The m/z limit of the ion trap can also be extended by reducing the diameter of the ion trap or by reducing the frequency of the RF; however, both of these solutions can have a negative impact on the mass spectrum due to an increase in the space charge effect . For ions with a m/z greater than 650 Daltons investigated for this dissertation, axial modulation was used to extent the mass range of the instrument.

Overview of Dissertation

The focus of this dissertation is on the development of a quadrupole ion trap laser microprobe instrument which is capable of mapping pharmaceutical compounds in intact tissue. Chapter 2 reviews the previous work done in this laboratory by Christopher D. Reddick who initially constructed the instrument (called Tubby, due to the large tub of a vacuum chamber in which it was constructed) used in these studies and the results of those initial studies which led to the current research. Christopher Reddick's

research centered on the initial construction of Tubby and the use of matrix-assisted laser desorption and ionization (MALDI) as a means of detecting pharmaceutical compounds in intact tissue. Those studies showed that the instrument was capable of detecting pharmaceutical compounds at levels which were compatible with dosing levels of most pharmaceutical compounds (approximately 50 ng/mg). The ability to spatially resolve the location of those compounds in the intact tissue mass was not accomplished during the initial studies with the instrument because of analyte migration during the MALDI preparation step. The ability to spatially resolve the location of pharmaceutical compounds in intact tissue formed the focus of my research.

Chapter 3 describes the first of two methods investigated to preserve the spatial distribution of pharmaceutical compounds in intact tissue: laser desorption coupled to chemical ionization (LD/CI). The chapter starts with an overview of the laser desorption process and gives a brief description of chemical ionization. Initial experiments were performed to demonstrate the viability of LD/CI for the detection of trace level compounds in intact tissue. A micro-manipulation stage was constructed so that selected locations on the surface of an intact tissue mass could be sampled. Final experiments were conducted which demonstrated the ability of LD/CI to preserve the spatial location of pharmaceutical compounds in intact tissue.

Chapter 4 describes the second method investigated to preserve spatial location information: the electrospraying of a MALDI matrix onto the

surface of tissue. The traditional method of MALDI is described (the drop method) and the blurring of spatial information is verified. An electrospray apparatus was constructed which was capable of electrospraying the MALDI matrix solution onto intact tissue. The method of electrospraying the MALDI matrix solution is demonstrated as being capable of preserving the spatial location information of pharmaceutical compounds in intact tissue.

Chapter 5 describes experiments preformed on both model and actual tissue samples to determine the location of drug compounds in intact tissue masses. The drug spiperone, at a level of 25 ng/mg of tissue, was mapped with a lateral resolution of 150 μm in a tissue sample by both LD/CI and the MALDI matrix electrospray method. An experimental drug which had been intravenously dosed to a level of 58.5 ng/mg in an animal, was mapped in a sample of tissue with a resolution of 150 μm by both methods.

In chapter 6, the final conclusions of the dissertation are presented and a brief description of future work which would be of interest to continuing the project is described.

CHAPTER 2
INITIAL STUDIES

Overview of Instrument

All experimental results presented here were obtained on a quadrupole ion trap instrument initially constructed at the University of Florida specifically for the analysis of pharmaceutical compounds in tissue by Christopher D. Reddick. A complete description of the instrument can be found in Chris' dissertation.[62]

The instrument consists of a Finnigan 4500 EI/CI ion source from Finnigan MAT (San Jose, CA) (Figure 2.1). One of the advantages of this ion source is that the ion volume can be changed with each sample to minimize carry-over effects. The only modification to the ion source was the blocking of the GC transfer line inlet hole so that a sufficient pressure of CI reagent gas (methane, ammonia, and isobutane were used where indicated for this dissertation) could be obtained for the LD/CI studies. The ion source and probe lock were mounted 90° in relation to the ion trap to allow the laser beam to be introduced into the source orthogonal to the probe face (Figure 2.2). This design assured that a small laser spot size with high power density could be obtained and that the ions would be desorbed in the direction of the ion extraction and focusing lenses. Additionally, the 90° design allows for future

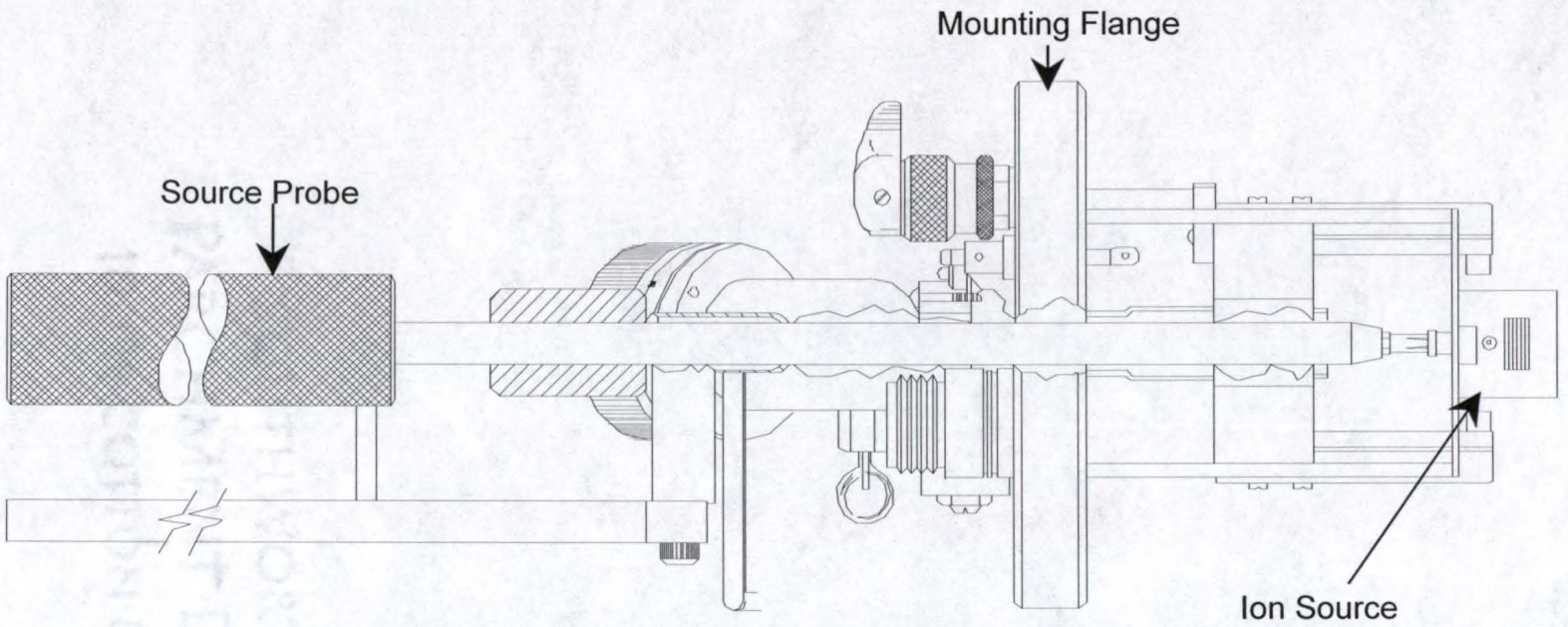

Figure 2.1. Schematic drawing of Finnigan EI/CI ion source used in instrument.

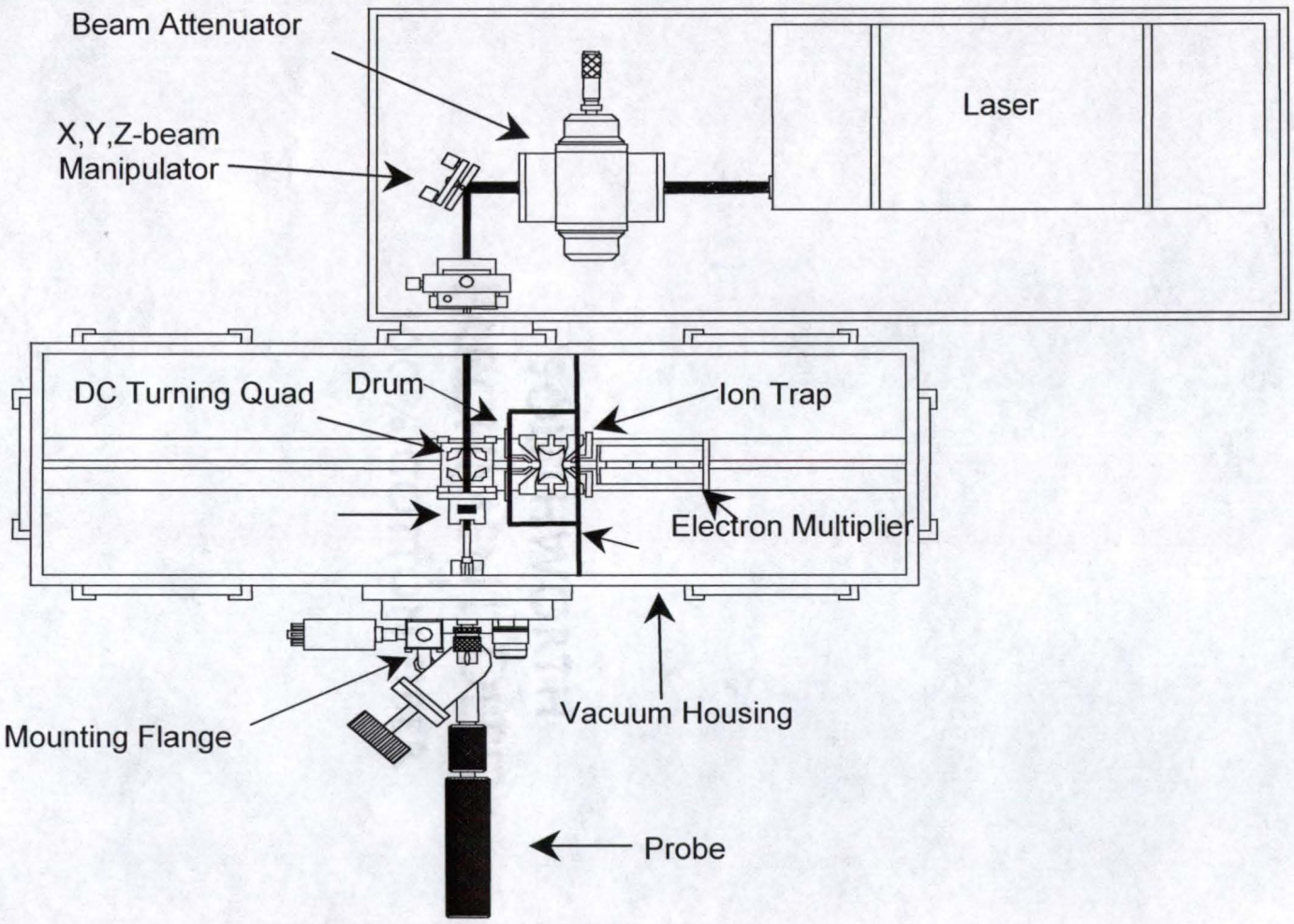

Figure 2.2. Schematic drawing of instrument Tubby.[62]

modifications to the instrument that will permit the viewing of the sample for laser desorption position selection.

To direct the ions from the ion source to the ion trap, a DC quadrupole was used as a 90^0 ion deflector as described by Pedder and Yost.[63] The deflector consisted of four quarter-round stainless steel rods with a radius of 0.5" and a length of 3.25". The rods were held in position by two anodized aluminum caps and were secured to the inside of the caps by Teflon screws to prevent grounding. Opposing rods were connected electrically so that a voltage could be applied to each pair of rods to turn the ions. A complete characterization of the DC turning quad has been given by Pedder.[64] A stainless steel tube lens was mounted to two of the quarter-round steel rods of the turning quad and served as the entrance lens into the ion trap.

The ion source and DC turning quad were housed in a differentially pumped, cradle-type vacuum chamber. The chamber was pumped by two TPH 300 L/s Balzers (Hudson, NH) turbomolecular pumps. The turbomolecular pumps were mounted directly to the stainless steel vacuum chamber (one in the source region and one in the analyzer region) through two 4.0" connection ports machined into the bottom of the vacuum chamber. Each turbo pump was individually backed by a 300 L/min mechanical pump (Alcatel Corporation, Hingham, MA). The pressure in each region was monitored by separate Bayard-Alpert type ion gauges (Granville-Phillips, Boulder, CO).

To minimize ion-molecule reactions between chemical ionization (CI) reagent gas introduced into the ion source during CI experiments and ions in the analyzer region, an aluminum dividing wall was added to the instrument between the source and analyzer regions as shown in Figure 2.2. With the installed wall, a pressure differential of approximately two orders of magnitude ($3x10^{-4}$ torr in the source region and $3x10^{-6}$ torr in the analyzer region) could be maintained during CI experiments.

MALDI

The initial studies which Chris Reddick performed on Tubby were designed to characterize the instrument's performance for use as a laser microprobe mass spectrometer with matrix-assisted laser desorption/ionization (MALDI). Since the results of those experiments led directly to my research, and because my research also involved the use of MALDI as a desorption and ionization method, a brief overview of the history and theory of MALDI is included here.

History

In the early 1980s, the desorption of bio-organic molecules for mass spectrometry above 10,000 Daltons was performed almost exclusively by plasma desorption.[65-66] Then in 1988 both Tanaka et al. in Japan and Karas and Hillenkamp in Germany published articles which described a method of

sample preparation that allowed the analysis by laser desorption mass spectrometry of bio-organic molecules of up 100,000 Daltons and 67,000 Daltons, respectively.[67-68] Both of the preparation methods involved the addition of a matrix to the sample which enhanced the desorption and ionization of large bio-molecules.

The method which Tanaka et al. described involved the dispersion of an ultra fine (about 300 Å diameter) cobalt power in glycerol which was dissolved in an organic solvent. This matrix solution was mixed with the sample (also in solution) before being applied to the sample holder. The matrix/analyte solution was allowed to dry before analysis. A nitrogen laser (337 nm wavelength) was used to desorb and ionize the sample, with the ions mass analyzed with a time-of-flight mass analyzer. The technique was called, "ultra fine metal plus liquid matrix method" and was able to demonstrate the detection of the $[7M+cation]^+$ ion of lysozyme from chicken egg white (lysozyme mw = 14306 Daltons). The metal powder served as a chromophore for absorbing the irradiating laser light and the glycerol served to disperse local heating and provide a renewable surface area for multiple laser shots.

The method developed by Karas and Hillenkamp was born out of an earlier observation that laser desorption of amino acids which had strong absorbance near the wavelength of laser light used (a Nd:YAG, frequency-tripled to 355nm or frequency-quadrupled to 266 nm) required a lower threshold irradiance (defined as the minimum laser power required to

produced ions from the sample) and produced a greater ratio of molecular-type ions to fragments than amino acids which had a lower absorbance at the selected wavelength.[69] As a test, the authors mixed a strongly absorbing amino acid (tryptophan) with a weakly absorbing one (alanine). The resulting spectrum showed alanine $[M+H]^+$, along with the tryptophan $[M+H]^+$, even though the laser power used was approximately one tenth of that necessary to produce ions from a sample of alanine alone. Based on these observations, Hillenkamp and Karas chose the UV absorbing compound nicotinic acid dissolved in water (at a concentration of 10^{-3} M) as their matrix and mixed an equal amount of matrix solution with sample solution (bovine albumin, mw = 67,000 in water at a concentration of 10^{-5} M). The mixture was air dried on a probe tip and desorbed and ionized by the frequency-quadrupled output of a Nd:YAG laser (at 266 nm) and the ions analyzed by time-of-flight mass spectrometry. Their method was called, "matrix-UVLD" where the UV stands for ultraviolet and the LD stands for laser desorption. After several name changes, today the most widely accepted name for this sample preparation method is MALDI (matrix-assisted laser desorption/ionization).

Theory of MALDI

Desorption

The desorption process of MALDI has been extensively researched and is fairly well understood qualitatively.[70] Most of the proposed models for

desorption of large bio-molecules by UV MALDI are variations of the same general theory.[71] That general, qualitative theory for the desorption of large bio-molecules by MALDI is well represented by the "hydrodynamic model" proposed by Vertes, Irinyi, and Gijbels.[72] The basics of the hydrodynamic model are that the incident laser light causes rapid heating of the solid (both matrix and analyte). Once the sublimation temperature of the matrix is achieved, rapid evaporation of both matrix and analyte produces an expanding plume of material into the gas phase by direct sublimation. The temperature, density, and velocity of the solid and expanding vapor can be calculated by application of a set of hydrodynamic equations (Figure 2.3). Figure 2.3A shows the calculated effect of a 10-ns laser pulse (Nd:YAG, frequency-quadrupled to 266nm) on temperature at the surface-vapor interface of a nicotinic acid sample. Note that after the end of the laser pulse (50 and 100 ns traces), both the surface of the sample and the vapor created during the desorption event are significantly cooled. The surface is cooled by the sublimation process and the vapor is cooled by the rapid expansion into the gas phase. Figure 2.3B shows the density distribution of the expanding vapor into the gas phase. The initial vapor density (10ns trace) is relatively thick and located, as expected, primarily within 4 μm of the surface. Once the irradiation stops (50 and 100 ns traces), the rate of evaporation quickly subsides due to the rapid cooling of the surface and the plume detaches from the surface and expands.

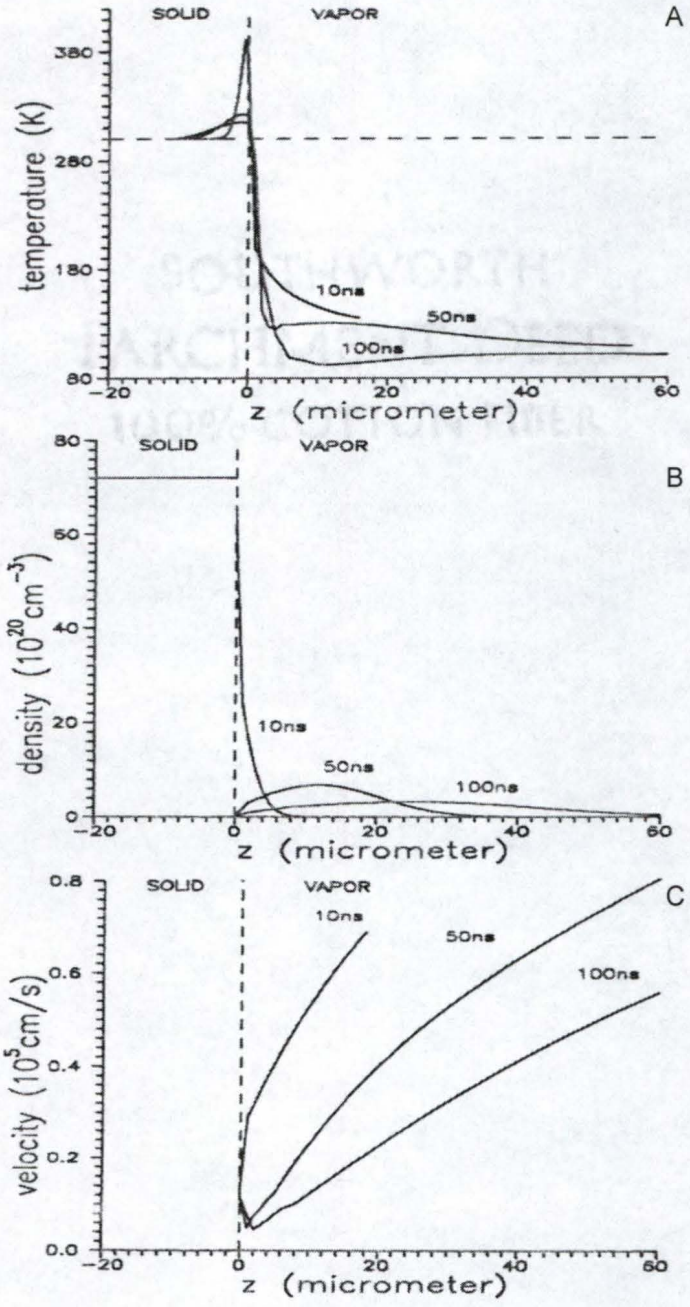

Figure 2.3. The calculated temperature(A), density(B), and velocities of particles desorbed (C) from a matrix of nicotinic acid by a 10 ns laser pulse (Nd:YAG, 266 nm wavelength with 10^7 W/cm^2 power) using the hydrodynamic model. Dashed vertical line indicates matrix/vacuum interface. The dashed horizontal line in (A) indicates 300 K.[72]

Using the same process, the velocity, density, and temperature were calculated for sinapinic acid desorbed by a 10 ns laser pulse (at 308 nm wavelength) (Figure 2.4). In Figure 2.4A, the density of desorbed molecules in the expanding plume was calculated and plotted for laser irradiances increasing from 2 $x10^5$ to 4 $x10^6$ W/cm^2 (the letters f through a indicate a regular increase of laser power by five steps of 7.6 $x10^5$ W/cm^2). The areas under the curves of Figure 2.4A were integrated to determine the total flux of molecules desorbed at each laser irradiance level; these were then plotted to show the increase of material ejected with increasing laser power (Figure 2.4B). The calculated desorption flux vs. irradiance was compared to experimental data collected on the MALDI of bovine insulin with sinapinic acid as the matrix and an excimer laser operating with 10 ns pulse at 308 nm wavelength (Figure 2.5).[73] The hydrodynamic model fits well with the experimentally calculated ion flux vs. irradiance; however, there were differences. In the experimental data, the threshold of ion production was found to be 2 $x10^6$ W/cm^2 while the threshold calculated from the hydrodynamic model was found to be 2 $x10^5$ W/cm^2. The authors suggest that the cause for this deviation may well be the optical constants that were used in their calculations. The absorbance coefficient used for sinapinic acid was from the solution-phase data, since that was the only value available. Another difference between the calculated values and the experimentally determined values was the slope of the flux vs. irradiance. The measured ion yield shows

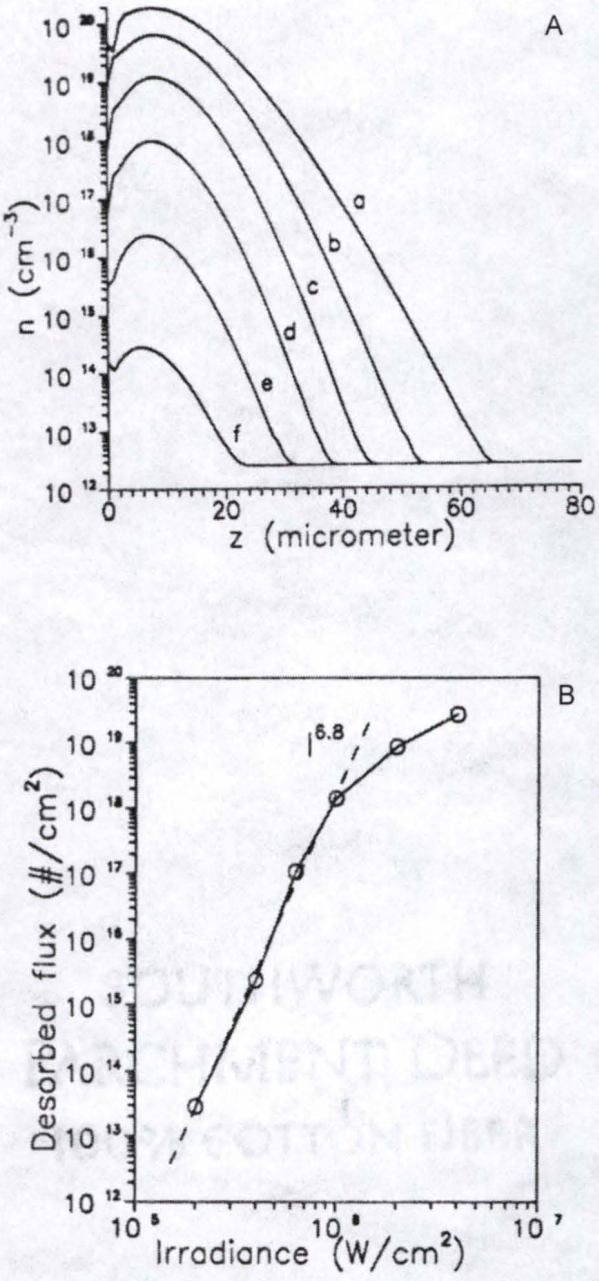

Figure 2.4. (A) shows calculated plume density profiles of matrix sinapinic acid matrix at 40 ns after 10 ns laser pulse (excimer laser, 308 nm wavelength). Letters f through a indicate varying laser irradiances (explanation in text). (B) shows plot of calculated desorbed matrix flux vs. laser irradiance.[72]

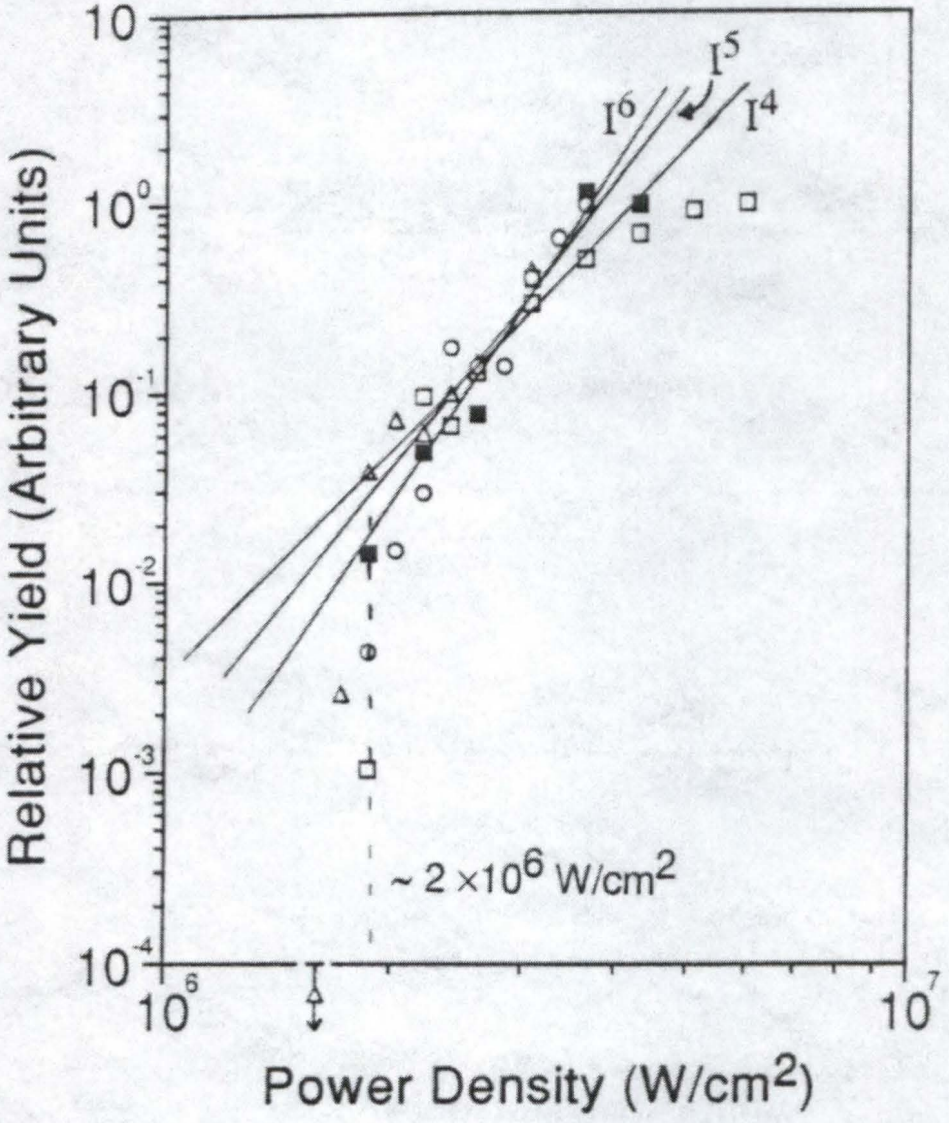

Figure 2.5. Plot of the dependence of molecular-ion yield, Y_I, of bovine insulin from sinapinic acid vs. laser irradiance level for excimer laser (at 308 nm wavelength with 10 ns pulse). The different symbols indicate different diameters of an iris placed in front of the microchannel plate detector to prevent saturation.[73]

a power law dependence with laser intensity of approximately $Y_i \propto I^6$, while the exponent derived from the hydrodynamic model was somewhat higher (6.8). The source of deviation between the two data sets can only be guessed; however, the authors suggest several possibilities: statistical error in the experimental data (no single power law exponent was given by the authors of the experimental measurements), that the measured ion yield may not be proportional to total desorbed molecule yield, and the assumption of a Gaussian fluence distribution on the sample surface in the hydrodynamic calculations. It is worth noting that both the experimental evidence and the hydrodynamic model predict a saturation-like behavior at high irradiance levels.

Velocity distributions were calculated for sinapinic acid and ferulic acid and then compared to experimental data gathered on both matrices. The calculated drift velocity (250 m/s) for ferulic acid *neutrals* compared well with the maximum measured *neutral* particle velocity of 300 to 400 m/s, while the calculated value for sinapinic acid *neutrals* (250 m/s) was found to be substantially lower than the experimentally measured *ion* velocity (1140 m/s) for sinapinic acid. The authors suggested that this difference might be the result of the high extraction field present in the experimental data. Even with the reported differences between the calculated and the experimental evidence, there is enough agreement to make the model important for a qualitative understanding of the MALDI desorption process.

One consideration worth noting is the fact that MALDI produces large, thermally labile, bio-molecule ions with little or no fragmentation, while the matrix itself often shows substantial fragmentation. This observation is not completely consistent with the simple heating of the matrix offered by the hydrodynamic model, since the analyte molecules would also be heated in the process. The authors suggest that this observation is the result of the energy-transfer pathways of the system. A model which offers an explanation for the observed intact bio-molecules desorbed during UV MALDI called, "The Homogeneous Bottleneck" model has been presented.[74] As with the hydrodynamic model, it is of value to understand the model for a clearer understanding of the MALDI process, and so it will be briefly presented here.

During solvent evaporation, the analyte molecules (called the guest in the homogeneous bottleneck model) are entrapped in the crystal lattice structure formed by the matrix molecules (called the host). The lattice bonds formed between host molecules will have a different vibrational frequency (and energy transfer coefficient) than internal bonds of the host molecules, and both of these bonds will be different than the bonds formed between host and guest. Figure 2.6 is a schematic representation of the bonds involved in the host/lattice and guest incorporation into a MALDI matrix. Several assumptions are made to produce the kinetic equations used to solve the energy transfer bottleneck in the model. One assumption is that the two most effective mechanisms by which the excited volume can be cooled is by evaporation and

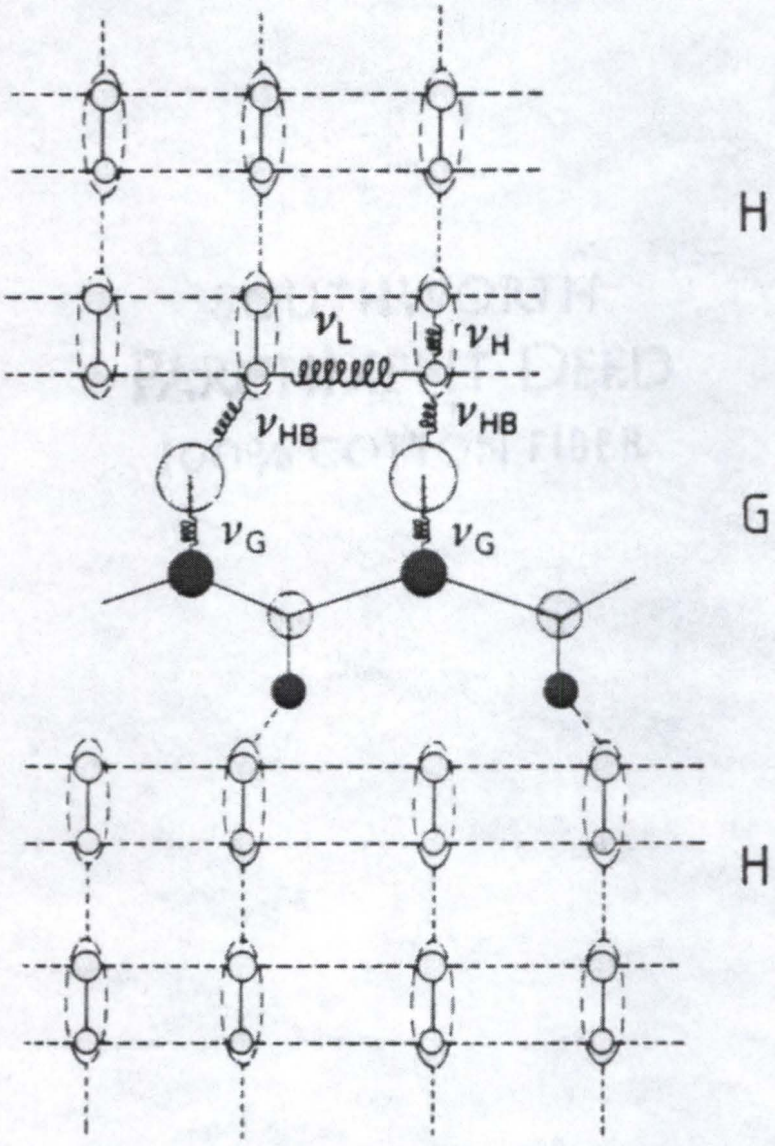

Figure 2.6. A schematic representation of the vibrational modes of the guest molecule (G) incorporated into lattice of host molecules (H). Solid lines represent chemical bonds and broken lines represent physical bonds. The springs represent the coupling modes of energy transfer. ν_{HB} represents the hydrogen bonds formed between host and guest and is the bond broken during release of the guest molecule.[74]

sublimation. The possible mechanism of cooling by heat conduction was ignored in the model because of the short timescale (10 ns) generally involved during UV laser irradiation of the solid. The possible cooling by volume evaporation was also ignored in the model because it has been shown to be important only with matrices which have low coefficients of absorbance (this process of cooling was included in a later publication which included IR MALDI).[75] Additionally, the laser pulse was assumed to have a purely Gaussian distribution across the surface.

The authors presented and solved a set of kinetic equations which were taken to be representative of the energy redistribution process during laser irradiation of the host/guest solid. The physical processes which were assumed in deriving the equations were as follows: the laser energy deposited on the solid primarily excited (electronically, because it was UV radiation) the host molecules. Since in typical MALDI conditions the host molecules are present at a ratio of 1,000:1 to 100,000:1 compared to the guest molecules, this seems to be a valid assumption. Through an extremely fast (approximately in the ps timescale) internal conversion processes, this deposited energy is converted to internal vibrational energy. The internal vibrational energy of the host is then transferred to lattice vibrational energy at a rate dependent on the specific kinetic rate constant. This vibrational energy is also transferred, via direct coupling, to the guest molecule vibrational energy, again at a rate dependent on the specific kinetic rate constant. The

lattice is cooled by phase transformations and by the transference of energy to the guest. The heating rate of the guest molecule is determined by the direct absorbance of energy from the laser light and by the transference of energy from both the lattice and directly from the host. In addition, both the guest and host molecules can be subjected to energy loss through irreversible fragmentation. It should be noted that this model deals with the volume energy density of the guest and not the energy content of the guest.

An energy bottleneck can form at any of these energy transference points if the transfer rate coefficient is extremely low in relation to the others. Solving the equations presented by the authors, there is found to be extremely efficient transference of energy between host and lattice due to the large number of couplings present in the system. Furthermore, the transference of energy would be expected to be efficient in the direct coupling between host and guest since the vibrational frequencies of the bonds can fall within the same range. There would be expected to be a bottleneck in energy transference at the direct host/guest bond based on the low concentration of the guest in the matrix (generally 10^{-4} to 10^{-6} for traditional MALDI). There would also develop a bottleneck at the bonds between the lattice and the guest because of the vibrational difference between these bonds. Figure 2.7 shows the time history plot of the energy deposition during MALDI of nicotinic acid with a frequency-quadrupled Nd:YAG. Figure 2.7(b) represents a pictorial summation of the proposed theory. The lattice and host molecules are in

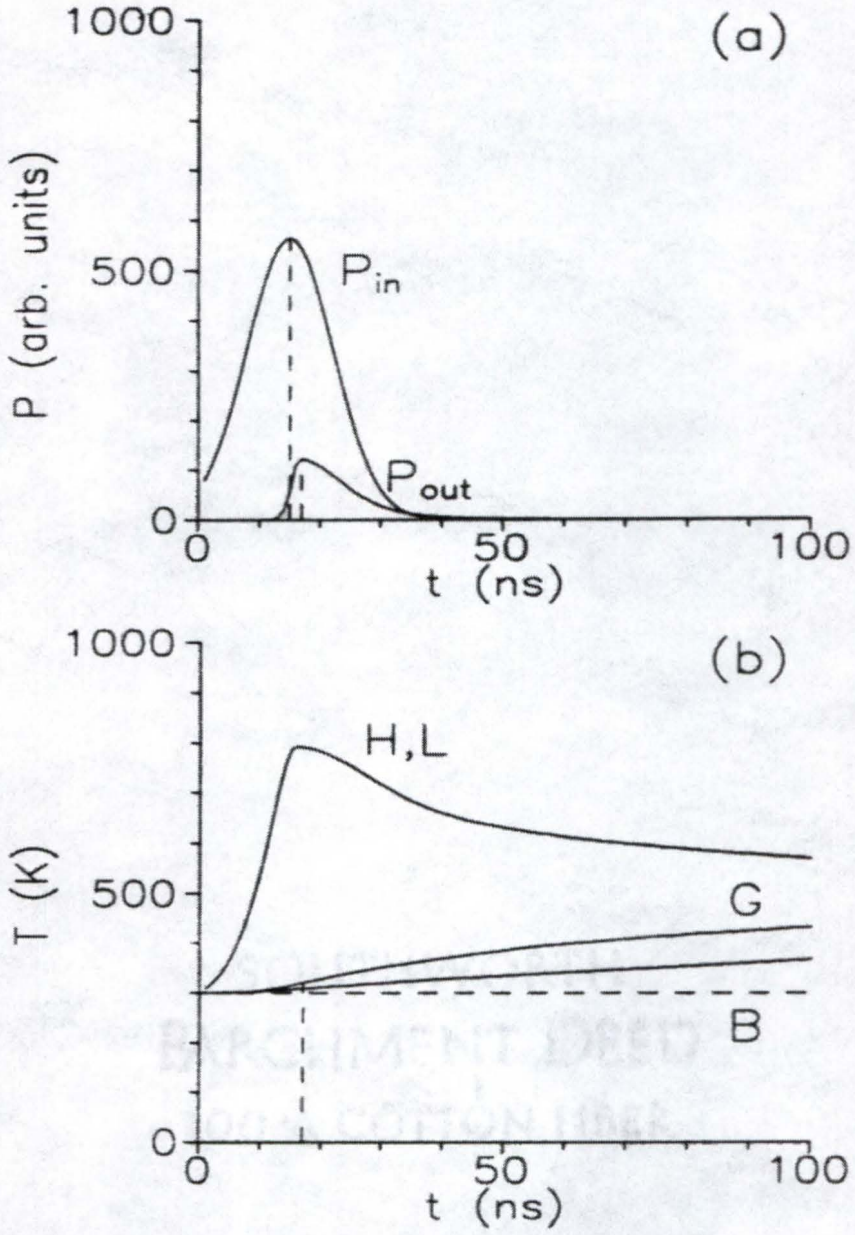

Figure 2.7. Calculated time history plots of energy deposition into matrix and guest. Plot (a) shows energy flux in (through laser irradiation) and out (through sublimation) of system. Note the slight time lag (indicated by the vertical dashed lines) between the maximum energy flux into the system and the maximum energy removed from the system. Plot (b) shows energy density of the host/lattice (H,L), guest (G), and thermally fragmented guest molecules (B). The dashed horizontal line shows room temperature across time of calculation. Note that for the timescale indicated, the lattice remains in equilibrium with host.[74]

thermal equilibrium during the rapid energy deposition by the laser irradiation due to efficient energy transference from host to lattice, while at the same time the guest molecules are thermally cooler. This reduction in temperature of the guest molecules compared to the host and lattice is a result of the bottleneck in vibrational energy transference due to the difference between the bonds formed between the matrix lattice and the bonds formed between the lattice and the guest.

Using the same equations, but with different initial conditions, the authors predicted the effects on the system for an increase in the concentration of the guest molecules in the matrix, a higher sublimation temperature for the host, and a lower power density with longer pulse length for the laser irradiation of the system (Figure 2.8). In Figure 2.8(a) the effect of increasing the fraction volume concentration of the guest molecules from 10^{-4} to 10^{-2} is shown. The increase in concentration of the guest molecule results in a greater efficiency of transfer of energy between the host and the guest. The greater efficiency results in an increase of guest temperature and an increase in the amount of thermal degradation (indicated by B in Figure 2.8). Additionally, since more of the available energy is transferred to the guest, there is less energy transferred into the lattice and so the rate of sublimation is reduced, which results in further heating of the guest and more thermal degradation.

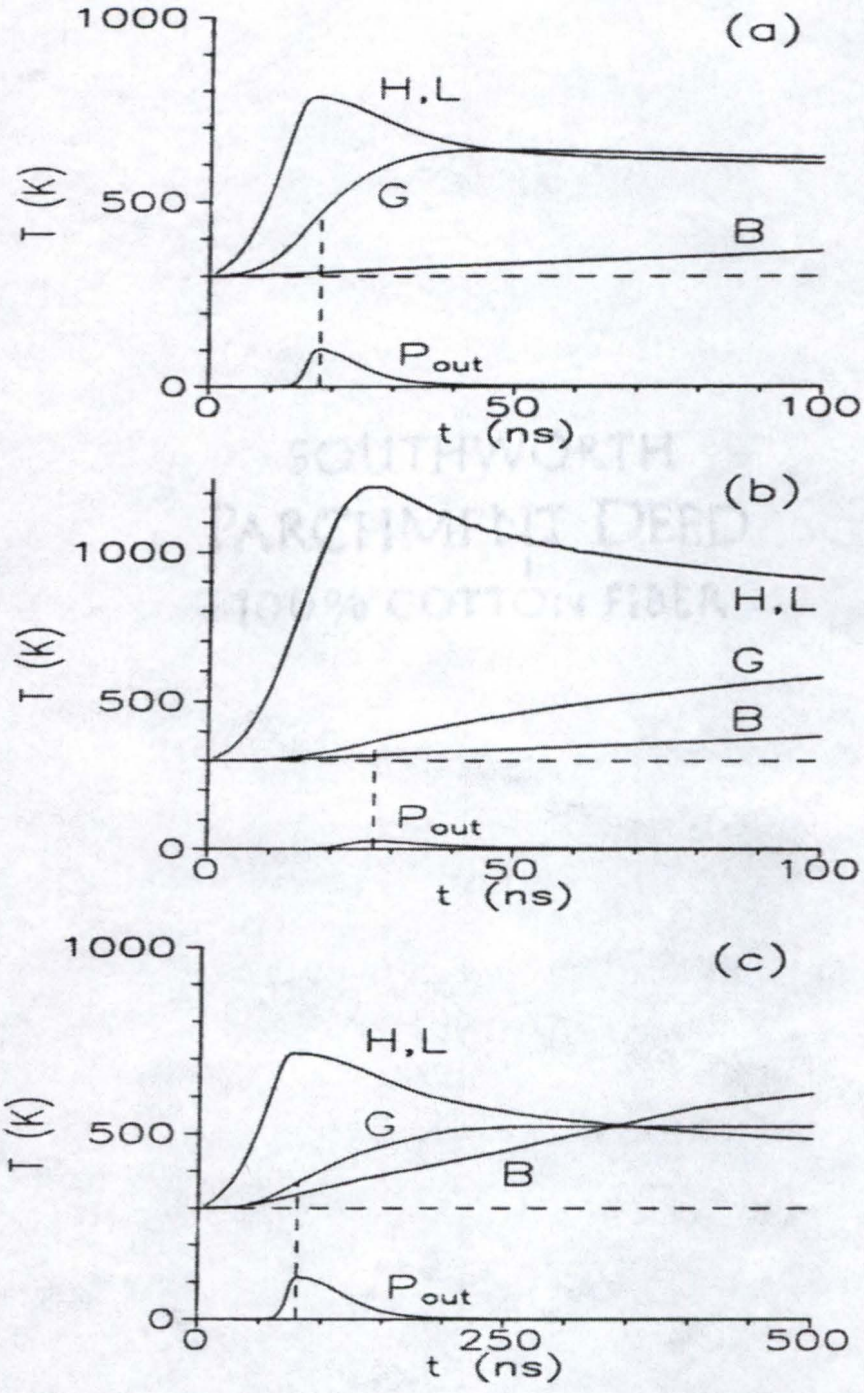

Figure 2.8. Homogeneous bottleneck model calculations for atypical MALDI conditions. Plot (a) demonstrates predicted behavior of system when concentration of guest is increased. Plot (b) shows predicted behavior when sublimation temperature of matrix is increased. Plot (c) shows predicted behavior when laser pulse is increased in duration while intensity of irradiance is decreased.[74]

Figure 2.8(b) demonstrates the effect of an increase in sublimation temperature for the host from 315 K to 400 K. The result of the increase of the sublimation temperature is what would be expected. The lattice and host are able to achieve higher temperatures before the onset of sublimation begins the cool the system. Because of this increase in temperature, more energy is transferred to the guest molecules and greater thermal degradation results. The authors also point out the advantage of a sublimating matrix as apposed to a melting matrix. If the matrix were to melt and evaporate, after melting the energy transfer process would be enhanced between the host and the guest. This increase in energy transfer might, if the melting temperature were high enough, result in sufficient transference of energy to the guest to bring about thermal degradation; however, this effect would be temperature dependent and is not a guarantee of increased degradation. Figure 2.8(c) demonstrates the effect of a longer laser pulse (increasing from 10 ns to 50 ns) along with a reduction in power (from 1 $x10^7$ W/cm^2 to 2 $x10^6$ W/cm^2). This change represents a 5-fold increase in pulse length and a 5-fold decrease in laser power. The net result is that the same energy is deposited in the sample, but the time over which the energy is delivered has been increased. This has a 2-fold effect on the embedded guest molecules. First, the cooling of the matrix by sublimation has been slowed due to the less rapid heating of the system from the reduced power. Secondly, increasing the pulse length increases the coupling time over which the host molecules can pump energy directly into the

guest. The combination of the two results, as expected, in an increase in fragmentation of the guest molecule.

While neither the hydrodynamic model nor the homogeneous bottleneck model can be taken as the only model to explain desorption during MALDI, like most chemical models, they offer a useful explanation of the process and summarize the current level of understanding of the process.

Ionization

While the desorption of neutrals and ions during MALDI is at least fairly well understood, the ionization process is not. There seem to be almost as many theories about the actual ionization process during MALDI as there are papers written about the process. One fact is fairly clear from the evidence presented so far, and that is that the ionization process for MALDI is a collective one, not a single process.[26] An excellent review has recently been published on the current theories for ionization during MALDI, and readers wishing for a more in-depth coverage of the process are referred there.[70] While the factors affecting the desorption event during MALDI are germane to this dissertation, the actual process of ionization is not. It is worthwhile, however, to briefly cover some of the currently postulated processes for a better understanding of MALDI. The following explanations were adapted from the previously cited review article.

The ionization process during MALDI can be split into two categories: primary ion formation and secondary ion formation. Primary ion formation covers those ions formed before (pre-formed ions in the matrix) or formed first during the ionization/desorption event (which would generally be matrix ions). Secondary ion formation covers those mechanisms which lead to those ions not generated during the primary ion formation process (which usually would be the analyte ions).

Primary ion formation

One of the ways by which the MALDI process helps to create ions is by reducing the energy necessary to produce the ions. This reduction is brought about by screening of the Coulombic charge on ions by solvation in the matrix. Transferring pre-formed ions from the solid-state to the gas phase, along with the removal of the matrix solvation shell, would negate any benefit gained by the screening of the Coulombic charges in the matrix; however, collisions during the plume expansion could serve to add the necessary energy needed to maintain separation of the pre-formed ions and reduce the incidence of charge recombination in the gas phase. Again, this is presumably not the major process of ion formation, only one of a collection of processes which could contribute to the overall production of ions during MALDI.

The mechanism of multiphoton ionization has been proposed to be one of the major mechanisms leading to ion formation during the MALDI process.[76] The mechanism is simple and can be presented as:

$$M \xrightarrow{n(h\upsilon)} M^{+\cdot} + e^{-} \qquad 2.1$$

where M represents the chromophore (matrix molecule) and e^{-} represents an ejected electron. This proposal is consistent with the observation that efficiency of MALDI is dependent on the absorbance coefficient of the matrix used.[70] The ionization energy of most MALDI matrices in bulk crystal form is still not known; however, the ionization energy of the individual matrix molecules appears to be greater than the 7.36 eV energy of two photons for the nitrogen (337 nm) lasers typically used in MALDI. Because of the low irradances typically used in MALDI ($\approx$1 x10^6 W/cm^2) the absorbance of more than two photons is unlikely. One possibility which has recently been proposed is that matrix molecules absorb two photons of laser energy and reach an excited state just below the threshold necessary for electron ejection.[77] During the plume expansion, where matrix/matrix collisions are numerous, a thermal distribution of vibrational energy is established which can then lead to the thermal emission of an electron from the electronically excited matrix molecules. This mechanism has been shown to be in good agreement with experimental observations.

Another proposed mechanism for achieving electron ejection without absorbance of more than two photons of energy is when two electronically

excited matrix molecules pool their energy to produce an ion.[78] The basis for this theory stems from the observation of matrix ion suppression when the analyte concentration is increased above normal (normal being ≈ 1:10,000 vs. matrix). The authors note that this cannot be simple proton affinity competition since, when the analyte preferentially cationizes, the matrix ions (of the $[M+H]^+$ form) are still suppressed. Also, when the primary form of analyte ion is $[M+H]^+$, this can suppress the formation of matrix ions of the $[M+Cation]^+$ form (Figure 2.9). The authors proposed a mechanism which involves two excited state matrix ions:

$$mH + h\upsilon \longrightarrow m^*H \qquad 2.2$$

$$m^*H + A \xrightarrow[m^*H]{} m^- + AH^+ \qquad 2.3$$

for protonation and a similar mechanism, where the proton (H) is replaced by a cation, for cationization. Both mechanisms predict an abundance of matrix $[M-H]^-$ ions during matrix suppression, even in the absence of $[M+H]^+$ matrix ions, and that prediction has been supported by experiment.

A similar proposed mechanism is simple excited-state proton transfer. This mechanism has been proposed since the seminal paper of Karas, Bachman, and Hillenkamp which led to MALDI as it is practiced today.[70] The proposed mechanism is the same as shown in equations 2.2 and 2.3, but instead of a second excited state matrix ion being required, the acidity of the excited state matrix ion formed in equation 2.2 is increased to the point that proton donation happens without the need for additional energy. The proton

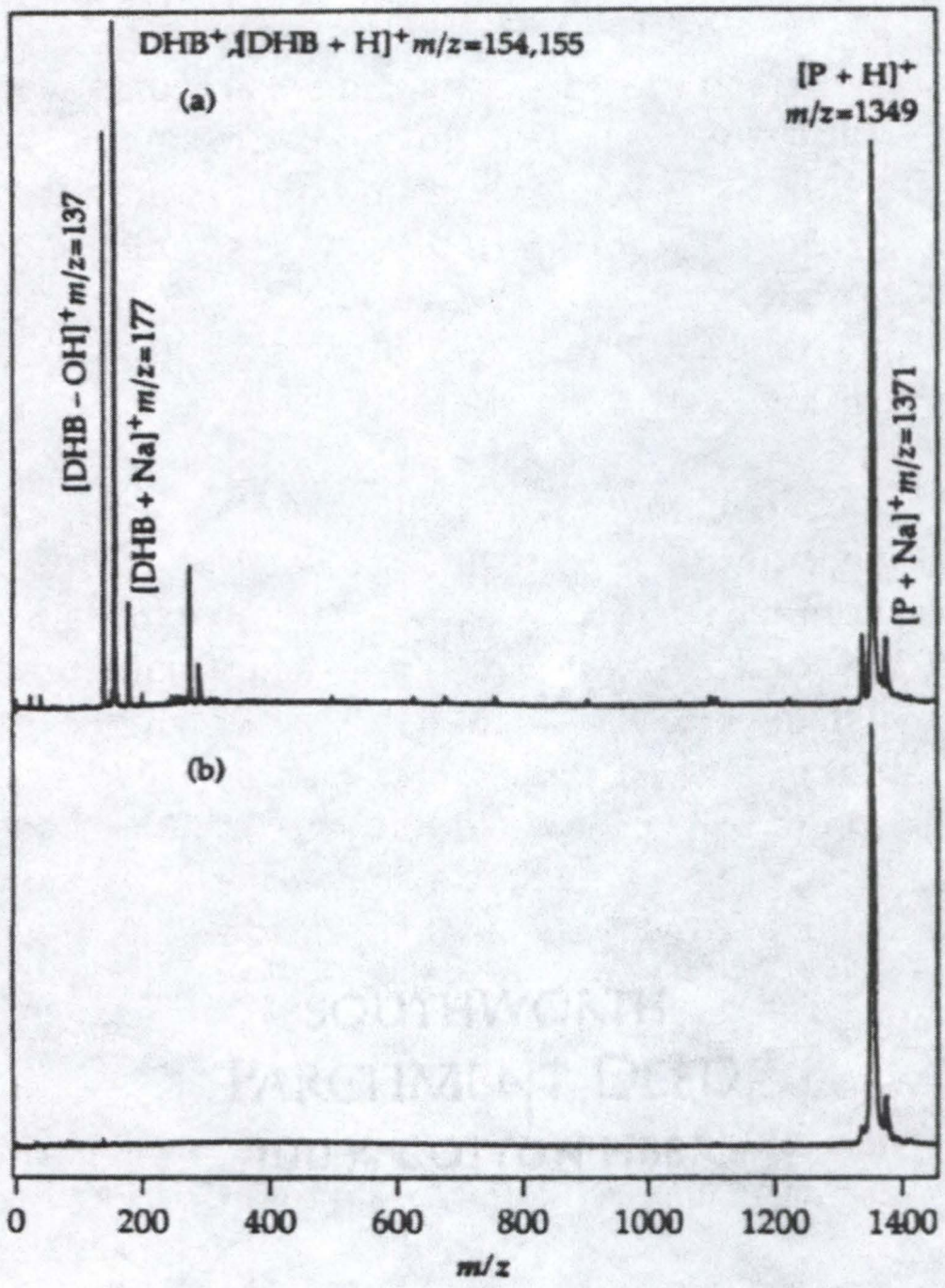

Figure 2.9. Spectrum (a) shows MALDI of substance P in matrix of 2,5-dihydroxy benzoic acid (DHB) where matrix-to-analyte ratio was 1000. The spectrum shows strong signals for matrix $[M+H]^+$ ion and cationization. Spectrum (b) shows MALDI with matrix-to-analyte ratio of 100. The spectrum shows strong signal for analyte ion of $[M+H]^+$. Note that all matrix signal was suppressed, as well as the $[M+Na]^+$.[78]

exchange between the excited state molecule (with increased acidity) and the analyte molecule could happen either in the solid state just prior to ejection, or in the expanding plume after desorption while the plume is still fairly dense.

The possible contribution to MALDI ions from pre-formed ions in the matrix prior to desorption has been proposed. It has been shown that ions are produced (in the cationized form) even when the laser beam impinged on the backside of a 200 nm thick gold foil (thus removing the possibility of photo-excited molecules), leading to the belief that these were thermally desorbed pre-formed ions.[79] It is difficult of course, to distinguish between pre-formed ions and those ions formed during early thick-plume formation.

For UV MALDI, the matrix is generally a strongly absorbing chromophore of the incident light; in IR MALDI, however, this is not generally the case. Because of the similar spectra produced by both IR and UV MALDI, mechanisms which do not require photo-excitation have been proposed to contribute to both forms of MALDI. Early work with simple laser desorption demonstrated the formation of the $[M+Na]^+$ ion of the sugar stachyose from a sugar and NaI mixture (at a ratio of 5:1) when the laser light was focused on the backside of a thin formvar film (with the mixture deposited on the opposite side).[80] When the formvar film and sample were not perforated (laser intensity of 1 $x10^{11}$ W/cm^2, sample 20 μm thick), the $[M+Na]^+$ ion was produced almost exclusively with very little fragmentation. This observation led to the proposed "shock wave" theory for desorption of ions. This proposal rules out the

possibility of simple thermal desorption of ions, since the large increase in temperature at those laser intensities would have produced extensive thermal degradation and fragmentation. The theory proposes that a thermally induced shock wave propagates through the solid leading to the desorption of pre-formed ions from the opposite side. This shock wave desorption is very similar to process developed for secondary ion mass spectrometry (SIMS). This model of desorption led to the proposal of the pressure pulse model for desorption and ion formation.[81] In the proposed model, two-center excited annihilation (the contribution of two excited state matrix molecules) may lead to ion formation with desorption the result of the pressure-driven shock wave. Another model, at least superficially similar to the pressure-driven model above, is the spallation theory proposed by Cramer, Haglund, and Hillenkamp.[82] Spallation is a process by which layers of material next to the free surface area are ablated by thermally induced stress which can build-up at rates faster than can be dissipated by acoustic waves, even though the energy densities are too low for the process to be simple vaporization. The proposed ionization occurs as a result of the bond-breaking (possibly a piezoelectric process) that occurs during spallation which allows free charge to develop at the fracture site. It should be noted that this ionization proposal was only mentioned as a possibility and no serious investigation has been conducted to prove or disprove the likelihood of it.

Secondary ion formation

Secondary ion formation would result from reactions within the expanding plume formed during MALDI. Since the plume above the irradiation site is considered to be dense enough for multiple molecule-molecule and ion-molecule collisions, one proposed theory is that of gas-phase proton transfer. Hydrogen atoms have been found in quantities which are considered to be significant in MALDI plumes.[83] This opens the door for a proposed mechanism similar to that in fast atom bombardment:[84]

$$M + e^- \longrightarrow (M - H)^- + H \cdot \qquad 2.4$$

where the matrix captures a free electron and then produces a hydrogen radical which is available for donation to analyte or matrix. Again the theory of photo-induced increased acidicty of matrix ions could produce proton transfer reactions in the expanding plume and result in protonated matrix and analyte ions.[70] Finally, in early work with laser desorption without MALDI matrices, it was shown that cationization of molecules occurred readily in the gas phase.[85] There is no reason to assume that a similar process would not also occur in MALDI.

It must be emphasized that none of the proposed mechanisms can be assumed to be the only mechanism by which ionization occurs in MALDI, but they all may be important to a greater or lesser degree for ionization depending on experimental conditions (i.e. matrix, solvent, analyte, wavelength, irradiation intensity, etc.).

Practical Aspects of MALDI on Tissue

In traditional MALDI, the analyte and matrix are co-dissolved in a solvent and pre-mixed before being deposited on the sample probe. The solvent is then allowed to evaporate, incorporating the analyte molecule into the crystal lattice structure formed by the matrix during drying. Because MALDI experiments performed in this dissertation involved with mapping of pharmaceutical compounds present in intact tissue, the matrix and analyte could not be pre-mixed before application of the MALDI matrix and solvent. This change in the MALDI preparation procedure had a direct effect on the results and methods presented in this dissertation and should be considered. For the MALDI experiments presented in this dissertation, the MALDI matrix was dissolved in a solvent which was capable of dissolving both the matrix and the analyte. A thin slice of tissue was placed on the probe tip and allowed to air dry. It was necessary to allow the tissue to thoroughly dry before analysis in the mass spectrometer because once introduced into the vacuum of the mass spectrometer solvent from the sample would evaporate at an elevated rate. This increase in the rate of evaporation of the solvent from the sample, beneath the MALDI matrix coating, would loosen or remove the MALDI matrix from the surface of the sample. Additionally, the evaporating solvent would disturb the surface of the sample and would be a source of gas-phase neutrals which could produce unwanted ion molecule reactions. Once the tissue had dried (usually one to two hours), the solvent and matrix were

then pipetted (or electrosprayed where indicated) onto the surface of the tissue and allowed to air dry (usually within one minute). Figure 2.10 shows a representative drawing of the MALDI preparation method used for tissue samples in this dissertation. The applied solvent (with matrix) served to extract the analyte from the tissue. The extracted analyte was then incorporated into the crystal lattice formed by the matrix molecules when the solvent evaporated.[62] The implications of the differences between this method and the traditional method used in MALDI preparation on spatial resolution will be made clear in chapter 3.

MALDI of Paclitaxel in Tissue

Paclitaxel is an anticancer drug from the Taxus alkaloid family of products found in the Pacific yew tree bark.[86] Paclitaxel functions as an anti-cancer drug by stabilizing microtubules (composed of tubulin) during cell division (mitosis).[87] While the function of paclitaxel is well known, there is a great deal of interest in how paclitaxel is delivered to and how it attacks the living tumor. Clinical studies indicate that paclitaxel first binds (reversibly, with low affinity) to plasma proteins.[88] The paclitaxel is then cleared from the blood and delivered to the tissue (including the tumor). This suggests the possibility that paclitaxel may be primarily delivered to the outer layers of a hard tumor. One of the long term goals of this research was to elucidate the delivery location of paclitaxel in a human tumor.

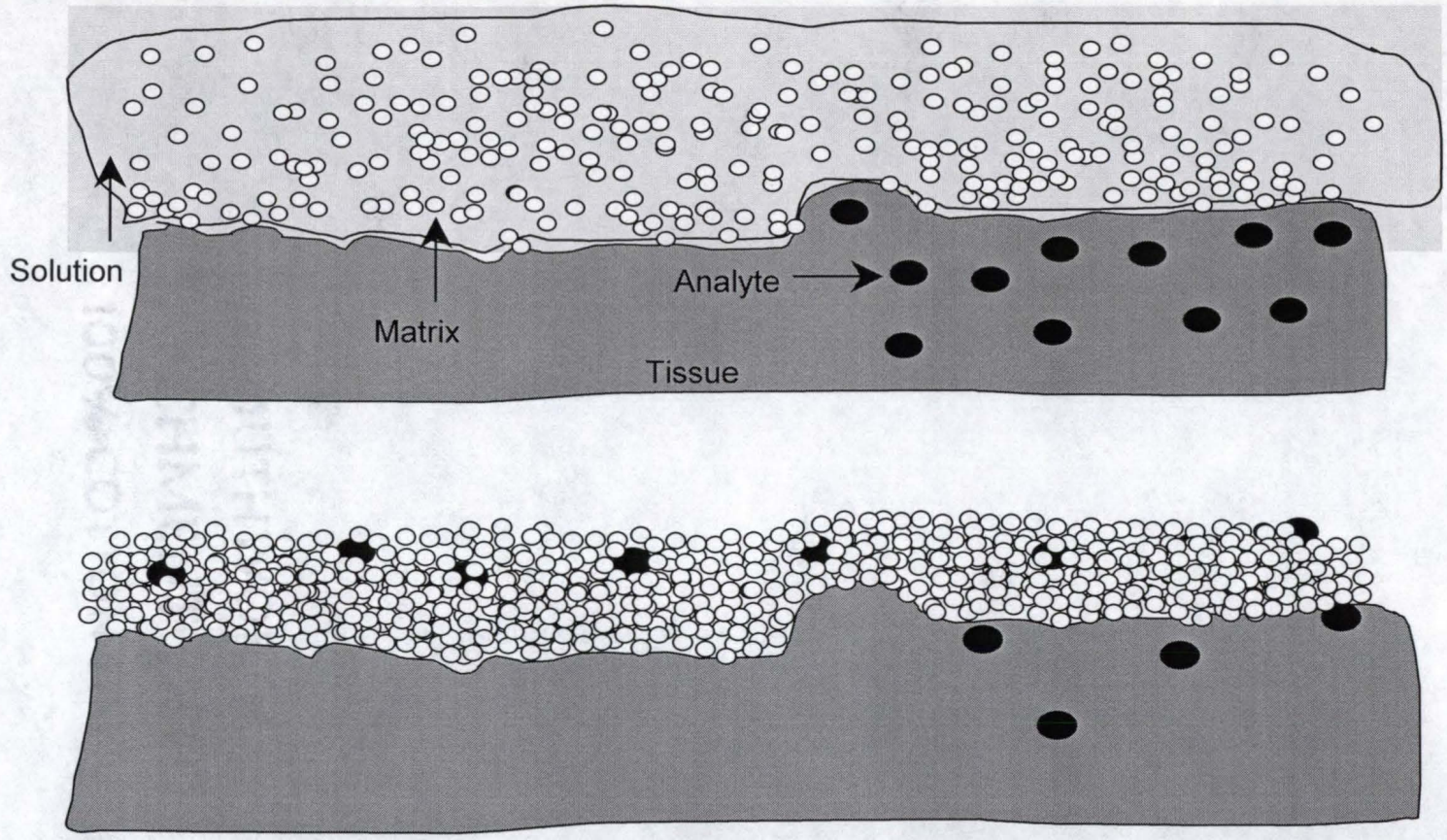

Figure 2.10. Drawing of MALDI process for tissue. Top drawing shows the MALDI matrix in solution deposited on top of tissue sample. The solvent extracts the analyte from the tissue sample into the solvent phase. Bottom drawing shows analyte incorporated into MALDI matrix after evaporation of solvent.

An ovarian tumor was obtained from Bristol-Myers Squibb Oncology Division (Princeton, NJ). The tumor was human in origin but had been implanted and grown to size (approximately 10 mm in diameter) in an immunodeficient, nude mouse. The mouse was administered a single dose of paclitaxel in a 10% cremphor, 10% ethanol, 80% saline solution intravenously. The concentration of paclitaxel in the tumor was reported by Bristol-Myers Squibb to be 10-50 ng/ mg of tumor. Approximately one hour after administration of the drug solution, the mouse was sacrificed and the tumor was excised. The tumor was then snap frozen and sent to the University of Florida packed in dry ice. The tumor was sliced thin (approximately 0.5 mm) while frozen and 5.0 μL of a 0.1 M 2,5-dihydroxy benzoic acid (DHB) in methanol solution was placed on top of the tumor section and allowed to air dry completely before analysis.

A UV laser was used for the MALDI experiments. The UV laser was a Laser Science Inc. (Cambridge, MA) model VSL-337ND pulsed nitrogen laser with a wavelength of 337.1 nm and a 3 ns pulse width (full width at half maximum). The laser is near-diffraction limited, which allowed the beam to be more easily focused to a tight spot. The maximum energy output was >250 μJ/ pulse with a peak power of 85 kW. The laser beam's intensity was adjusted between 10^6-10^7 W/cm^2 using a wheel attenuator (Newport Corp., Irvine, CA). The position of the laser beam was adjusted manually with an x,y,z-micromanipulator attached to the beam deflector (Newport Corp.).

The top panel (A) of Figure 2.11 shows the MALDI MS spectrum (an average of 30 laser shots) of the ovarian tumor after forward/reverse scan isolation of a 50-dalton-wide window around the $[M+H]^+$ ion of paclitaxel (m/z 854). Because of the wide window used (to maximize sensitivity) both the $[M+H]^+$ ion (m/z 854) and the $[M+Na]^+$ (m/z 876) can be seen. The $[M+Na]^+$ ion was chosen for fragmentation because it typically represented the most abundant paclitaxel ion (although the $[M+H]^+$ is the most abundant ion in panel (A), this was not typical for other locations on the tissue sample). The laser beam was moved to a new location on the sample and a daughter ion spectra of the $[M+Na]^+$ ions from another 30 laser shots were acquired and averaged. The center panel (B) of Figure 2.11 shows the MS/MS daughter ion spectrum of the $[M+Na]^+$ ion of paclitaxel from the tumor; this spectrum was reproducible and so could be used for the detection of paclitaxel in tissue. The daughter ion spectrum of the paclitaxel $[M+Na]^+$ ion from the ovarian tumor shows an almost identical pattern to that of the daughter ion spectrum of the $[M+Na]^+$ ion of a paclitaxel standard, as shown in panel (C) of Figure 2.11 and in Figure 2.12. In both cases the $[M+Na]^+$ ion intensity was reduced in the daughter ion spectrum because it was selectively fragmented by CAD. Figure 2.13 shows the structure of paclitaxel and the proposed fragmentation pathways of the daughter ions observed in Figure 2.12. Visual inspection of the tumor after analysis showed that the laser had burned completely through the tissue (a depth of 0.5 mm). The holes blasted in the tissue were measured to be

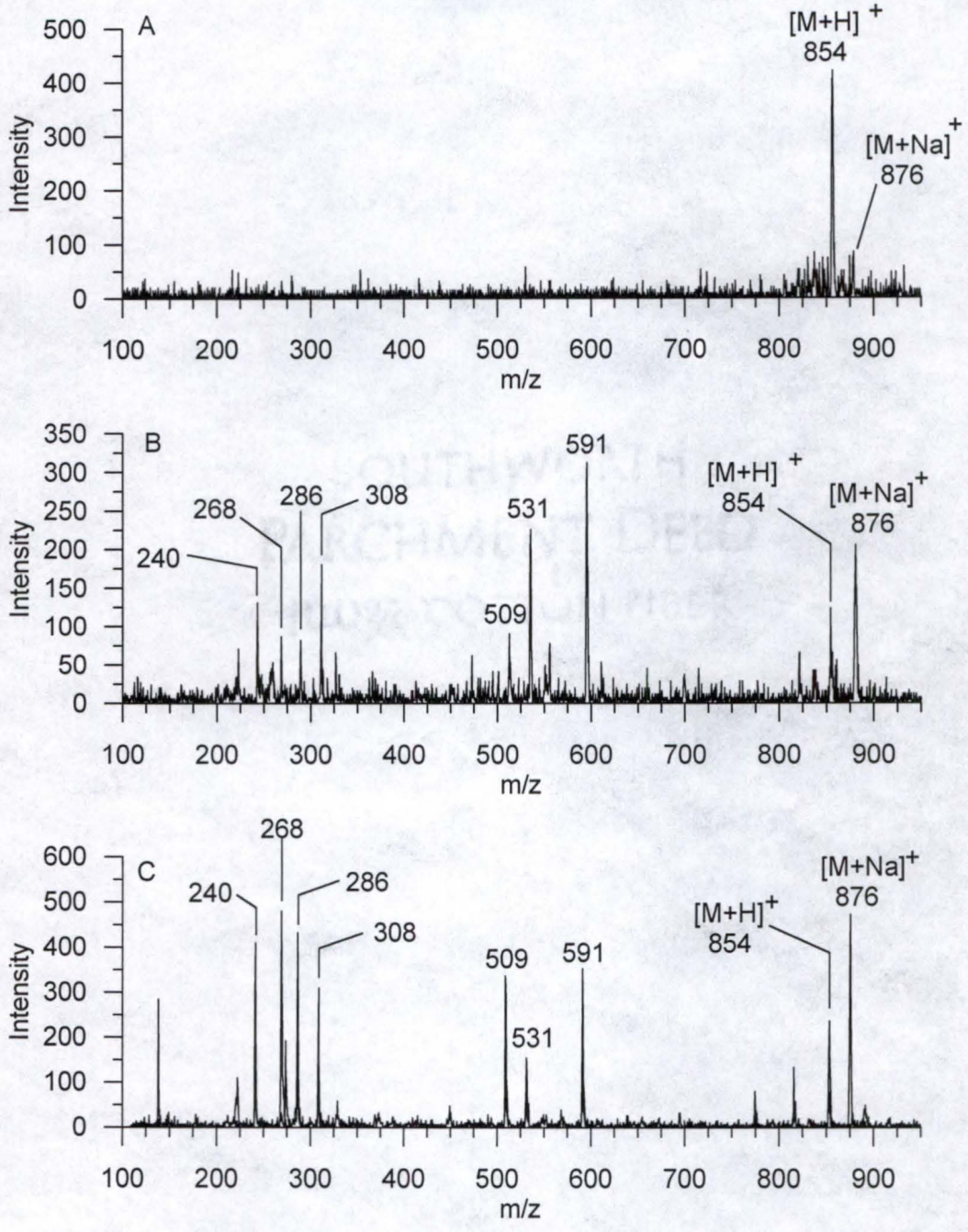

Figure 2.11. Spectrum A shows the MALDI spectum for paclitaxel in an ovarian cancer tumor after isolation of the region around the $[M+H]^+$ ion at m/z 854. Spectrum B is the daughter ion spectrum of the $[M+Na]^+$ ion from a different location on the same sample. Spectrum C is the daughter ion spectrum of the $[M+Na]^+$ of a paclitaxel standard.[62]

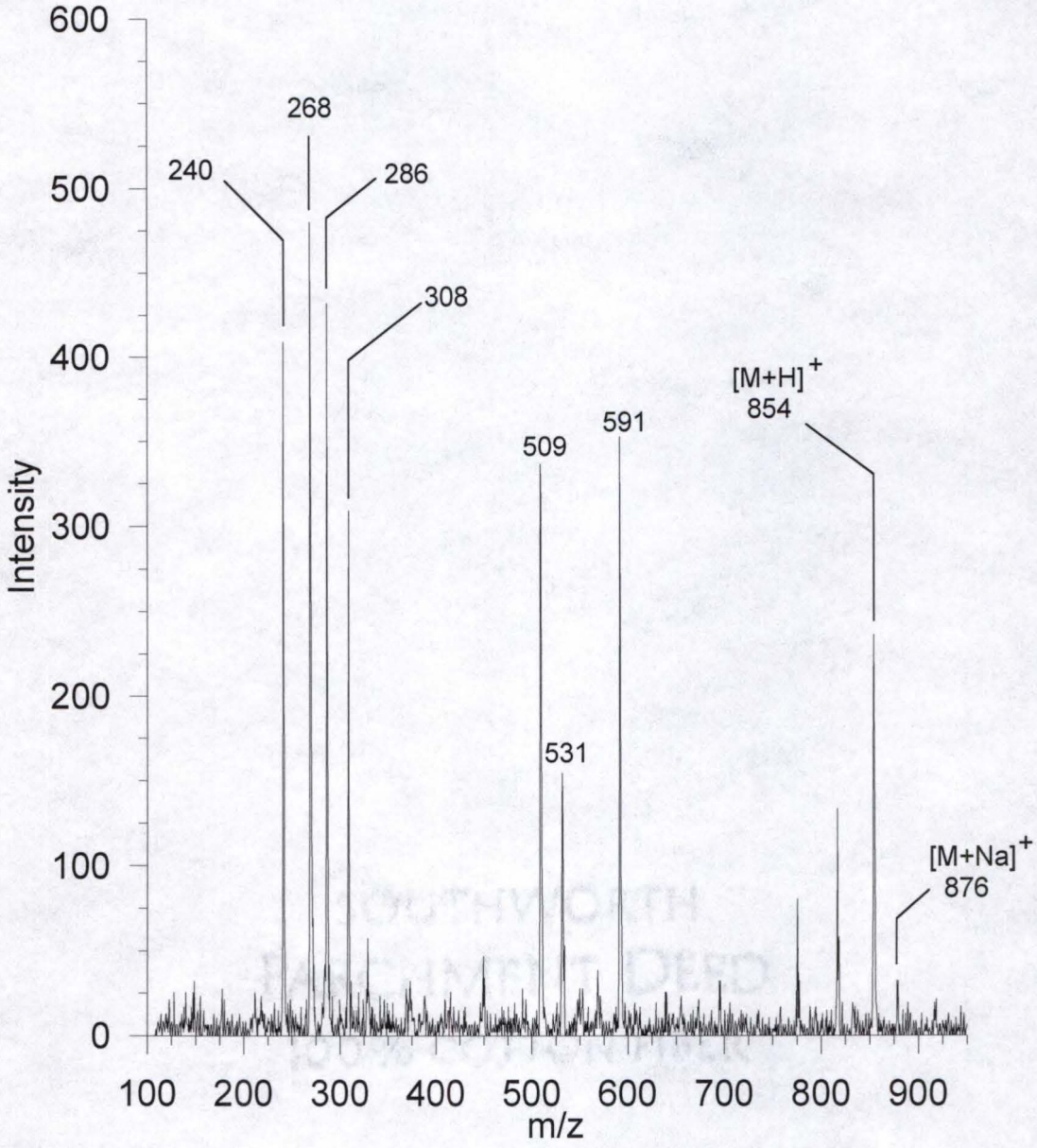

Figure 2.12. Daughter ion spectrum of $[M+Na]^+$ standard of paclitaxel by MALDI.[62]

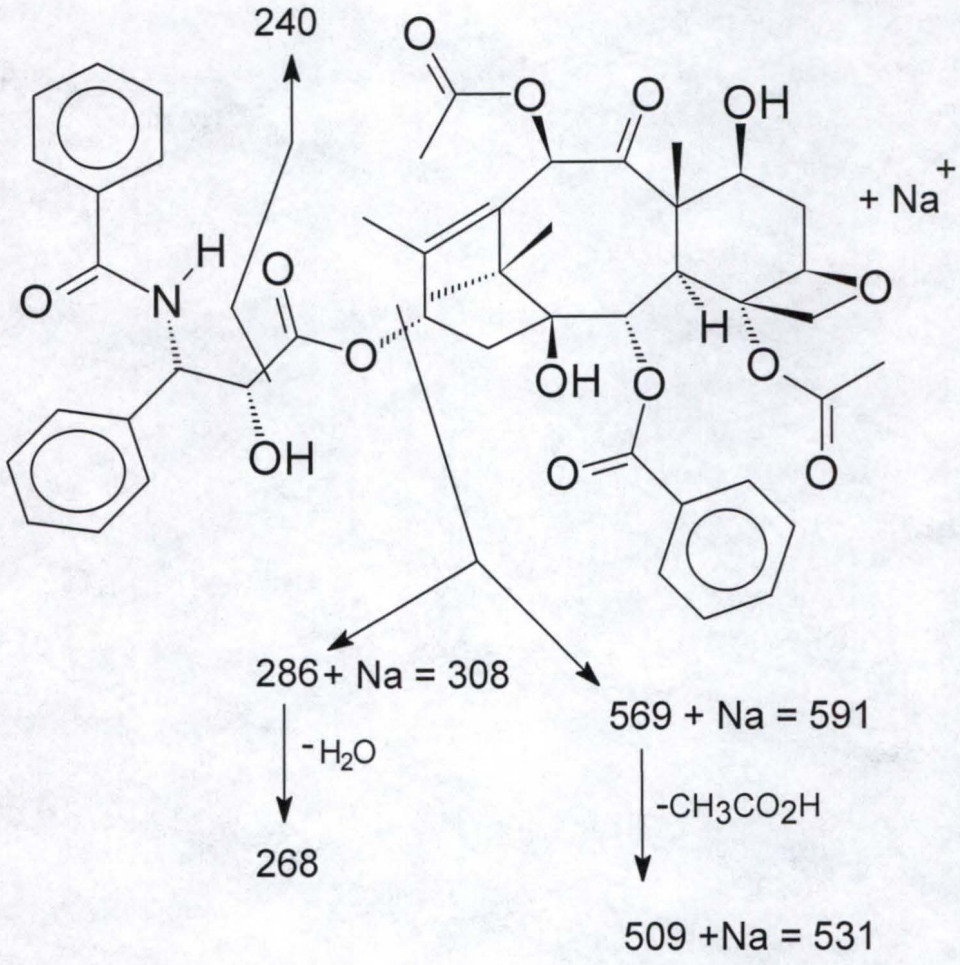

Figure 2.13. Proposed fragmentation pathways of paclitaxel that lead to observed daughter ion spectrum seen in Figure 2.12.

approximately 100 μm in diameter; thus the ablated tissue was estimated to be approximately 0.09% of the total tissue mass on the probe (6.5 mg). Based on the reported amount of paclitaxel in the tissue (50 ng/mg), the spectra in Figure 2.11 (A) and (B) each represent approximately 290 pg of paclitaxel ablated. The detection of paclitaxel at physiological trace levels satisfied the first goal for the ion trap laser microprobe instrument; however, the second goal, the identification of the location of paclitaxel within the tissue mass, was not achieved. The thick (DHB) crystal matrix coating on top of the tissue slice, coupled with the inability to visually inspect the tissue during analysis, prevented any correlation of acquired spectra with a specific region of the tissue.

CHAPTER 3
LASER DESORPTION / CHEMICAL IONIZATION

The results of the initial experiments performed on the instrument, demonstrated the ability of the instrument for the detection of pharmaceutical compounds at trace levels in intact tissue; however, the ability to map the location of the compounds was not accomplished. The application of the MALDI matrix onto the surface of the tissue during sample preparation obscured visualization (after solvent evaporation and crystal formation) of the tissue surface below. Additionally, experiments performed in our lab, as well as experiments in other labs, indicated that the spatial location of a compound extracted from a surface into the solvent and matrix mixture during MALDI preparation allowed the analyte to migrate before crystallization of the matrix.[37,62,89] The primary cause of the migration of the analyte has been given as convection currents induced in the solvent during the crystallization process.[37] The theory is that the growth of the crystals in the solvent creates currents. The currents caused by crystal formation, as well as currents due to evaporative cooling of the solvent surface, move the analyte and blur the spatial location after crystallization is complete.

Because of the need for an accurate representation of the pharmaceutical compound's spatial location within the intact tissue mass

under investigation, two alternative methods to the simple pipetting of the MALDI matrix onto the surface of the tissue were investigated. The first of these alternative methods was laser desorption coupled to chemical ionization (LD/CI), which is described in this chapter. The second method was the electrospraying of the MALDI matrix solution onto the surface of the tissue, which is described in chapter 4.

LD/CI

In Chapter 2, the theory behind MALDI was separated into two parts: desorption and ionization. The two events were treated as separate but inter-linked events. In LD/CI the process of desorption is truly separated from the process of ionization. Each will be treated separately in this chapter.

Laser Desorption

Much of the early work with laser desorption mass spectrometry was done on inorganic samples (looking for elemental information), where fragmentation was not an issue.[90] In 1968, Vastola and Pirone used a pulsed ruby laser to desorb and ionize polycyclic aromatic hydrocarbons (PAHs), alkyl compounds, and the amino acid leucine.[91] The amino acid was extensively fragmented by the desorption and ionization process, while the PAHs showed good results by forming radical molecular ions, $M^{+\cdot}$. Two years later, the same group showed the laser desorption/ionization of the alkali salts of 1-hexyl

sulfonate.[92] This time the major ions produced from a series of four different alkali salts was the alkali-cation form of the molecular ion, $[M+cation]^+$. Almost ten years after the original work of Vastola and Pirone, Posthumus et al. presented the laser desorption/ionization mass analysis of digitonin (a large thermally labile, non-volatile, organic molecule) which was detected as the $[M+Na]^+$ ion.[93] It is this work by Posthumus et al. which has been credited with creating interest in the laser desorption/ionization of organic compounds.[90] Since that time, all manner of lasers and mass analyzers have been put together to do laser desorption/ionization mass spectrometry.

The desorption of large, thermally labile organic compounds by laser desorption can be broken into three different types of processes (as with MALDI, the contribution of these processes is dependent on experimental conditions). For low power density conditions ($\leq 1x10^8$ W/cm^2), where the substrate beneath the sample has a higher absorbance than the sample, a simple thermal process is assumed to dominate.[94] Thermal desorption of thermally labile compounds without extensive fragmentation would seem to be contradictory; however, it is the rate at which the sample is heated and the high temperatures attained by the laser beam irradiance which allows this process to produce intact molecular-type ions. Figure 3.1 shows an Arrhenius plot of the temperature-dependent nature of vaporization and decomposition of thermally labile compounds.[95] For a compound to be non-volatile and thermally labile, the activation energy for desorption would have to be higher

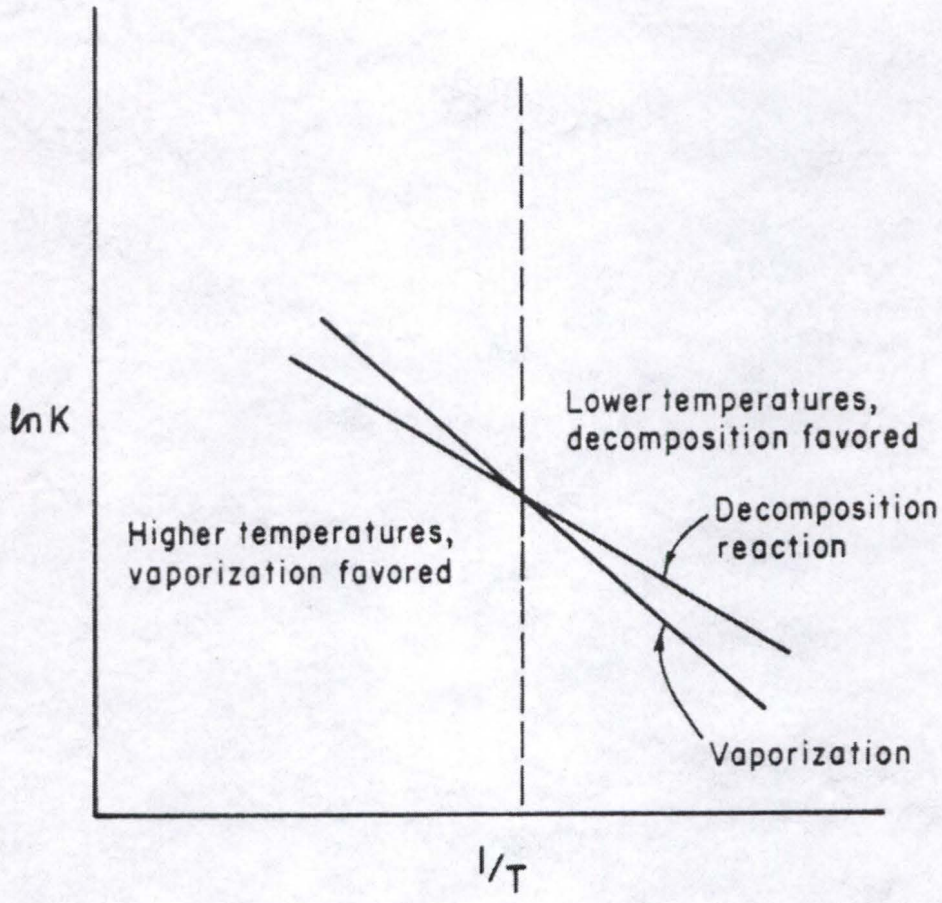

Figure 3.1. The relationship between the temperature-dependent nature of vaporization and decomposition. The two processes are represented by Arrhenius plots of the rates of vaporization and decomposition. At a sufficiently high temperature (the left side of the plot) the rate of vaporization proceeds faster than decomposition. Laser heating produces extremely high temperatures at a rate fast enough to move the sample to the left side of the plot (where vaporization is preferred) before extensive fragmentation can occur. The desorbed compounds are then cooled by expansion into the gas phase.[95]

than the activation energy for decomposition. However, If the temperature is raised high enough, fast enough, the rate of vaporization can exceed the rate of decomposition and the compound can be evaporated into the gas phase without decomposition. The vaporized material is then cooled during expansion into the gas phase in much the same way that the matrix molecules and analyte were cooled by expansion for MALDI. The major form of ions formed during thermal desorption of organic compounds has been seen to be the $[M+Cation]^+$ form.[96] It has been proposed that this form of ion is produced by the thermal emission of alkali-metal ions from the hot center of the laser beam spot (which interacts mainly with the substrate beneath the sample). The alkali-metal ions then combine in the gas phase with thermally emitted neutral organic molecules produced mainly from the cooler outer edges of the laser spot on the sample.[97]

When the laser power is increased (>1 $x10^9$ W/cm^2) and the sample is thick (which reduces the influence of the substrate beneath the sample) a different desorption process has been observed, one which has been called pressure-wave-driven desorption.[98] The proposed mechanism is similar to that which was previously covered in the MALDI section of the last chapter of this dissertation. Basically, the rapid rise in temperature of the substance under investigation produces an explosive decomposition of material, which in turn produces a compression wave that is driven through the material. At the surface, this pressure wave causes the ejection of particles (including intact

molecular-type ions) into the gas phase. The experimental evidence for this proposed theory came in a series of experiments where thin layers of carbolfuchsin were electrosprayed onto a thin gold film (5 μm thick).[98] The laser (a frequency-quadrupled Nd:YAG, 266 nm wavelength) impinged upon the film from the backside (the side opposite that where the sample was deposited). When the power density was high (~ $x10^9$ W/cm^2) and the film and sample layers were perforated by the laser beam, numerous fragment ions of carbolfuchsin were observed along with ions from the gold foil. However, when the foil was not perforated(power density ~ $x10^8$ W/cm^2) , the primary ion desorbed was the $[M+H]^+$ ion of carbolfuchsin and there was no fragmentation. This was taken to be indicative of a pressure-wave-driven desorption mechanism.

The third type of desorption process seen in laser desorption is the MALDI process, where the absorbance of the laser light by the substance plays a major role in the desorption process. As in MALDI, this process is a collective process where thermal desorption and many other process play a part, depending on experimental conditions. The original research by Karas et al. demonstrated the importance of the laser wavelength in laser desorption/ionization. Since this subject was already covered in chapter two, it will not be duplicated here.

Chemical Ionization

It was noticed early on that during laser desorption the ionization process appeared to happen primarily during the time when the laser beam interacted with the substance, but that neutral molecules continued to be desorbed from the surface for some time after the laser irradiation ceased. During the first organic application of laser desorption/ionization by Vastola and Pirone, it was noticed that ions were emitted for a 200-400 μs period, which seemed to correspond to the peak of the laser pulse (800 μs).[91] Neutral molecules (ionized by an electron beam) were observed to be produced for several hundred microseconds after the end of the laser pulse. Van Breeman, Snow, and Cotter in 1983 showed that a 40 ns laser pulse (a CO_2 laser was used) produced neutral molecules for 4-10 ms after the laser pulse ended (Figure 3.2).[99] The investigators demonstrated that under high pressure source conditions (a CI reagent gas of isobutane was maintained at a pressure of 0.5 torr in the source region), the time over which ions left the source was extended from 1 μs to 4-10 ms. This extension in time allowed for better mass analysis by a scanning magnetic sector instrument since an extended time period is required for the analyzer to scan the mass range. This experiment also showed that chemical ionization could be used to increase the number of analyte ions produced by the desorption event which could be used to lower the limit-of-detection of the method. Figure 3.3 shows the results of laser desorption of tetramethylammonium chloride during the first 500 μs

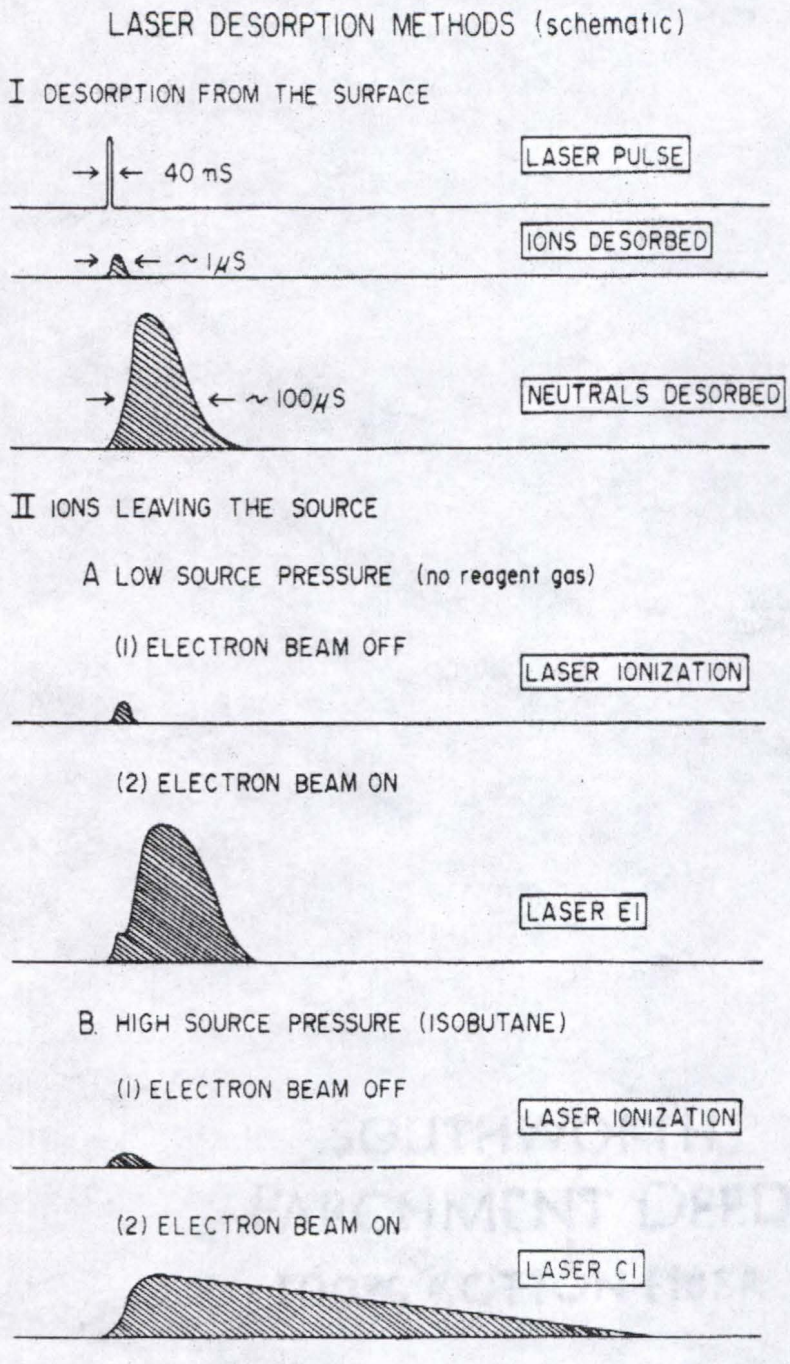

Figure 3.2. A schematic representation of the ions and neutrals produced by a 40 ns CO_2 laser pulse. The diagram shows the detected ion as a function of time under different conditions. A scanning magnetic sector instrument was used to produce the results.[99]

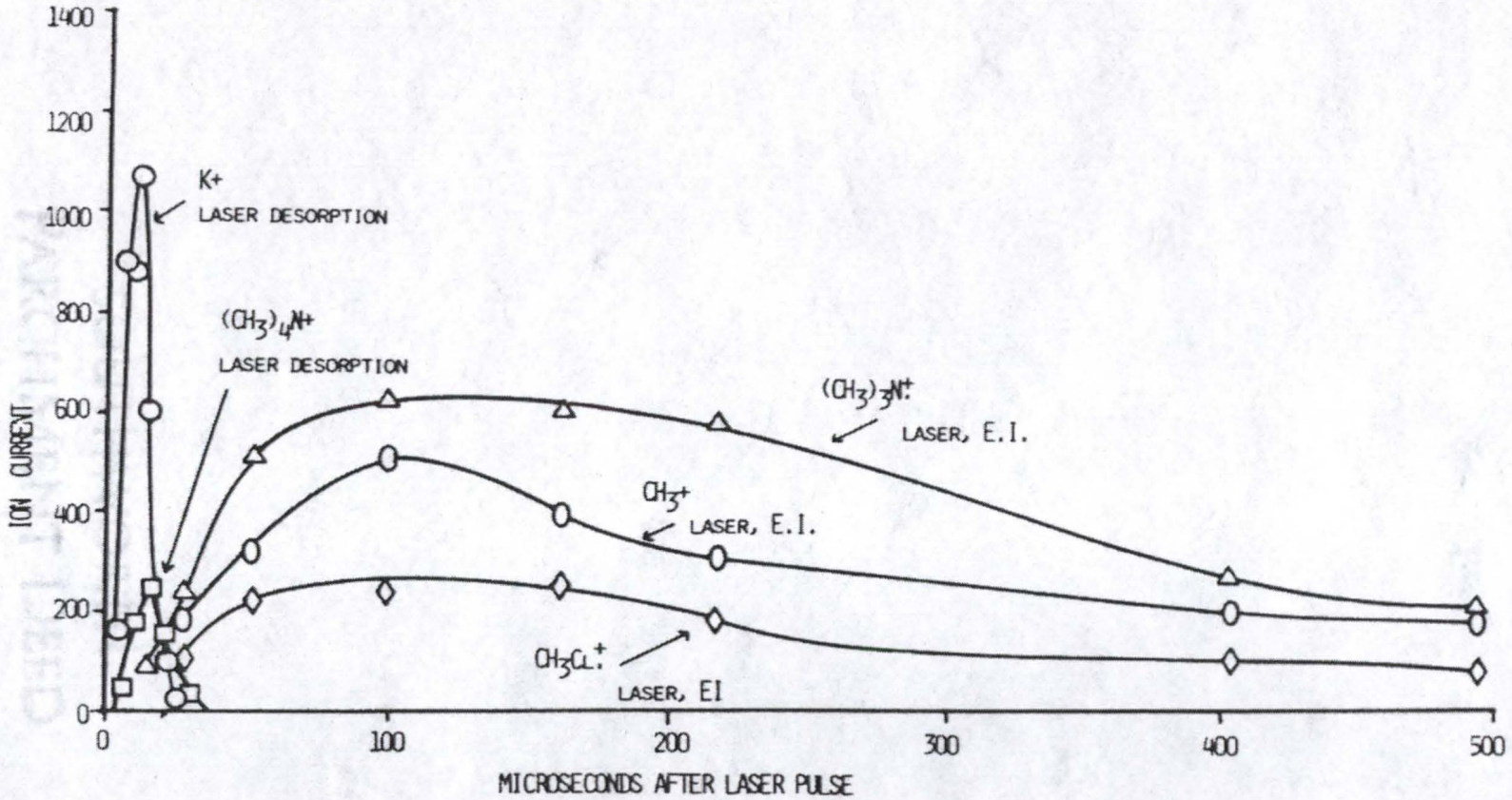

Figure 3.3. The intensity of ions detected during the first 500 μs after laser pulse in the desorption of tetramethylammonium chloride.[99]

following a CO_2 laser pulse.[99] A TOF mass analyzer was used for these experiments and the ions were extracted from the ion source at different times by means of a drawout pulse which was delayed for a variable period after the laser pulse event. An electron beam was used to ionize the neutrals desorbed after the laser pulse. The interesting thing about Figure 3.3 is the intensity of the ions produced. The intensity of the ions produced by the electron beam ionization of neutral molecules desorbed after the laser pulse is approximately three times that of the laser ionization alone. In our own lab, Robert Perchalski studied the use of chemical ionization for extending the ion production lifetime of several compounds sampled by laser desorption.[100] He concluded that there were two processes underlying the extended lifetime of ion production noted in LD/CI. The first processes was the chemical ionization of laser produced molecules, simple LD/CI. The second process was the vaporization of the analyte from the sample surface by the action of the reagent gas (termed desorption chemical ionization-DCI). Even when the reagent gas entering the source was blocked from direct interaction with the sample, the process of DCI could be initiated by the input of thermal energy in the form of the laser beam. The DCI process was dependent on the ion source temperature, and the signal lifetime was dependent on the melting point of the compound and the size of the sample.

Because we were interested in mapping the location of trace level pharmaceutical compounds in intact tissue, it was decided to try chemical

ionization in conjunction with laser desorption. Laser desorption of the intact tissue meant that no matrix needed to be added to the tissue surface (which was the cause of analyte migration). Chemical ionization was used so that desorbed neutral molecules would be ionized for a lower limit-of-detection.

Chemical ionization is a general term used to describe the ionization of molecules by ion-molecule reactions in the gas phase. Harrison offers a comprehensive review of chemical ionization mass spectrometry; those wishing a more detailed description of the process are refereed to his book.[101] The basic concept of chemical ionization is as follows: a reagent gas is introduced into the ion source at sufficient pressure (generally between 0.5 and 1 torr) to assure that an adequate number of collisions result between reagent ions (produced by electron ionization) and the neutral reagent gas molecules. Since the reagent gas partial pressure in the source is in large excess of that of the analyte (usually 1,000 to 10,000 times greater) the reagent gas preferentially undergoes electron ionization. Once ionized, reagent gas ions react with the large number of reagent gas neutrals present to form a steady state of reagent ions (for methane the major reagent ions are CH_5^+ and $C_2H_5^+$). If a collision between one of the reagent ions and an analyte neutral occurs, and the gas-phase proton affinity (PA) of the analyte is greater than the proton affinity (PA) of the conjugate base of the reagent ion, then a proton exchange reaction can occur to from an $[M+H]^+$ ion of the analyte:

$$[X+H]^+ + M \rightarrow [M+H]^+ + X \qquad 3.1$$

where $[X+H]^+$ is the reagent ion, X is the conjugate base of the reagent ion, and M is the analyte molecule. The difference in gas-phase proton affinity of M and X determines the amount of energy deposited into M by the proton transfer process. By selection of the proper reagent gas (to form ions whose conjugate base PA is close to the PA of the analyte), the primary ion produced by the CI reaction is the $[M+H]^+$ ion and the number of fragment ions can be reduced. In MS/MS, the molecular-type ion is preferred because it is more structurally characteristic of the intact analyte. Furthermore, selecting an ionization method which produces only molecular-type ions, with no fragmentation, concentrates the ion current in a single ion. This production of a single-type ion reduces the limit-of-detection for MS/MS.

LD/CI of Spiperone in Intact Tissue

To demonstrate the ability of LD/CI to detect pharmaceutical compounds in intact tissue, a laser of sufficient power to desorb intact tissue was needed. The laser used in the previous MALDI experiments (a VSL-337ND pulsed nitrogen laser from Laser Science Inc., Cambridge, MA) had a maximum energy output of approximately 250 μJ per pulse with a 3 ns pulse length. This gave a power output of approximately 83 kW per pulse. Focussed down to a spot size of 100 μm diameter, the power density on the tissue was 1×10^9 W/cm^2 which is considered to be sufficient to produce vaporization of some material.[90] However, since the sample was thick

(approximately 0.5 mm) interaction of the laser beam with the substrate (the probe tip beneath the tissue) was not significant. This meant that the tissue itself needed to have sufficient absorbance to produce desorption. The absorbance of the tissue at 337 nm was not sufficient to desorb enough analyte neutrals or ions from the surface of the tissue for detection. As was pointed out earlier, in laser desorption/ionization where thick samples are used a power density of greater than 1 $x10^9$ W/cm^2 is generally used. While the power density for the desorption of neutrals is considered to be lower than that of laser desorption/ionization, the inability of the UV laser to produce sufficient neutrals made it necessary to find a laser which would produce a consistent desorption process. For that reason, a Lumonics (Ontario, Canada) series TE-860-4 excimer CO_2 IR laser with a wavelength of 10.6 μm and a maximum energy output of 6 J per pulse (here typically 2.6 J per pulse) and a pulse duration of 2 ns to 1.5 μs was used for the initial LD/CI experiments. The beam size of the CO_2 laser was reduced by physically blocking it from a 25 x 13 mm rectangular spot down to a round spot with a diameter of 4 mm before focusing. The physical blocking reduced the energy per pulse used in these experiments to approximately 115 mJ (assuming an even energy distribution across the beam and simple reduction in beam size). It was necessary to reduce the energy per pulse from the CO_2 laser because early experiments indicated that so much tissue was ablated at full laser power that the inside of the ion volume was coated by the ablated material after a single laser pulse.

The coating of the inside of the ion volume allowed it to become electrically charged (by the electron beam used in CI), dramatically reducing ion transmission after a single laser shot. The spot size after focusing had a diameter of 750 μm, making the power density approximately 3×10^7 W/cm^2. Although this power density was less than that of the UV laser, the CO_2 laser produced consistent desorption of the tissue samples.

The laser was focused into the mass spectrometer chamber by a single zinc-selenide focusing lens (Melles-Griot, Irvine, CA) with a focal length of 25.4 cm. The laser was externally triggered after a 1 ms delay by a custom built electronic circuit. The delay of the laser trigger was necessary to assure that the ion gate (the electrostatic lens in the ion source just before the turning quad) had sufficient time to switch from +170 V to –25V (the typical voltage applied to the lens during ion transmission. The software (Gatorware) used to control the scan and acquisition of the ITS-40 was written by Tim Griffin and Nathan Yates at the University of Florida.[102,103] Methane gas was introduced into the ion source of the instrument for chemical ionization. The pressure reading (uncorrected) in the ion source side of the vacuum housing was 4×10^{-4} torr. A capacitance manometer, connected to the ion source by a hollow probe shaft, showed that this chamber pressure produced a CI ion source pressure of 0.5 torr. This CI source pressure was high enough to produce good chemical ionization spectra of perfluorotributylamine (PFTBA, mw = 671), a calibration compound commonly used for EI and CI in mass

spectrometers. The ionization was considered good chemical ionization when the PFTBA fragment ion at m/z 502 (a common EI fragment ion of PFTBA) was less than 10% of the PFTBA ion at m/z 652 (a common CI fragment ion of PFTBA).

For the initial LD/CI studies, the drug spiperone was chosen as the target compound. Spiperone, developed as an antipsychotic drug, belongs to a class of compounds known as azipirones which are similar to serotonin in structure and so bind to the 5-HT_{1A} receptors in the central nervous system.[104] In vivo neural recording studies of spiperone have shown that it binds not only to the 5-HT_{1A} receptors in the brain, but also to 5-HT_2 receptors.[104] Because these receptors are present at various densities throughout the brain, there is considerable interest in determining the concentration of spiperone in different cerebral regions. Spiperone was chosen as a model compound because in previous studies in our lab it had been demonstrated to be very stable over time (solutions of spiperone did not significantly degrade over more than a year) and it had been shown to be easily incubated into tissue samples.[62] Additionally, spiperone has been the subject of previous MS studies in our lab and so has been well characterized.[105,106] Figure 3.4 shows the LD/CI MS/MS daughter ion spectrum of the $[M+H]^+$ ion (at m/z 396) of a spiperone standard. After isolation (a 5-dalton-wide window by the forward/reverse scan method), the $[M+H]^+$ ion was fragmented by CAD to produce the daughter ion spectrum shown. The major daughter ions produced are at m/z 165 and 291; daughter

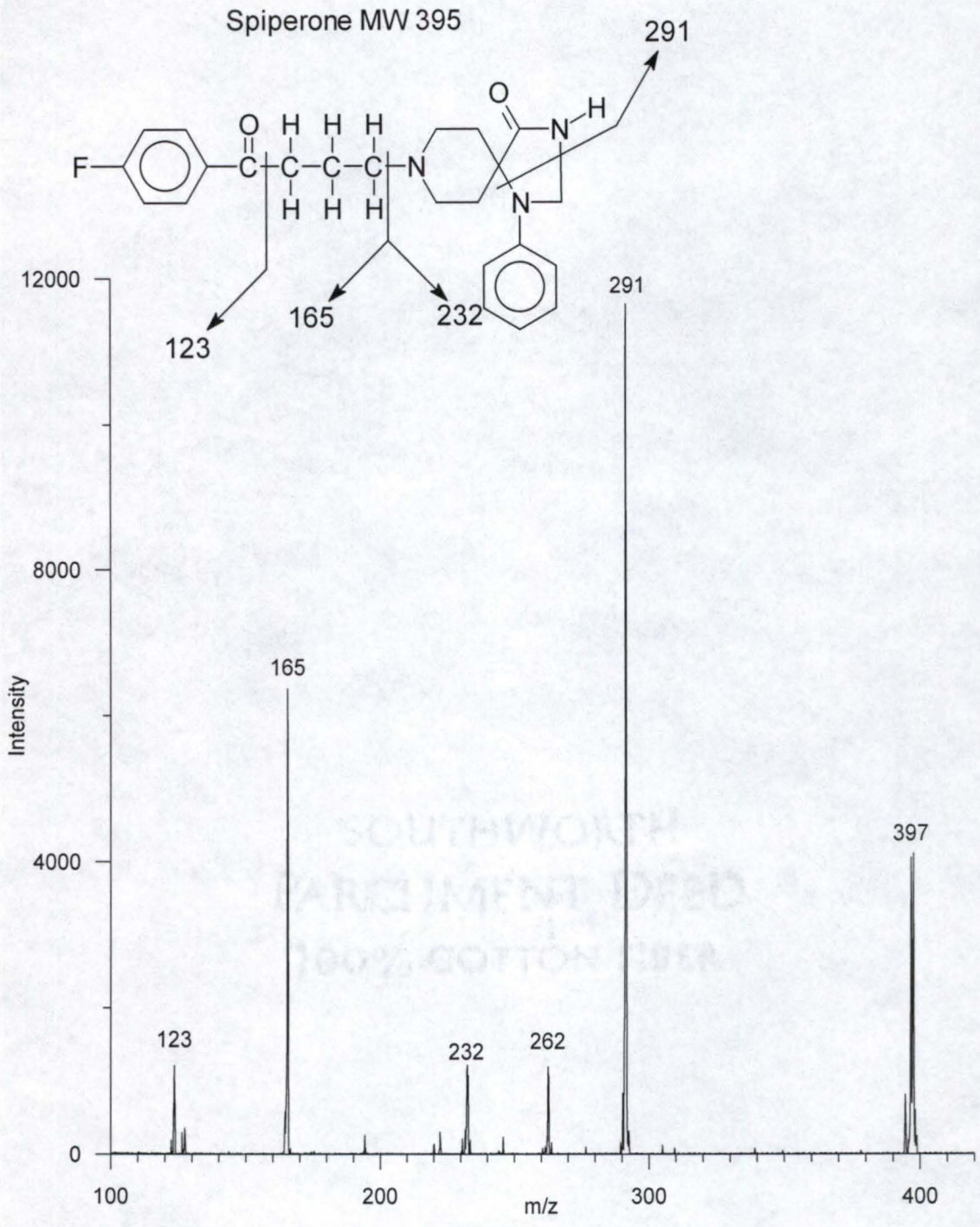

Figure 3.4. The LD/CI MS/MS spectrum of the $[M+H]^+$ ion (m/z 396) of the drug spiperone. The peak at m/z 397 is the ^{13}C isotope of the $[M+H]^+$ ion of spiperone left after resonant excitation of the m/z 396 ion.

ion peaks also appear at m/z 123, 232, and 262. The drawing above the spectrum in figure 3.4 shows the molecular structure of spiperone and the proposed fragmentation pathway which produced the observed daughter ions.

A whole liver was obtained from a male Sprague-Dawley rat after sacrifice. The liver tissue was directly transferred to storage in a -20^{0}C freezer. A 7.9 mg piece of frozen liver tissue (a slice of approximately 0.5 mm thickness) was placed in a shallow stainless steel well. 4 μL of a 100 ng/μL solution of spiperone in 1% aqueous acetic acid (HOAc) was placed on top of the tissue. The tissue was allowed to incubate for one hour and was then washed with several aliquots of 1% HOAc solution followed by several aliquots of deionized water. The liver tissue was then blotted dry, placed on the probe tip, and allowed to dry completely (approximately 1.5-2 hours) before analysis. To determine the amount of spiperone absorbed by the tissue, the 1% HOAc washings of similar liver samples incubated in spiperone were collected and analyzed by LC/MS. The same liver tissue samples (after washing) were extracted with a solvent (with sonication), and the extract was analyzed. The results of duplicate washing and extraction experiments indicated that 50% of the collected spiperone was found in the washings and 50% was found in the tissue extracts. For this reason, all concentration values for spiperone in spiked tissue in this dissertation are given as 50% of the amount of spiperone applied to the tissue. For all experiments, blank tissue samples were analyzed to assure that there was no carry-over of analyte.

Figure 3.5 shows the LD/CI spectrum (5 laser shots) of a rat liver tissue slice which was spiked to a level of approximately 25 ng/mg of tissue with spiperone. Note that the peak at m/z 396, which corresponds to the $[M+H]^+$ ion, is completely buried in the tissue matrix noise (see inset for close-up view of region around m/z 396). The ion injection time used during the acquisition of this spectrum was only 90 μs (in contrast to the 4 ms used in the other LD/CI spectra presented here) to preserve close to unit resolution. When the tissue was desorbed with an ionization time of 4 ms without the isolation of a narrow m/z range, space charging shifted and broadened the peaks, rendering the spectrum meaningless. It is obvious from Figure 3.5 that without the capability for mass isolation and MS/MS available with the quadrupole ion trap, the target drug could not be positively detected at such low levels. In fact, we found that LD/CI of tissue produced such intense interference ions that the standard forward/reverse scan isolation would not adequately isolate the m/z region of interest. The tissue matrix ions apparently continued to fragment during the forward and reverse stages of isolation (the low m/z ions are ejected during the first (forward) step of the two-step isolation), leaving ions at m/z values below the isolation region (data not shown). Switching to SWIFT isolation waveforms, which provide axial modulation at all frequencies around a notched set of frequencies selected by the operator, overcame these problems. In this way the higher and lower m/z interfering ions are ejected out of the trap at approximately the same time. If a

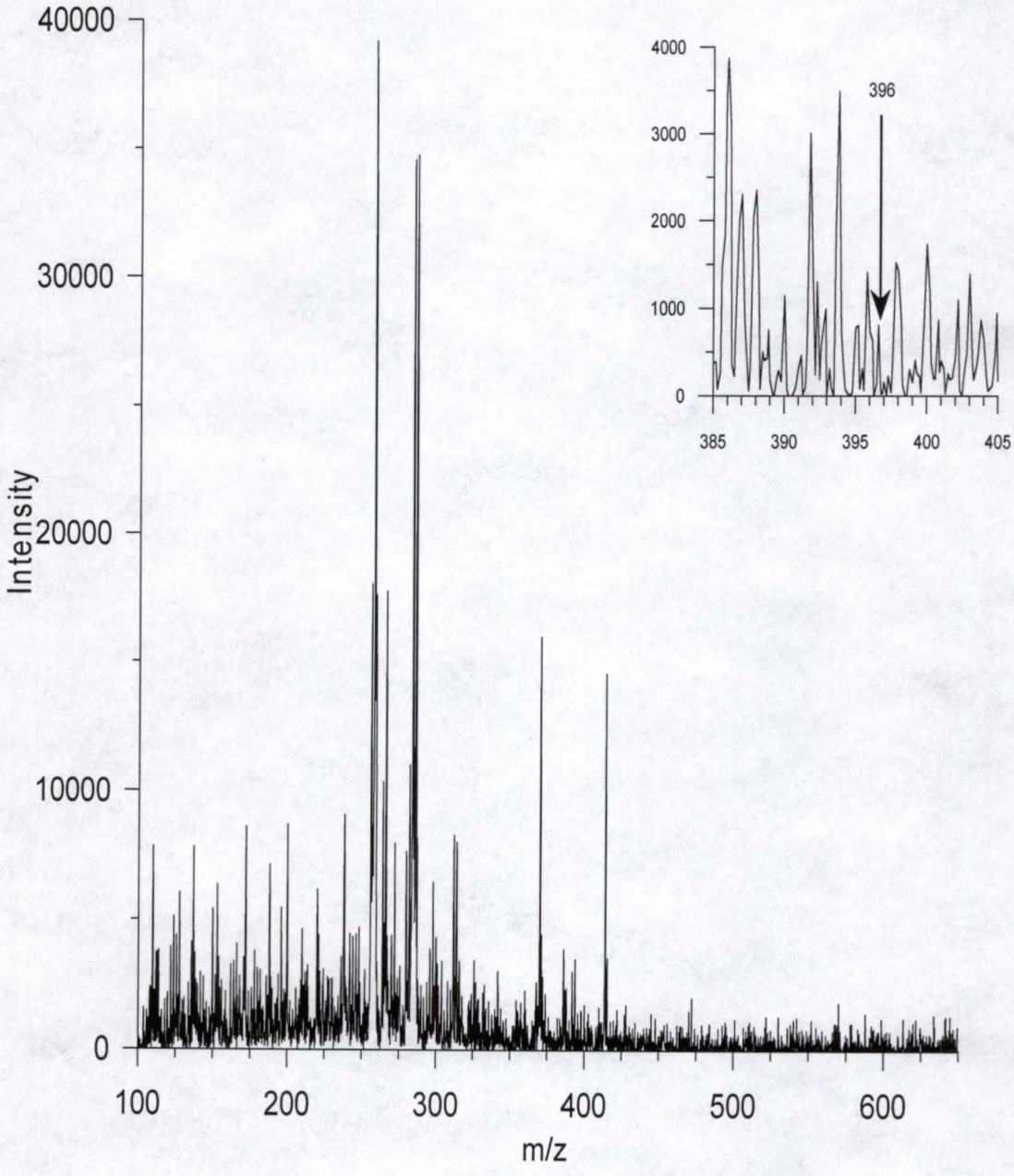

Figure 3.5. LD/CI MS spectrum of rat liver tissue spiked with the drug spiperone to a level of 25 ng/mg. The inset shows a close up of the region around the spiperone $[M+H]^+$ ion at m/z 396. The arrow indicates the peak at m/z 396 which corresponds to the $[M+H]^+$ ion of spiperone.

higher m/z interferent ion did fragment during isolation, the fragment ions produced would still be given sufficient energy to be ejected from the trap. A Stanford Research Systems (Sunnyvale, CA) model DS345 synthesized function generator was used to generate the SWIFT waveforms used for waveform isolation of ions in the ion trap during LD/CI experiments. The waveforms were created with a computer program which was written at the University of Florida by Peter Palmer which created isolation waveforms similar to those described in a paper by Chen et al.[107] Each SWIFT waveform isolation burst took approximately 8 ms (7 bursts per scan were used for a total isolation time of 56 ms), whereas the high mass ejection step of the two-step isolation technique took 50 ms. This isolation technique produced significantly better results.

Using the same tissue sample as above (with the probe tip rotated to present a new area on the tissue to the laser beam), another LD/CI mass spectrum of the spiked rat liver tissue was obtained (Figure 3.6). This time, however, a 10-dalton-wide window around m/z 396 was isolated by SWIFT waveform isolation following a 4 ms ion injection time. Once again, the peak at m/z 396, which corresponds to the $[M+H]^+$ ion of spiperone, is not the most intense peak in the isolated region of the spectrum (see inset for close-up of area). Note that the isolation of the region around the m/z of the ion of interest leaves the lower m/z region relatively empty so that daughter ions produce by CAD during MSA/MS can be easily identified.

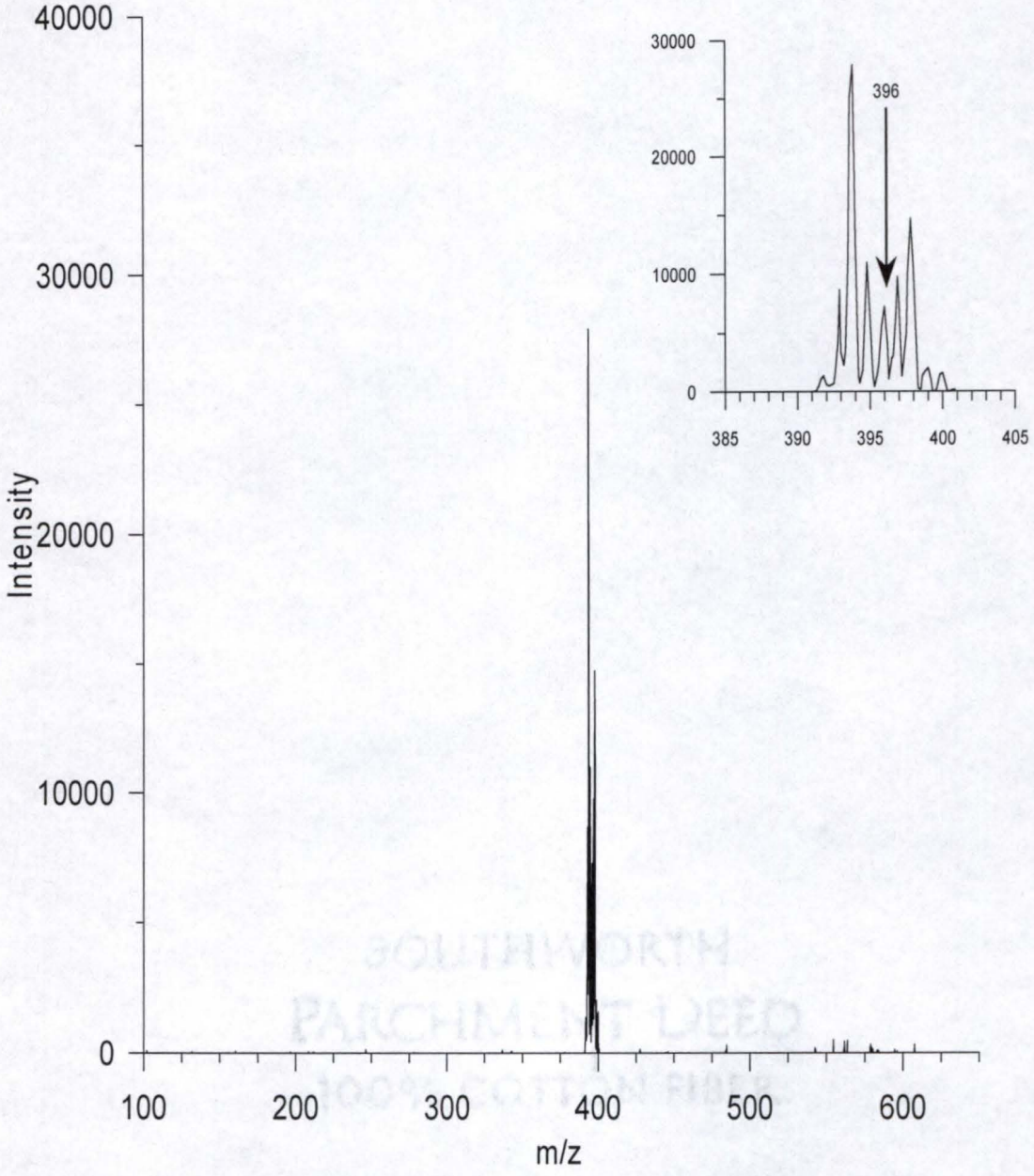

Figure 3.6. LD/CI mass spectrum of rat liver tissue spiked with the drug spiperone at a level of 25 ng/mg. A 10-dalton-wide area around the $[M+H]^+$ ion of spiperone (m/z 396) was isolated by use of the SWIFT isolation method. Inset shows a 20-dalton-wide window around m/z 396. Note that peak at m/z 396 is still not the largest peak in the isolation window.

Figure 3.7 shows the daughter ion spectrum produced by CAD from another new location on the same rat liver sample. The daughter ions produced by CAD of the ion at m/z 396 match the daughter ions produced by CAD of the neat spiperone sample under similar instrumental conditions (see Figure 3.4 for comparison). This demonstrated the ability of laser desorption coupled to chemical ionization (LD/CI) for the detection pharmaceutical compounds at trace levels in intact tissue; however, the issue of spatial resolution was still not addressed.

One of the difficulties in selecting specific points on the tissue mass for laser desorption during LD/CI was the small opening in the ion volume used for chemical ionization. Because relatively high pressures are needed during CI to ensure an adequate number of collisions between reagent ions and analyte neutrals, the ion volume used for CI has and ion exit hole of only 1mm diameter. This small opening necessitated the construction of an X,Y-stage to move the sample while inside the vacuum chamber moving the sample inside of the vacuum chamber.

The X,Y-Stage

The Finnigan 4500 ion source used on the instrument consists of a 1.25" by 1.05" stainless steel block with a 1.15" diameter by 0.6" deep hole machined into the front of the block to allow the placement of the extraction lens stack (drawing B in Figure 3.8). The lens stack used in the laser

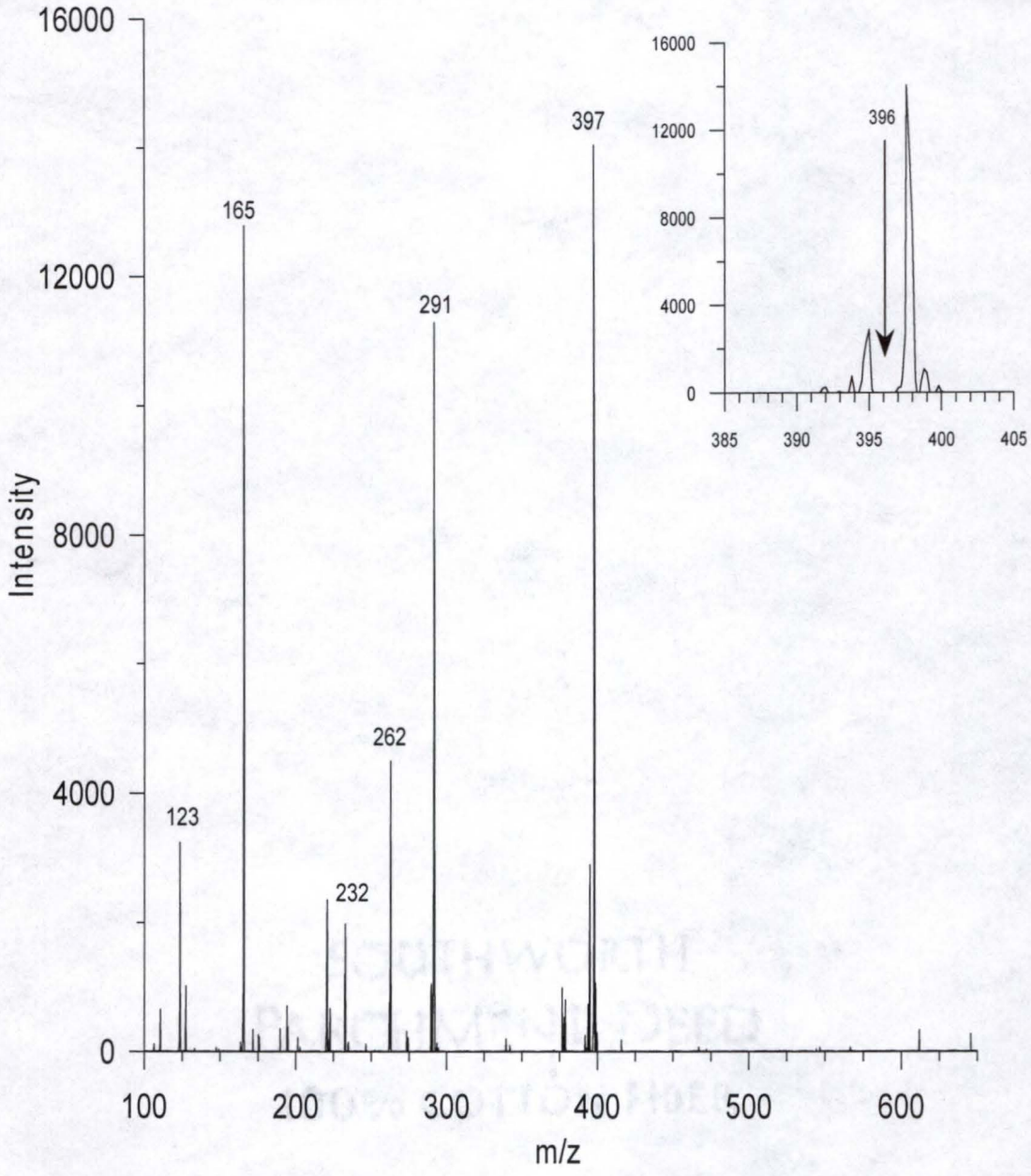

Figure 3.7. LD/CI MS/MS daughter ion spectrum of m/z 396 ion from rat liver tissue spiked with spiperone (mw=395). The daughter ions shown in spectrum match daughter ions observed from LD/CI MS/MS daughter ion spectrum of neat spiperone (Figure 3.4). Inset shows close-up of region around m/z 396. Note that only the m/z 395 and 396 ions were fragmented by CAD.

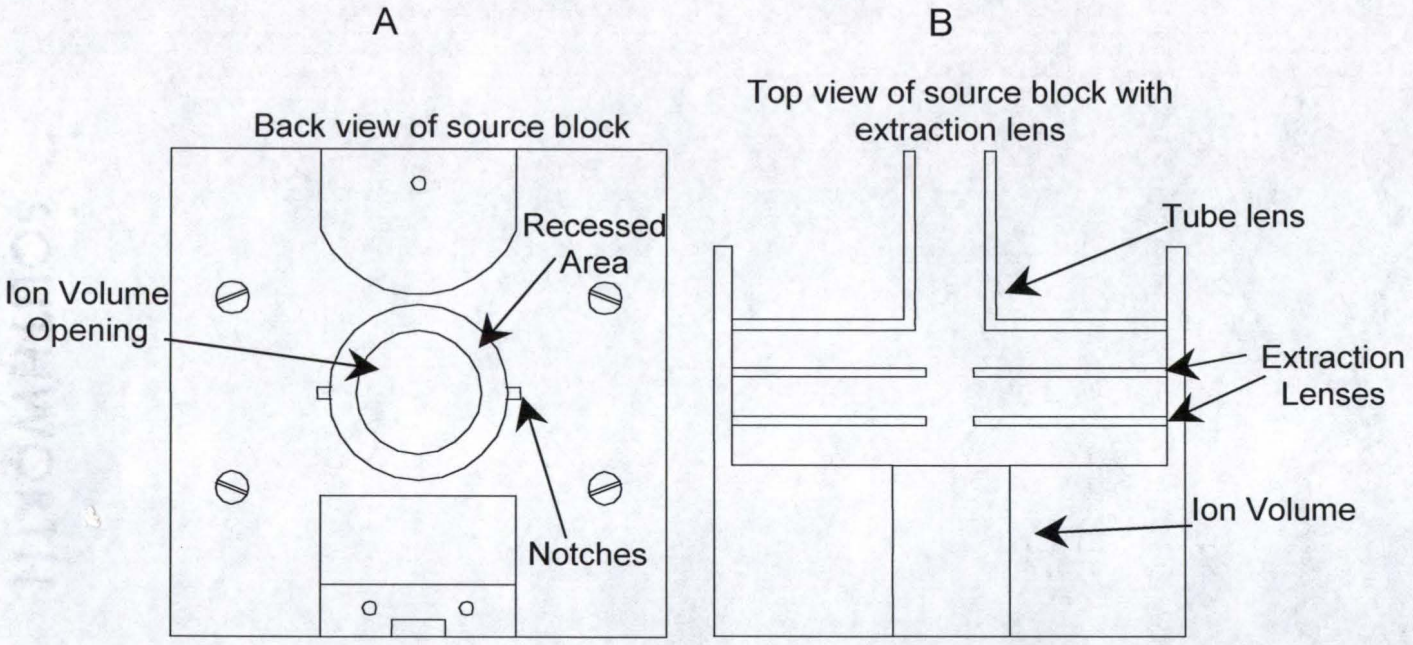

Figure 3.8. Schematic drawing of Finnigan 4500 ion source block. Drawing (A) is a view of the back of the source block showing the opening for holding the ion volume and the small notches used to orient the ion volumes. Drawing (B) shows a cut-away top view with extraction lenses included.

microprobe instrument consists of two, flat stainless steel focusing lenses and a third exit tube lens (0.270" length). The ion volumes used in the 4500 source consists of thin (0.005" thick) stainless steel sleeves which are connected to the probe tip by a metal clip (Figure 3.9). Two small (0.025") notches machined into the sides of the ion volume opening of the ion source block serve as a guide for the wire clip when the ion volume is placed in the source block (Figure 3.8 A). The electron ionization (EI) ion volume of the 4500 is 0.5" in length and extends out of the front of the ion volume opening to just before the first extraction lens. The front of the EI ion volume is open and allows the UV laser beam used in the MALDI studies to be positioned by means of an X,Y,Z-beam manipulator placed in the beam path prior to entering the vacuum chamber (Figure 2.2). Because the CI ion volume has only a 1mm opening (Figure 3.9), the option of manipulating the laser beam prior to entering the vacuum chamber was not available. This led to the decision to manipulate the position of the probe tip itself as a means of moving selected areas on the tissue sample to a position where the incoming laser beam (through the 1 mm opening in the CI volume) would strike a selected spot on the tissue sample. To accomplish this, an X,Y- stage was constructed which would manipulate the sample probe.

The X,Y-stage consisted of a base plate, an X-stage, and a Y-stage (Figure 3.10). The base plate (the first level) of the X,Y-micro-manipulation stage was constructed from a 0.25" thick stainless steel plate machined into a

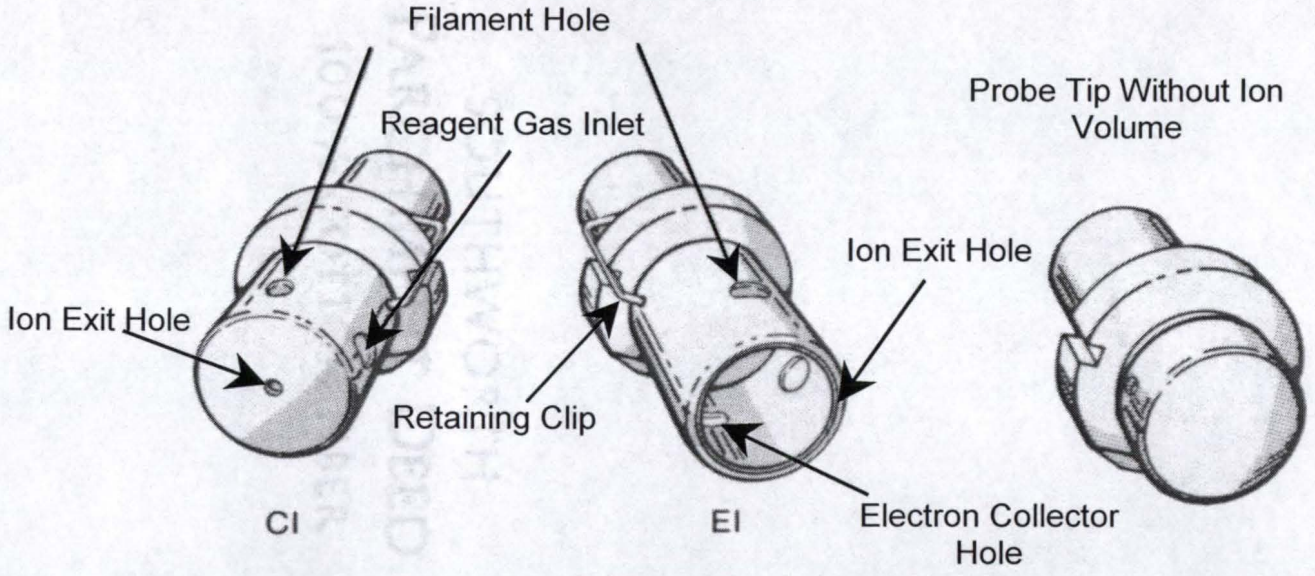

Figure 3.9. Finnigan 4500 probe tips with typical EI and CI ion volumes attached. Note the retaining clip which attaches the probe tip to the ion volume. Probe tip on right shows the tip without the ion volume attached.[108]

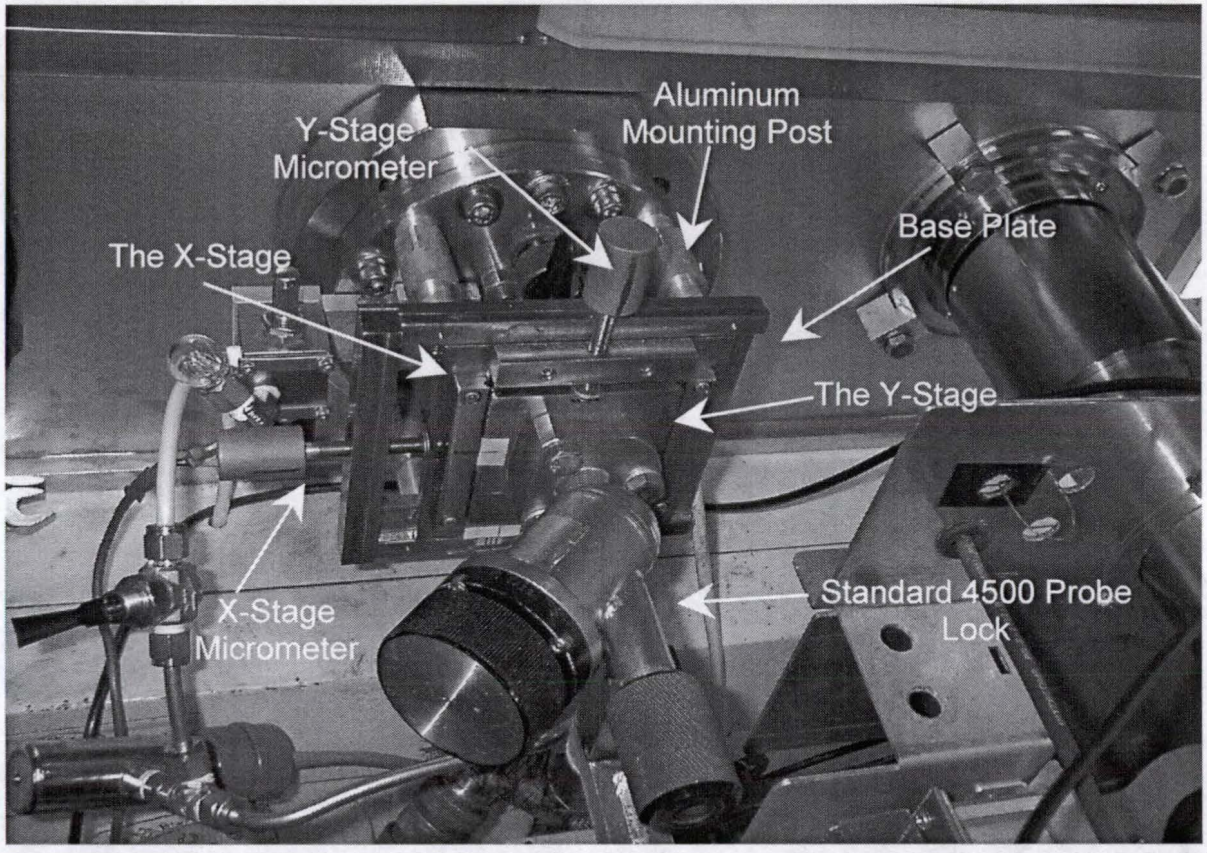

Figure 3.10. Picture of the finished X,Y-micro-manipulation stage mounted to the instrument. The micrometer attached to the X-stage was able to manipulate the probe lock in the X-direction (left and right) while the micrometer attached to the Y-stage was able to manipulate the probe lock in the Y-direction (up and down).

5.55" by 5.05" rectangle (Figure 3.11). The inside area of the plate was machined away leaving a 1.0" bridge-piece across the top and bottom portion of the square and a 0.5" wide bridge-piece along either side. Holes were drilled and tapped at locations on the plate to serve as bolt holes to attach an upper and lower V-groove rail which served as a ball bearing guide along which the X-stage would slide (see Figure 3.12). A 0.5" by 5.05" stainless steel block was machined for a micrometer holder and a hole was drilled through the center of the block. The hole was tapped (80 threads per inch) to accommodate a 0.25" diameter micrometer which was machined out of a 1.0" round by 5.0" piece of stainless steel. The micrometer was machined smooth (the threads were removed) along a 0.35" section at one end with the final diameter of that section being 0.185". A 2.0" section at the other end of the micrometer was left 1.0" round and served as a handle to turn the micrometer. The 0.35" smooth section had a 0.0355" thick groove cut into it 0.15" from the end. This groove served as an attachment place for a C-clip which was used to secure one end of the micrometer to the 0.25" stainless steel plate of the X-stage. The C-clip served to attach the micrometer to the moveable X-stage in such a way that micrometer would freely turn and the movement of the micrometer (in and out) of the mounting rail would move the X-stage left and right. Four 0.5" holes were drilled into the base plate to form a 4.75" square which corresponded to four bolt holes (which were tapped to accept a 0.5" bolt) in the vacuum mounting flange which held the ion source block (Figure

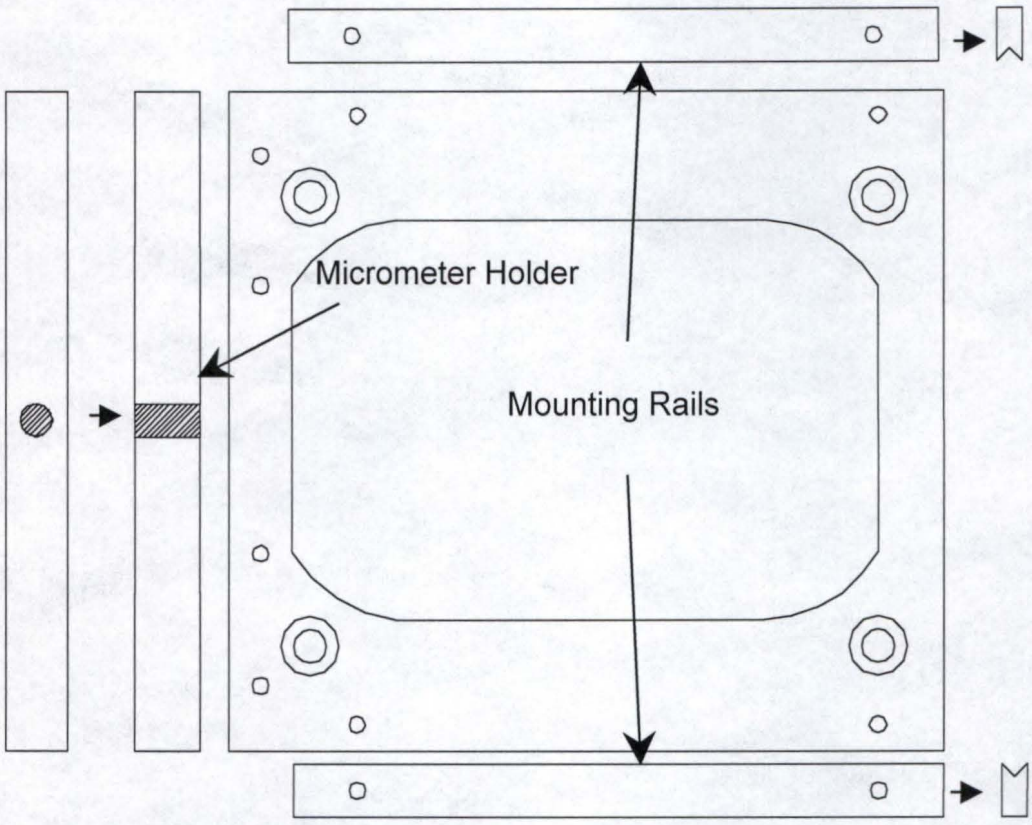

Figure 3.11. Drawing of the base plate of the X,Y-micro-manipulation stage constructed to allow spatial selection of locations on the sample probe. The small arrows indicate V-groove machined into the edges of the top and bottom rails. Rails were mounted to the base plate to serve as ball bearing guides for connection to the X-stage. Small arrow on left hand side indicates a top view of the rail through which the micrometer was screwed to serve as manipulator of X-stage (Figure 3.12).

3.10). Four 1" diameter by 3.0" aluminum posts were machined out of block aluminum. Holes (0.5") were drilled and tapped into both ends of the posts. Into one end of the posts a short (1.0") piece of (0.5") all-thread was screwed into the post. The other end of the piece of all-thread was screwed into the tapped bolt holes of the vacuum mounting flange. The other ends of the posts (the end not attached to the vacuum mounting flange) were bolted to the base plate of the X,Y-micro-manipulation stage and held it firmly in place 3.0" away from the vacuum mounting flange. Two rails (5.05" by 0.4" by 0.2") were machined out of stainless steel block. A V-groove was machined into the 5.05" by 0.2" face of each rail to a depth of 0.125". This V-groove served as a ball bearing guide to hold eight 0.125" stainless steel bearings which were evenly spaced out along the groove and held in place by a 0.005" by 0.2" by 4.25" strip of brass. The bass strip had 0.125" holes drilled into it evenly spaced along the 0.2" face to serve as a cage to hold the ball bearings in place. In the center of the brass strip a small hole was drilled which accommodated a pin press-fit into the center of the opposing V-groove machined into the upper and lower sides of the X-stage plate (figure 3.12). The X-stage plate of the X,Y-micro-manipulation stage was similar to the base plate except that the plate from which it was machined was small enough (4.25" square) so that the entire plate fit between the two ball bearing rails attached to the base plate. A 3.25" by 2.85" hole was machined into the center of the X-stage. V-grooves were machined into the top and bottom

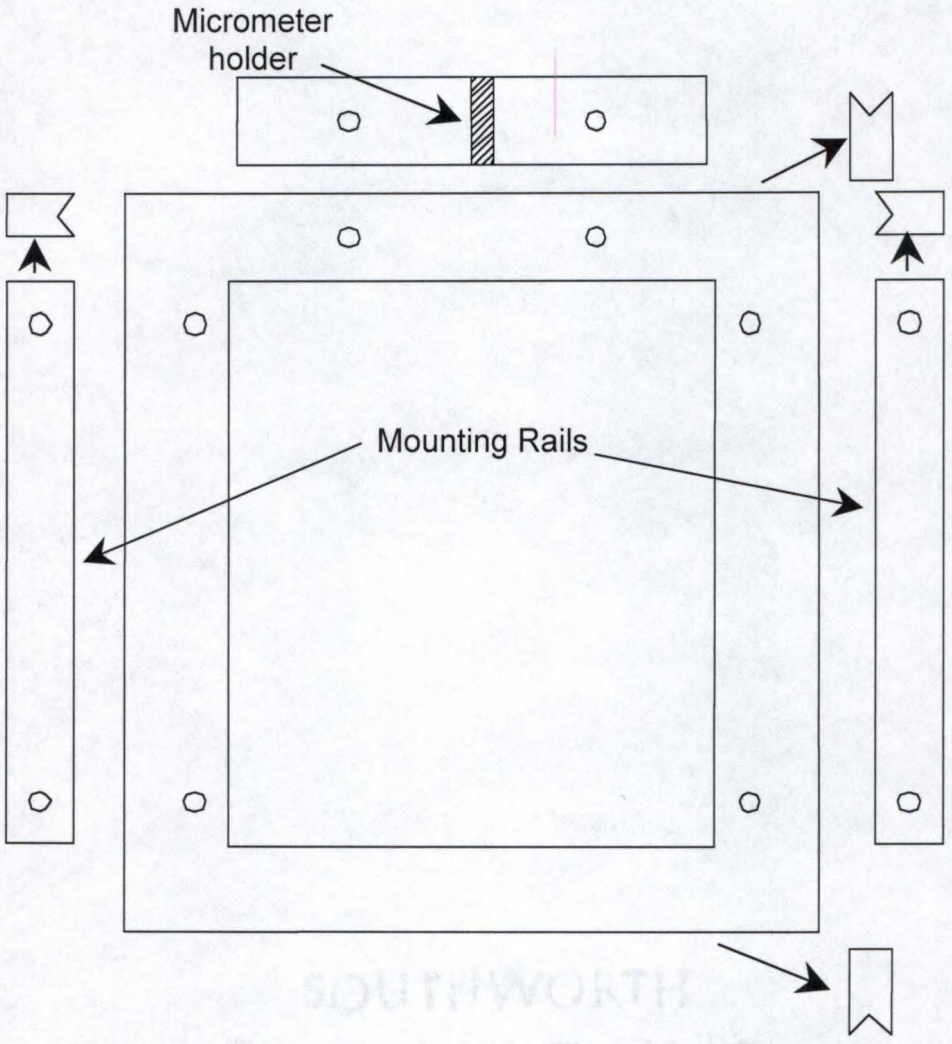

Figure 3.12. X-stage of micro-manipulation stage. Arrows indicate the machine V-groove cut into the upper and lower edges of stainless steel plate and into the inside edge of left and right rails. The left and right rails served as ball bearing holders for the Y stage to slide along.

portions of the X stage so that they matched the V-groove of the mounting rails of the base plate of the stage. With the ball bearings placed into the V-grooves between the base plate mounting rails and the X-stage plate, the X-stage would easily slide left and right along the surface of the base plate (movement in the X-direction). As was done with the base plate of the stage, mounting rails with V-grooves were attached to the X-stage; however, this time they were attached to the left and right of the opening in the plate (Figure 3.12).

The Y-stage of the micro-manipulation stage was constructed out of a 0.25" stainless steel plate machined to 2.75" square (Figure 3.13). Holes were drilled into the plate and tapped so that they matched the standard bolt hole pattern of the Finnigan 4500 probe lock. The left and right sides of the Y-stage had V-grooves machined into them that matched the V-grooves machined into the mounting rails attached to the X-stage. As was done with the base plate of the stage, a thin strip of brass was machined to hold the stainless steel 0.125" ball bearings in place between the X-stage mounting rails and the Y-stage plate. With the Y-stage in place, and the ball bearings in place between the plate and the mounting rails, the Y-stage freely moved up and down (motion in the Y-direction). A second micrometer was constructed in a similar fashion to the first and was attached to the Y-stage in the same manner as was done with the first. With the micrometer screwed through the micrometer holder attached to the X-stage plate, turning the micrometer

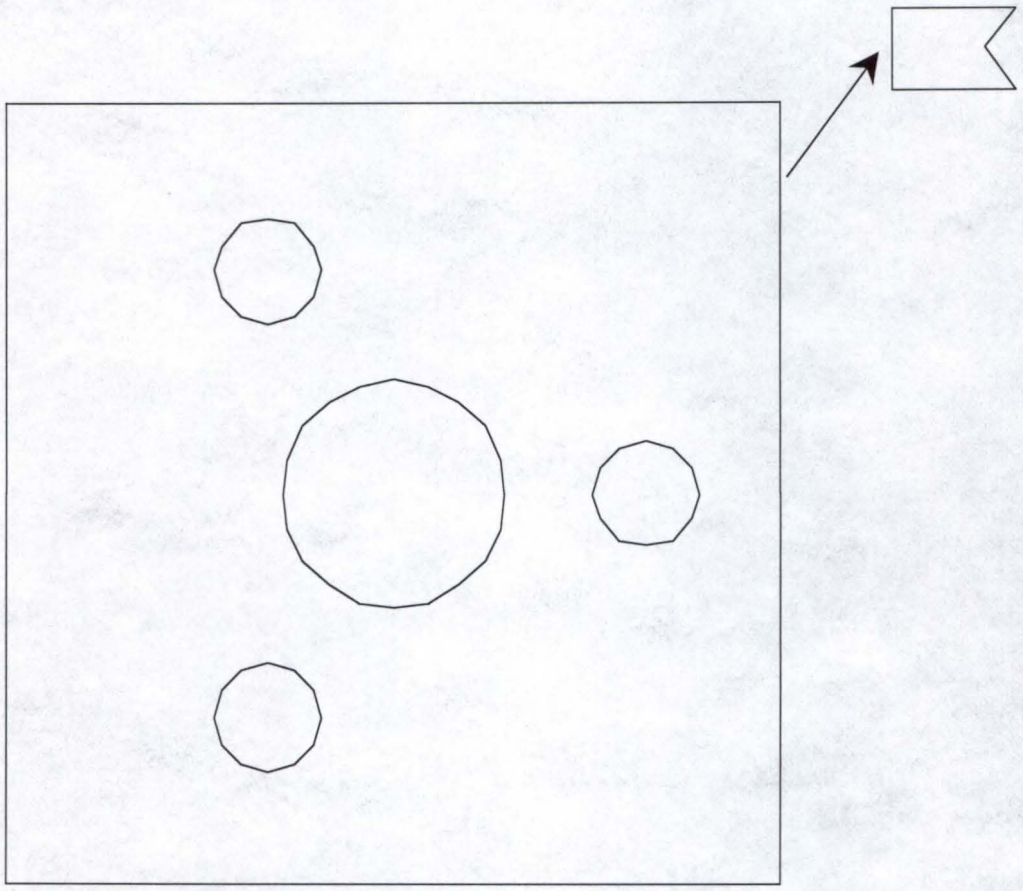

Figure 3.13. The Y-stage. A 0.25" stainless steel plate with holes drilled into the plate to match the bolt holes of the standard Finnigan 4500 probe lock. Arrow indicates the V-groove machined into both left and right sides of plate.

handle would move the X-stage up and down. Once the Finnigan 4500 probe lock was bolted to the Y-stage plate, the probe lock and entire Y-stage could be manipulated in the X and Y direction by turning the micrometers in and out. With a probe secured in the probe lock, it too could be manipulated in the X and Y direction.

The probe lock's new location (on the Y-stage) was 3.5" away from the vacuum mounting flange (where the probe lock originally was attached). To maintain a vacuum seal between the vacuum mounting flange on the instrument and the back of the third level of the stage, a piece of 1.1" inner diameter stainless steel flexible tubing was brazed into a groove machined into the back side of the third level of the stage. Because the probe lock had originally mounted directly to the vacuum mounting flange on the instrument by means of a 1.4" outer diameter o-ring (the groove for the o-ring was machined into the face of the probe lock which was now used to seal the probe lock to the third level of the stage), a replacement piece had to be created to seal the flex tubing to the vacuum mounting flange (Figure 3.14). The piece was machined out of a 0.25" stainless steel plate. A 1.4" outer diameter o-ring groove which matched the o-ring groove on the probe lock's interface was machined into one side of the new flange. In addition, a 1.1" outer diameter nipple (0.25" in height) was machined on the side of the flange opposite the o-ring groove. The nipple was used to braze the stainless steel flexible tubing to the flange. With the new flange attached to the vacuum

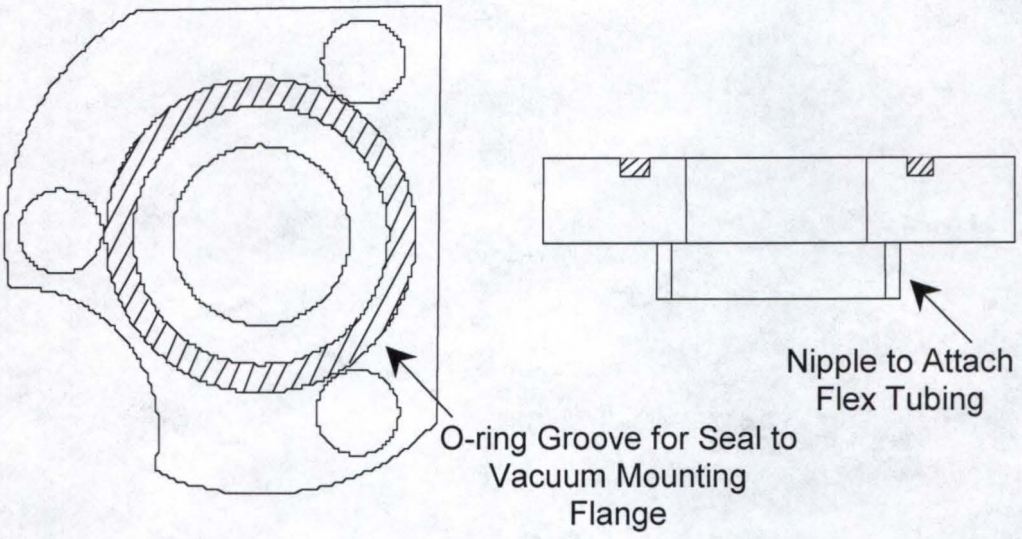

Figure 3.14. Flange machined to connect stainless steel flex tubing to vacuum mounting flange of instrument. Left hand side is view of face which bolted to vacuum mounting flange. Right hand side is side view showing nipple used to attach flange to stainless steel flex tubing to flange.

mounting flange on the instrument, the stainless steel flex tubing provided a flexible vacuum seal between the instrument and the third level of the stage. A probe, locked into the probe lock on the third level of the stage, could now be manipulated up and down and left and right while inside the instrument under vacuum conditions.

The original design of the probe tips used with the Finnigan 4500 instrument called for the probe tip to be clipped to the ion volume (Figure 3.9). This arrangement did not allow for movement of the probe tip while it was attached to the ion volume. In addition, the probe tip itself was used to hold the ion volume in place by aligning the small wire clip into the notches in the ion volume opening in the ion source block (Figure 3.9). To allow the movement of the probe tip (by means of the new X,Y-stage), an alternative method of holding the ion volume in the ion source block had to be devised. The ion volume still had to be removable by means of a probe inserted through the probe lock for several reasons: ablation of tissue by laser desorption would eventually coat the inside of the ion volume and reduce ion transmission (by allowing the ion volume to be electrically charged from the electrons used to ionize the reagent gas); the possibility of carry-over signal of the analyte from sample to sample due to contamination of the ion volume; and the inconvenience of having to shut the instrument down to switch from EI volumes (used during MALDI experiments) to CI volumes (used during LD/CI experiments). Since the ion source block had 0.025" notches cut into the

block on either side of the ion volume opening to accommodate the clips used to attach the probe tip to the ion volume (Figure 3.9), small pieces of 0.025" wire were welded to the outside of the ion volumes at the locations where the retaining clips originally were attached. When the ion volume was slid into the source block, the small wire pieces served to guide the ion volumes into the opening and then hold them there in the correct position. The ion volumes needed to be oriented in the correct position so that the holes in the sides of the ion volumes for reagent gas, electron beam, and the electron collector (Figure 3.9) lined up with the corresponding holes in the ion source block. To insert and remove the modified ion volumes, a custom probe needed to be created. The new probe had an expandable front piece which fit into the open end of the ion volumes. Expanded, the front piece of the probe would tightly hold the ion volume while it was inserted into the instrument (or removed). Relaxed, the front piece of the probe would allow the ion volume to be left in place in the source block, held there by the wire pieces welded to the outside of the volumes.

The original probe tips used with the Finnigan 4500 mass spectrometer had a sample surface which was 0.3" in diameter (Figure 3.9). The face of the probe tip completely filled the back of the ion volume ,forming a tight seal. This arrangement did not allow for movement of the probe tip face within the ion volume. New probe tips were designed and constructed which allowed movement of the probe tip within the ion volume while still

maintaining a tight seal at the back of the ion volume (to maintain adequate reagent gas pressure during CI). To allow the entire face of the new probe tip to be sampled, the new probe tip's face was 0.155" in diameter. This allowed the entire probe tip surface to be manipulated into the area where the laser beam would strike the sample through the 1 mm opening in the CI ion volume. To maintain a tight seal when the new probe tip was manipulated within the ion volume, a 0.45" diameter shoulder was machined into the probe tip 0.125" back from the tip surface. This shoulder (when butted up against the back of the ion volume) set the probe tip surface to the correct depth in the ion volume and maintained a good seal at the back of the ion volume even when the tip was manipulated to its maximum distance from center (0.075" to either side or up or down). The original ion source block had a 0.08" deep recessed area machined into the ion volume opening which served to help hold the original probe tips in place (Figure 3.8). To allow full movement of the new probe tips across the back surface of the probe source (while maintaining a tight enough seal to allow for good CI pressures), the recessed area was increased to form a 0.525" square smooth surface across the back of the ion source around the ion volume opening.

One full turn of a micrometer on the new X,Y-stage moved the probe tip approximately 300 μm in the ion volume. To asses the reproducibility of the new X,Y-stage, the MALDI matrix DHB was applied to a new probe tip and allowed to dry. After drying, the probe tip with the DHB was inserted into the

mass spectrometer and the X,Y-stage was adjusted so that the left edge (in the X direction) of the middle of the probe tip (in the Y direction) was approximately in the center of the ion volume (where the UV laser beam was positioned to strike). The UV laser was fired 20 times (enough to remove the DHB matrix from the surface of the probe tip) at one location, then the X,Y-stage was moved one turn of the X micrometer to position the probe tip approximately 300 μm to the right of the previous location. At each location across the surface of the probe tip the laser was fired 20 times. After sampling the surface over the entire 4 mm distance of the probe tip (13 spots in 12 turns of the micrometer), the probe tip was removed and inspected under a 30X microscope. Visual inspection showed that spots of approximately 50 μm diameter had been formed by removal of the MALDI matrix at intervals of approximately 300 μm (the spot sizes and distances moved were measured with a micrometer under the microscope), resulting in a even distribution of spots across the middle of the probe tip. The MALDI matrix was removed and a new layer of DHB was applied to the surface of the probe tip. Again, the X-stage was adjusted so that the left edge of the middle of the probe tip was under the location of the UV laser beam. As was done previously, a line of spots were formed in the MALDI matrix across the probe tip at 300 μm intervals (from approximately 0 to 4 mm across the tip). Once the right edge of the probe tip was reached, the Y-stage was adjusted down one turn of the micrometer (moving the location where the laser beam struck the probe tip

approximately 300 μm in the Y direction). Because the sample, not the laser beam, was adjusted, moving the sample down in the Y direction was equivalent to moving the laser beam up on the sample surface. Once the Y-stage had been adjusted, the laser was again fired 20 times to mark the spot on the probe tip where the laser beam stuck the surface. As was done with the first set of marks across the probe tip, the X-stage micrometer was adjusted one turn (this time in the opposite direction) and 20 laser shots were used to mark the location of the laser beam at each sampling spot across the probe tip. After adjusting the X-stage back to its original location (with the Y-stage adjusted 300 μm lower), the probe tip was removed and visually inspected under the microscope. The first set of laser spots formed in the MALDI matrix appeared similar to those formed in the first evaluation of the stage. The location of the second set of spots (those formed after the adjustment of the Y-stage one turn) appeared approximately 300 μm above the first set of laser spots. By visual inspection, it appeared that each upper laser spot was approximately (± 25 μm in the X direction) above the corresponding laser spot from the first set of laser markings. These experiments were repeated several times and similar results were found. One problem was noted: when the probe tip contacted the back of the ion source (by adjustment of the probe distance in the Z direction), the tip would catch on the ion source and bind. This binding of the probe tip with the ion source would cause the movement in the X direction to the be off by as much as 100

μm. Because of this, care was taken to adjust the length of the probe so that the probe tip was close to but not touching the ion source.

With the stage finished, the next step was to test the ability of LD/CI to map the location of a drug compound at trace levels in intact tissue.

LD/CI with Spatial Resolution

Because the CO_2 laser used in the previous LD/CI experiments had required extensive attenuation of the beam to reduce the energy per pulse, a new CO_2 laser was purchased to continue the laser desorption experiments. A μ-TEA CO_2 laser (Laser Science, Inc., Franklin, MA) was purchased and used for all further LD/CI experiments. The μ-TEA laser featured a 125 ns laser pulse (FWHM) at 10.6 μm wavelength with an output of 15 mJ of energy per pulse. The beam diameter was 2.5 mm. The beam's diameter was adjusted prior to focusing by means of a stainless steel iris (Edmund Scientific, Barrington, NJ.) adjustable from 0.8 mm to 5 mm. The laser beam was attenuated to an approximately 1.25 mm diameter prior to focusing. In order to reduce the size of the focussed beam, a new zinc-selenide, positive meniscus lens with a focal length of 3.75" was used. The new lens, along with the smaller beam, allowed the focussing of the beam to a spot size of < 100 μm diameter.

A probe tip was constructed with a 100 μm slot cut into the face of the probe so that it was divided approximately into half (Figure 3.15). A 100 μm

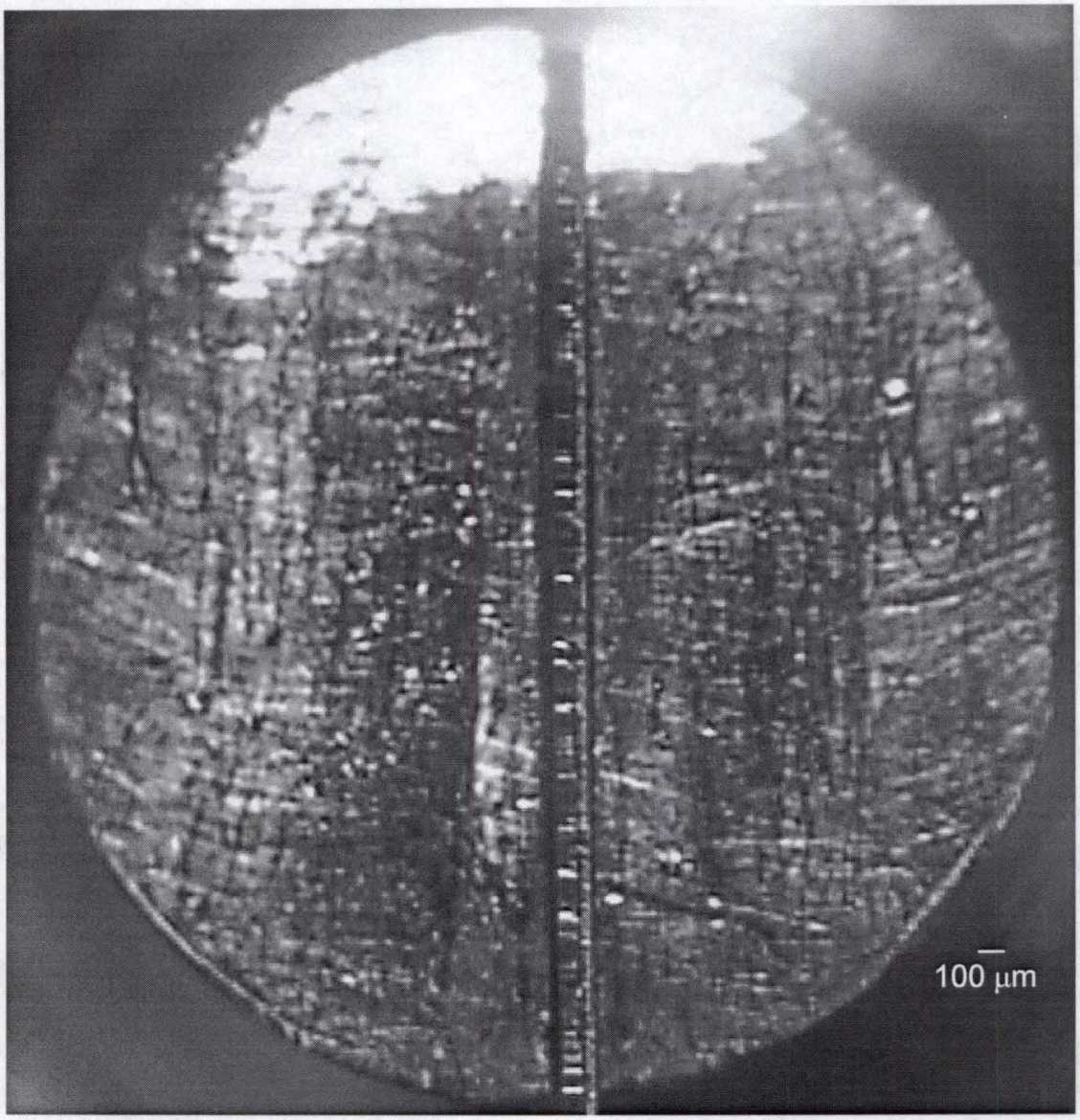

Figure 3.15. Split probe tip used for spatial resolution studies with laser microprobe instrument. The 100 μm thick dividing wall extended approximately 20 μm above surface of probe tip.

thick piece of stainless steel was placed into the slot to form a barrier 20 μm high between the two sides. A thin slice of rat liver tissue (1.8 mg) was placed in a shallow stainless steel well. 0.9 μL of a 100 ng/μL solution of the drug spiperone dissolved in aqueous 1% acetic acid was pipetted unto the surface of the tissue. The well was covered and left alone for one hour. Another thin slice of rat live tissue (2.7 mg) was placed in a separate stainless steel well and 1.0 μL of aqueous 1% acetic acid with no spiperone was pipetted onto the tissue and allowed to sit covered and undisturbed for one hour. Both pieces of tissue were rinsed with several aliquots of 1% aqueous acetic acid solution and then blotted dry. The tissue pieces were placed on different sides of the divided probe tip (carefully, to prevent mixing of the fluids retained in the tissue) and allowed to air dry (approximately 1.5 to 2 hours).

Figure 3.16 shows a drawing of the divided probe tip used in the spatial study. The MS/MS spectra above the drawing were collected from the indicated locations across the front of the probe tip. One full turn of the X-stage micrometer (equally approximately 300 μm) was used to move the sample to a new position between each sampling. The spectra represent the average of 3 collected laser desorption and mass analysis events at each location (3 micro-scans averaged into an analytical scan). The characteristic daughter ions of spiperone (Figure 3.4) at m/z 291, 232, 165, and 123 were detected from each of the selected spots across the probe tip's surface that corresponded to the spiperone spiked tissue (all spectra not shown). In

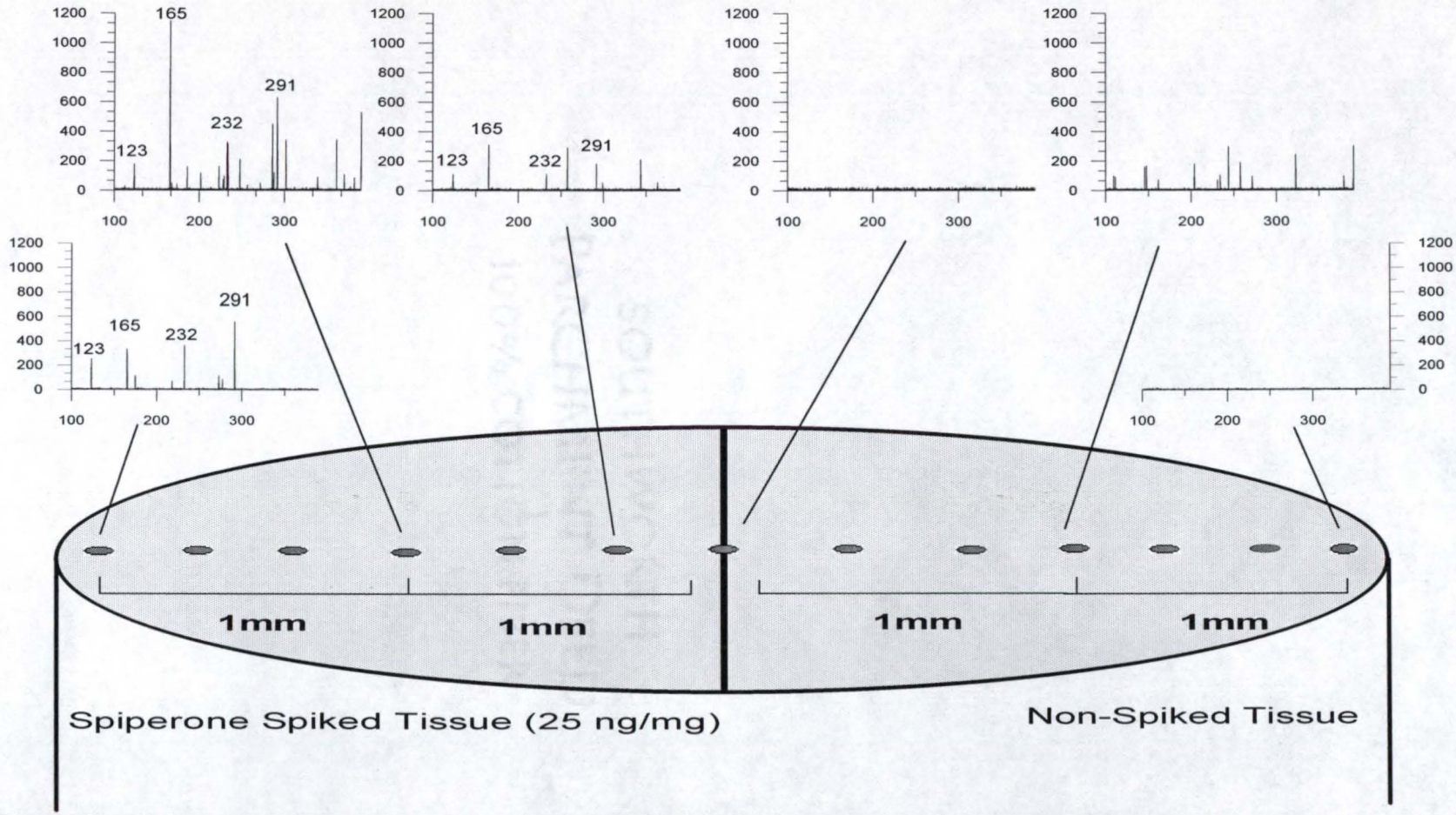

Figure 3.16. Drawing of divided probe tip with representative MS/MS spectra at selected locations across the probe tip. The daughter ion spectra were produced by CAD of ion at m/z 396 which corresponds to the $[M+H]^+$ ion of spiperone. Note that ions indicated from spots selected from spiperone spiked side of tissue sample are characteristic daughter ions of spiperone. Similar daughter ions were not detected on the non-spiked side of the tissue sample.

contrast, no characteristic daughter ions of spiperone were detected from the sampling of the non-spiked side of the probe tip.

Figure 3.17 shows a photomicrograph of the tissue after analysis. Each sampling spot is clearly visible and could be related back to the data collected across the surface. The size of each spot was approximately 100 μm in diameter and represented the damage caused 12 laser shots. The representative spectra shown in Figure 3.16 were collected in the first 3 laser shots; however, additional laser shots were taken at each spot to clearly mark the location of the laser beam. After the first 3 laser shots, the level of detected spiperone on the spiked side of the tissue decreased dramatically. No spiperone was detected during the third set of 3 laser shots. It was not clear whether the decrease in detected spiperone was the result of decreased efficiency of laser desorption due to damage caused by the first 6 laser shots, degradation (thermal or photo) of the spiperone in the tissue, or whether the decrease in detected spiperone indicated that the drug had not penetrated for below the surface of the tissue. There was a decrease in the intensity of the ion signal (based on the signal observed in the isolation window around m/z 396) after the first 6 laser shots which seemed to indicate that the surface of the tissue had been damage by the laser interaction and was no longer as easily ablated.

The results of the above experiment clearly demonstrated that laser desorption coupled to chemical ionization on the laser microprobe instrument

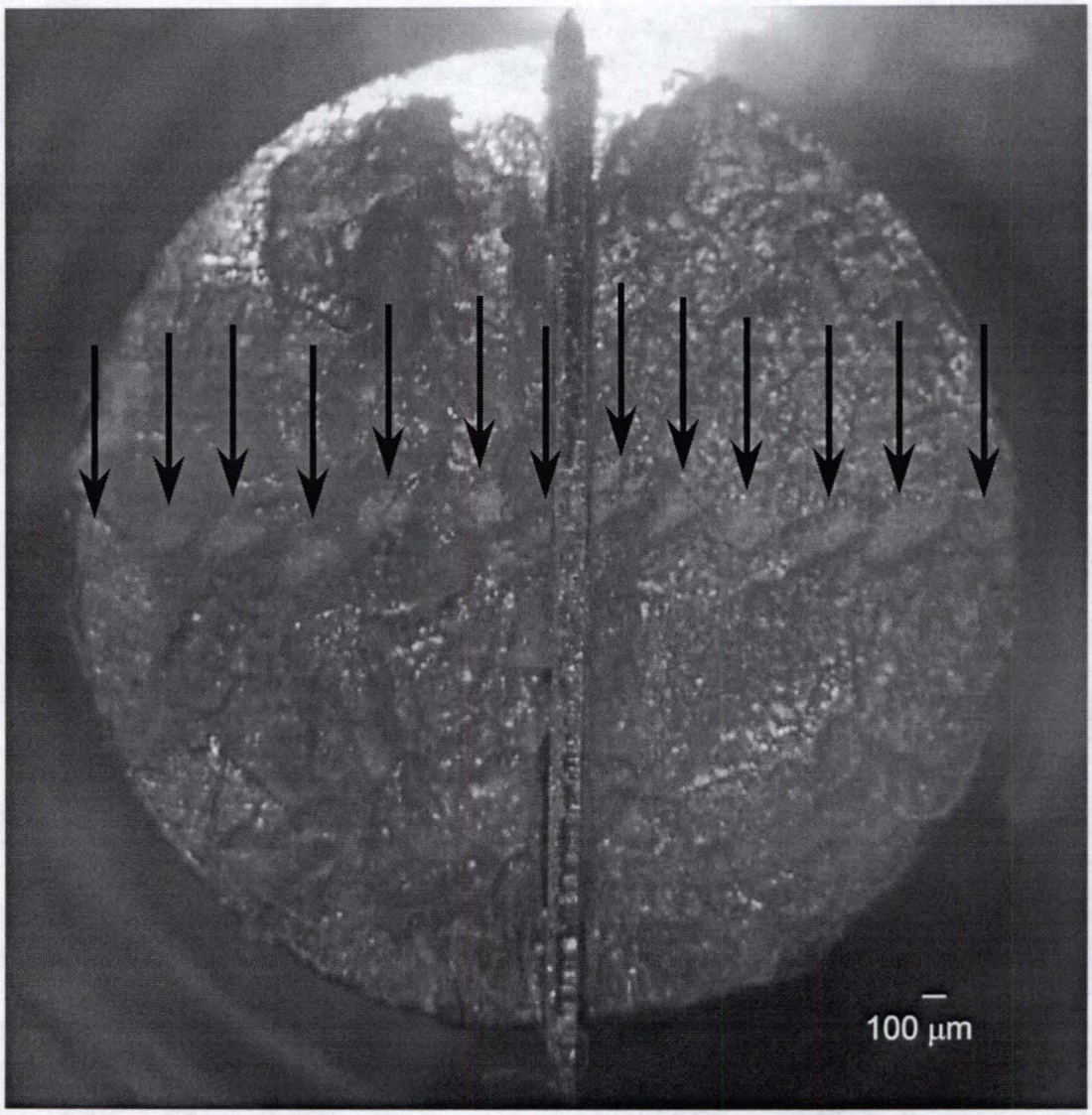

Figure 3.17. Photomicrograph of tissue sampled by LD/CI. Tissue on left hand side of probe tip was spiked with drug spiperone (25 ng/mg), while tissue on right hand side was not spiked with drug. The arrows indicate the location of laser sampling.

was capable of mapping the location of a pharmaceutical compound in an intact tissue mass. Additionally, as Figures 3.5 through 3.7 showed, the ability of the quadrupole ion trap to isolate and then selectively fragment (by CAD) the ion of interest was crucial in the unambiguous detection of trace level compounds in the complex matrix of tissue.

CHAPTER 4
ELECTROSPRAYING OF THE MALDI MATRIX

As was noted in the beginning of chapter 3, the pipetting of the MALDI matrix onto the surface of the tissue blurred the spatial location of compounds in tissue. To verify this, a series of experiments were performed.

MALDI Drop Method

In experiments preformed previously in our lab, it was demonstrated that spiperone was capable of a lateral migration of at least 300μm when the MALDI matrix solution was allowed to sit on top of the tissue for up to five minutes before drying.[62] In a typical MALDI drop experiment (where the matrix solution is applied as a drop onto the surface of the tissue), the matrix solution can evaporate in as few as 30 seconds. To determine the extent of lateral migration of the drug compound during routine MALDI drop applications, the split probe tip (shown in Figure 3. 15) was again employed.

A 2.4 mg thin slice of rat liver tissue was placed in a stainless steel well and 1.2 μL of a 100 ng/μL solution of spiperone in aqueous 1% acetic acid was pipetted on top of the tissue. A similar piece (2.6 mg) of rat liver tissue was placed in a comparable stainless steel well and 2 μL of an

aqueous 1% acetic acid solution with no spiperone was pipetted onto the top of the tissue. Both tissue pieces were allowed to soak undisturbed in the solution for one hour. At the end of one hour, the two pieces of tissue were rinsed with several aliquots of aqueous 1% acetic acid, blotted dry, and placed on different sides of the split probe tip and allowed to air dry (1.5 hours). As before, care was taken to ensure that fluids from the two different tissue masses were not allowed to intermingle. Once dry, 4 μL of a saturated DHB in methanol solution was pipetted onto the surface of the tissue and allowed air dry (approximately 30 seconds). Once the matrix had fully dried and crystallized, the sample was interrogated with the laser microprobe instrument beginning on the non-spiked side of the probe tip. Figure 4.1 shows a photograph of the tissue after the matrix solution had crystallized. Note that the tissue beneath the crystallized matrix has been obscured by the MALDI matrix. Figure 4.2 shows a drawing of the probe tip with representative MS/MS spectra (of the m/z 396 ion corresponding to the $[M+H]^+$ ion of spiperone) from selected locations across the surface (approximately every 300 μm). The ions marked with numbers indicate the characteristic daughter ions of spiperone (at m/z 123, 232, 165, 291). It is clear from Figure 4.2 that because of the MALDI matrix application during the preparation of the tissue sample, all spatial information about the location of spiperone in the tissue mass had been lost. Since the intended purpose of the project was to map the location of the drug compound in the tissue mass, this procedure of applying

Figure 4.1. Photomicrograph of MALDI matrix covering rat liver tissue used in MALDI drop experiment to demonstrate the loss of spatial resolution during matrix application.

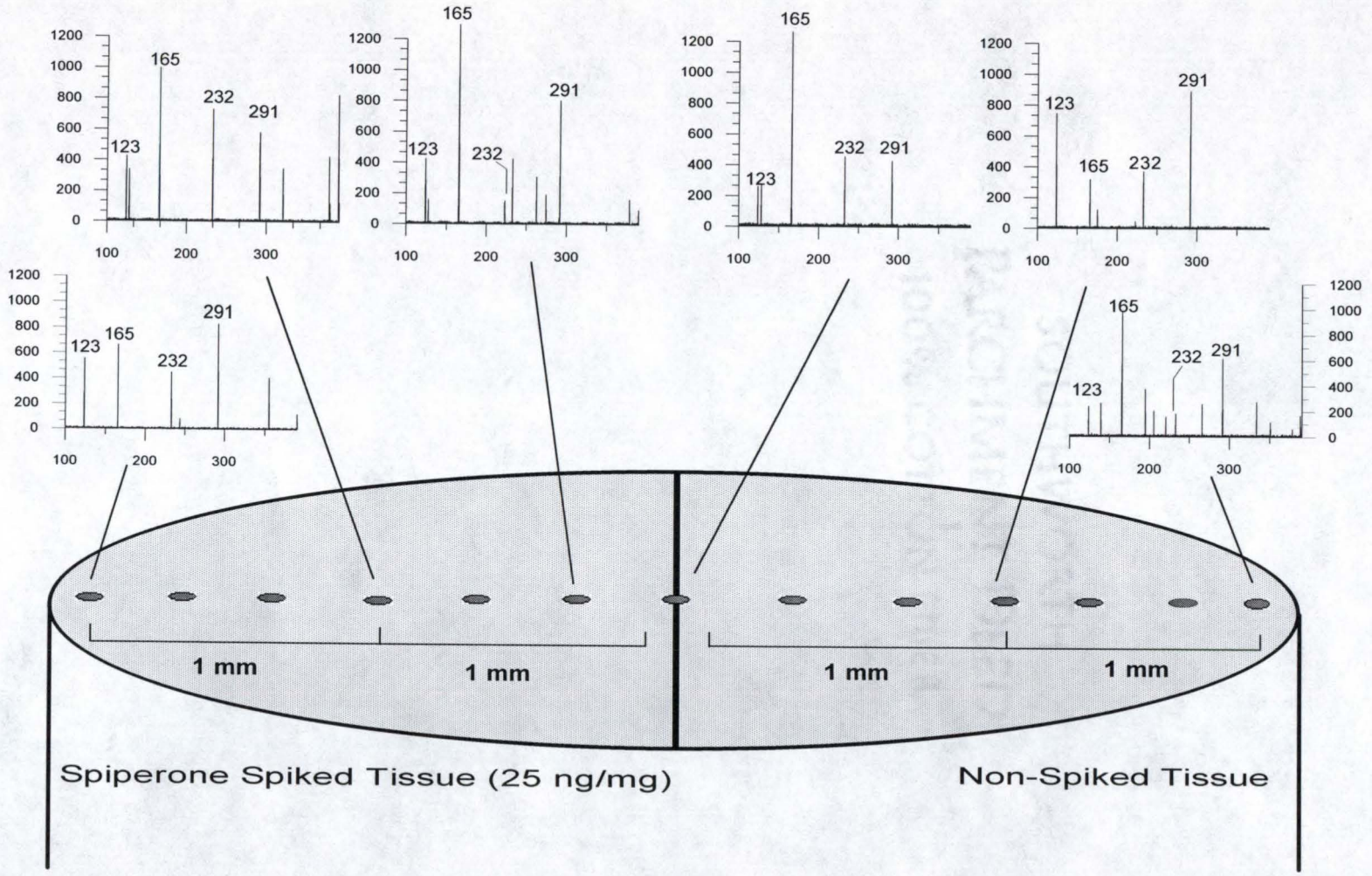

Figure 4.2. Drawing of probe tip and representative daughter ion spectra from selected locations across the surface. Ions marked with m/z numbers are ions which correspond to characteristic daughter ions of spiperone.

the MALDI matrix in a drop fashion was unacceptable. As an alternative method of applying the MALDI matrix, electrospraying of the matrix solution onto the surface of the dried tissue was evaluated.

The Electrospray Apparatus

In order to reproducibly electrospray the MALDI matrix solution onto tissue samples, an apparatus needed to be constructed. Since high voltages are used during electrospraying (+4 kV in experiments preformed here), the electrospray apparatus was constructed out of plastic.

The electrospray apparatus used an Analytica (Branford, CT) electrospray probe, high voltage power supply, and gas distribution box. The electrospray probe was constructed of stainless steel and featured two housings (one inside of the other) which provided the ability to use a sheath gas during the electrospray procedure (Figure 4.3). The inner stainless steel housing (called the needle) held the fused silica capillary (50 μm inner diameter and a 150 μm outer diameter) used to deliver the matrix solution to the tip of the needle. The fused silica capillary protruded from the tip of the needle approximately 10 μm so that solution flowing from the capillary would readily contact the needle and be subjected to the potential applied to it. Sheath gas in typical electrospray mass spectrometry is used to help desolvate the solution clusters formed during electrospray. For the electrospraying of the MALDI matrix solution, the sheath gas provided a

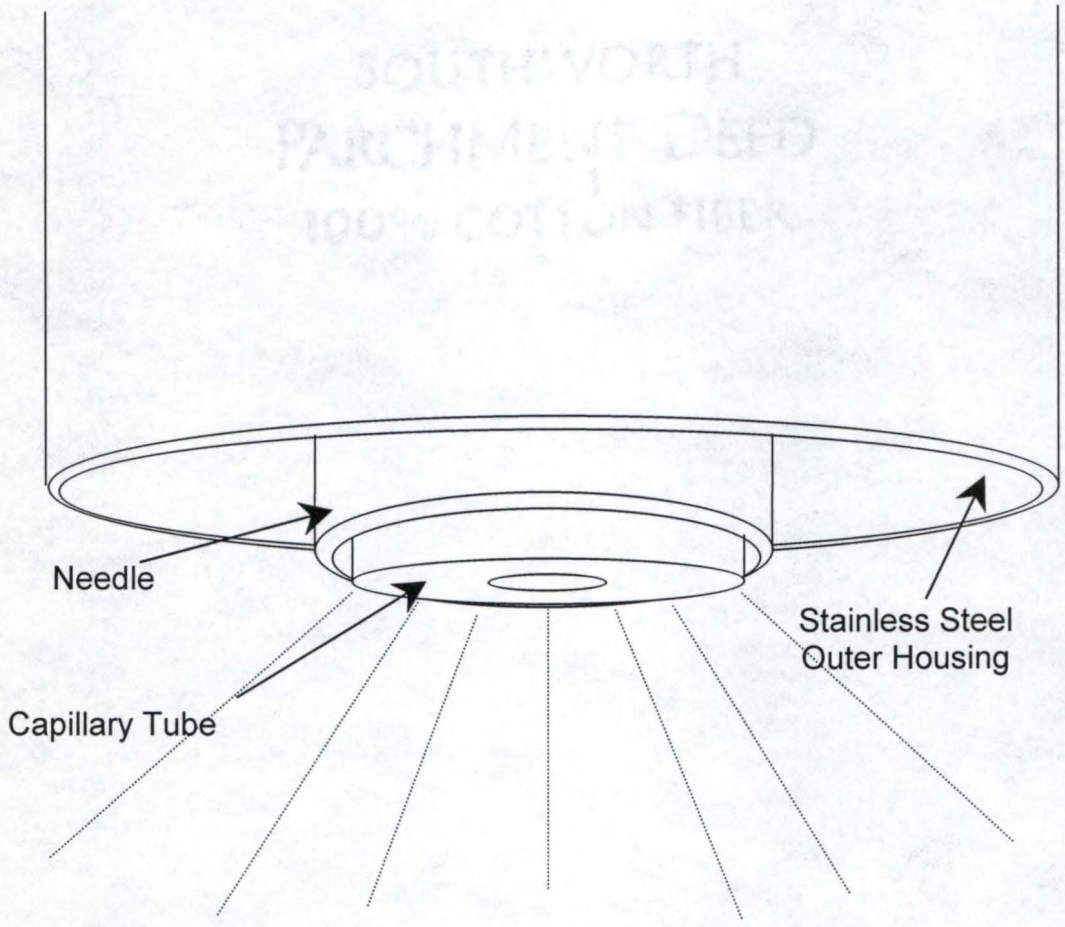

Figure 4.4. Drawing (not to scale) of the Analytica electrospray needle tip. Sheath gas flowed between inner housing and outer housing.

continuous flow of gas across the sprayed surface which assisted in the evaporation of solvent . For all electrospray experiments preformed here, +4 kV of potential was applied to the needle while the sample was held at ground. This voltage was found to produce the best electospraying of the MALDI matrix solution.

The physical box which held the electrospray probe at the proper position above the sample probe tip was machined out of 0.25" plastic (Figure 4.5). The sides of the box were 7" deep and 6" high. The back of the box was 6.5" across and 6" high. A 6.5" by 6.5" block of 0.75" thick plastic was used to form the top of the electrospray box. A second 0.75" thick block of plastic was machined into a 6.4" by 6.5" rectangle and was used as the platform on which the sample probe tip would be placed during electrospraying. Two 0.25" wide slots 2.75" long were machined through each of the side panels. The middle of these slots were spaced 2.5" from the bottom edge of the side panels and were located 2" in from the front and the back of the panels. Holes were drilled and tapped on both sides of the platform piece so that plastic bolts could be fed through the slots in the side panels and be used to hold the platform in place inside of the box. The height of the platform, and thus the distance between the electrospray needle tip and the probe tip, was adjustable by loosening the bolts and sliding the platform up or down. Two 0.25" thick and 0.1" deep slots were machined into the inside edge of the side panels of the box 0.25" in from the front. A 0.25" thick panel measuring 6.6" by 7" was

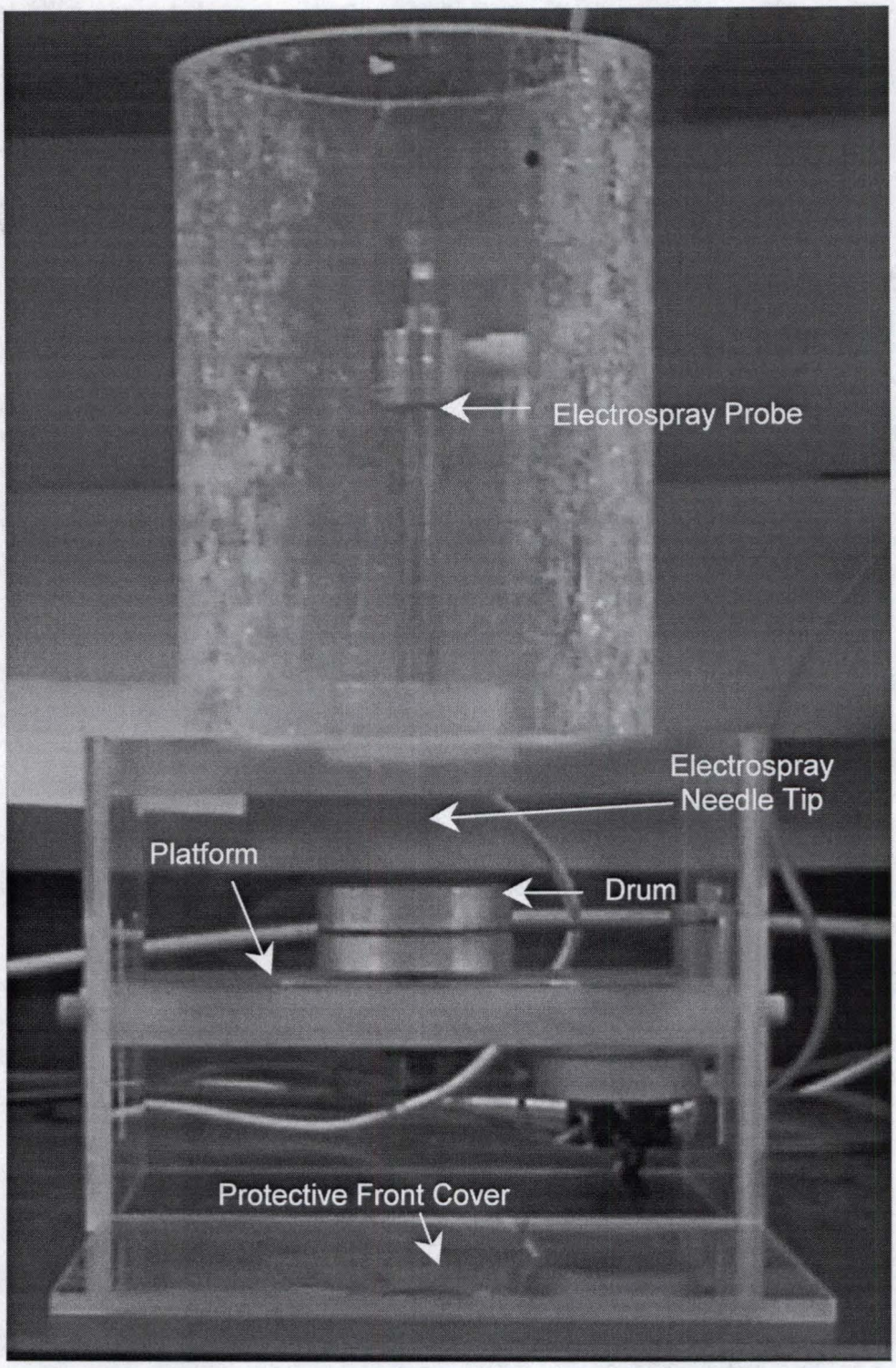

Figure 4.5. The completed electrospray apparatus. The platform, on which the rotating drum was set, was adjustable up and down to set the distance between the probe tip and the electrospray needle.

machined so that it would slide into the slots of the side panels when the box was finished and form a protective front cover. To supply the potential to the electrospray needle, an aluminum block measuring 2" square and 1" thick was machined. A slight depression (0.2" deep) was machined into the center of the top of the box. A 0.3" hole was drilled in the center of the aluminum block to a depth of 0.75". In the center of the 0.3" hole, a 0.01" hole was drilled. A similar 0.3" hole was drilled through the top of the box in the center of the depressed area machine for the aluminum block. When the electrospray probe was placed in the 0.3" hole (the size of the hole corresponded to the outer diameter of the electrospray probe), the tip of the electrospray needle protruded approximately 0.2" beyond the inner side of the box top. This arrangement allowed a potential to be supplied to the aluminum block which was in physical contact with the electrospray probe and positioned the electrospray needle in the center of the box.

A small aluminum drum (2.0" diameter) was machined and placed on a post which had been pressed into an aluminum plate. The aluminum plate was placed into a depression which was machined into the top surface of the platform. The platform was attached to the ground of the high voltage power supply and provided a ground which was in contact with the metal drum. With the platform inside of the box, the drum was positioned below the electrospray needle tip; by moving the platform, the top of the drum could be moved as close as 1" and as far as 3" away from the electrospray needle tip. A small

electric motor (taken from a clock) was mounted one of the side panels of the box and was attached to the drum by an o-ring which acted as a drive belt so that when the motor was turned on the drum rotated slowly (approximately one revolution per minute). A 4" outer diameter plastic tube (0.5" thick) was placed around the electrospray probe to prevent accidental touching while potential was applied. The matrix solvent was pumped to the electrospray needle by a syringe pump (Harvard Apparatus, South Natick, MA). Figure 4.6 is a photograph of the completed electrospray apparatus. Nitrogen gas was used as a sheath gas and was supplied by a tank of nitrogen attached to the standard Analytica gas distribution box.

Experiments showed that the best electrospray conditions were a flow rate of 5 μL per minute, a sheath gas flow of 50 mL per minute, and an electrospray voltage of +4 to +5 kV. The sample probe tip was placed in the center of the rotating drum and positioned 1 cm below the electrospray needle. Several matrix solvent compositions were tried; while most electrosprayed well, a solvent composition of 70% methanol 30% aqueous 1% acetic acid solution was finally chosen. This solvent composition was found to electrospray well and provided the necessary organic composition needed to dissolve some of the pharmaceutical compounds investigated while preventing the spread of those compounds across the surface of the tissue.

The matrix used was DHB and was sprayed from a solution of 10 μg/μL of solvent solution. Experiments showed that the surface of the tissue

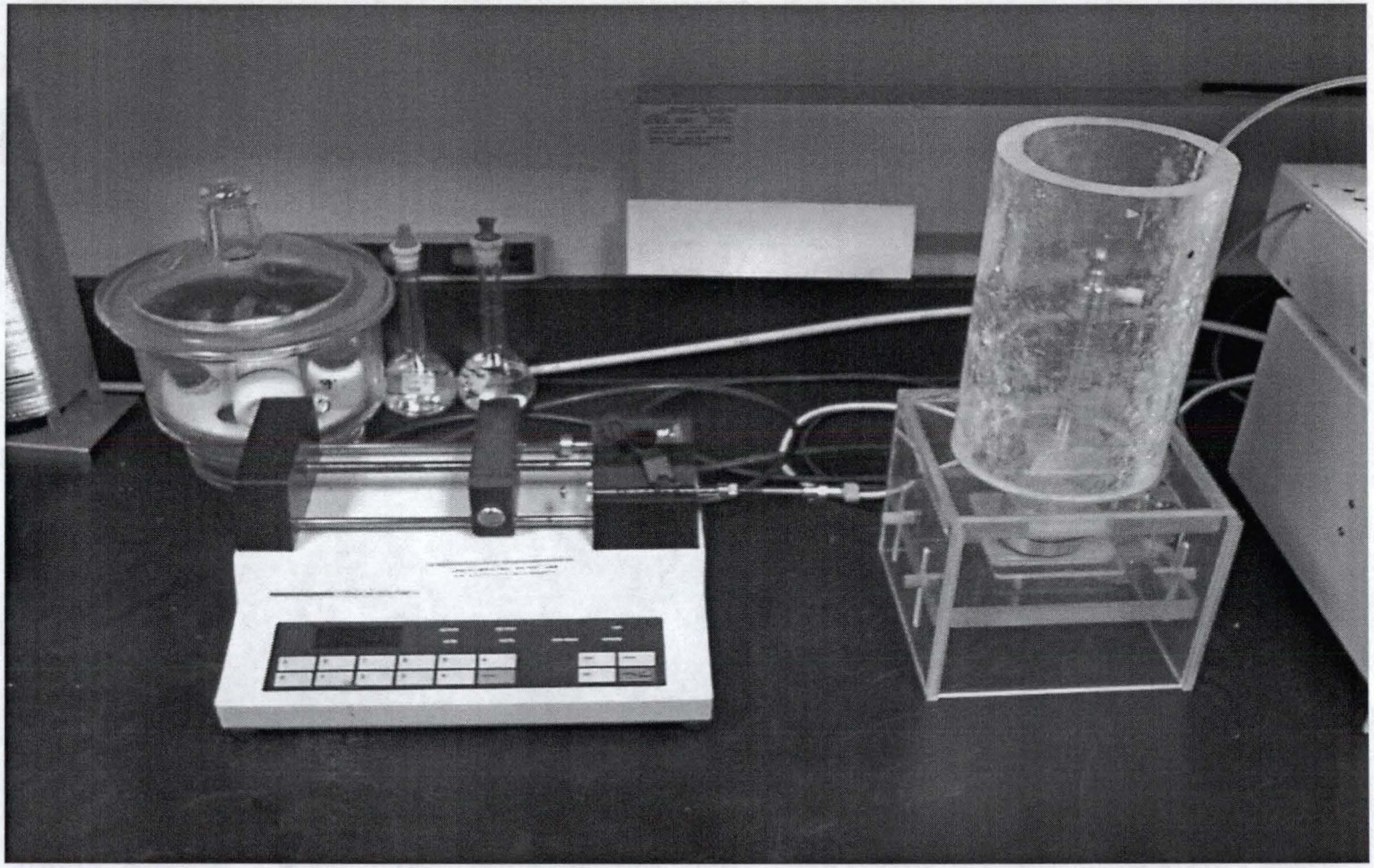

Figure 4.6. A photograph of the finished electrospray apparatus. The syringe pump supplied the matrix solution to the electrospray tip. Note the heavy plastic sleeve used to protect 4kV electrospray tip from being touched accidentally.

was coated with a thin layer of matrix after electrospraying for 7 to 10 minutes. Electrospraying of the matrix solution for longer that 10 minutes still provided good results, but produced a thick matrix layer (approximately 2 to 3 μm thick by visual inspection) which did not produce compound ions for the first 5 to 10 laser shots. It was believed that this was the result of a layer of matrix crystals being deposited over an already crystallized portion of matrix which contained the extracted analyte.

Electrospraying of the MALDI Matrix

The electrospraying of a MALDI matrix has recently been demonstrated to preserve the spatial distribution of compounds.[18,109] However, in these cases the analyte under investigation was a major compound present in the sample. It was not clear that trace level analytes would be extracted from the tissue to sufficient levels to be detected. As was done in previous experiments, two thin slices of rat liver tissue were prepared. One of the tissue slices was spiked with the drug spiperone while the other was not. The two tissue slices were placed on opposite sides of the split probe tip and allowed to air dry.

The dried tissue was electrosprayed with a MALDI matrix solution for 10 minutes at a potential of +4.0 kV and a current of 50 nA. The syringe pump was turned off after 10 minutes and the current was allowed to drop to zero before the high voltage was turned off. Figure 4.7 shows a photograph of the

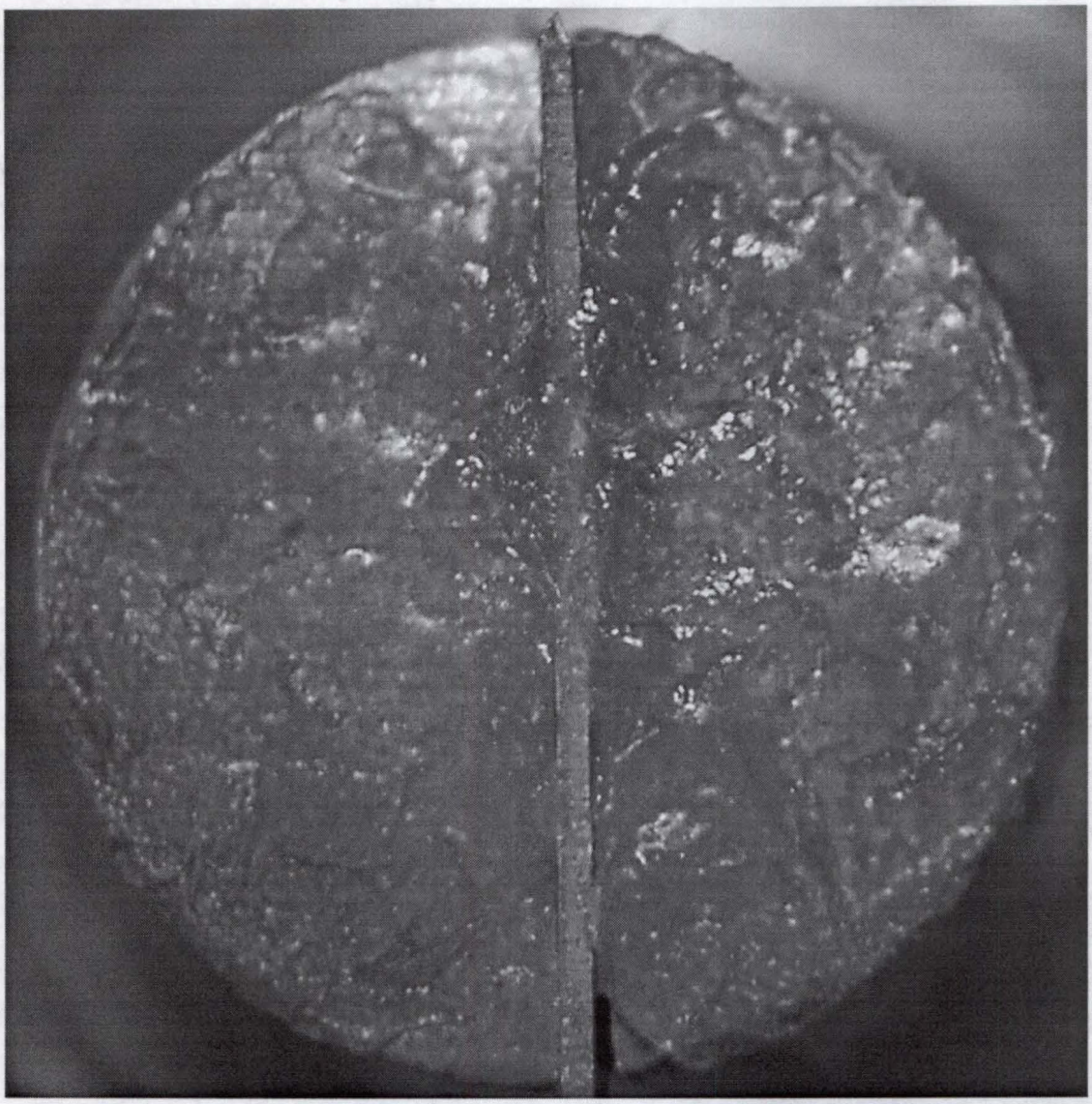

Figure 4.7. Tissue after electrospraying of the MALDI matrix. Note that tissue is clearly visible beneath the thin matrix coating on the surface.

tissue after electrospraying. Note that the tissue surface was still visible beneath the thin matrix coating. The matrix appeared as a shiny coating over the tissue and was only clearly visible as a frosting of the metal surfaces of the probe tip around the tissue. Figure 4.8 shows the MS/MS spectra of the m/z 396 ion across the surface of the sample (with a resolution of 300μm). The ions marked with m/z numbers (123, 165, 232, and 291) correspond to the characteristic daughter ions of spiperone. The intensity of the ions varied across the surface; however, daughter ions of spiperone were only noted on the side of the tissue which had been spiked with spiperone.

These experiments demonstrated the ability of electrospraying the MALDI matrix onto the surface of the tissue to preserve the spatial location of the drug compound. It was expected that the electrospray process would seriously reduce the ion intensity by reducing the amount of extracted drug from the tissue (because of the short contact time between application and evaporation of the matrix solution). While no specific experiments were preformed to explore whether or not this was true, it is interesting to note that the intensity of the daughter ions in Figure 4.2 (the MALDI drop method) are slightly higher than the intensity of the daughter ions in Figure 4.8 (the electrospray method). The intensity scale in both figures are the same; however, it must be noted that in Figure 4.2 the extracted drug was distributed across the entire surface of the probe tip (due to migration of the drug after extraction into the matrix solution) while in Figure 4.8 the drug was only

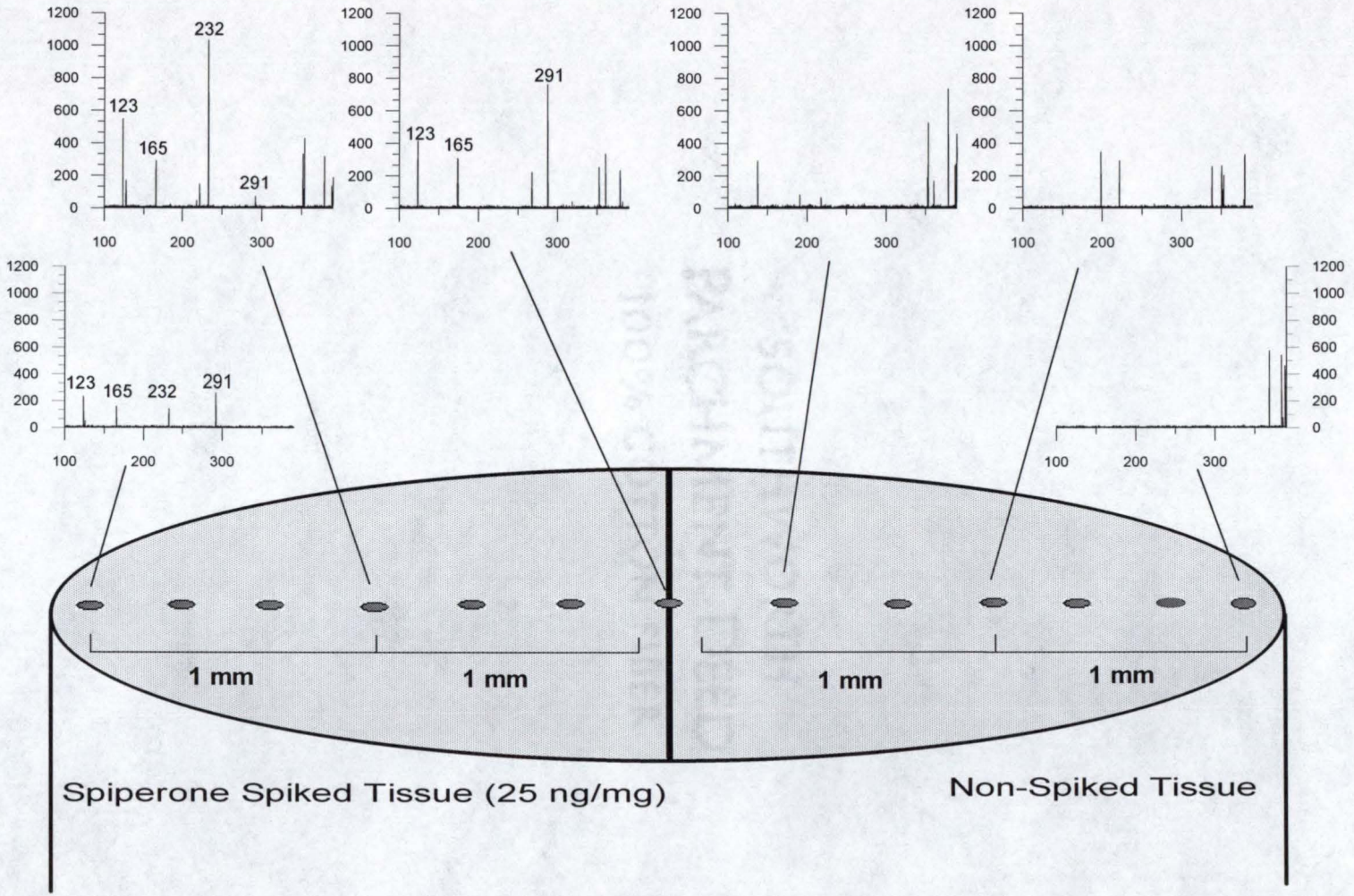

Figure 4.8. MS/MS spectra of m/z 396 ion at selected locations across probe tip after electrospraying of MALDI matrix. Ions marked with m/z values correspond to characteristic daughter ions of spiperone.

detected in the spiked half of the probe tip which indicated that the drug was only located in the matrix above half of the surface.

Infrared MALDI

Both of the alternative methods (LD/CI and electrospraying of the MALDI matrix) were successful in preserving the spatial resolution of the drug compound in the intact tissue samples. The next logical step was to compare the two techniques to see if one would be more sensitive than the other (under a specific set of experimental conditions). In order to do a direct comparison, as many experimental conditions as possible needed to be held constant. Since the UV laser was not powerful enough to perform laser desorption without the added MALDI matrix, it could not be used for both LD/CI and MALDI experiments. Instead, the infrared laser (TEA-CO_2) was tested for its ability to do MALDI.

IR lasers have been used for MALDI by several groups.[110-115] However, in most of these cases the IR laser used was an Er:YAG laser with a wavelength of 2.94 μm or a tunable laser which was operated at wavelengths around 2.94 μm. CO_2 lasers with a wavelength of 10.6 μm have also been used in a few cases.[116,117] In a direct comparison of IR and UV MALDI, it was noted that the IR MALDI yielded superior spectra.[118] It was assumed that this was the result of a lower degree of metastable decay and adduct ion formation which led to greater resolution in a time-of-flight mass analyzer. The authors

noted that the fraction of laser shots which led to a discernable signal with IR MALDI (even when operated well above threshold intensity) was much lower than those found in UV MALDI. In assessing the performance of an Er:YAG laser for IR MALDI, it was noted that 100 –1,000-times more material was ablated during IR MALDI compared to UV MALDI with a comparable spot size.[119] Since single laser shots produced spectra of comparable intensity, this meant that the ionization efficiency of IR MALDI (compared to the amount of analyte desorbed) must have been 2 to 3 orders of magnitude less than that of UV MALDI.

To investigate the possibility of using a CO_2 laser for MALDI (for a comparison of sensitivity between MALDI and LD/CI), several different MALDI matrices were evaluated. DHB, sinapinic acid, and caffeic acid were all tried as matrices for IR MALDI. All of these matrices had recently been used for IR MALDI by various groups. The matrices were dissolved in methanol to produce solutions of 10 μg/μL. Spiperone was used as the analyte for the evaluation of the different matrices. A 10 μL aliquot of the DHB matrix solution was mixed with a 10 μL aliquot of a 1.0 μg/μL solution of spiperone prepared in aqueous 1% acetic acid solution. A 1.0 μL drop of the above mixture was pipetted onto a probe tip and allowed to air dry. While the ratio of analyte to matrix in this composition was higher than what is normally used in MALDI (1:10 in these experiments compared to1:1,000 in traditional MALDI), earlier experiments with a concentration of matrix one and two orders of magnitude

more did not produce significantly different results. The ratio was kept low to minimize the amount of material ablated in later experiments where the electron ionization (EI) filament was turned on during the MALDI desorption event. The CO_2 laser spot size was adjusted (by using the iris to block the beam before focusing) to a round spot approximately 100 μm in diameter (measured by visual inspection). Since the probe tip was 4 mm in diameter, the laser beam irradiated approximately $1/1600^{th}$ of the total surface area of the probe. The 1.0 μL of the applied mixture had 0.5 μg of spiperone; assuming a uniform distribution across the probe tip face (as it appeared when viewed under a microscope at 30X power), each sampling spot represented a total of 310 picograms of spiperone. Initial experiments were tried with an order of magnitude less spiperone but it was found that this level was below the threshold of consistent detection.

Figure 4.9 shows a spectrum produced by one laser shot of IR MALDI with DHB as the matrix. The inset of figure 4.9 shows a close up of the region around the spiperone $[M+H]^+$ ion at m/z 396. Inspection of the probe tip after a single laser shot revealed that all of the DHB crystals from a spot of 100 μm in diameter had been removed. The spectrum in figure 4.9 represents a typical single shot spectrum out of a total of 20 collected across the probe tip (the location was changed for each laser shot).

Sinapinic acid and caffeic acid were next evaluated using the same procedure as that used for DHB. Figure 4.10 and figure 4.11 show a typical

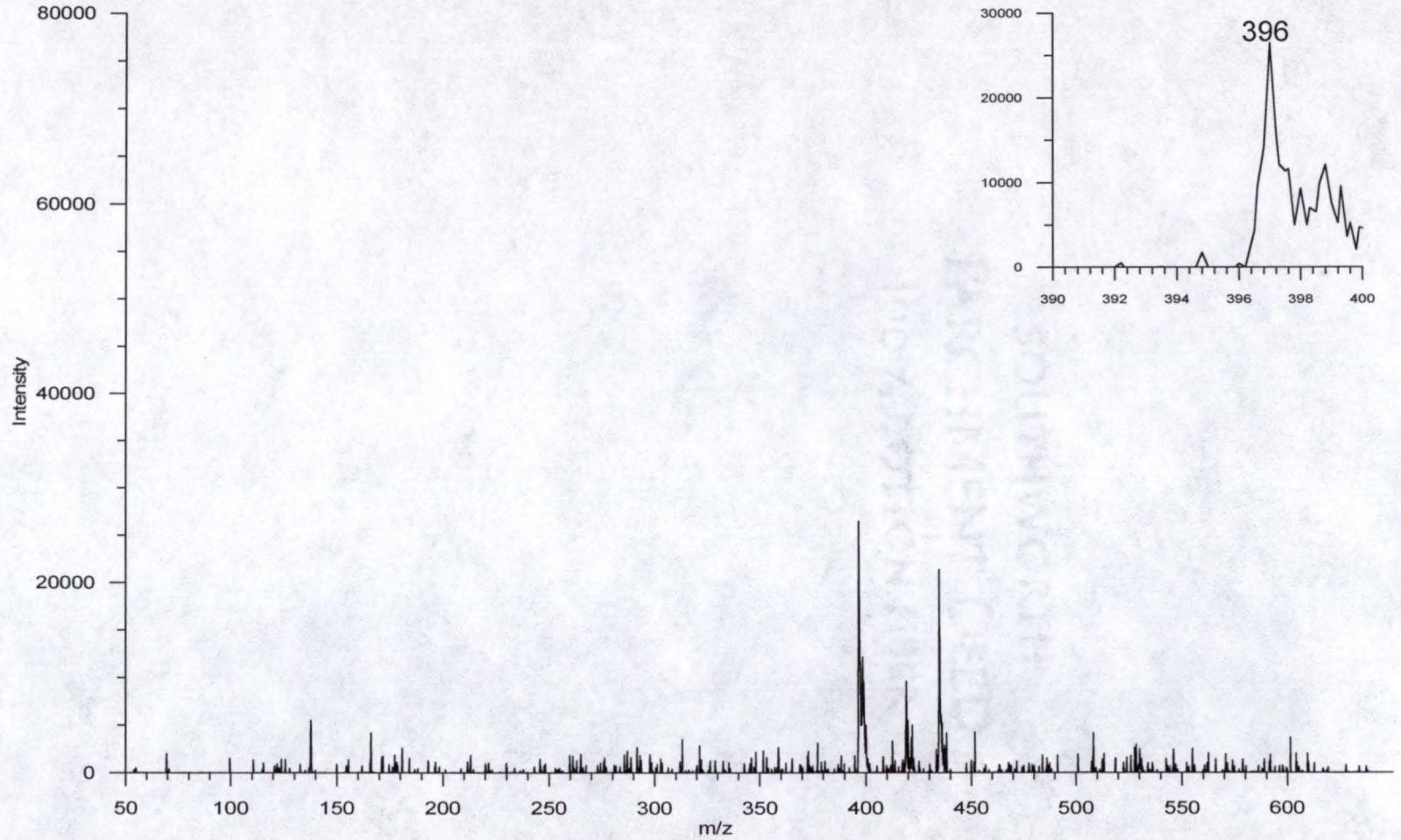

Figure 4.9. Infrared MALDI of spiperone using CO_2 laser and DHB as matrix. Spectrum represents one laser shot (310 picograms of spiperone). Inset shows ion at m/z 396 which corresponds to spiperone $[M+H]^+$ ion.

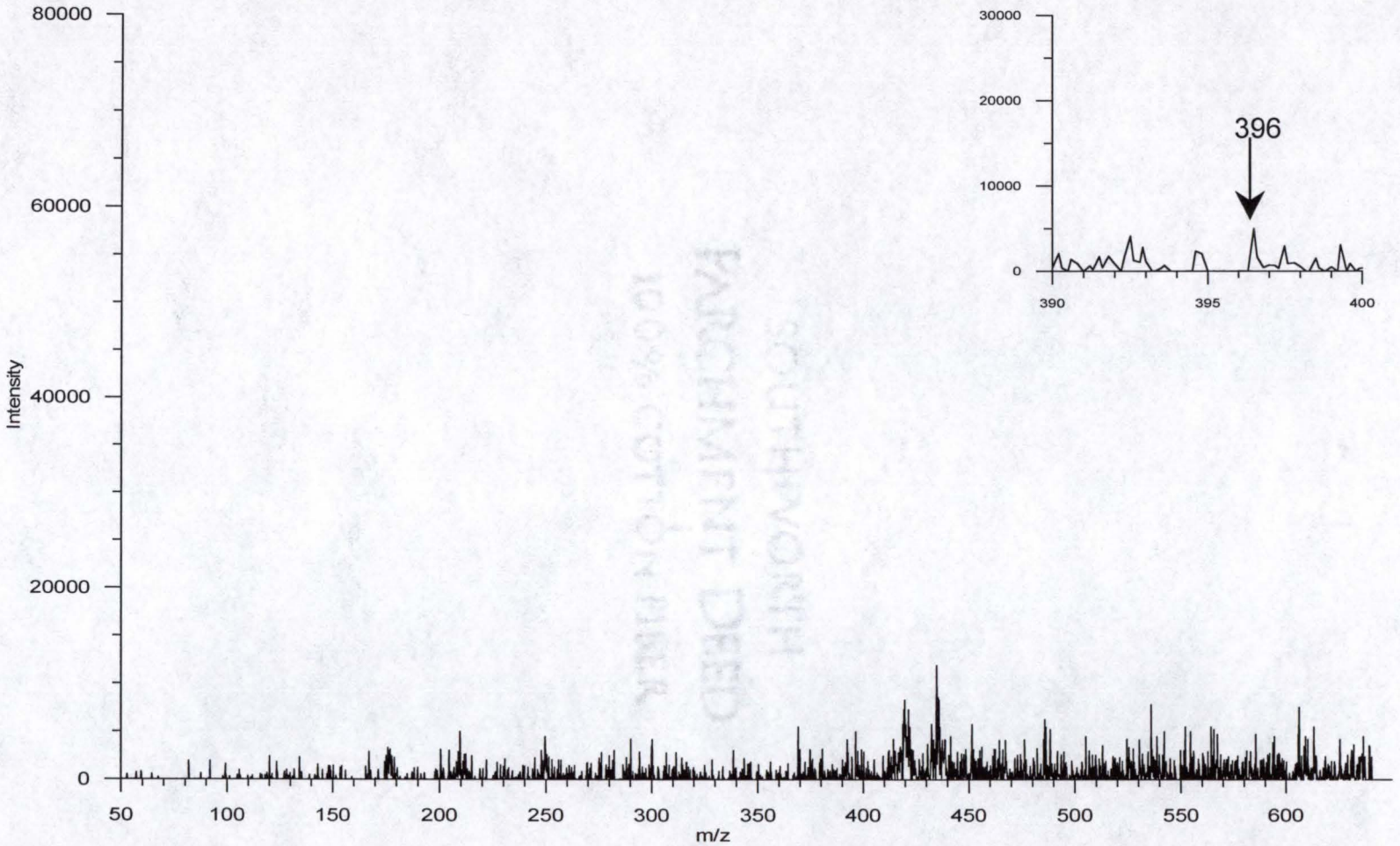

Figure 4.10. Infrared MALDI of spiperone using CO_2 laser and sinapinic acid as the matrix. Spectrum represents one laser shot (310 picograms of spiperone). Inset shows ion at m/z 396 which corresponds to spiperone $[M+H]^+$ ion.

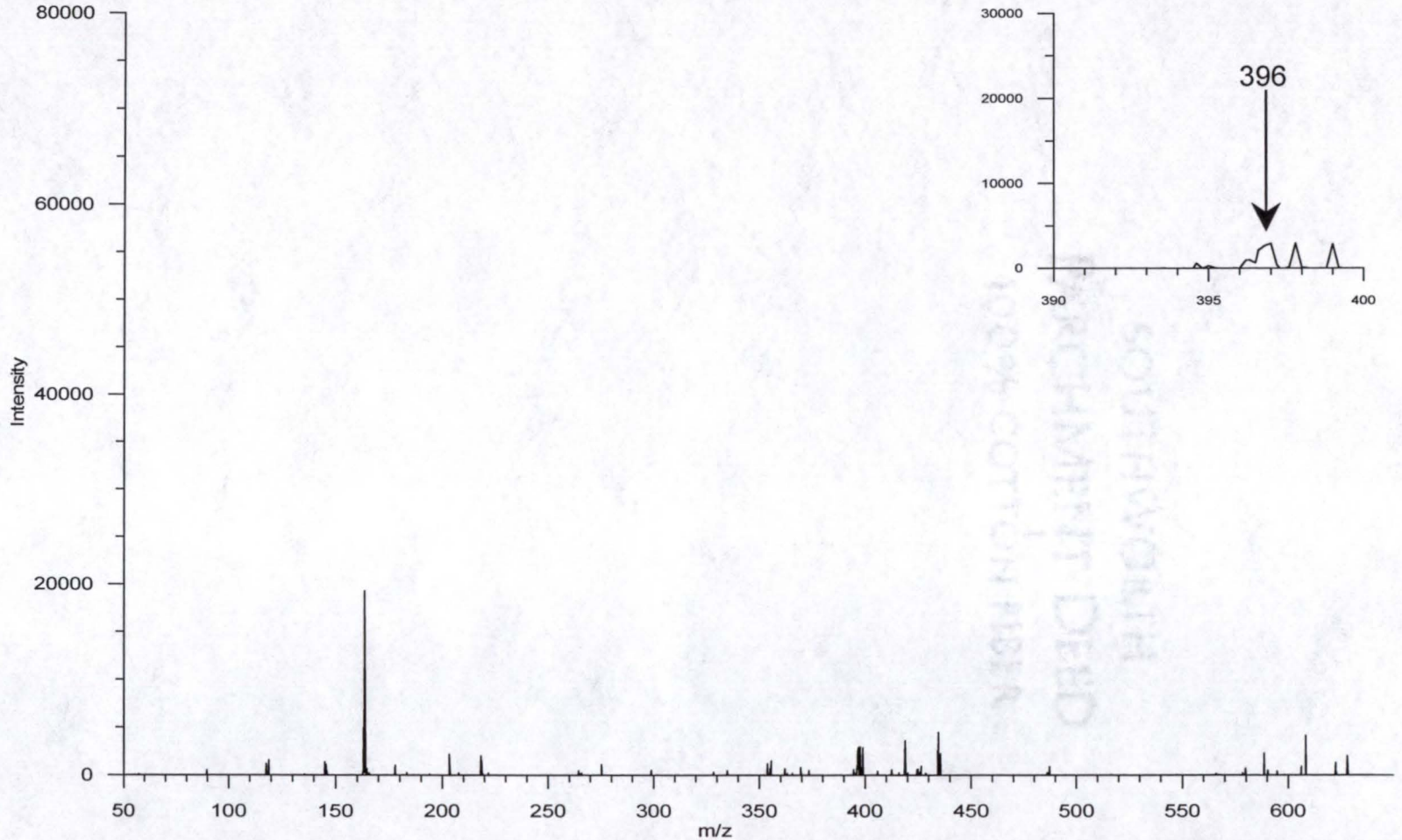

Figure 4.11. Infrared MALDI of spiperone using CO_2 laser and caffeic acid as the matrix. Spectrum represents one laser shot (310 picograms of spiperone). Inset shows ion at m/z 396 which corresponds to spiperone $[M+H]^+$ ion.

single shot spectrum for sinapinic acid and caffeic acid respectively. The intensity scale on all three figures was held constant so that the relative ionization efficiency could be evaluated. It is easy to see from a comparison of figures 4.9 through 4.11 that the matrix DHB provided superior ionization efficiency (approximately 28,000 counts compared to approximately 500 counts for sinapinic acid and caffeic acid). However, the purpose of the experiments was to compare the sensitivity of MALDI to that of LD/CI. In order to the compare the relative ionization efficiencies of IR MALDI to LD/CI, 10 μL of a 1.0 μg/μL of spiperone in aqueous 1% acetic acid solution was mixed with 10 μL of neat methanol. As was done in the MALDI experiments, 1.0 μL of the mixture was pipetted onto a probe tip and allowed to air dry. Figure 4.12 shows the spectrum produced by a single laser shot under conditions of methane CI. The maximum of the intensity scale for the LD/CI spectrum was increased to the maximum for the instrument and represented a 1.5 X increase in intensity over that used for the IR MALDI experiments; even so, the ion at m/z 396 (the $[M+H]^+$ ion of spiperone) was off-scale in intensity.

To verify that the low signal intensity seen from IR MALDI compared to LD/CI was the result of IR MALDI and not of the MALDI process in general, the same solutions used in the IR MALDI experiments were used for a series of UV MALDI experiments. The UV laser beam was adjusted by defocusing to a round spot of approximately 100 μm diameter (the same size as the laser spot used in the IR MALDI experiments). In order to remove all of the material

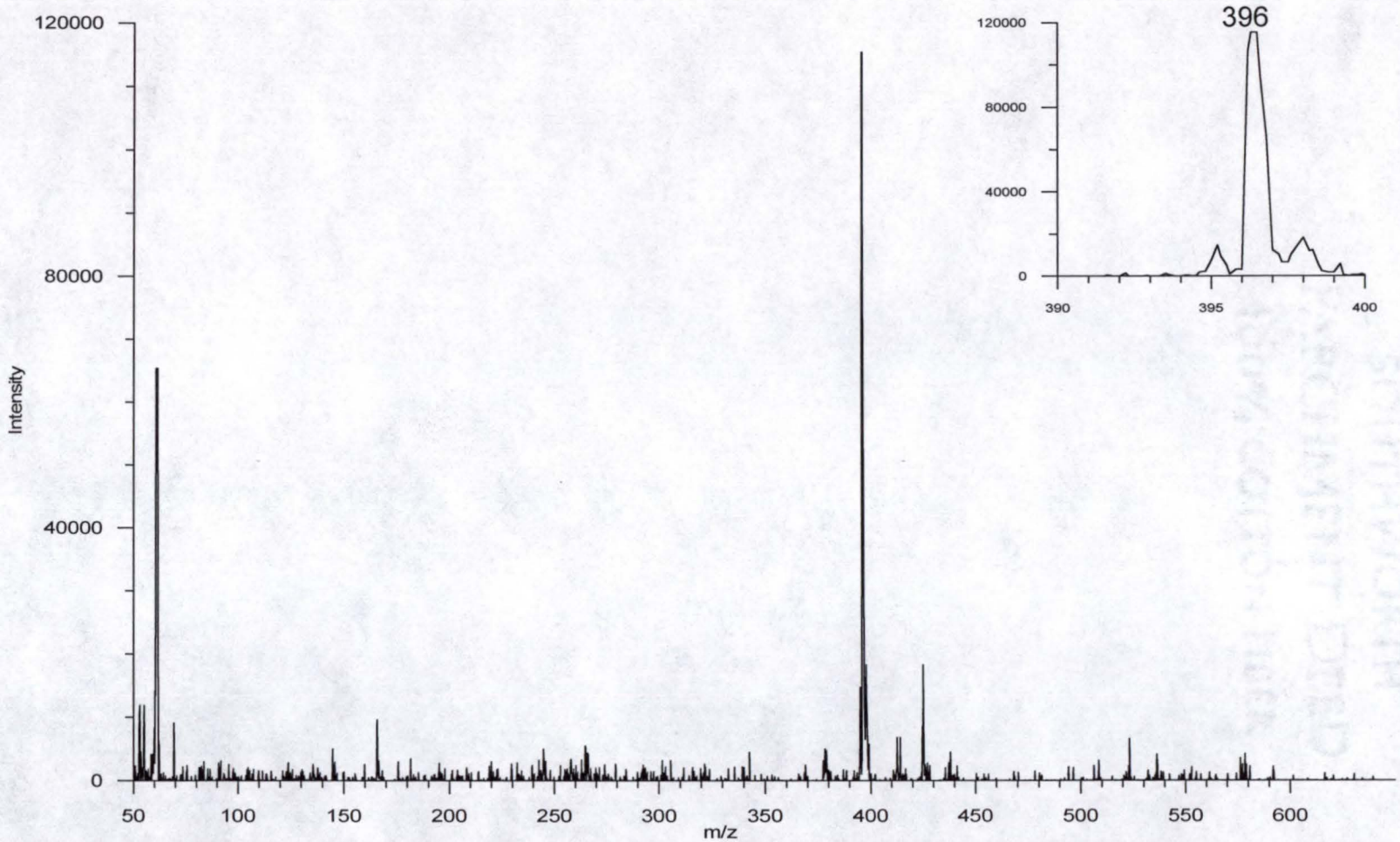

Figure 4.12. Methane LD/CI of spiperone using CO_2 laser. Inset shows the area around m/z 396 which corresponds to the spiperone $[M+H]^+$ ion. Note that the ion intensity scale is 1.5 times the MALDI ion intensity scale and that ion at m/z 396 is off-scale.

during sampling (as was done in IR MALDI), the number of laser shots per micro-scan was increased to 5. Each micro-scan is averaged to produce an analytical-scan, and 4 micro-scans (of 5 laser shots each) were used for each analytical scan in the UV MALDI experiments. The spectra presented in figures 4.13 through 4.15 represent the average of 4 micro-scans (of 5 laser shots each) for a total of 20 laser shots during each sampling event. After 20 laser shots, visual inspection showed that most of the material on the probe tip was removed from a spot size of approximately 100 μm in diameter. A comparison of figures 4.9 through 4.11 to figures 4.13 through 4.15 clearly show that UV MALDI produced a significantly greater signal intensity per amount of material ablated. Considering that the UV MALDI spectra represent the average of 4 micro-scans, it can be assumed that if all 20 laser shots were summed (the instrument could not be operated in a summing mode), the intensity of the m/z 396 ion would be even greater. These results were consistent with what had been observed in past comparisons of LD/CI and UV MALDI, that the two techniques produce similar signal intensity.

It was obvious from the above experiments that IR MALDI (under the conditions used for these experiments) was not as sensitive as UV MALDI and therefore should not be used to compare the sensitivity of electrosprayed MALDI and LD/CI from tissue samples. However, it was of interest to verify that the amount of material ablated during the IR MALDI event was greater

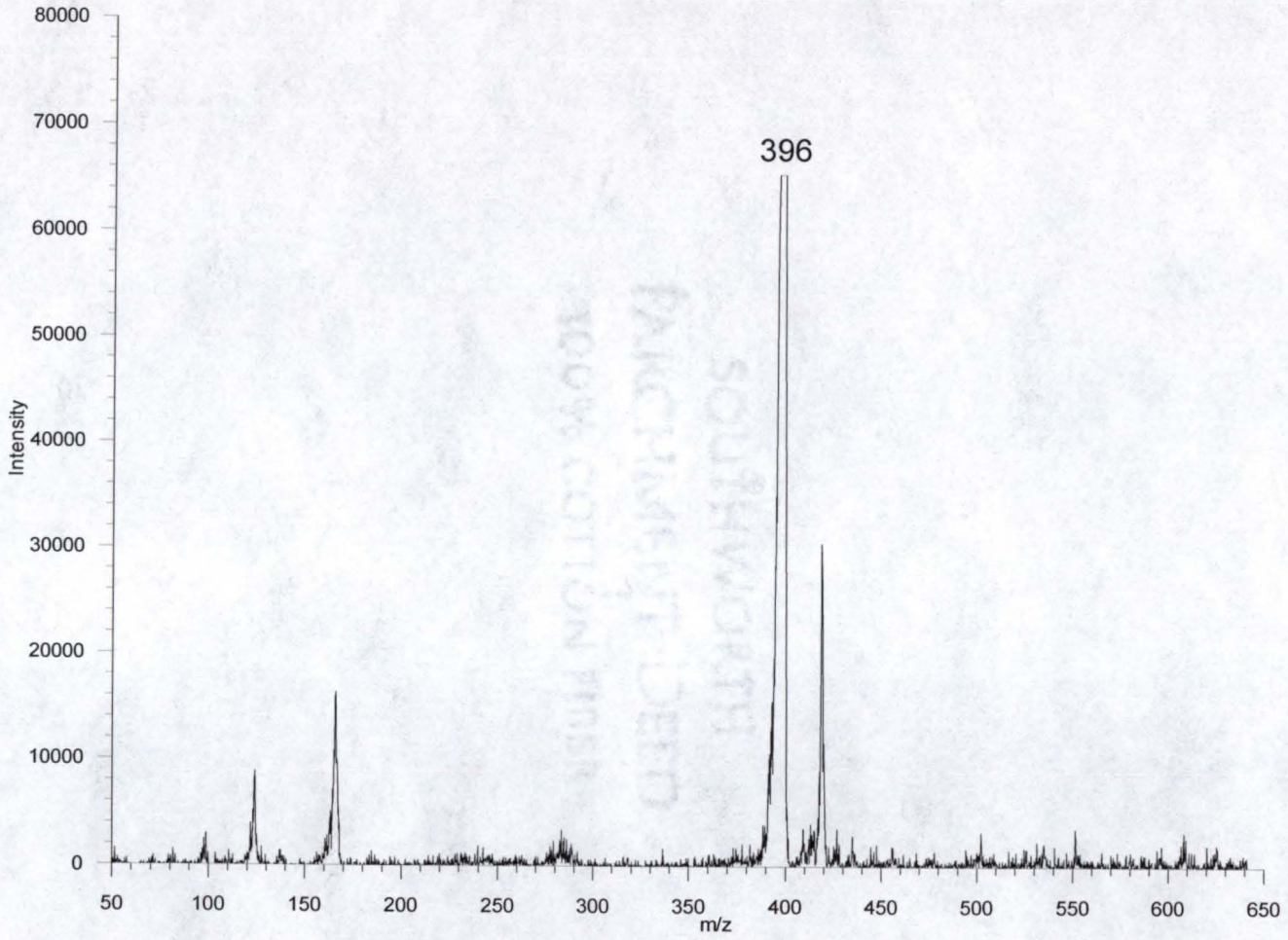

Figure 4.13. UV laser MALDI of spiperone in DHB. Ion intensity scale is same as in IR MALDI experiments. Note that peak at m/z 396 is off-scale.

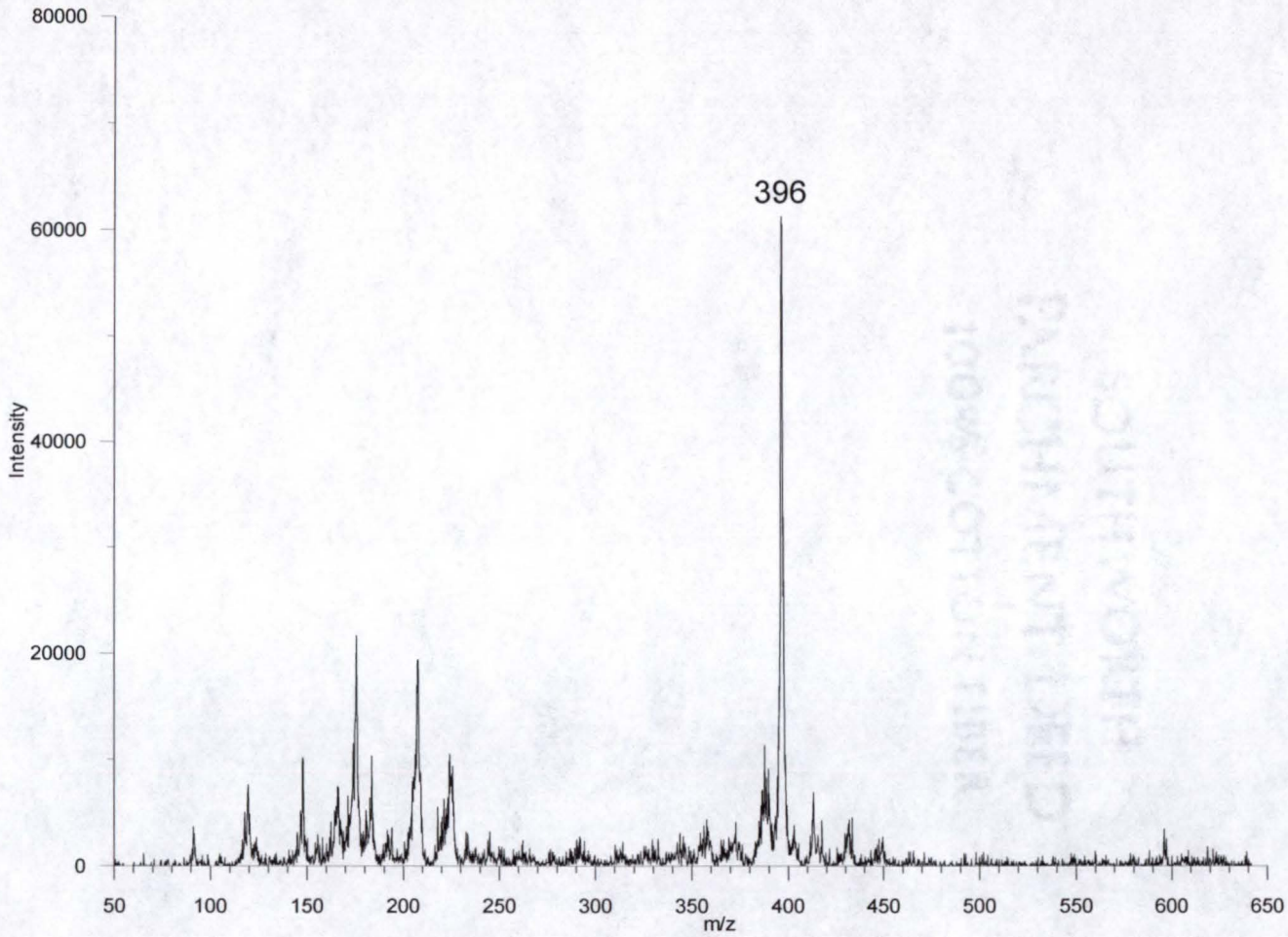

Figure 4.14. UV laser MALDI of spiperone in sinapinic acid. Ion intensity scale is same as in IR MALDI experiments.

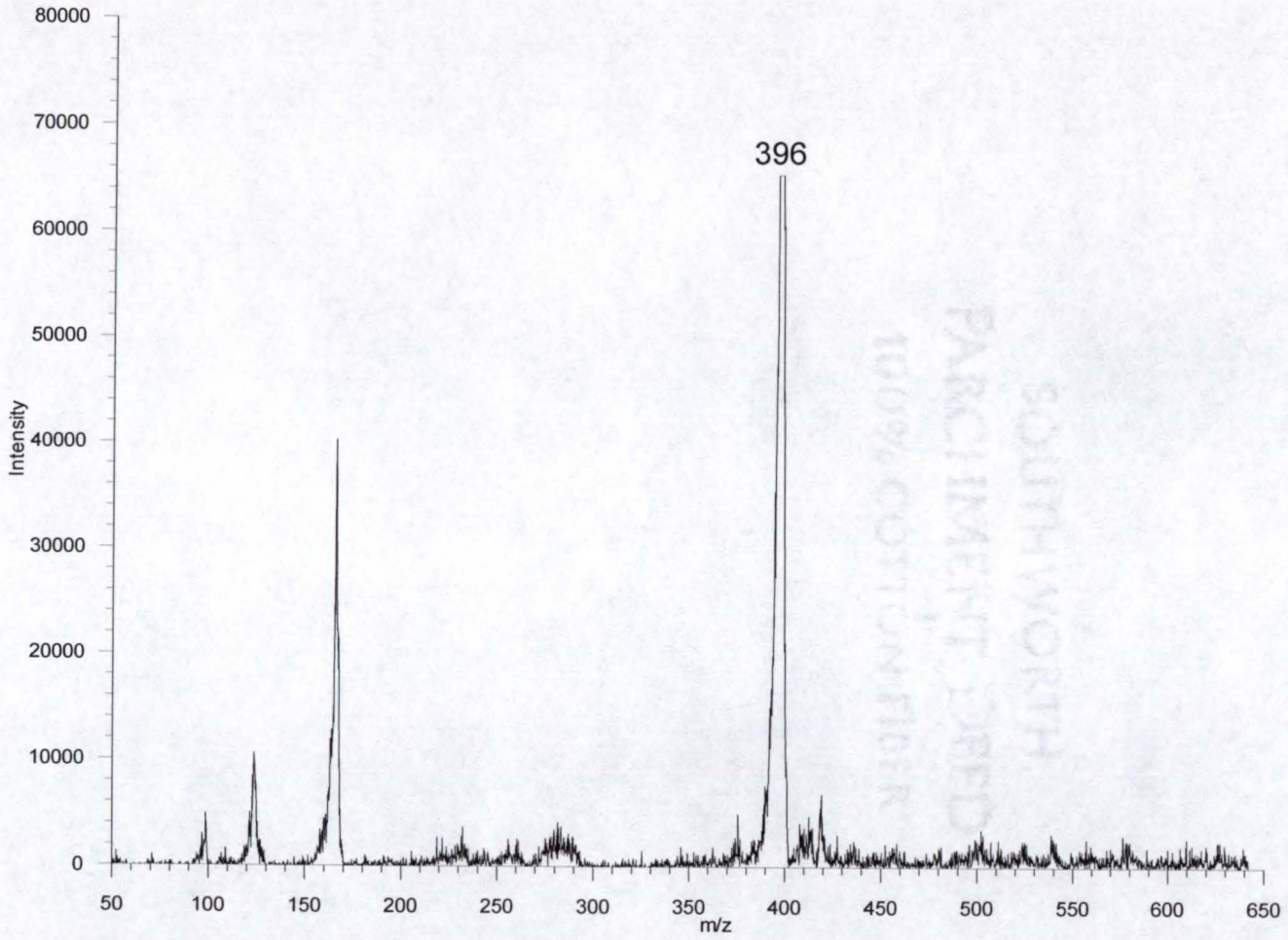

Figure 4.15. UV laser MALDI of spiperone in caffeic acid. Ion intensity scale is same as in IR MALDI experiments. Note that peak at m/z 396 is off-scale.

than that indicated by the ion intensity. Visual inspection showed that the amount of material (matrix) removed during IR and UV MALDI experiments was the same; however, it was possible that during IR MALDI the matrix was ejected from the surface as large crystal fragments which were too large to enter the gas phase. To verify that it was the ionization efficiency of IR MALDI, not the desorption event, which led to the low signal intensity, the electron beam was turned on during the laser desorption event. The electron beam will ionize some of the ablated material which is desorbed as neutrals during IR MALDI. All experimental parameters were the same as in the IR MALDI experiments. Figures 4.16 through 4.18 show the results of a single CO_2 laser shot with the electron beam turned on. The flattening of the low m/z ions (from the matrix) indicates that the amount of material ablated and ionized by the electron beam produced a signal which was off the scale of the instrument. The signal of the matrix ions in figure 4.16, 4.17, and 4.18 was significantly greater than that detected with the electron beam turned off (figures 4.9, 4.10, and 4.11). This indicated that a large portion of the gas-phase material produced during IR MALDI was neutrals. For comparison, the electron beam was turned on during the desorption event while performing UV MALDI under the same set of experimental conditions as was used in the previous UV MALDI experiments (Figure 4.19). As was seen in IR MALDI, there was an increase in matrix ion intensities between UV MALDI with the electron beam on as compared to UV MALDI with the electron beam turned off

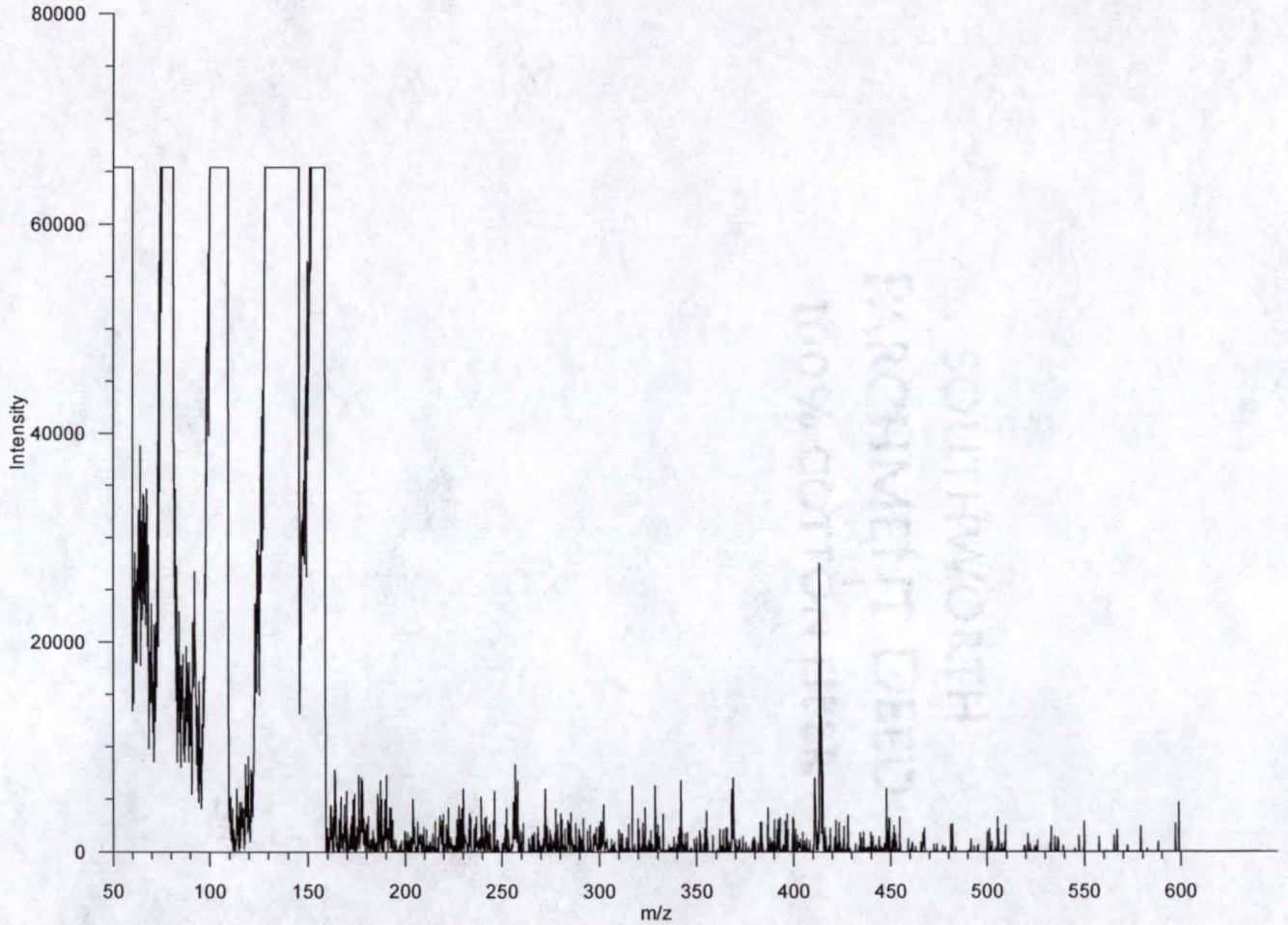

Figure 4.16. IR MALDI of spiperone in DHB. Electron filament was turned on during desorption event. The flat tops of the low m/z ions (from matrix) indicate that ion intensity was significantly off-scale.

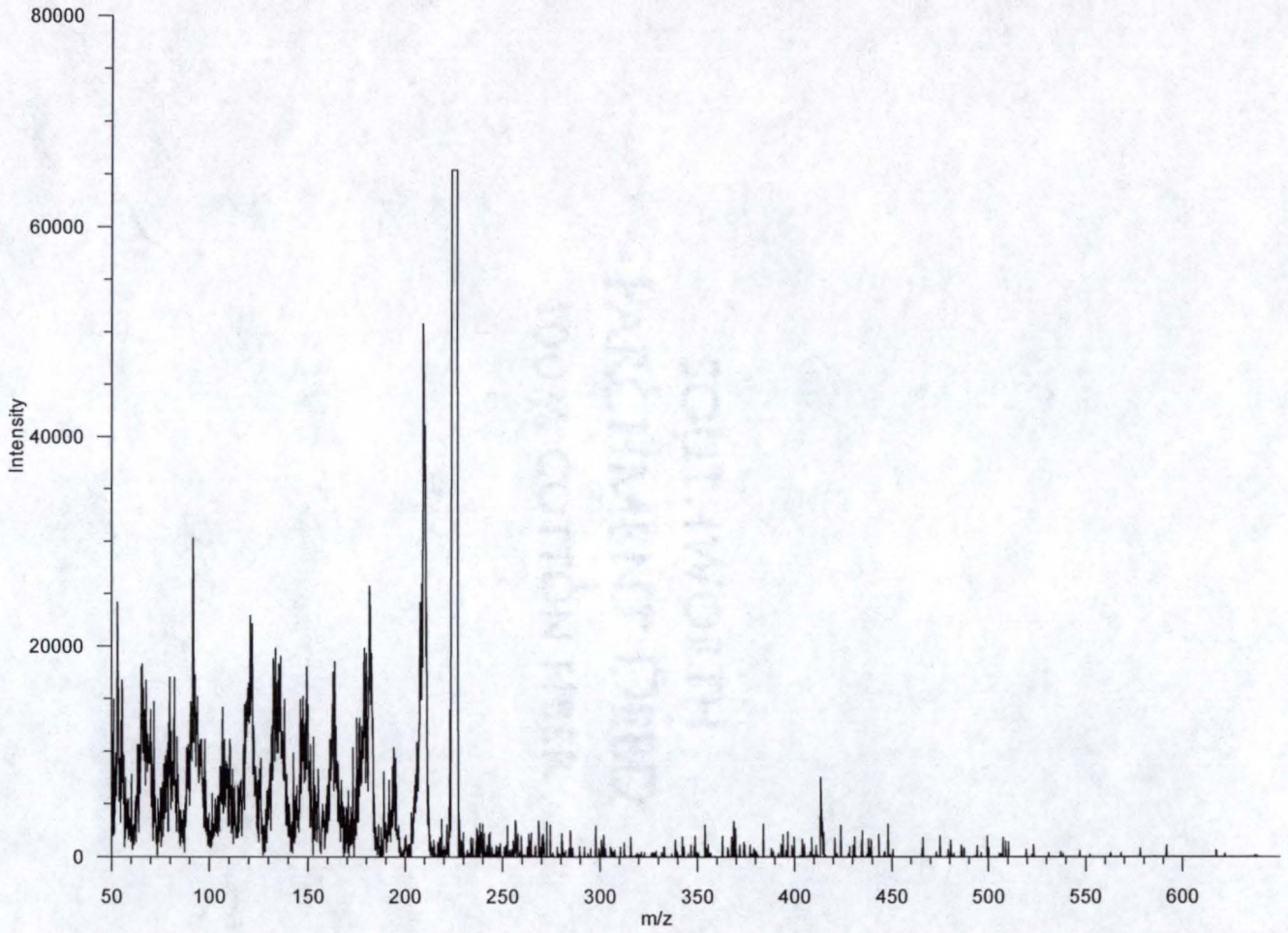

Figure 4.17. IR MALDI of spiperone in sinapinic acid. Electron filament was turned on during desorption event. The flat top of the ion at m/z 225(from matrix) indicate that the ion intensity was off-scale.

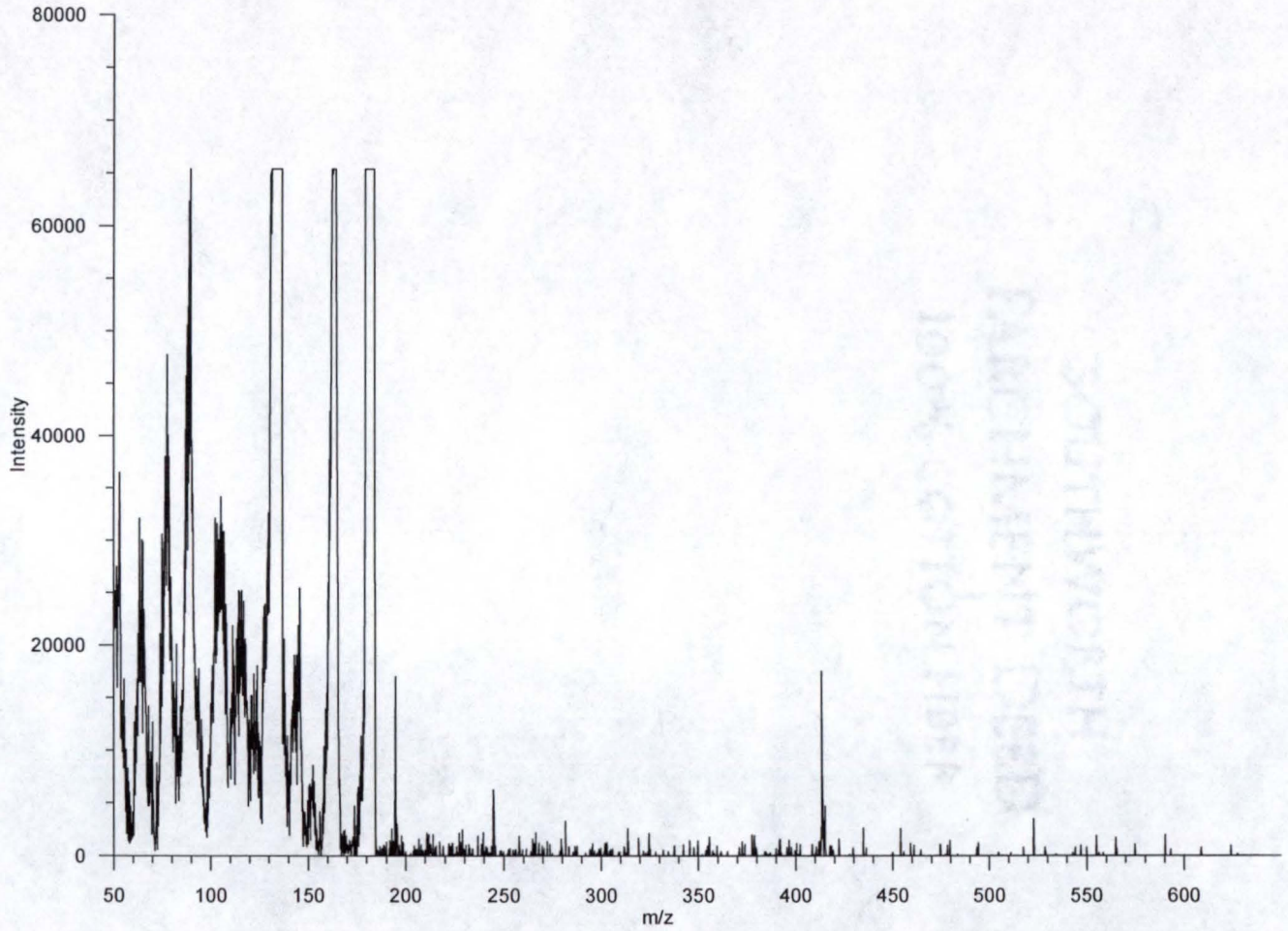

Figure 4.18. IR MALDI of spiperone in caffeic acid. Electron filament was turned on during desorption event. The flat tops of the low m/z ions (from matrix) indicate that ion intensity was significantly off-scale.

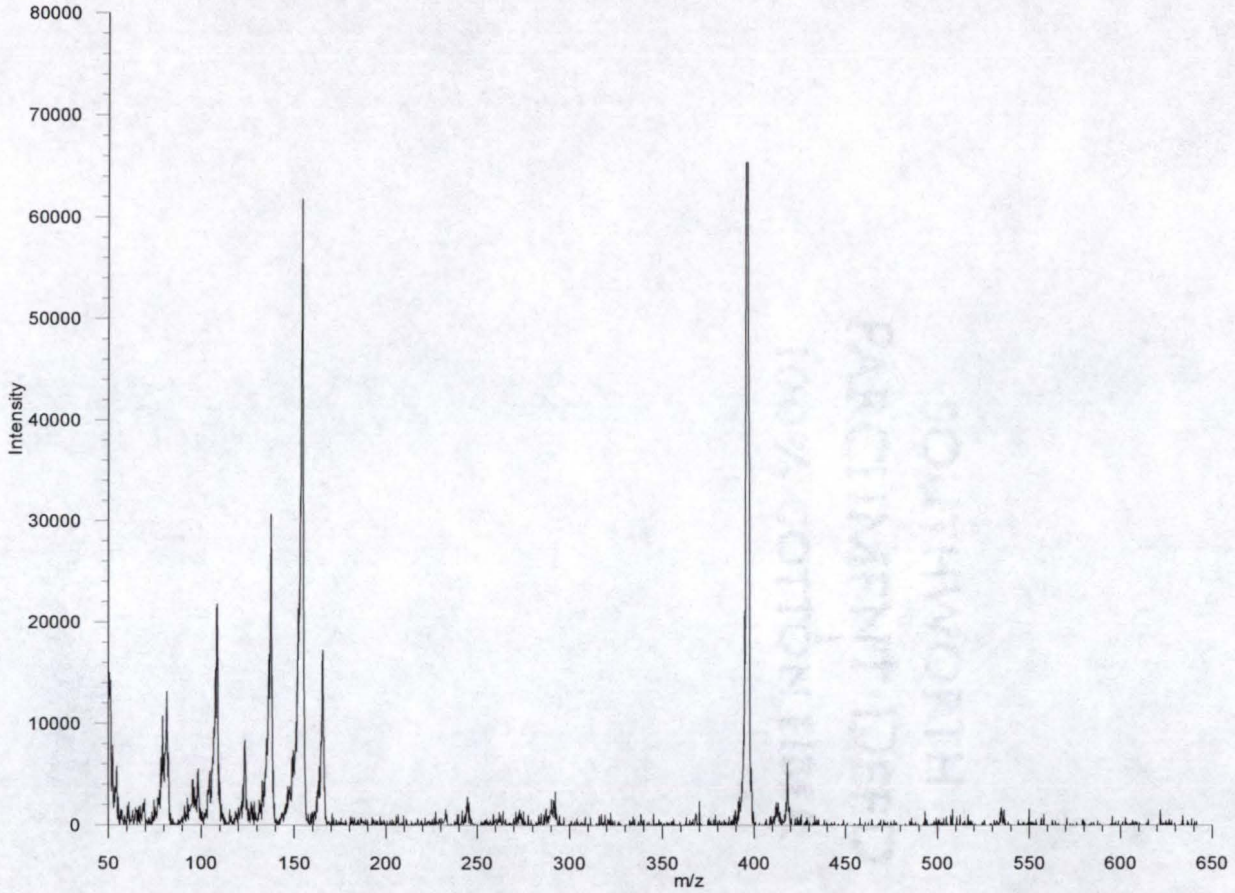

Figure 4.19. UV MALDI of spiperone in DHB matrix with electron filament turned on. Note that the intensity of the low m/z ions are not as large as those during IR MALDI with electron filament turned on. This would suggest that even with 5 laser shots, the amount of ablated matrix in the UV MALDI experiments was not as great as in the IR MALDI experiments.

(comparing figures 4.13 and 4.19. Because the intensity of the matrix ion signals produced during IR MALDI with the electron beam turned on were off the scale of the instrument, it is impossible to make a direct comparison between the neutral material desorbed during IR MALDI and the neutral material desorbed during UV MALDI, but considering that the spectrum in figure 4.19 (UV MALDI) was the average of 4 micro-scans, this suggests that the amount of neutral gas-phase material ablated in the IR MALDI experiments was comparable to the amount of neutral gas-phase material ablated in the UV MALDI experiments. It should be noted that the ion at m/z 414 in the IR MALDI spectra with the electron beam turned on was believed to be the $[M+H_2O+H]^+$ ion of spiperone; however, MS/MS was not performed to verify this.

While these experiments evaluated only three MALDI matrices which are commonly used both in UV and in IR MALDI, the results were consistent with what had been noted by other groups investigating the IR MALDI process: that the ionization process during IR MALDI (comparing the amount of ablated material to the ion signal intensity produced) is about 2 to 3 orders of magnitude less efficient than that of UV MALDI.[119]

Since the UV laser was not capable of consistently producing ions during laser desorption of tissue and the IR laser produced inferior sensitivity during MALDI, a direct comparison of laser desorption coupled to chemical ionization and MALDI was not possible.

CHAPTER 5
APPLICATION OF ELECTROSPRAYED MALDI MATRIX SOLUTION AND LD/CI TO THE MAPPING OF PHARMACEUTICAL COMPOUNDS IN INTACT TISSUE SAMPLES

In order to verify that the quadrupole ion trap laser microprobe instrument was capable of mapping the location of pharmaceutical compounds at trace levels in intact tissue, a series of experiments was performed to demonstrate the ability to differentiate between tissue spiked with pharmaceutical compounds and non-spiked tissue. Both LD/CI and MALDI were evaluated in these experiments.

Spiperone

As in the previous spatial experiments, the drug spiperone was used as a model pharmaceutical compound for investigations into the mapping ability of the instrument. A 3.6 mg thin slice of rat liver tissue was placed in a stainless steel well. A 1.8 μL aliquot of a100 ng/μL solution of spiperone in aqueous 1% acetic acid solution was pipetted onto the tissue. A similar (5.3 mg) slice of rat liver tissue was placed in a similar well and 2.5 μl of an aqueous 1% acetic acid solution was pipetted onto the tissue. Both samples were left undisturbed for the next hour. At the end of one hour, the non-spiked tissue sample was removed and rinsed with several aliquots of aqueous 1%

acetic acid solution and then blotted dry. Approximately one half of the non-spiked tissue sample was placed on one side of a stainless steel probe tip. After placing the non-spiked piece on the probe tip, the tissue piece which had been spiked with spiperone was removed from its well and washed with several aliquots of aqueous 1% acetic acid solution. The spiked tissue was blotted dry and then placed on the probe tip next to non-spiked piece of tissue. The remaining half of the non-spiked rat liver tissue was then blotted dry and placed on the other side of the spiked piece of tissue. Figure 5.1 shows the final arrangement of tissue pieces on the probe tip. The spiked tissue piece formed a slice of tissue in the middle of the two non-spiked tissue pieces that lay to either side. The sample was allowed to air dry (approximately one hour). After drying, the tissue had visibly shrunk and the three different regions of the tissue were more easily discernible (Figure 5.2). The sample was electrosprayed with a solution of 70% methanol and 30% aqueous 1% acetic acid which had 10 μg/μL of the MALDI matrix DHB dissolved in it. The tissue sample was sprayed for approximately 7 minutes (at a rate of 5 μL/min this delivered 350 μg of matrix). After electrospraying, the tissue was clearly visible beneath the thin matrix coating (Figure 5.3). The sample was then investigated using the quadrupole ion trap laser microprobe instrument. Each micro-scan collected consisted of four laser shots; four micro-scans were averaged into each analytical-scan. At each spot sampled across the surface of the tissue, four analytical scans were collected. The X,Y-stage micrometers

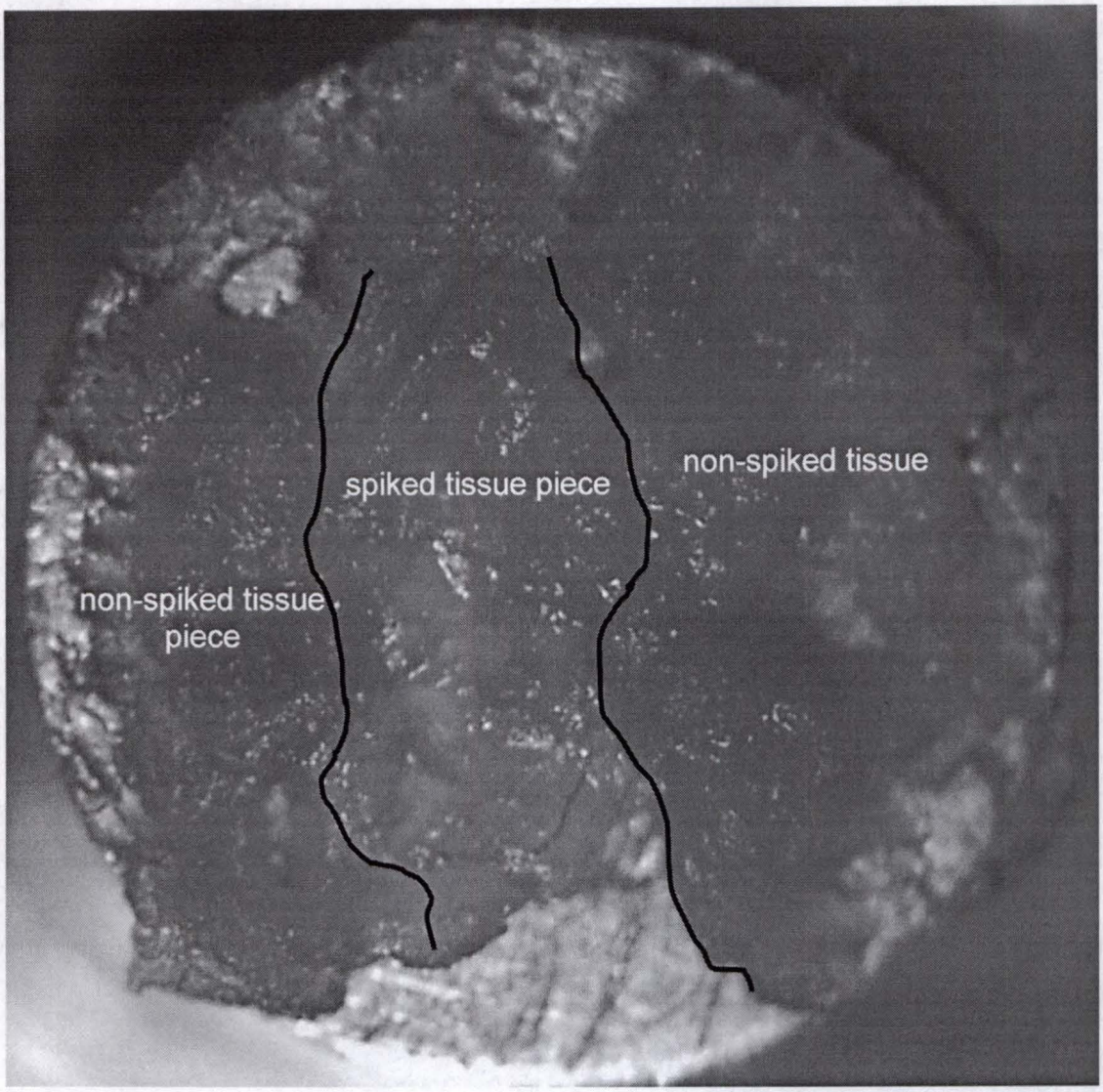

Figure 5.1. Photomicrograph of three different tissue pieces placed side by side on probe tip to simulate a continuous piece of tissue. The lines dividing the three regions of tissue have been added to mark the three different pieces. The tissue piece in the middle was spiked with the drug spiperone at a level of 25 ng/ mg of tissue.

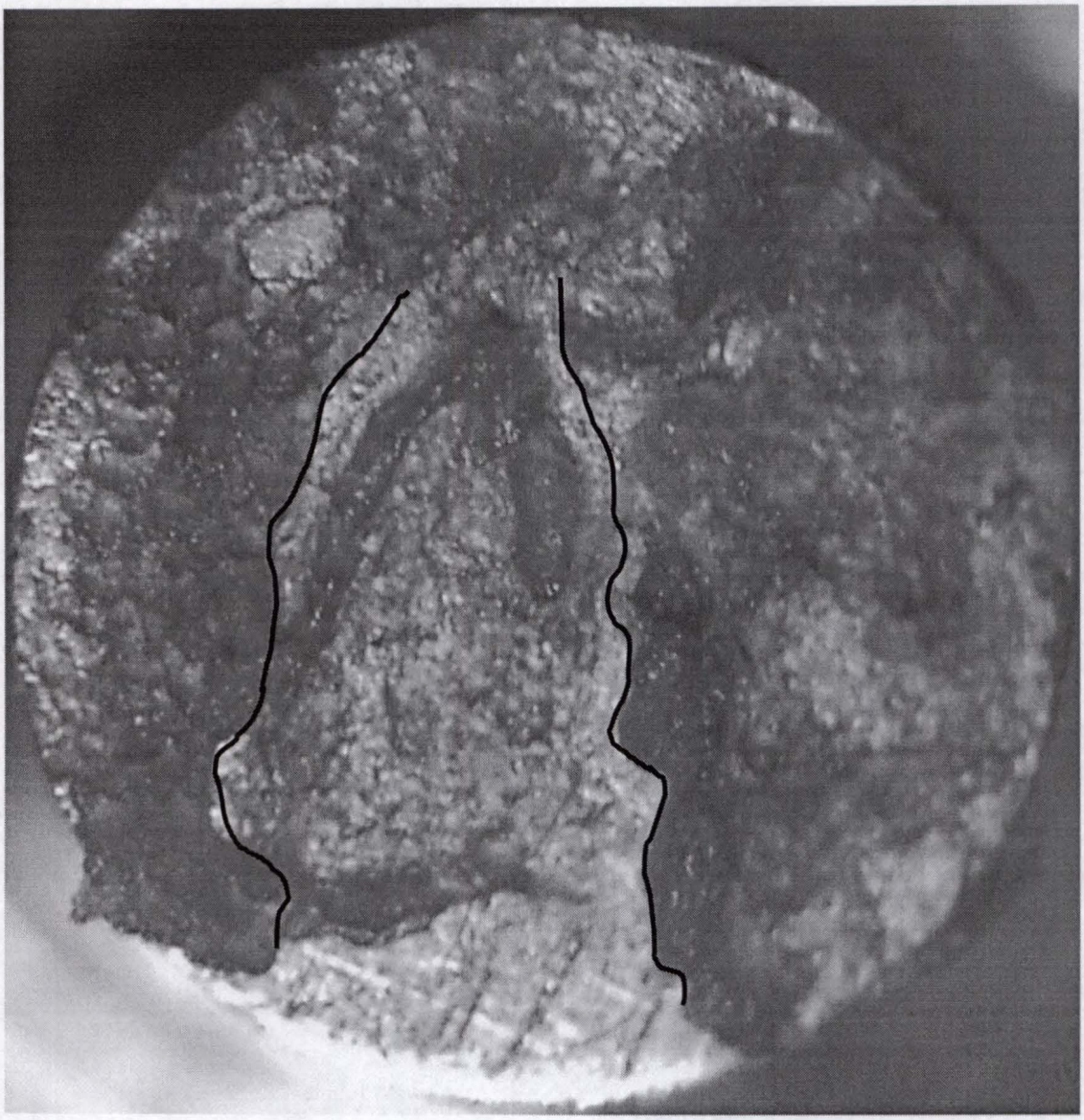

Figure 5.2. Photomicrograph of tissue sample in figure 5.1 after one hour of drying. The three regions of tissue were more easily visible after the tissue was allowed to dry. The lines have been added to the photomicrograph to aid in the identification of the three different tissue pieces.

Figure 5.3. Photomicrograph of tissue sample from figure 5.1 after electrospraying of MALDI matrix DHB onto surface. The tissue was still clearly visible beneath the thin coating of MALDI matrix. The lines have been added to the photomicrograph to indicate the different tissue pieces on the probe tip.

were turned one half turn after each sampling to move the location of the tissue beneath the laser beam approximately 150 μm each time. Figure 5.4 shows the tissue sample after investigation (the arrows in Figure 5.4 point to the spots across the surface of the tissue sample where the laser beam sampled the surface). The 64 laser shots at each point produced a spot of approximately 50 μm in diameter (as measured by visual inspection). It is interesting to note that in several locations the MALDI matrix took on an opaque, white appearance that obscured visualization of the tissue beneath it after sampling. There are several possible explanations for this phenomena. The most likely explanation for the change in the appearance of the MALDI matrix is that trapped moisture beneath the matrix coating (whether from the tissue or from the MALDI matrix solvent electrosprayed onto the tissue) evaporated during the time which the sample was under vacuum. This evaporation of solution may have caused the tissue to pull away slightly from the matrix coating. While this made easy visualization of the tissue sample beneath the matrix difficult, many of the major areas on the tissue were still visible. MS/MS by CAD was performed on the m/z 396 ion (which corresponds to the spiperone $[M+H]^+$ ion) at each sample location. The sum of the characteristic daughter ions of spiperone (at m/z 123, 165, 232, and 291) was calculated for each analytical scan. The mean intensity of the summed ion intensities for each of the four analytical scans at each location across the surface of the tissue is plotted at each sampled location in figure 5.5. The

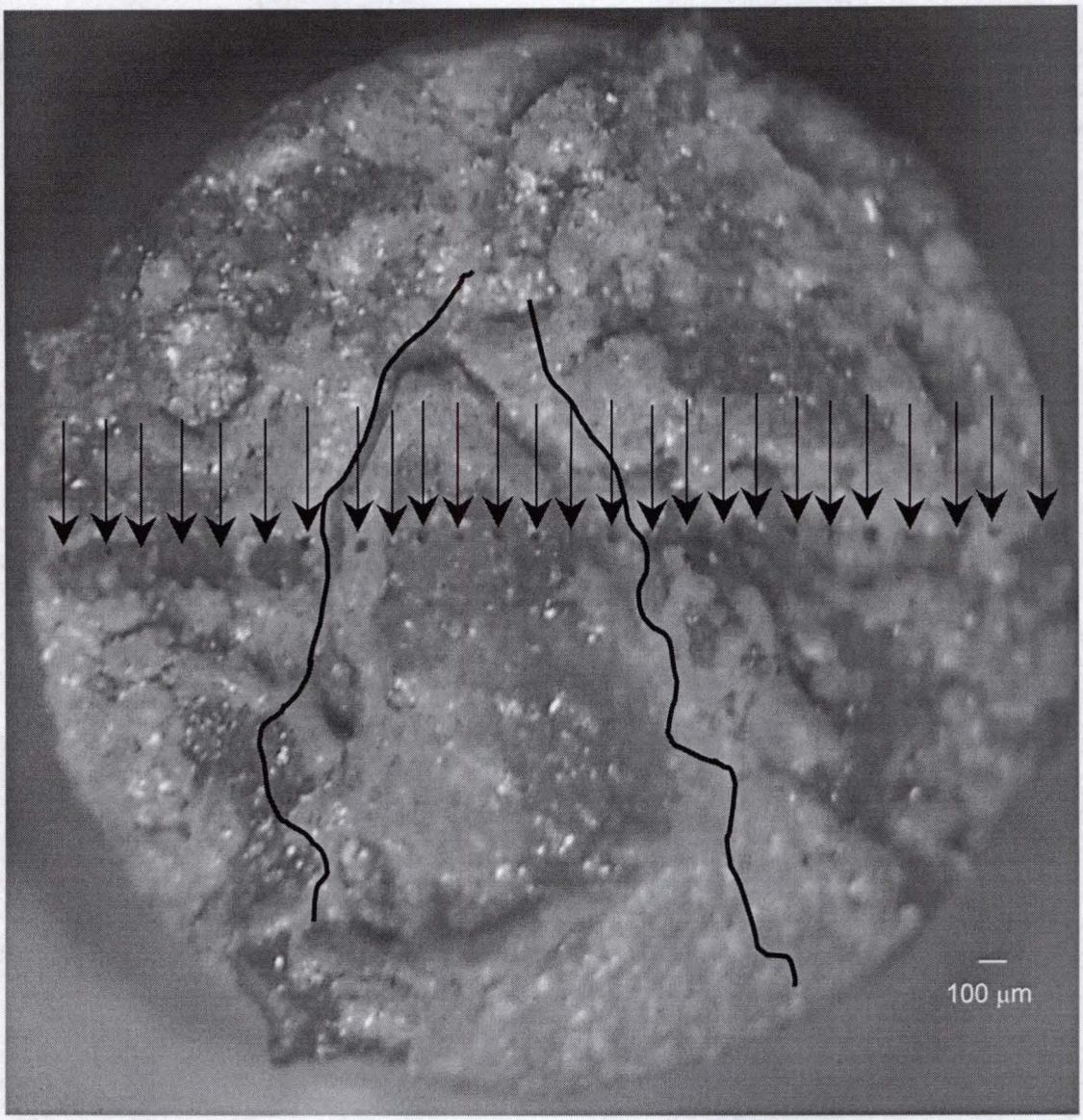

Figure 5.4. Electrosprayed tissue sample after investigation. Note that the tissue is not as clearly visible beneath the MALDI matrix coating. It is believed that during investigation (under vacuum) the tissue continued to shrink due to evaporation of solvent trapped beneath the matrix, or from evaporation of moisture retained in tissue. Arrows have been added to indicate sampling locations.

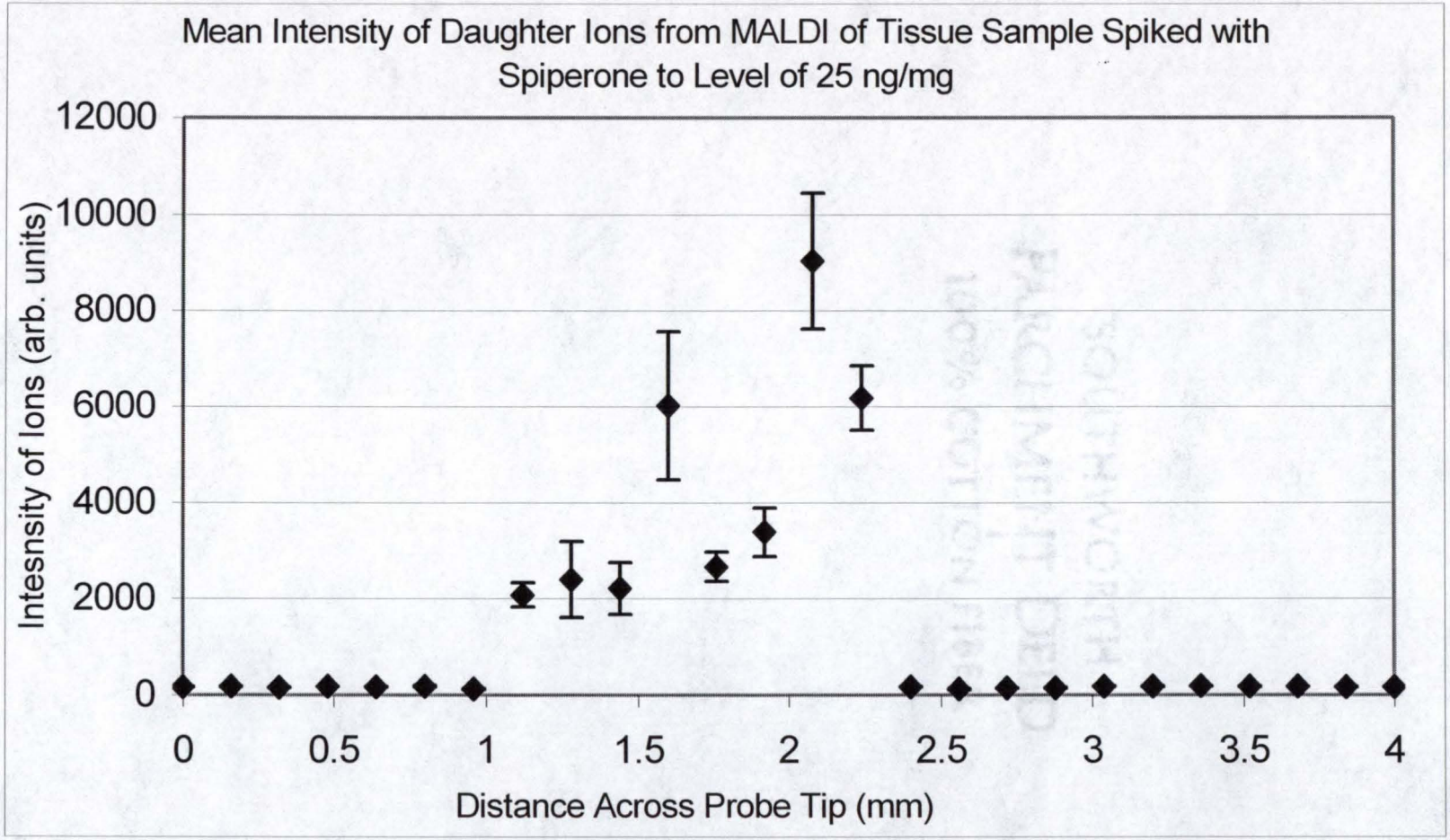

Figure 5.5. Plot of the mean of the sum of characteristic daughter ions (at m/z 123, 165, 232, and 291) from locations across surface of tissue sample electrosprayed with MALDI matrix. The error bars represent ± 1 standard deviation of the mean from the four analytical scans averaged.

spots which produced daughter ion intensities above that of random noise (points 8 through 15, going from left to right across the tissue surface) correspond exactly with the spots produced by the laser beam on the tissue sample spiked with spiperone.

It should be noted that this technique is not designed to quantitate the amount of detected spiperone in the tissue sample. Figure 5.5 shows the rather large variation in the mean daughter ion intensity at selected locations; this presumably reflects the imprecision of the measurement, since there is no reason to believe that the concentration of spiperone across the spiked tissue sample varied significantly. For the mapping of a pharmaceutical compound in an intact tissue mass, the simple presence or absence of the analyte may be adequate. It remains to be established whether semi-quantitative results can be obtained. Of course the ability to map a compound will be dependent on the concentration of the compound within the sample. If the concentration of the compound is below the limit of detection of the instrument, a false negative would result and the map would indicate that the compound was not present.

To estimate the amount of spiperone in each of the spots sampled in figure 5.4 we can first assume that the spiperone spiked tissue (spiked with a total of 90 ng of spiperone) represents approximately 1/3 of the total probe tip area (the total area of a 4.0 mm diameter probe tip) and that the MALDI matrix extracted only the top half of the tissue sample. This gives a total of 45 ng of spiperone spread out over a total surface area of 4 $x10^6$ μm^2. The 50 μm

diameter sampling spot size meant that only 1/2000 of the total surface area was investigated at each point across the surface. Each analytical scan (the scan which produced a final spectrum) was the average of four micro-scans, and each spot was sampled four times. This means that each analytical scan was the average of approximately 1.5 pg of spiperone. Since the signal for spiperone was detected for more than just the four samplings used to produce figure 5.5, it can be assumed that the actual amount of spiperone detected was significantly less than this amount (the signal was sometimes detected for 10 to 15 analytical scans at one spot).

To assess the capability of LD/CI to map pharmaceutical compounds in intact tissue, a procedure similar to that used in the electrosprayed MALDI matrix solution experiment was conducted. A 4.0 mg thin slice of rat liver tissue was spiked with 2.0 μL of a 100 ng/μL solution of spiperone in aqueous 1% acetic acid solution. A similar thin slice of rat liver tissue (4.6 mg) was incubated in neat aqueous 1% acetic acid solution for one hour. Both pieces was rinsed with several aliquots of aqueous 1% acetic acid solution and blotted dry. The tissue slices were arrange on the probe tip as they had been for the electrospraying experiments (with the spiked piece of tissue situated between two non-spiked pieces of tissue).

Figure 5.6 shows the tissue samples after analysis. The distance between sampling spots was approximately 150 μm and the spot size of the laser beam was approximately 50 μm in diameter. The spots in the

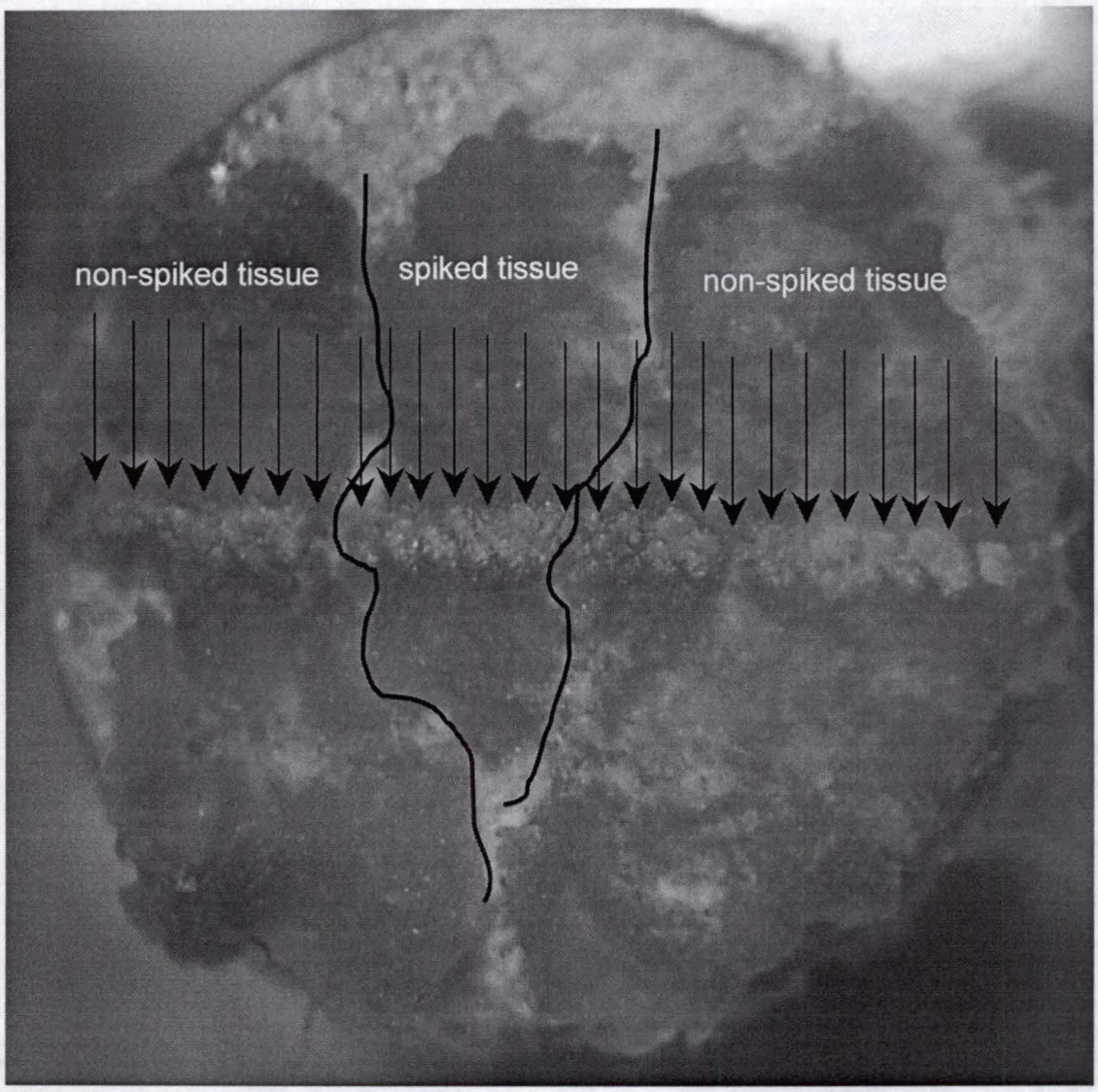

Figure 5.6. Photomicrograph of the tissue sample used for mapping of spiperone by LD/CI. Arrows indicate laser sampling locations across the surface of the tissue. The lines indicate the division between spiked tissue (center piece) and non-spiked tissue.

photomicrograph appear larger than 50 μm in diameter because the laser was fired approximately 10 to 20 times after the data had been collected to ensure that the surface was well marked for correlation to the spectra (the actual beam profile was that of an ellipse, which shows in the damaged area around each spot). Each analytical scan consisted of a single laser shot. Each location was sampled four times and, as was done in the electrosprayed experiments, MS/MS was performed on the ion at m/z 396 (with isolation and CAD). The sum of the intensity of the four characteristic daughter ions of spiperone (at m/z 291, 232, 165, 123) was calculated and the mean intensity of the four analytical scans was plotted, as shown in figure 5.7. As was found in the electrospraying experiments, the plotted data matched the tissue sample investigated. The data plotted between approximately 1 and 2 mm in distance across the tissue surface (from left to right across the probe tip) showed an increase in signal intensity for the daughter ions of spiperone. These locations on the tissue matched the sampling spots which were produced on the surface of the spiperone spiked tissue (Figure 5.6).

Experimental Pharmaceutical Compound

The results of the mapping of spiperone in spiked rat liver tissue demonstrated the ability of the instrument to map the location of a pharmaceutical compound in intact tissue incubated in a solution of the drug by both the electrospray and LD/CI methods; however, it was desirable to test the ability of the instrument in the mapping of a pharmaceutical compound in

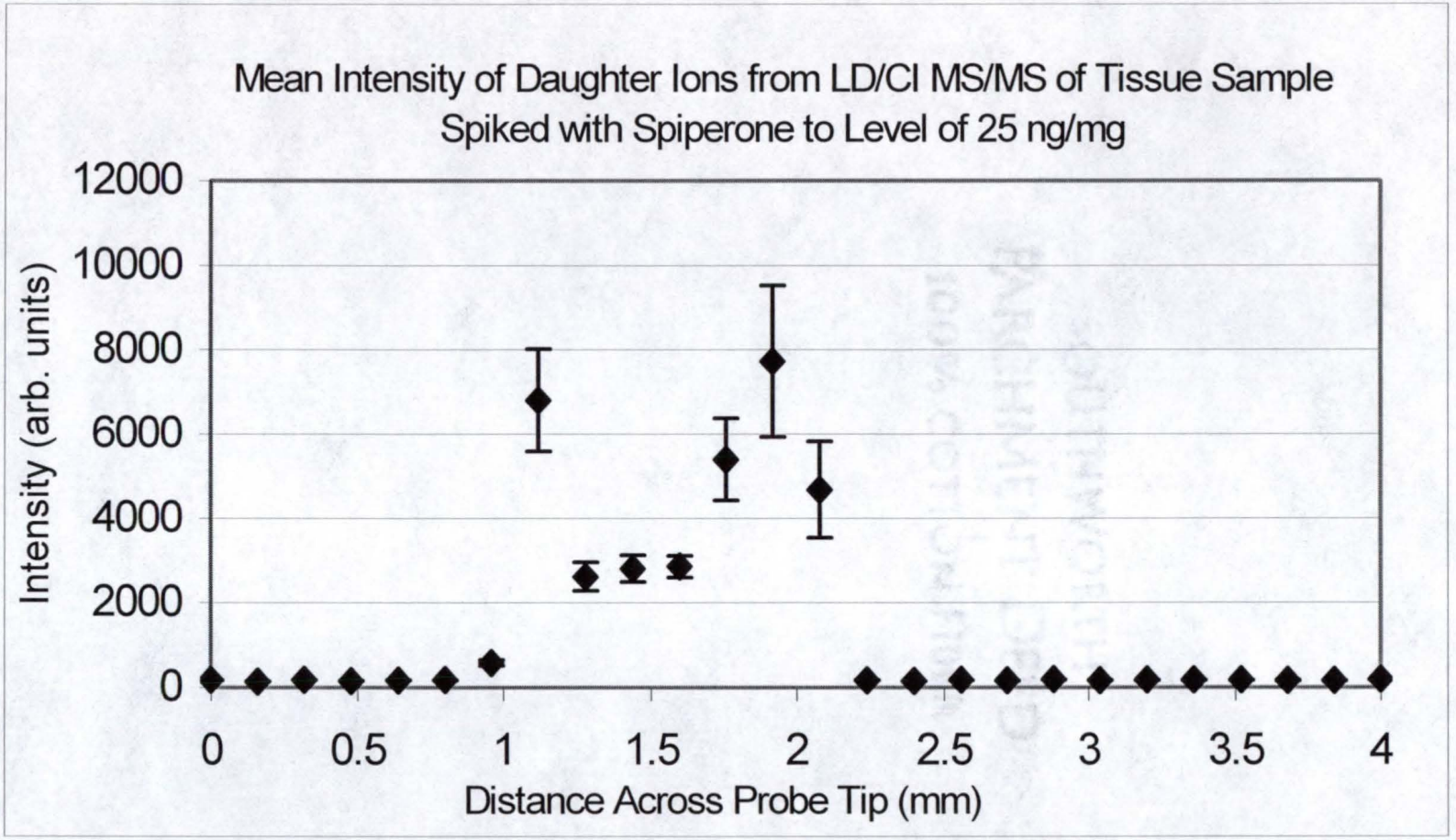

Figure 5.7. Plot of mean intensity of characteristic daughter ions of spiperone detected by LD/CI MS/MS from rat liver tissue sample (shown in figure 5.6). Each spot was sampled four times. The error bars indicate ± 1 standard deviation of the mean. Note that error bars on low intensity spots are covered by plotted spot.

an intact tissue sample where the compound had been administered to a test animal by conventional methods. We had available to us tissue samples from a dog which had been administered a pharmaceutical compound that was currently under investigation by the Bristol-Myers Squibb Co.. The compound was a multiply substituted quinoline with a molecular weight of 426 Daltons. Figure 5.8 shows the MALDI MS/MS daughter ion spectrum of the $[M+H]^+$ ion (m/z 427) of a neat sample of the experimental compound. The daughter ions in the spectrum which appear at m/z 327, 367, and 381 were produced by CAD of the ion at m/z 427.

The salt form of the experimental compound, which had been radio-labeled with ^{14}C to a specific activity of 0.1 μCi/ mg, was administered to the dogs intravenously at a dose 100 mg/kg for a period of 14 days. A thin slice of dog esophageal tissue (Figure 5.9) was removed from a frozen sample (approximately 2 grams in weight) which had been gathered from the animals 7 days after last administration of the compound. The level of the compound in the esophageal tissue was estimated as 59 mg/kg based on the concentration of radioactivity detected in a similar tissue sample. The thin slice (approximately 0.5 mm thick) was placed on a probe tip and allowed to air dry. The esophageal tissue slice was taken transversely so that the 4 mm diameter piece included tissue from the mucosa and muscularis regions of the esophagus. The mucosa consists of the epithelial layer which lines the lumen of the esophagus and the submucosa layer composed of connective tissue

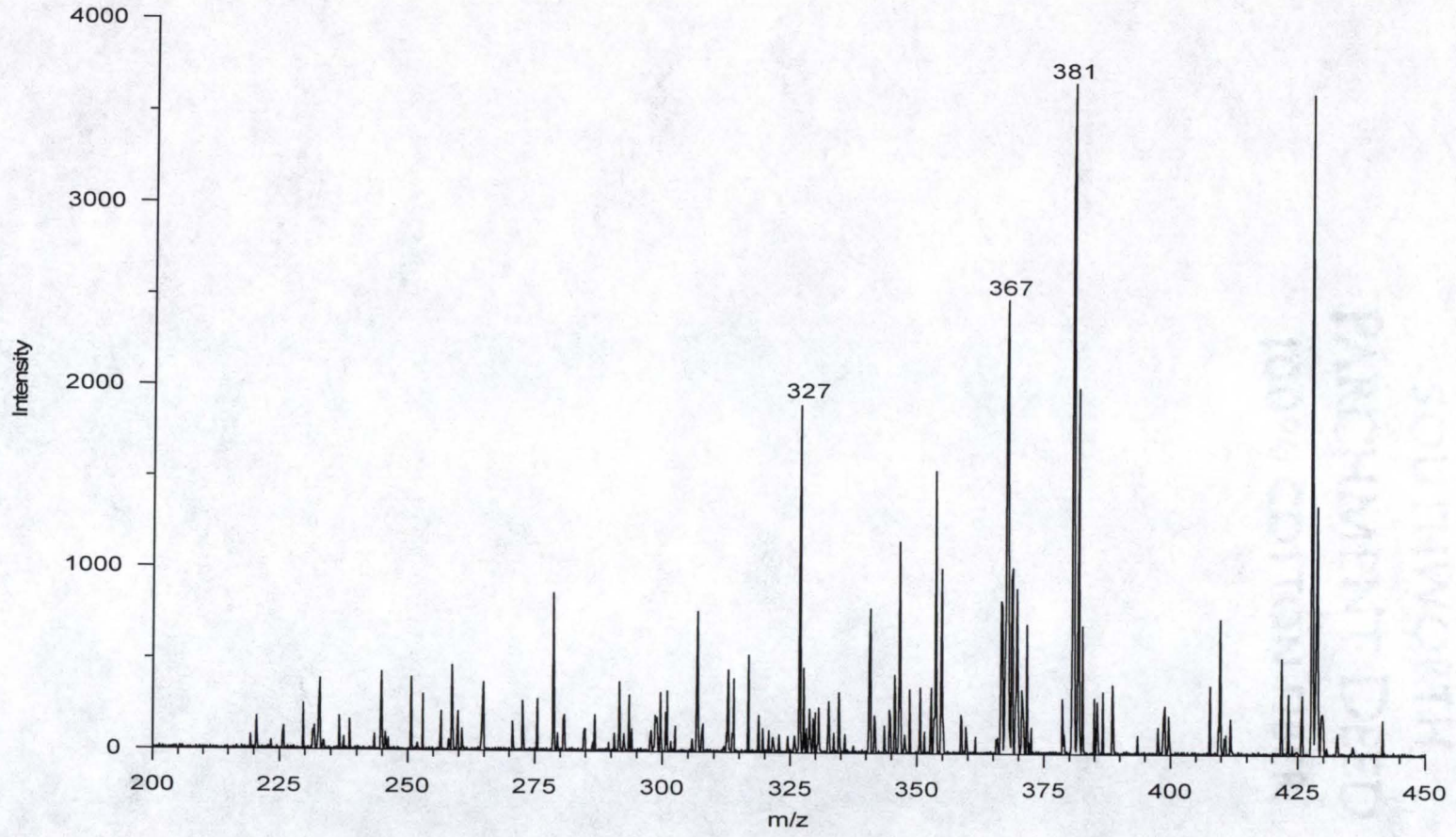

Figure 5.8. The MALDI MS/MS daughter ion spectrum of the $[M+H]^+$ ion at m/z 427 of the experimental compound. The most prominent daughter ions are labeled. They appear at m/z of 327, 367, and 381.

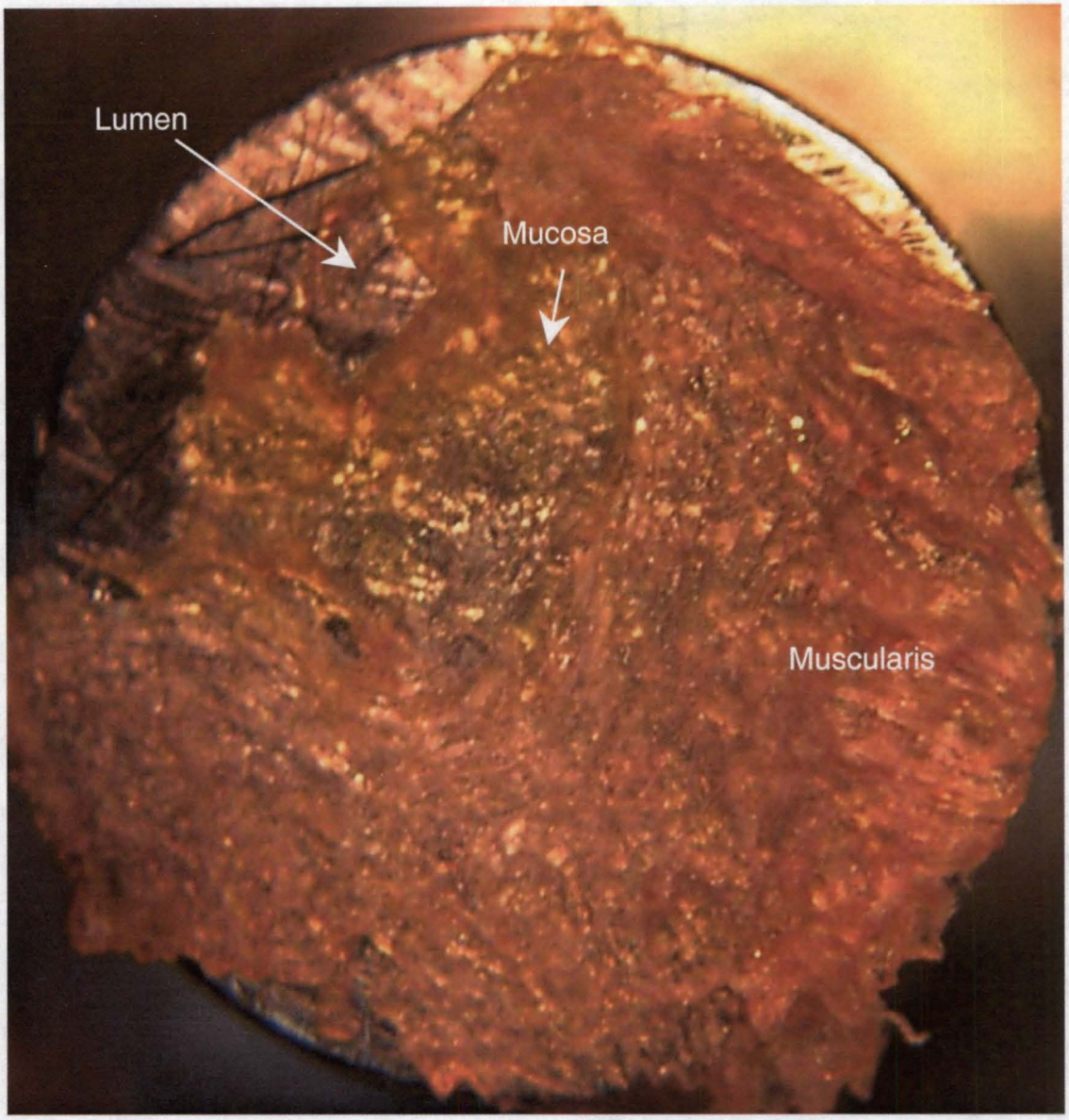

Figure 5.9. Photomicrograph of the thin slice of dog esophageal tissue used for the electrospray MALDI MS/MS mapping of the experimental compound. Note that the tissue appears yellowish around the lumen and becomes pinkish farther away (from left to right).

that binds the epithelial tissue to the muscularis. The muscularis of the esophagus consists of two layers of smooth muscle (an inner layer of circular muscle and an outer layer of longitudinally arranged muscles). This tissue sample was selected because there were clearly two different regions of tissue visible in the sample (believed to be the two regions discussed above). The area around the lumen of the esophagus was colored yellow, while the region farther away from the lumen (believed to be the muscularis) had a pinkish color. The lining of lumen had a dark brownish hue that appeared dark pink after being sliced thin (Figure 5.9). While there was no reason to believe that the experimental compound was unevenly distributed within the tissue mass, the sample represented a test of the instrument's ability to map the location of the compound and determine its location within the different sections of the tissue.

After the tissue slice had dried (approximately 1.5 hours), the probe tip with the sample was electrosprayed with a MALDI matrix solution of 70% methanol and 30% aqueous 1% acetic acid which contained 10 μg/μL of DHB. The electrospray conditions were the same as those used in the electrospraying of the rat liver tissue in the spiperone experiments presented in Chapter 4. After electrospraying the tissue for seven minutes, the sample was analyzed with the microprobe instrument.

Figure 5.10 is a photomicrograph of the tissue sample after analysis. The spacing between sampling locations across the tissue surface was

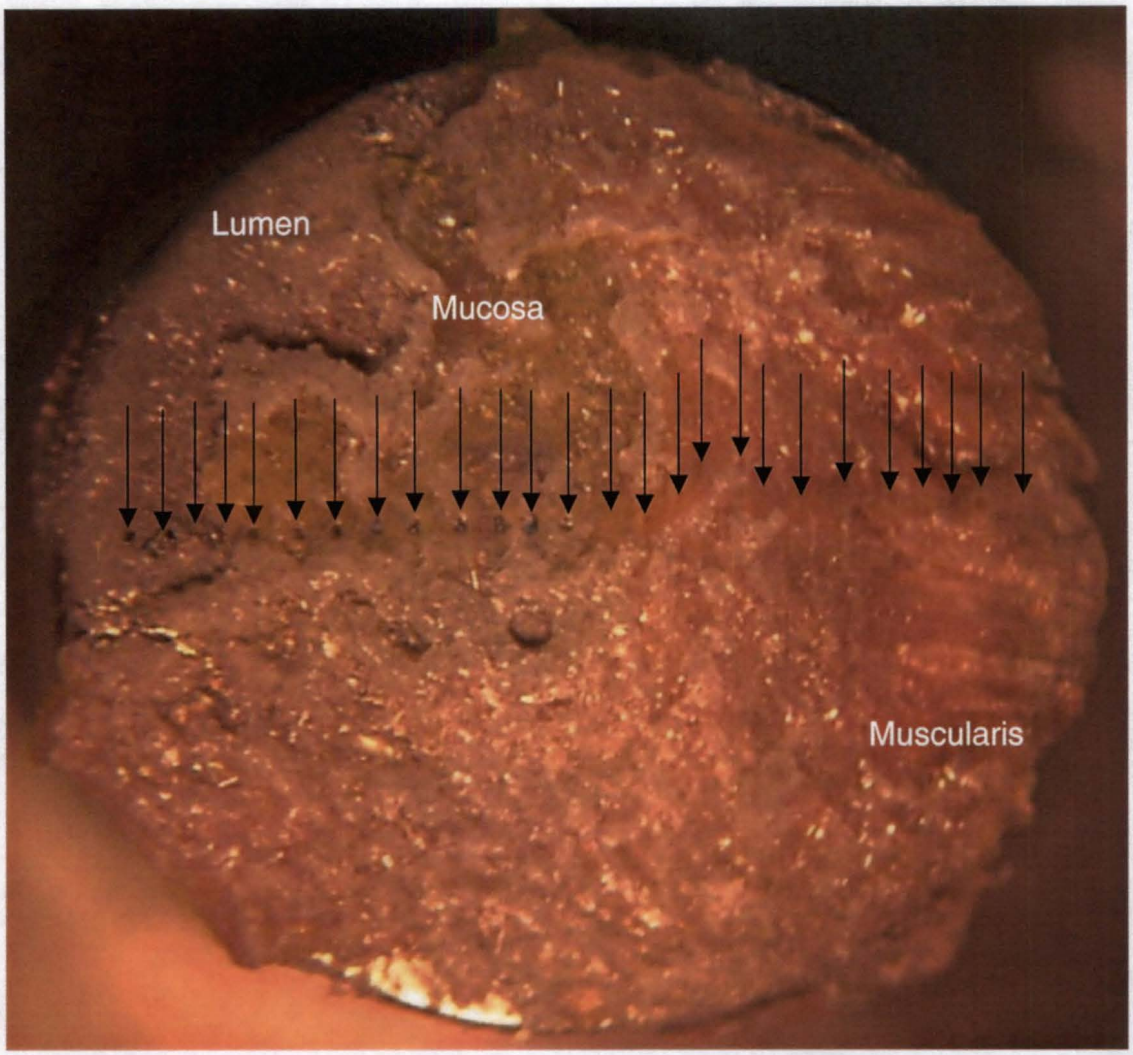

Figure 5.10. Photomicrograph of esophageal tissue in figure 5.9 after electrospraying of the MALDI matrix MS/MS analysis. Arrows indicate the location of laser beam sampling across the surface. The distance between each sampling is approximately 150 μm. Note that (moving from left to right) the tissue color changes from a yellow to a pink hue. Also, note that the two sampling spots on the far left side of the probe tip were off the edge of the tissue sample.

approximately 150 μm. Each spot was analyzed four times (with each analytical scan consisting of four micro-scans of four laser shots each) and, as was done in the spiperone experiments, MS/MS was preformed on each analytical scan (with isolation and CAD of the ion at m/z 427). The intensities of the daughter ions at m/z 327, 367, and 381 were summed for each analytical scan and the mean of the summed intensities was plotted. Figure 5.11 shows the plot produced by the sampling of the esophageal tissue by MALDI MS/MS.

It appears from figure 5.11 that the experimental compound was not evenly distributed in the tissue mass. The two sample spots on the far left side of the plot were actually not of tissue but of MALDI matrix electrosprayed onto the sample probe (see Figure 5.10). These two spots thus could serve as a baseline with which to compare the rest of the plotted intensities. In a separate experiment, a similar thin slice of dog esophageal tissue from an animal which had not been administered the experimental compound was analyzed under similar conditions. The MS/MS spectrum from the blank dog esophagus tissue did not produce the characteristic daughter ions of the experimental compound (m/z 327, 367, and 381). The summed intensities of the ions at m/z 327, 367, and 381 from MS/MS of the blank tissue were comparable to the summed intensities of those ions from the MS/MS of the sample spots taken off the edge of the tissue (in Figure 5.10).

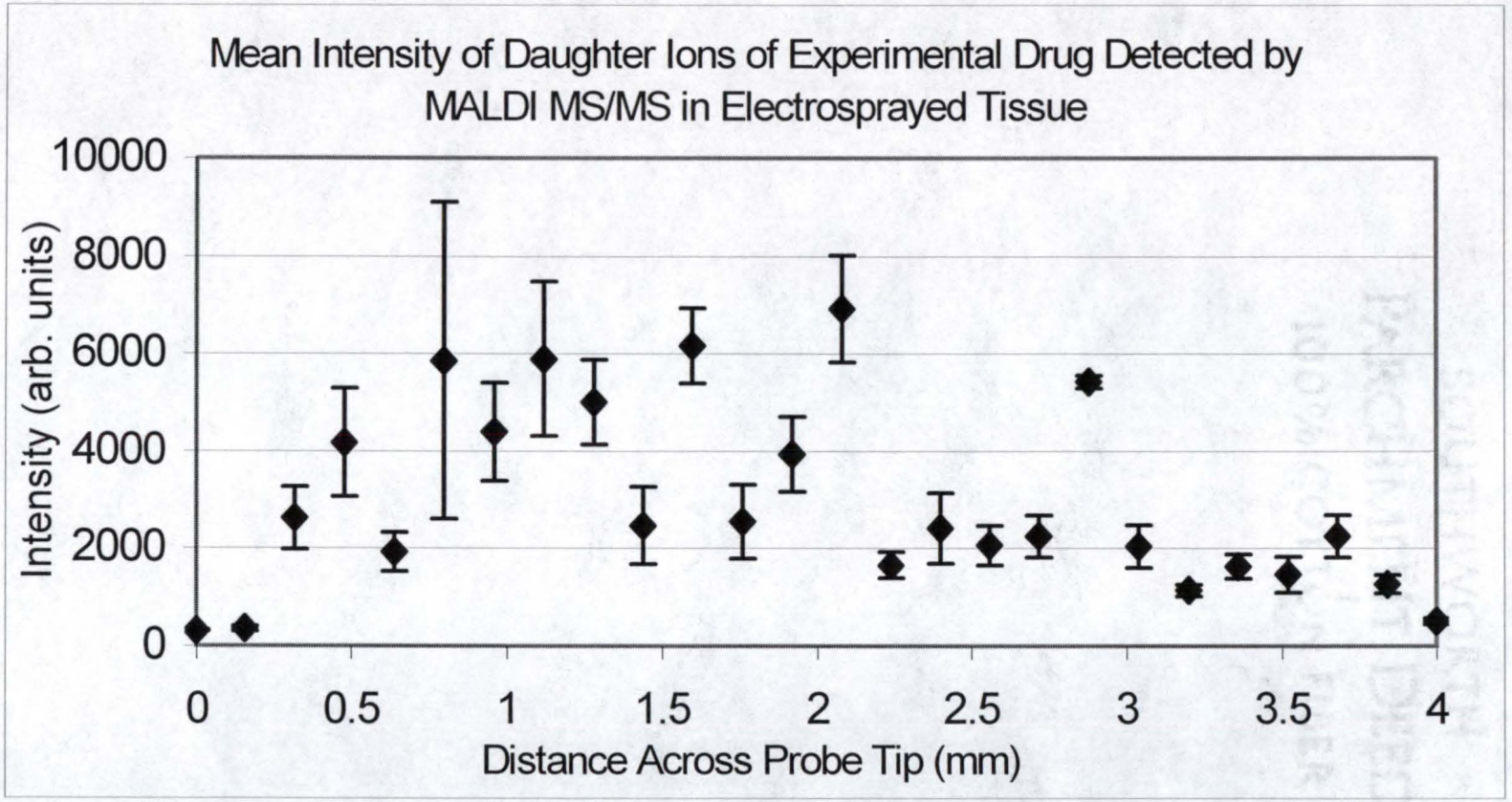

Figure 5.11. Plot of the mean daughter ion intensity produced by CAD of the ion at m/z 427 which corresponds to the $[M+H]^+$ ion of the experimental compound in the dog esophageal tissue (figure 5.10). The error bars indicate ± 1 standard deviation of the mean.

It is interesting to note that the plotted intensities between 2 mm and 4 mm were of lower intensity and smaller standard deviation of the mean than the spots sampled between the left side of the tissue and 2 mm. This was interesting because the change in intensity occurs at approximately the same location on the tissue as the change in color (going from yellow to pink when moving from left to right). While it is tempting to assume that this change in intensity was the result of a change in concentration of the experimental compound, that conclusion is questionable. Neither MALDI nor LD/CI are good quantitative techniques. The change in color (and possibly a corresponding change in tissue type) could indicate that the extractability of the compound may differ in the two regions. This could result in a greater amount of compound being extracted into the MALDI matrix from one region of tissue (the yellow region for instance) as compared to the other region. Additionally, visual inspection of the tissue after drying indicated that the yellow section of tissue was thinner than the pinkish section (although both were approximately the same thickness before drying). Extraction of the MALDI matrix solution may have been more efficient in the thinner tissue. For example, if the experimental compound was of uniform concentration in both regions of tissue prior to drying, and the MALDI matrix solution extracted the compound from the same depth of tissue, the thinner tissue would be expected to yield a greater amount of compound (the compound would have been concentrated in the thinner tissue region during drying). Furthermore,

upon visual inspection of the tissue mass after sampling, it was noted that the laser beam had penetrated completely through the thinner yellow tissue, exposing the surface of the probe tip below. The depth of penetration of the laser beam into the (thicker) pink region of tissue was approximately the same as the depth of penetration into the thinner yellow region, but due to the difference in thickness, the laser beam penetrated less than half way through the thicker tissue mass. Both of these effects could account for the higher intensities observed from the yellow section.

Another possible source for the variation in intensity of the mean of the summed daughter ions in the different tissue regions would be the variation in the absorbance of the incoming laser beam and thus the extent of the ablation of material. Without extensive experimental investigation, it clearly cannot be concluded that the intensities of the ion signals in the particular tissue sections correlate directly with the concentration of the experimental drug in those tissue sections.

Next, LD/CI was used to map the experimental drug in a similar tissue slice. Another, thin tissue slice of dog esophageal tissue (approximately 4 mg) was taken from the bulk frozen sample and placed on a probe tip to air dry. After drying, the tissue sample was analyzed with the quadrupole ion trap laser microprobe instrument. Figure 5.12 is a photomicrograph of the tissue after sampling by LD/CI. The different regions (colored pink and yellow) of tissue are clearly visible in the photomicrograph, pink on the left and yellow on

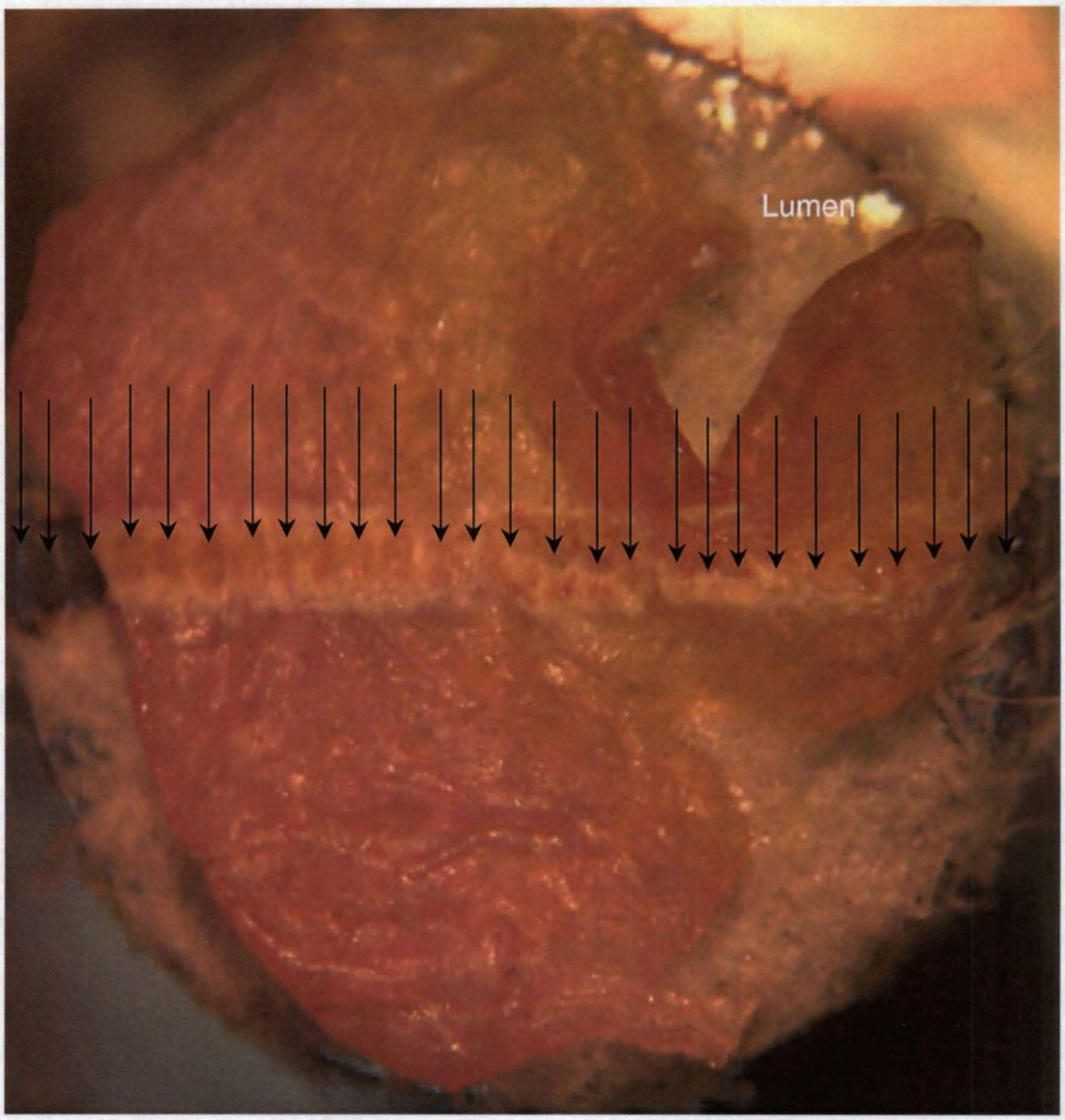

Figure 5.12. Dog esophageal tissue which had been dosed with an experimental drug to a level of 58.5 ng/µg. Arrows indicate the spots on the tissue surface which were sampled with a CO_2 laser for LD/CI. Note that the first two spots on the far left and the spot on the far right were not of tissue but of the probe surface.

the right. The spot size of the CO_2 laser beam used in sampling was approximately 50 μm in diameter and each spot on the tissue was sampled four times (each analytical scan consisting of a single laser shot). Again, as was done in the electrospray experiment, MS/MS was performed during sampling with isolation of the region around m/z 427 (which corresponds to the $[M+H]^+$ ion of the experimental drug) and CAD, to produce daughter ions. Figure 5.13 is a plot of the mean intensity of the sum of the characteristic daughter ions (m/z 327, 367, and 381) of the m/z 427 ion.

As was observed in the electrosprayed sample, there is a region of the tissue that produces a more intense response than other regions. The region that produced the more intense response was again the yellow section of tissue around the lumen of the esophagus. In figure 5.13, that region is between 2 and 3 millimeters in from the left hand side of the sample. In the photomicrograph, that region includes the dark band (assumed to be the epithelial layer of the mucosa) around the lumen of the esophageal tissue and some of the yellow region. Again, it should be emphasized that the increase in response does not necessarily indicate an increase in drug concentration in the tissue but could be the result of increased ablation due to differences in the tissue (absorbance, thickness, etc.). As was seen in the MALDI electrospray experiment on the dog esophagus tissue, visual inspection of the tissue sample showed that the yellow region of tissue was thinner than the pink region (after drying). As was previously discussed, this thinning of the

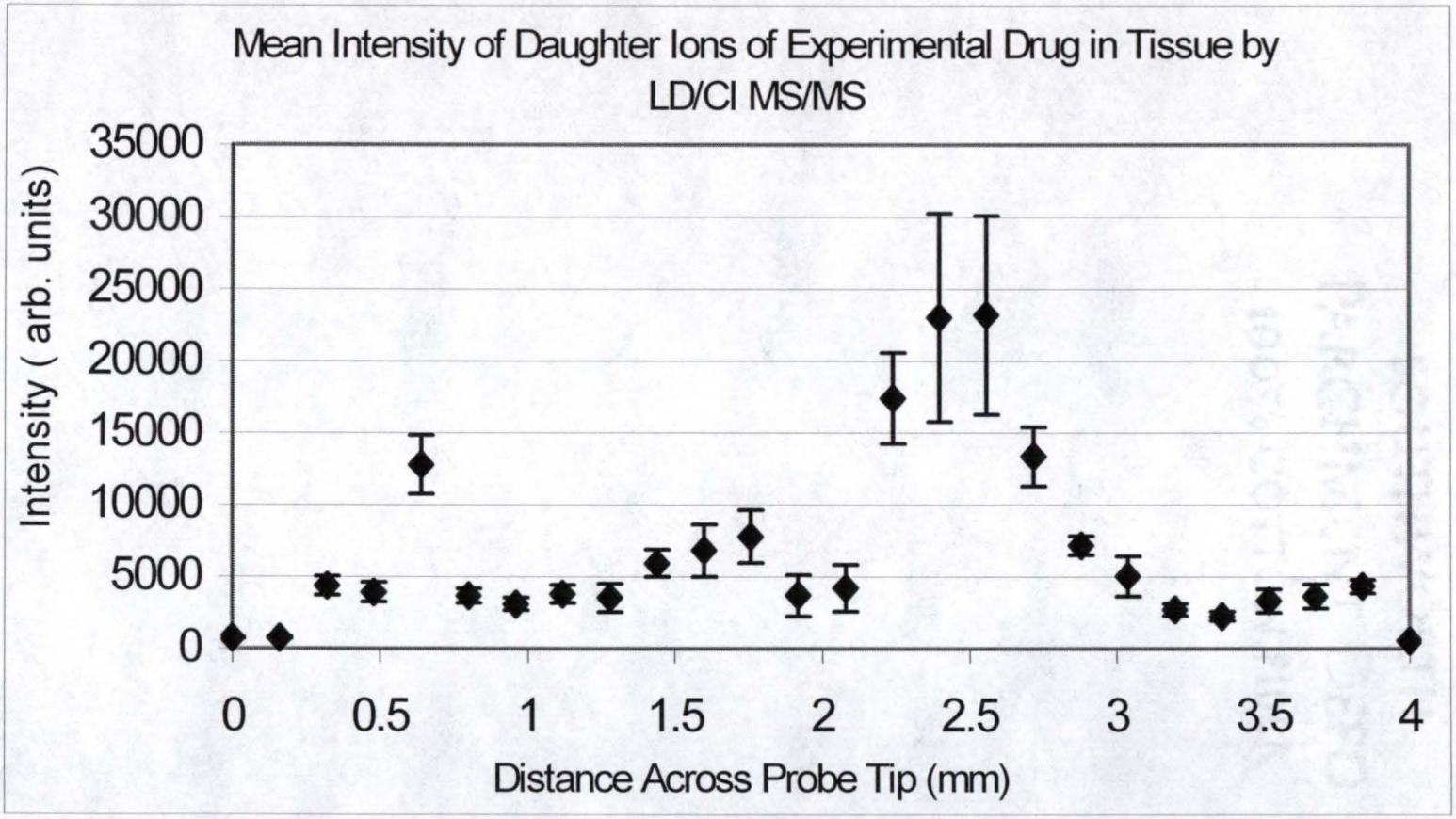

Figure 5.13. A plot of the intensity of the sum of the characteristic daughter ions of the experimental pharmaceutical compound in esophageal tissue. Each spot is the mean intensity of four samples gathered at each spot. The error bars are ± 1 standard deviation of the mean.

tissue could result in an artificial increase in the concentration of the drug within the thin tissue region which would not be present in the natural state of the tissue.

Also noteworthy is the fact that the mean intensity of the summed daughter ions (m/z 327, 367, and 381) of the m/z 427 ion in the yellow region of tissue located to the right of the dark pink band around the lumen of the esophagus was not greater than the mean intensity of the summed daughter ions from m/z 427 in the pinkish region (see Figure 5.12). An examination of the esophageal tissue prior to sampling (Figure 5.14) shows that the region to the right of the lumen (and slightly below) was not as thin as the region to the left of the lumen. Again, this is a possible reason for the observed variation in response.

Paclitaxel

Because one of the long-term goals of this research was to map the location of paclitaxel in an ovarian tumor, it was of interest to evaluate both LD/CI and the electrospraying of the MALDI matrix solution for paclitaxel in tissue. There was no ovarian tumor sample available, so paclitaxel was studied by incubating it in rat liver tissue.

The first step in the investigation into the mapping of paclitaxel in intact tissue was to determine the ability of LD/CI to produce significant ions of adequate intensity from paclitaxel for identification by MS/MS. One μL of a

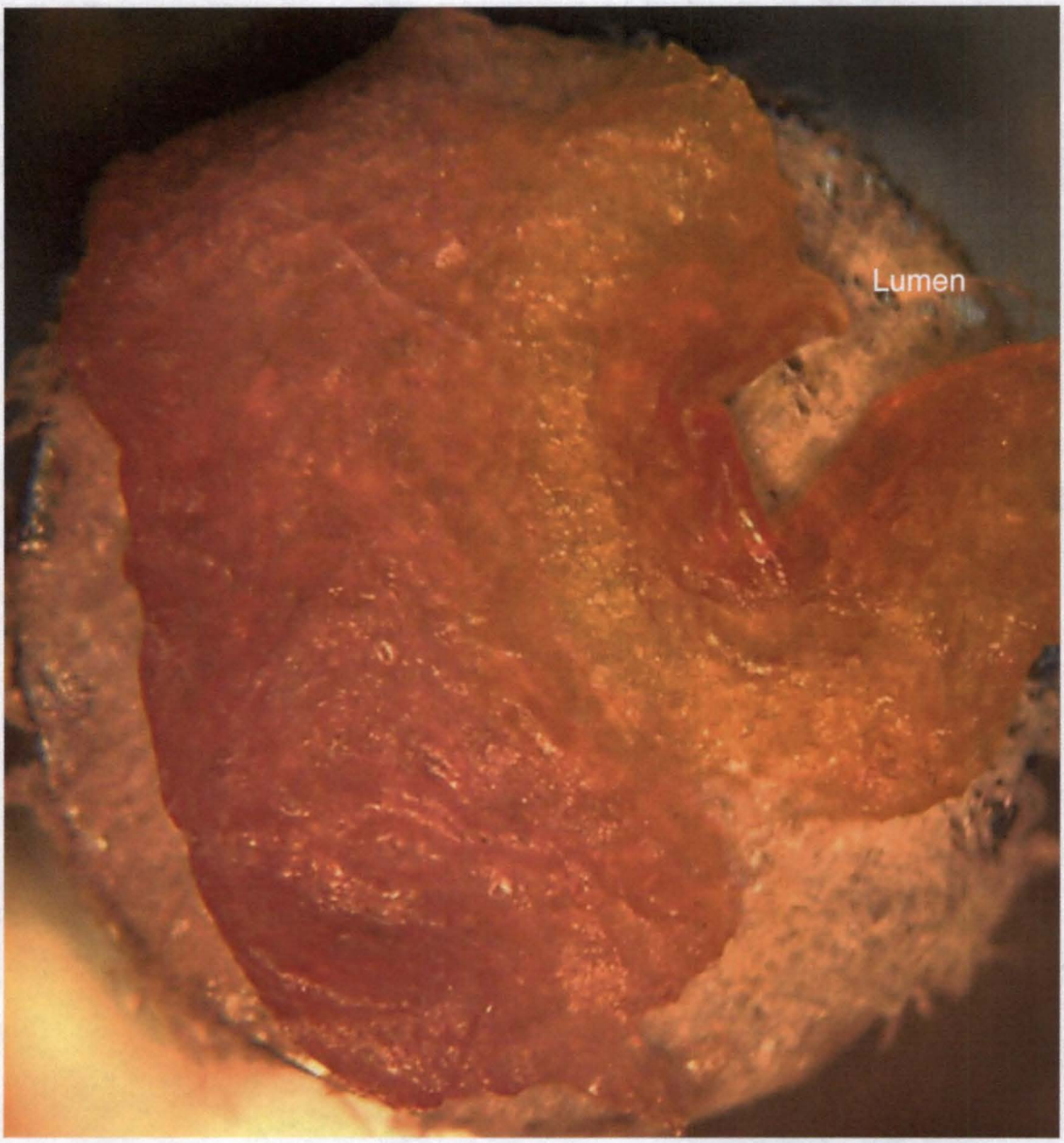

Figure 5.14. Photomicrograph of dog esophageal tissue prior to analysis with quadrupole ion trap laser microprobe instrument. Note that the region of tissue to the right (and slightly below) the lumen appears slightly thicker and is not as brightly colored yellow as the region to the left of the lumen (for comparison to photomicrograph of same region after sampling as seen in figure 5.12)

paclitaxel standard in methanol (approximately 5 μg/μL) was pipetted onto a stainless steel probe tip and allowed to air dry. The sample was interrogated with the μ-TEA CO_2 laser using a spot of approximately 50 μm in diameter. Figure 5.15 shows the LD/CI mass spectrum of the paclitaxel standard using methane as the reagent gas. Figure 5.16 shows the proposed fragmentation pathways for the observed fragment ions observed. There were nine major fragmentation ions produced during the LD/CI of the paclitaxel standard. The $[M+H]^+$ ion (at m/z 854), however, was only a minor ion in the spectrum. Since MS/MS was used for positive identification of the compound in the complex matrix of tissue, the extensive fragmentation of paclitaxel during ionization would seriously reduce the sensitivity for detection of the compound in tissue. It should be noted that the ion at m/z 794 (in figure 5.15) which corresponds to the $[M-CH_3COOH+H]^+$ ion of paclitaxel was selected for MS/MS because it was structurally significant and had an ion current of approximately 3 times that of the $[M+H]^+$ ion; however, in tissue spiked with paclitaxel to a level of 500 ng/mg the characteristic daughter ions of this fragment ion were not detected (data not shown). Because of this, different CI reagent gases were tried.

The proton affinity (PA) of the conjugate base (C_2H_4) of the major reagent ion in methane CI ($C_2H_5^+$) is 162.6 kcal/mol.[101] The PA of the conjugate base (C_4H_8) of the major reagent ion of isobutane CI ($C_4H_9^+$) is 195.9 kcal/mol.[101] Since the amount of energy deposited in the analyte

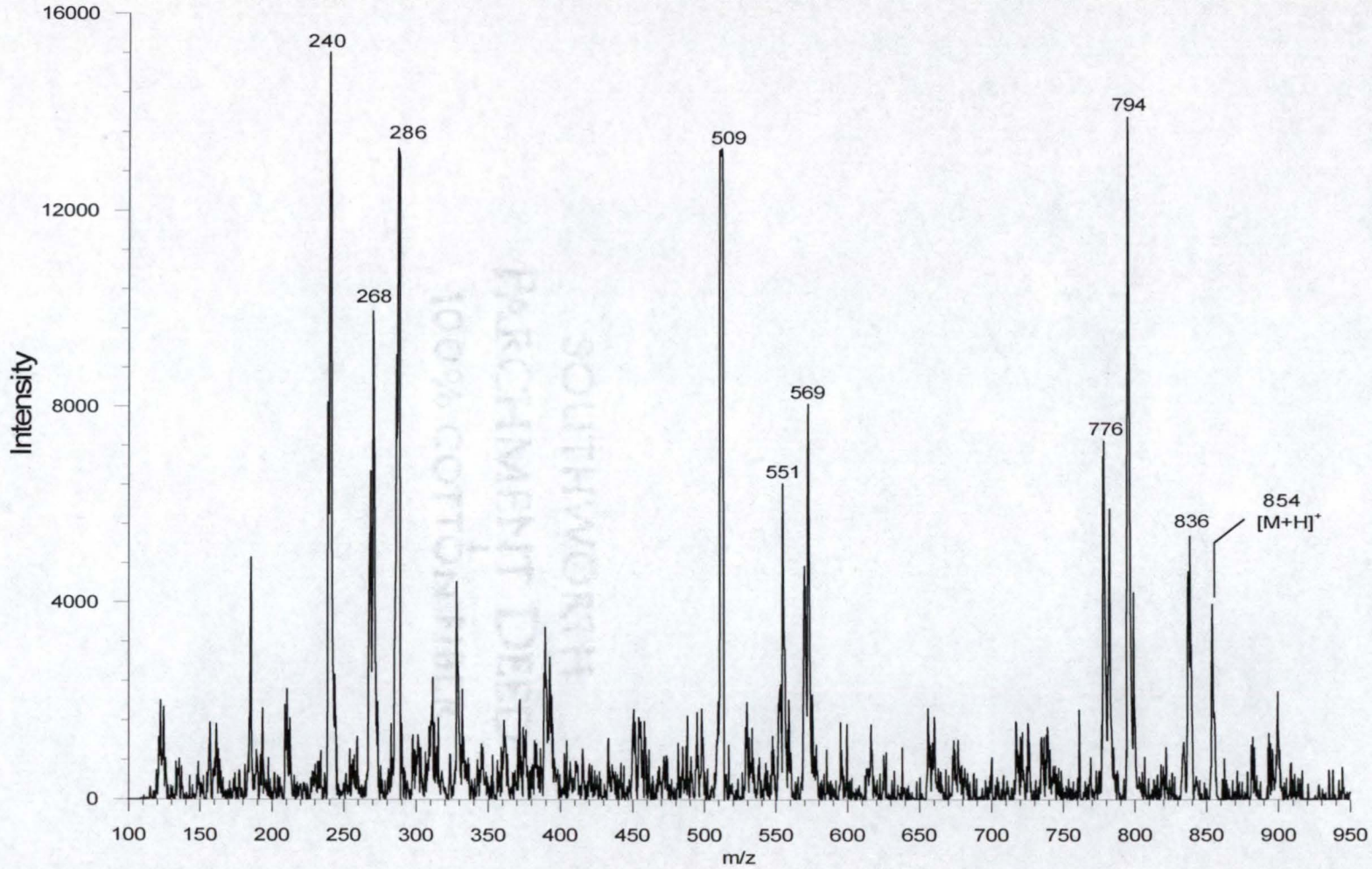

Figure 5.15. LD/CI MS of neat paclitaxel using methane reagent gas. Note that the $[M+H]^+$ at m/z 854 is only a minor peak in the spectrum.

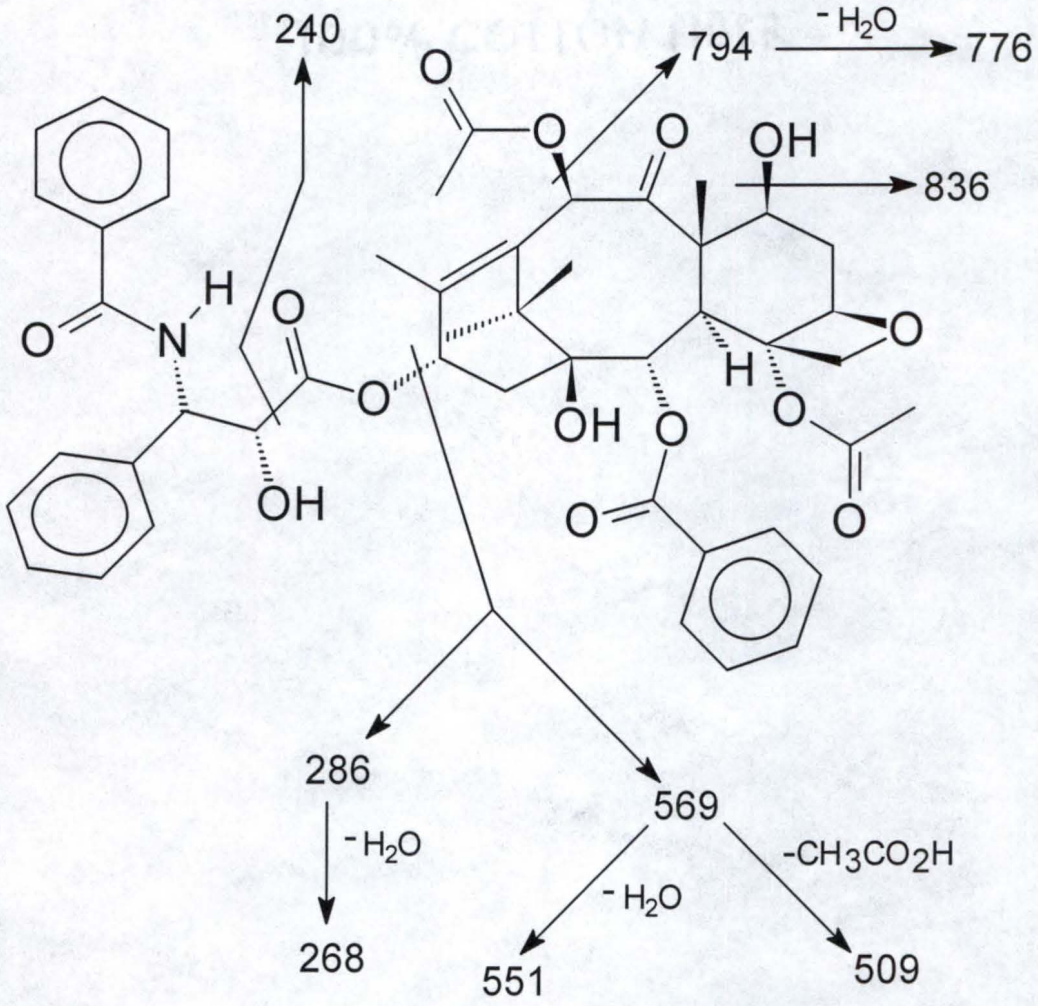

Figure 5.16. Proposed fragmentation pathways of paclitaxel during LD/CI.

molecule during ionization is a function of the difference in PA between the proton donor and the proton acceptor (PA_D-PA_A), the greater PA of C_4H_8 results in less energy being deposited in the $[M+H]^+$ ion during isobutane CI (a reduction of 33.3 kcal/ mol). This reduction in deposited energy should reduce the amount of fragmentation observed during LD/CI of paclitaxel. Figure 5.17 shows the LD/CI mass spectrum of a paclitaxel standard using isobutane as the reagent gas. While the fragmentation of the paclitaxel was reduced (the $[M+H]^+$ ion is approximately 10 times that from figure 5.15), there was still extensive fragmentation.

To further reduce the fragmentation during the ionization of paclitaxel, ammonia was evaluated as a reagent gas. The PA of the conjugate base (NH_3) of the major reagent ion (NH_4^+) in ammonia CI is 204.0 kcal/ mol.[101] Figure 5.18 shows the LD/CI mass spectrum of paclitaxel using ammonia as a reagent gas. The use of ammonia as a reagent gas reduced the fragmentation of the paclitaxel during ionization to only a few minor fragments. The major ion produced was the $[M+NH_4]^+$ ion (ammonium adduct ion) of paclitaxel. The formation of an adduct ion under these conditions of CI is generally accepted as being the result of the PA of the analyte being close in value to that of the reagent gas but still less than the PA of the reagent gas.[101] In this case the PA of paclitaxel would have to be between the PA of isobutane (195.5 kcal/mol) and ammonia (204.0 kcal/mol).

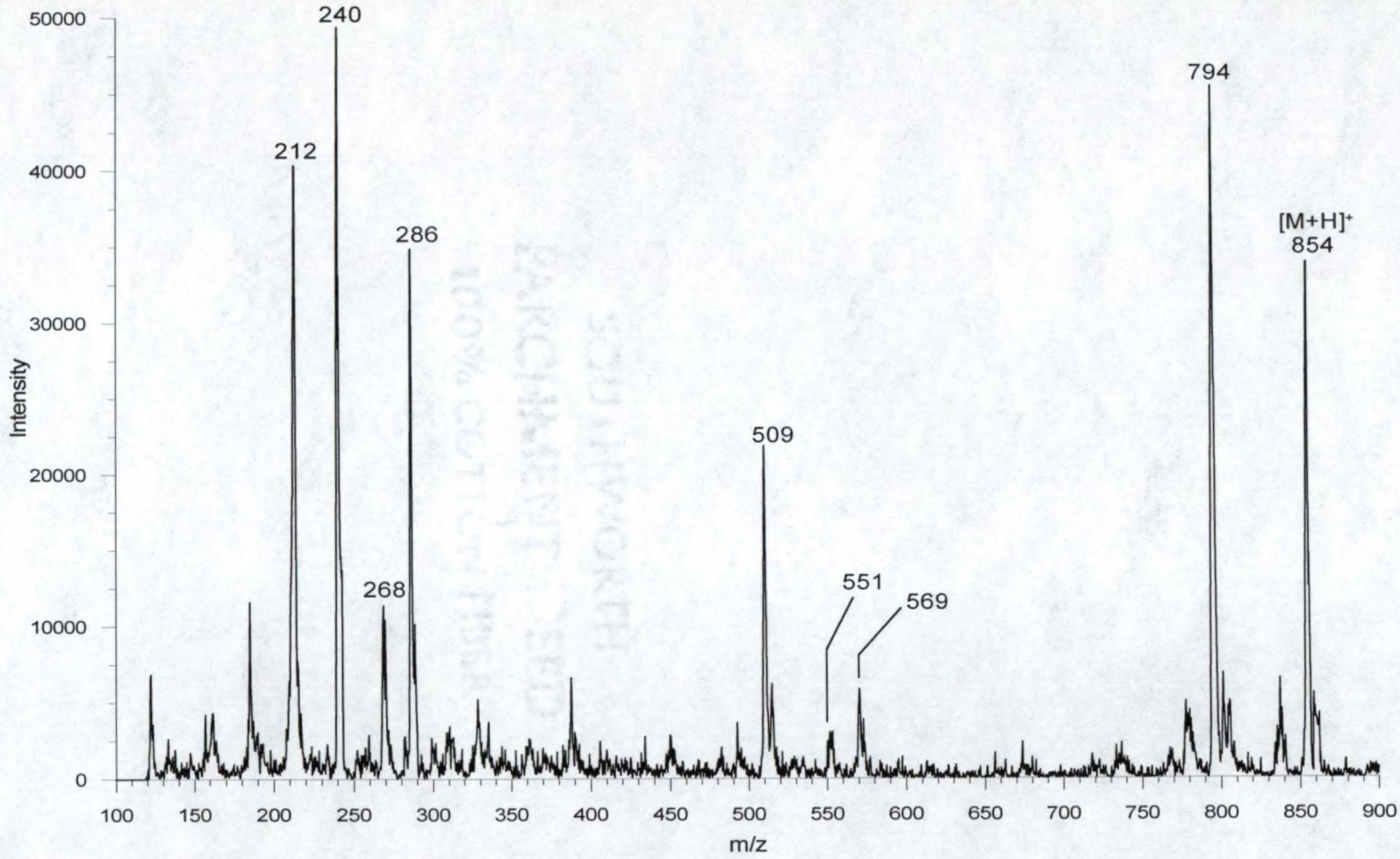

Figure 5.17. LD/CI MS of neat paclitaxel using isobutane reagent gas. Note that the $[M+H]^+$ ion (m/z 854) is approximately 10 times more intense that in figure 5.15.

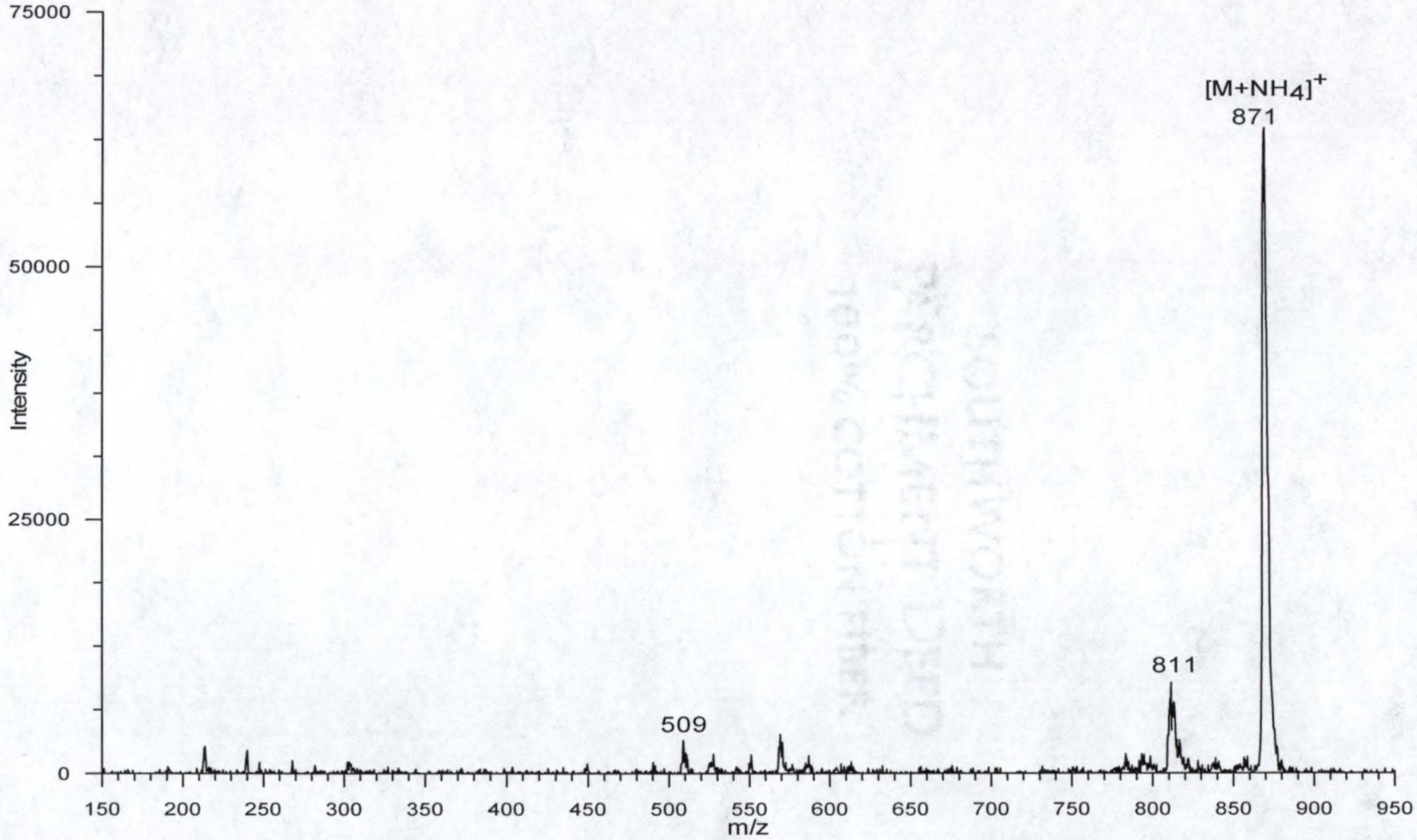

Figure 5.18. LD/CI of paclitaxel standard using ammonia reagent gas.

While paclitaxel formed a strong ammonium adduct ion when the standard was investigated, subsequent experiments with rat liver tissue incubated with paclitaxel to a level above 500 ng/mg (more than ten times the levels used for spiperone) did not produce the $[M+NH_4]^+$ ion at a sufficient level for detection by MS/MS. Because of this, LD/CI with ammonia as the reagent gas (under the experimental conditions used here) was not considered a viable method for the mapping of paclitaxel in tissue.

While the fragmentation of paclitaxel using isobutane as the reagent gas was less than that observed when using methane as a reagent gas, there were still four fragment ions of equal or greater intensity than the $[M+H]^+$ ion (figure 5.17). Thus, any ion selected (whether one of the fragment ions or the $[M+H]^+$ ion) for MS/MS would have a signal intensity of less than $1/5^{th}$ the total ion current from paclitaxel. Since the aim of this research was to map the location of trace level compounds in intact tissue, it was decided that more extensive research was needed to determine the optimal conditions for chemical ionization of paclitaxel.

Earlier experiments (Chapter 2) had shown that paclitaxel was detectable in tissue by MALDI; however, detection is not the same as mapping. With detection, the sample surface may be analyzed many times at many different locations before a positive detection result is observed. A false negative detection at one location on the sample surface does not necessarily effect the overall positive detection result found for the entire sample. When

analyzing a 4 mm diameter sample with a 50 μm diameter laser beam, only 1/6,400th of the total surface area is analyzed at each spot. For mapping, however, a false negative at one location across the sample surface changes the map produced by those results. Therefore, with mapping, it is desirable to have several positive detection events at each spot designated positive in the map (provided the analyte concentration at that location is sufficient for detection). The additional requirements for the mapping of compounds in tissue required that the electrospraying of the MALDI matrix solution provide adequate extraction of the analyte (and thus adequate signal intensity) for more than one positive detection event at each location where a positive result was found.

In initial MALDI electrospraying experiments using spiked rat liver tissue at a level of 50 ng/mg with paclitaxel, there was no detection of the characteristic daughter ion fragments of the $[M+Na]^+$ ion of paclitaxel (the most abundant molecular-type ion for MALDI of paclitaxel) by MS/MS. When the tissue was spiked to a level of 100 ng/mg, the electrosprayed tissue sample did produce a detectable signal by MS/MS; however, the detection of the characteristic daughter ions of the $[M+Na]^+$ ion of paclitaxel was not sufficiently reproducible enough from scan to scan to permit the mapping of the compound (the signal was detected sporadically across the tissue surface).

One of the reasons for the increased level of paclitaxel necessary for detection as compared to the other pharmaceutical compounds tested was the fact that paclitaxel was so labile that it fragmented under the normally gentle ionization conditions of MALDI. Figure 5.19 shows the MALDI MS spectrum of a neat sample of paclitaxel. The two most abundant ions in the spectrum are from the matrix (DHB). The ions at m/z 137 is the $[M-H_2O+H]^+$ ion of DHB and the ion at m/z 273 is the $[2(M-H_2O)+H]^+$ ion of DHB. The most intense fragment ion of paclitaxel was the ion at m/z 240. The extent of fragmentation by MALDI (in figure 5.19) is similar to that seen in LD/CI using isobutane as the reagent gas (in figure 5.17).

It was decided to evaluate electrospray MALDI for the mapping of paclitaxel in tissue. Despite the fact that the fragmentation during MALDI of paclitaxel was similar to that of LD/CI using isobutane as the reagent gas, MALDI offered advantages over LD/CI for the mapping of paclitaxel in tissue. During LD/CI, the interaction of the laser beam with the tissue surface often dramatically reduced the ion signal from the surface after only 6 to 10 laser shots at a location (as mentioned at the end of Chapter 3). Additionally, as was discussed in Chapter 3, ablation of an excessive amount of tissue would coat the inside of the ion volume and reduced the transmission of ions, thus reducing the sensitivity of the instrument. This phenomena was seen in some of the early mapping work of spiperone in tissue using LD/CI when several laser shots were averaged into each scan taken at a sampling location. For

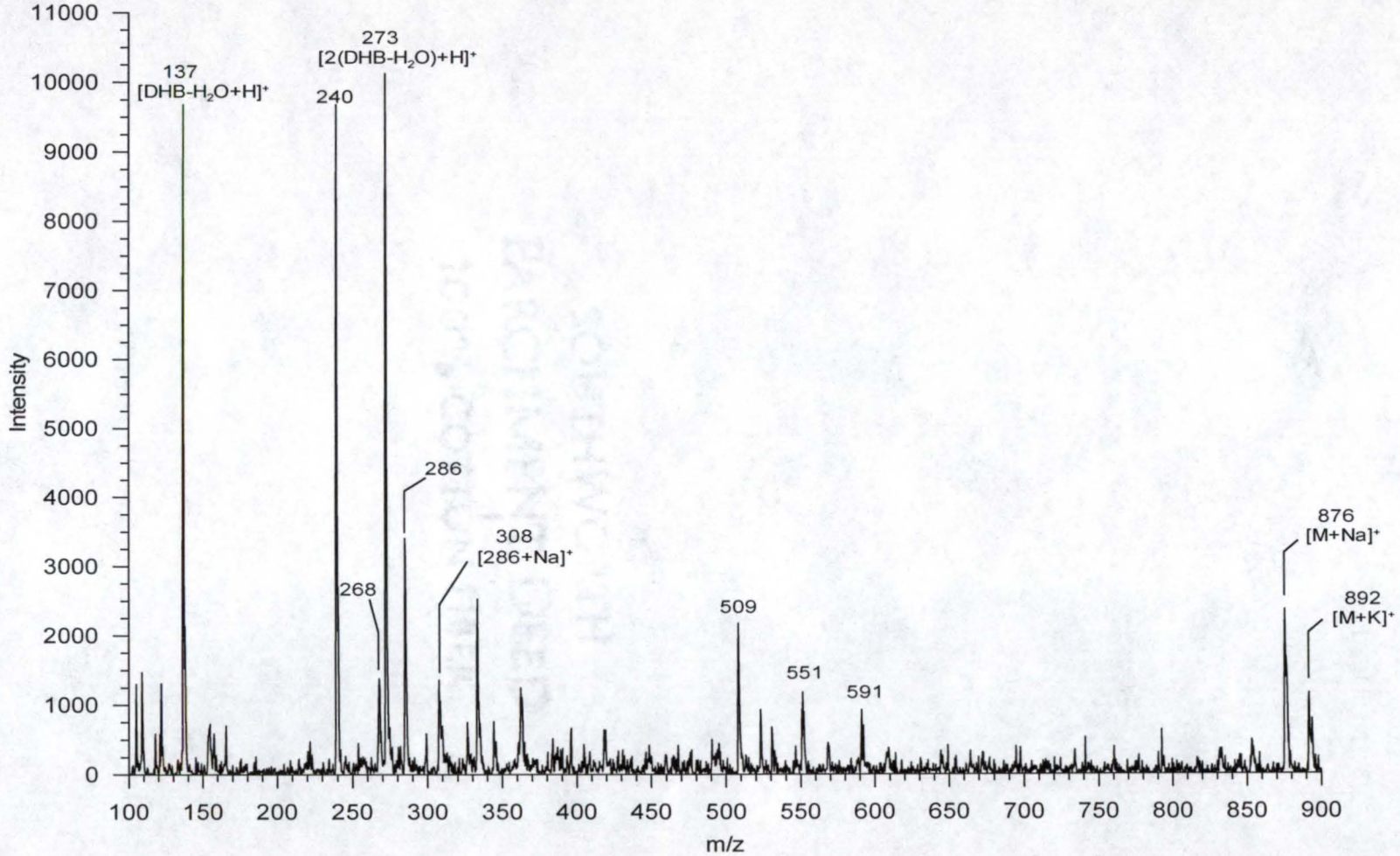

Figure 5.19. MALDI MS spectrum of paclitaxel standard. The two most abundant ions are matrix ions from DHB. The ion at m/z 137 is the $[M\text{-}H_2O+H]^+$ ion from DHB, and the ion at m/z 373 is the $[2(M\text{-}H_2O)+H]^+$ ion of DHB.

the mapping of compounds in tissue by LD/CI presented in this dissertation, a single laser shot was used for each analytical scan. These problems were not observed during the MALDI experiments. The ion signal of MALDI MS from a single spot would often persist for more than a hundred laser shots. This allowed the use of multiple laser shots for each micro-scan and for several micro-scans to be averaged into each analytical scan. For the mapping of compounds in tissue by electrospray MALDI presented in this dissertation, four laser shots were summed in each micro-scan and four micro-scans were averaged into each analytical scan. A comparison of figure 5.5 and 5.7 shows that for spiperone, the mean intensity of the MS/MS daughter ion signal from four analytical scans (a single laser shot each) by LD/CI was similar to the mean intensity of four analytical scans (consisting of four micro-scans of four laser shots each-16 total laser shots per analytical scan) by electrospray MALDI, and the signal for electrospray MALDI was seen to persist for more than the four analytical scans collected. This suggested the possibility of using more laser shots per sampling in electrospray MALDI as a way of increasing the reproducibility and intensity of the paclitaxel daughter ions signal by MS/MS.

As was done in the mapping experiments with spiperone, a thin slice of rat liver tissue (3.5 mg) was placed in a stainless steel well and 0.7 μL of a 1.0 μg/μL solution of paclitaxel in acetonitrile was pipetted onto the tissue. After the acetonitrile evaporated, the tissue was rinsed several times with

aliquots of aqueous 1% acetic acid solution and then blotted dry. If all of the paclitaxel remained in the tissue, its concentration would be 200 ng/mg. The spiked tissue slice was placed in the middle of a stainless steel probe tip and allowed to air dry. A similar thin slice (4.8 mg) of rat liver tissue was placed in a stainless steel well and 1.0 μL of acetonitrile was pipetted onto its surface. After the acetonitrile dried, the non-spiked tissue was rinsed several times with aliquots of aqueous 1% acetic acid solution and blotted dry. The non-spiked rat liver tissue was divided into two pieces and each piece was placed on different sides of the piece of rat liver tissue that had been spiked with paclitaxel. After all three pieces had dried (approximately 1.5 hours), the probe tip was placed into the electrospray apparatus and the surface of the probe tip was electrosprayed with a solution of 10 μg/μL of DHB in 70% methanol and 30% aqueous 1% acetic acid solution.

Figure 5.20 is a photomicrograph of the tissue sample after analysis with the laser microprobe instrument. The arrows in the photograph indicate the location of sampling. The black lines indicate the location of the different tissue pieces (the tissue spiked with paclitaxel was located in middle). Ten laser shots were summed in each micro-scan, and four micro-scans were averaged into each analytical scan. Four analytical scans were collected at each spot and MS/MS was performed on each. The most abundant daughter ions produced by the MS/MS of the $[M+Na]^+$ ion of paclitaxel (m/z 876) were at m/z 308, 531, and 591 (see figure 2.13). The intensities of these characteristic

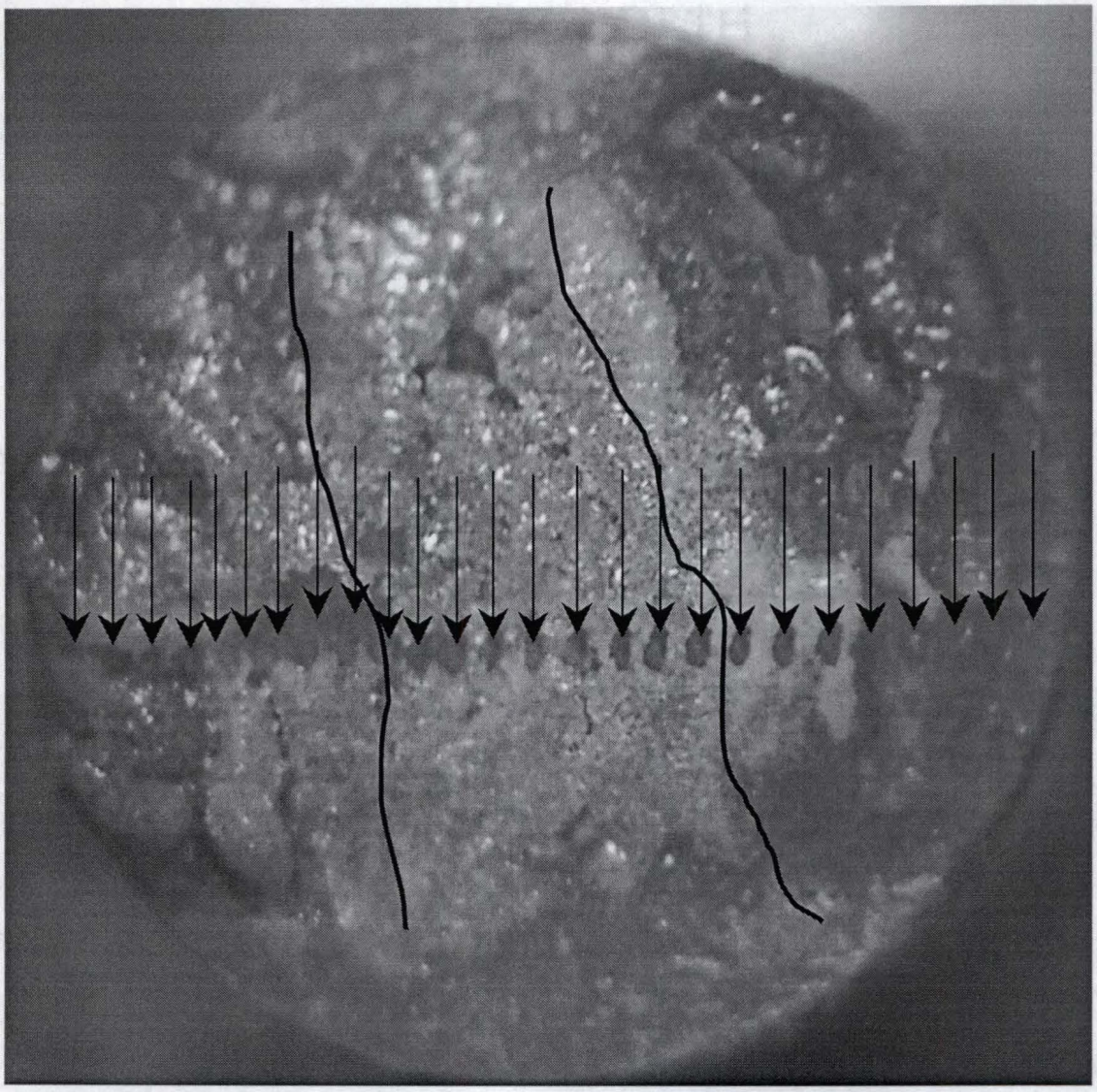

Figure 5.20. A photomicrograph of the rat liver tissue spiked with paclitaxel to a level of 200 ng/mg (center piece) between two outer pieces of rat liver tissue which were not spiked. Arrows indicate the spots sampled with the UV laser. Black lines have been added to indicate the location of spiked and non-spiked tissue samples.

daughter ions were summed for each analytical scan (figure 5.21). As was seen in the mapping of the rat liver tissue spiked with spiperone, the points on the plot which indicate a mean intensity above baseline correspond to the sampled spots on the tissue which were spiked with paclitaxel.

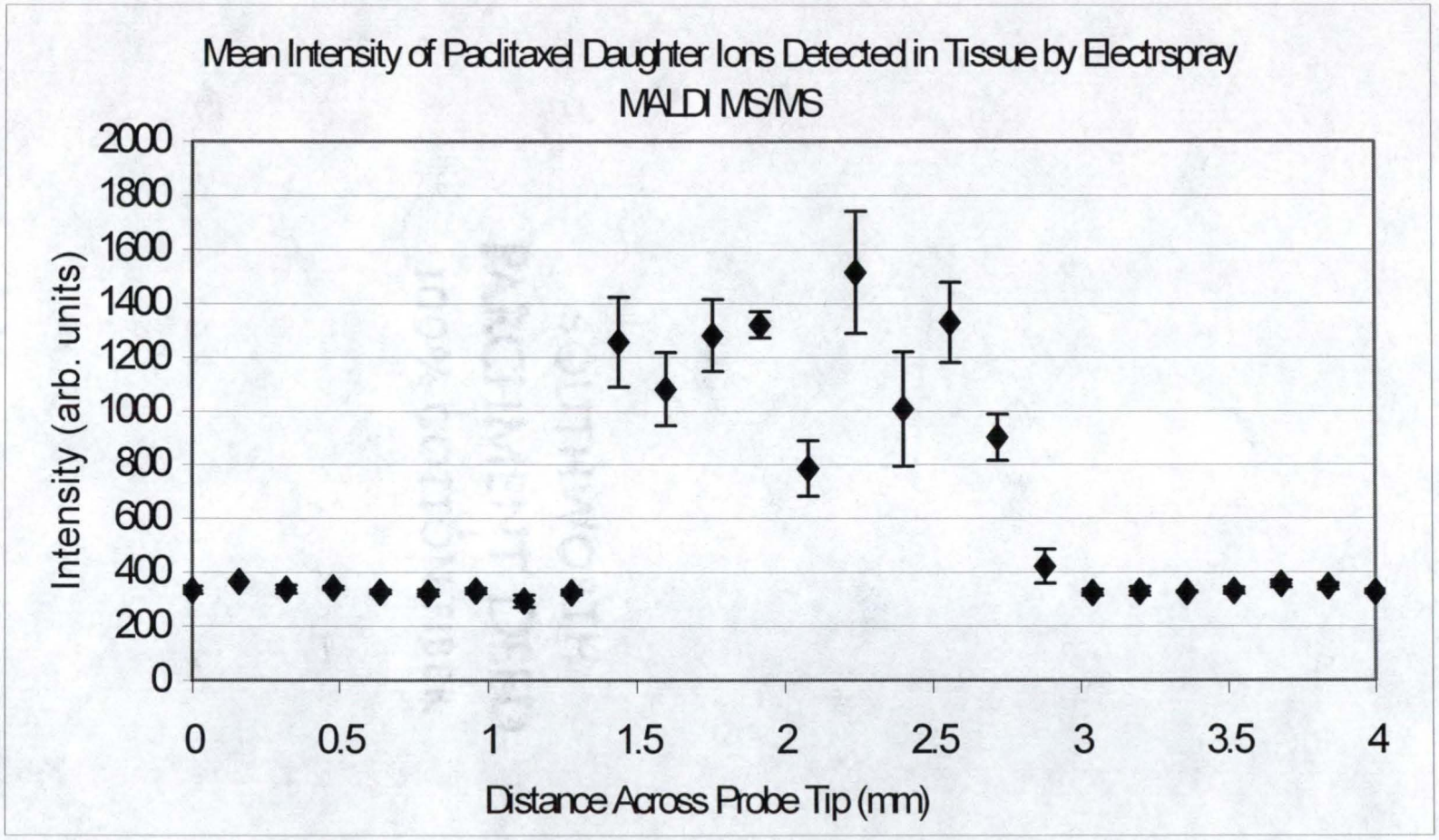

Figure 5.21. A plot of the mean of the summed intensities of the characteristic daughter ions of the $[M+Na]^+$ ion of paclitaxel in the rat liver tissue sample shown in figure 5.20. The error bars are ± 1 standard deviation of the mean.

CHAPTER 6
CONCLUSIONS AND FUTURE WORK

The goal of this project was to design, construct, and evaluate an instrument capable of mapping the location of pharmaceutical compounds in intact tissue masses at normal physiological levels. Early work demonstrated the ability of the instrument for the detection of pharmaceutical compounds in intact tissue at normal physiological levels; however, the spatial distribution of those compounds in the tissue could not be determined. The early work with the instrument used matrix-assisted laser desorption/ionization (MALDI) as a preparation technique to enhance the desorption and the ionization of pharmaceutical compounds. In the preparation process, the thin tissue slice (approximately 0.5 mm thick) had several microliters of a solution containing a MALDI matrix pipetted onto the surface and allowed to air dry (typically between 15 and 60 seconds). During the evaporation of the solution, cooling of the solution surface, as well as the formation of matrix crystals in the remaining solution, produce currents in the solution that allow the extracted analyte to migrate across the surface of the sample. Simple diffusion is not expected to play a major role in this migration: consider that the diffusion coefficient for glycine (mw=75) at 25^0 C in water is1.05×10^{-3} mm/s. Although

methanol is less viscous than water (methanol viscosity = 0.555 $x10^{-3}$ kg m^{-1} s^{-1}, water viscosity = 0.891 $x10^{-3}$ kg m^{-1} s^{-1}), spiperone is of higher molecular weight than glycine. Even imagining an order of magnitude difference in the diffusion coefficient for spiperone in methanol would result in less than 0.25 mm of migration in 15 seconds. The migration of analyte was shown to be as far as 2 mm (half the diameter of the probe tip used in the instrument) in as little as 15 seconds. The migration of the extracted analyte over such a distance completely removed spatial distribution information needed to map the location of the pharmaceutical compound in the tissue mass.

To preserve the spatial distribution of the pharmaceutical compounds in the intact tissue sample, both an alternative preparation method and an alternative ionization method were evaluated. The alternative ionization method was laser desorption (without the addition of a matrix for assistance) coupled to chemical ionization (CI). Because CI creates analyte ions in the gas phase, after desorption of the material from the solid surface, there was no reason to apply the matrix solution which allowed the migration of the compound. The first experiments were designed to determine if laser desorption coupled to chemical ionization (LD/CI) was capable of detecting pharmaceutical compounds in intact tissue samples at physiological levels. The drug spiperone was detected in rat liver tissue at a level of 25 ng/mg of tissue using a CO_2 laser for desorption and methane as a reagent gas for chemical ionization. The MS/MS capability of the quadrupole ion trap (first to

isolate a group of ions around the m/z of the ion of interest and then to selectively fragment the ion by CAD producing the characteristic daughter ions of the pharmaceutical compound for unambiguous identification) was crucial for the detection of trace level compounds in the complex tissue matrix.

The alternative preparation method tested was the electrospraying of the MALDI matrix solution onto the surface of the intact tissue mass. By electrospraying the matrix solution onto the surface of the tissue mass, the evaporation of the matrix solution was accelerated which in turn reduced the ability of the extracted analyte to migrate across the surface. Again, rat liver tissue was incubated with the drug spiperone to a level of 25 ng/mg. A MALDI matrix solution consisting of 70% methanol and 30% aqueous 1% acetic acid solution with 10 μg/μL of the MALDI matrix 2,5-dihydroxybenzoic acid (DHB) was electrosprayed onto the surface of the sample. The drug spiperone was sufficiently extracted from the tissue for detection without migration across the surface of the tissue mass within the spatial resolution of the experiment (300 μm).

Both methods were used for the mapping of spiperone in intact tissue samples where the compound was selectively located. The spatial resolution used in the mapping procedure was approximately 150 μm; however, based on the spot sizes used in the experiments it is reasonable to expect that a resolution of 25 μm would be possible.

Both methods were also used to map the location of an experimental compound which was administered to dogs intravenously. The concentration of the compound in the tissue sample was estimated to be 59 ng/mg based on the specific activity of the ^{14}C radiolabeled compound. The mapping of the compound by both LD/CI and MALDI with electrosprayed matrix showed spatial variation of the MS/MS signal across the tissue mass and again demonstrated the capability of the instrument to map a pharmaceutical compound in an intact tissue mass at normal physiological levels. It is not yet possible, however, to confirm that the variation in MS/MS signal directly correlates with variation in the concentration of the drug compound. Other possible causes for variation of the MS/MS signal across the tissue include changes in the tissue thickness in different regions during the drying of the tissue mass, possible changes in the extractability of the analyte based on different tissue types across the tissue mass, and differences in the absorbance characteristics of the different tissue types.

Finally, the electrospraying of the MALDI matrix was evaluated for the mapping of paclitaxel in tissue. A thin slice of rat liver tissue spiked with paclitaxel to a level of 200 ng/mg was placed between two non-spiked pieces of rat liver tissue. The entire tissue surface was electrosprayed with a 70% methanol 30% aqueous 1% acetic acid solution containing 10 μg/μL of DHB. The location of the spiked piece of rat liver tissue was mapped using a resolution of 150 μm by MALDI MS/MS.

While the ability to map the location of pharmaceutical compounds in intact tissue masses has been demonstrated, there are several areas where additional experiments are needed. Additional experiments for the electrospraying of the MALDI matrix solution include: an evaluation of the distance of migration of an analyte electrosprayed with various MALDI matrix solution compositions, an evaluation of the effect of different flow rates (for control of drop size) used in the electrospraying of the MALDI matrix solution, the evaluation of different classes of pharmaceutical compounds (based on their solubility in aqueous solutions) and the electrospraying of the MALDI matrix solutions, and the evaluation of different MALDI matrices to see if the sensitivity of the instrument can be improved for experiments using the electrospraying of the MALDI matrix.

The composition of the solution mixture in the electrospray experiments was not rigorously investigated. All of the pharmaceutical compounds tested dissolved completely in the 70% methanol 30% aqueous 1% acetic acid solution. This solution mixture was used because it offered a high percent of organic content which evaporated at a faster rate than a purely aqueous solution, thus minimizing the evaporation time during which the compound was capable of migrating. Preliminary experiments indicated that spiperone was capable of migration in a solution where the aqueous phase was greater than 50% (the balance was methanol); however, the extent of that migration and the extent of migration for other classes of compounds (based

on their solubility in different solvents) should be explored. There is expected to be a trade off from increasing the aqueous phase (and so the contact time between the solvent and the surface): a longer contact time is expected to give better extraction of the analyte while a shorter contact time should reduce the migration of the analyte.

The electrospraying of the matrix solution offers some control of drop size (through flow rate of the applied matrix solution and the potential applied); however, establishing and maintaining a good electrospray spray is essential. In the early evaluation of the electrospray apparatus it was found that low matrix solution flow rates (1 μl/min) and low sheath gas flow rates (less than 20 mL/min) caused the electrospray apparatus to 'spit' large droplets onto the surface of the tissue which allowed the extracted compound to migrate across the surface. Flow rates higher than 5 μL/min might provide a better wetting of the tissue surface (again for better extraction of the analyte) without increasing the migration of the analyte across the tissue surface (depending on solution composition).

All of pharmaceutical compounds investigated in the experiments presented in this dissertation were soluble in organic solvents (to a level of at least 1 mg/mL). It would be worthwhile to evaluate compounds that were not appreciably soluble in organic solvents. The challenge of minimizing the migration of compounds when electrospraying a high percentage of aqueous MALDI matrix solution would be expected to be great.

For the tissue experiments presented here, only one MALDI matrix was used (there were alternative matrices used in the IR MALDI section of chapter 4, but not on tissue samples). DHB was used as a matrix because it had been demonstrated in earlier research to be a good universal matrix for the investigation of pharmaceutical compounds by MALDI.[62] It is possible that other matrices may offer benefits such as increased detection of certain classes of pharmaceutical compounds. A more rigorous study of different matrices for different classes of pharmaceutical compounds (along with the matrix solvent solution used in the electrospraying of the matrix) would be of great interest.

Another area which is of interest is the tissue preparation step. For the experiments presented in this dissertation the tissue samples were prepared by cutting a thin slice of frozen tissue with a scalpel. It is possible that the thickness of the tissue sample would have an effect on the sensitivity of the MALDI method. A series of experiments investigating the effect of tissue slices prepared with a microtome (ranging in thickness from 10 μm to 500 μm) would be of interest. In addition, the effects of sample preparation for microtome cutting would be interesting (cutting a frozen sample to prevent the blurring of the compound's location within the tissue mass).

For the mapping of compounds in intact tissue by LD/CI, additional experiments which should be preformed include: the optimization of chemical

ionization conditions to reduce the fragmentation of paclitaxel, and the addition of better optics to better collimate the laser beam used for LD/CI.

As was discussed in Chapter 5, the chemical ionization of paclitaxel caused extensive fragmentation. Reagent gases other than the three evaluated for this dissertation (methane, isobutane, and ammonia) should be explored. Additionally, because there was no fragmentation of paclitaxel when ammonia was used as a reagent gas, a mixture of ammonia with other reagent gases might increase the sensitivity for paclitaxel. According to Harrison, the addition of methane to ammonia has been shown to increase the formation of the ammonia adduct ion.[101] This might allow ammonia to be used for the chemical ionization of paclitaxel in tissue.

In the experiments presented in this dissertation, the spot size of the CO_2 laser beam was reduced by physical blocking (with a metal iris). In conversations with laser optical experts, it was suggested that the beam could be reduced and collimated at the same time (this avenue has not been extensively investigated). A more collimated laser beam may reduce the damage caused to the tissue surrounding the area of the laser spot and may allow more laser pulses to be used before reduction of the ion signal occurs. Additionally, the use of filters to reduce the laser power (rather than the metal iris) should provide greater control of the laser spot size and energy used in LD/CI. If the amount of ablated material from each laser pulse was minimized

to the amount needed for detection of the analyte this may allow for an increase in the number of laser pulses from each spot analyzed by LD/CI.

One area of LD/CI which would be of interest to explore is the use of frozen samples. It has been reported that the water molecules in a frozen sample can act as a MALDI matrix to enhance desorption and ionization from frozen samples.[120] This would require the construction of a frozen finger device to keep the sample frozen while inside of the mass spectrometer. This technique may offer the advantages of MALDI (using the water as the matrix) without the disadvantages of having to electrospray the tissue sample.

Experiments which would also be of interest would be the evaluation of spot size versus sensitivity. A smaller spot size would reduce the amount of material ablated (and so reduce the sensitivity). The eventual maximum spatial resolution achievable with the instrument will be the smallest laser beam spot possible. The size of that laser beam spot may be dictated by the physical constraints of the laser light, or more likely, by the sensitivity of the instrument and the need to increase the spot size used for sampling to increase the amount of material ablated to permit trace level detection.

Another area which should be explored is the determination of detection limits for the mapping of various compounds in different tissue types. Considering that a more reproducible signal is necessary for the mapping of compounds than for their simple detection, it would be of great interest to determine the limits of detection for several compounds where the instrument

may be used in the future. The drug compound to be investigated and the tissue type where that drug will be found more than likely will have an effect on that limit of detection.

Also of interest would be studies to evaluate the response of specific pharmaceutical compounds in heterogeneous tissue samples. Because it is expected that the sensitivity of the instrument moving from one tissue type to another (within the same mass) may be dependent on the compound and tissue type, these studies would be restricted to specific examples; however, once determined for those examples, better semi-quantitative (or relative quantitative) analysis of the distribution of the compound in those examples should be possible.

Because the spatial distribution of pharmaceutical compounds in the tissue masses used for the mapping experiments in this dissertation were artificially arranged (except for the experimental compound), there need to be more studies done for the mapping of pharmaceutical compounds in tissue samples where the distribution of the compound is natural (the drug was administered by traditional methods). Also, the instrument could be evaluated for the mapping of biological structures in intact tissue masses. This use would allow the comparison of a visual map to the daughter ion intensity map.

In addition to the above mentioned experiments, some considerations for the next generation instrument are of interest. One area which is in need of improvement from the current instrument is the ion source . The current ion

source used in the instrument was a modified version of the Finnigan 4500 ion source. The size of the ion volumes (0.3" in diameter) used with the 4500 ion source were very restrictive. To allow full movement of the sample past the opening in the CI ion volume, the probe tip was restricted to a diameter of 0.155". A larger ion source which would be able to accommodate samples of 1 cm in diameter would allow for the mapping of larger samples. In addition, a larger ion source may make visualization of the sample (while the sample is in the mass spectrometer under investigation) easier. Currently, the major restriction to adding a method to visualize the sample while it is being interrogated with the laser beam is the need for a restricted ion volume when performing CI. A larger ion source would allow easier access (possibly with an endoscope) for visualization of the sample. By adding visualization of the sample while it is in the mass spectrometer, better control of where the laser beam strikes the surface of the sample would be possible (by adding a visual spotting laser to the optics of the system).

The movement of the sample by the X,Y-stage while the sample was in the mass spectrometer was not as reproducible as it could be. The X,Y-stage control of the probe was several inches away for the probe tip. This resulted in a variation of ±25 μm when sampling back and forth across the sample surface. In addition, the location of the sample in the ion volume (and so the location of the laser beam on the surface of the sample) varied by as much as 100 μm each time the probe was removed and inserted into the mass

spectrometer. Direct control of the probe tip (and so the sample) while inside of the mass spectrometer should reduce this variation. Computer control of the micrometers would also be desirable as a first step toward automating the instrument.

Finally, the research undertaken to demonstrate the ability of the quadrupole ion trap laser microprobe instrument to date has focused exclusively on the detection of pharmaceutical compounds in intact tissue; however, the ability of the instrument to detect compounds in a complex solid matrix has other applications. The instrument has been used to detect acetylcarnitine in whole human blood (results not included in this dissertation). As was seen in the detection of pharmaceutical compounds in tissue, the ability to perform MS/MS for the unambiguous identification of acetylcarnitine in whole blood was crucial. Because several metabolic disorders have been linked to carnitine levels in humans, there has been a growing interest in easily and rapidly determining the level of acylcarnitines in a variety of metabolic fluids.[121] Recently the levels of acylcarnitines in human urine were measured by MALDI MS.[122] Although the MALDI process used did not require the derivatization of the carnitines, they were extracted from the urine prior to detection. With the MS/MS capabilities of the quadrupole ion trap instrument, no prior extraction was needed to detect the acylcarnitines in blood.. This demonstrates the ability of the instrument to perform other tasks for which it was not specifically designed to do.

LIST OF REFERENCES

1. Smith, C.G. *The Process of New Drug Discovery and Development.* CRC Press: Boca Raton, **1992**, 8-9.

2. Stahl, E. *Drug Analysis by Chromatography and Microscopy.* Ann Arbor Press: Ann Arbor, **1973**, 57-81.

3. Perun, T. J. ; Propst, C. L. *Nucleic Acid Targeted Drug Design.* Marcel Dekker Press: New York, **1992**, 619-720.

4. Lee, M.; Kerns, E.; Hail, M.; Lui, J.; Volk, K. *LC-GC* **1997**, 15, 542-558.

5. Honig, R. E. and Woolston, J. R. *App. Physics Lett.* **1963**, 2(7) 138-139.

6. Castaing, R. and Slodzian, G. *J. Microscopie* **1962,** 1, 395-410.

7. Fragu, P.; Briancon, C.; Fourre, C.; Clerc, J.; Casiraghi, O.; Jeusset, J.; Omri, F.; and Halpern, S. *Biol. Cell* **1992,** 74, 5-18.

8. Short, R.; Ameen, A.; Jackson, S.; Pawson, D.; O'Toole, L.; and Ward, A. *Vacuum* **1993,** 44, 1143-1160.

9. Grimm, C.; Short, R.; and Todd, P. *Am. Soc. Mass Spectrom.* **1991** 2, 362-371.

10. Gusev, A.; Proctor, A.; Rabinovich, Y.; Hercules, D. *Anal. Chem.* **1995**, 67, 1805-1814.

11. McMahon, J,; Short, R.; McCandlish, C.; Brenna, J. Todd, P. *Rapid Comm. Mass Spectrom.* **1996**, 10, 335-340.

12. Neilsen, J.; Abildtrup, A.; Christensen, J.; Watson, P.; Cox, A.; McLeod, C. *Spectrochim. Acta B* **1998**, 53, 339-345.

13. Mansoori, B.; Johnston, M.; Wexler, A. *Anal. Chem.* **1994**, 66, 3681-3687.

14. Xie, C.; Mattson, M.; Lovell, M. Yokel, R. *Brain Res.* **1996**, 271-277.

15. Mathey, A.; Vaeck, L. V.; Steglich, W. *Anal. Chim. Acta* **1987**, 195, 89-96.

16. Todd, P.; McMahon, J.; Short, R.; McCandlish, C. *Anal. Chem.* **1997**, 69 , 529A-535A.

17. Pacholski, M.; Cannon, D.; Ewing, A.; Winograd, N. *Rapid Comm. Mass Spectrom.* **1998**, 12, 1232-1235.

18. Caprioli, R.; Farmer, T.; Gile, J. *Anal. Chem.* **1997**, 69, 4751-4760.

19. Kovalev, I. D.; Maksimov, G. A.; Surkov, A. I.; Larin, N. V. *Int. J. Mass Spectrom. Ion Physics* **1978**, 27, 101-137.

20. Conzemius, R. J.; Capellen, J. M. *Int. J. Mass Spectrom. Ion Phys.* **1980**, 34, 197-271.

21. Cotter, R. J. *Anal. Chim. Acta* **1987**, 195, 45-59.

22. Struyf, H.; Vaeck, L. V.; Poels, K.; Grieken, R. V. *J. Am. Soc. Mass Spectrom* **1998**, 9, 482-497.

23. Tsugoshi, T.; Chiba, H.; Yokoyama, T.; Furuya, K.; Kikuchi, T. *J. Trace Microprobe. Techniq.* **1998**, 16, 47-57.

24. Muddiman, D.; Gusev, A.; Proctor, A.; Hercules, D.; Venkataramann, R.; Diven, W. *Anal. Chem.* **1994**, 66, 2362-2368.

25. Chew, A.; Sykes, D. E.; Waddilove, A. E. *J. Anal. Atomic Spectrom.* **1997**, 12, 1101-1103.

26. Spengler, B.; Karas, M.; Hillenkamp, F. *J. Phys. Chem.* **1987**, 91, 6502-6506.

27. Cotter, R. *Anal. Chem.* **1992,** 64, 1027A-1039A.

28. Hillenkamp, F.; Unsold, E.; Kaufmann, R.; Nitsche, R. *Appl. Phys.* **1975**, 8, 341-348.

29. Vogt, H.; Heinen, H.; Meier, J.; Wechsung, R. *Fresenius Z. Anal. Chem.* **1981**, 308, 195-200.

30. Van Vaeck, L.; Claereboudt, J.; Waele, J.; Esmans, E.; Gijbels, R. *Anal. Chem.* **1985**, 57, 2944-2951.

31. Hachimi, A.; Van Vaeck, L.; Poels, K.; Adams, F.; Muller, J. *Spectrochim. Acta B* **1998**, 53, 347-365.

32. Pogue, R.; Zhang, W.; Wonkka, R.; Majidi, V. *Microchemical J.* **1994**, 50, 301-309.

33. Van Vaeck, L.: Van Espen, P.; Adams, F.; Gijbels, R. *Biomed. Eviron. Mass Spectrom.* **1989**, 18, 581-591.

34. Feigl, P.; Schueler, B.; Hillenkamp, F. *Int. J. Mass Spectrom. Ion Phys.* **1983**, 47, 15-18.

35. Novak, F.; Hercules, D. *Anal. Lett.* **1985**, 18, 503-518.

36. Kubis, A.; Somayajula, K.; Sharkey, A.; Hercules, D. *Anal. Chem.* **1989**, 61, 2516-2523.

37. Gusev, A.; Vasseur, O.; Proctor, A.; Sharkey, A.; Hercules, D. *Anal. Chem.* **1995**, 67, 4565-4570.

38. Wilk, Z.; Hercules, D. *Anal. Chem.* **1987**, 59, 1819-1825.

39. Tsugoshi, T.; Furuya, K.; Kikuchi, T.; Kobayashi, H.; Ueno, M. *Mikrochim. Acta.* **1994**, 113, 261-267.

40. Novak, F.; Wilk, Z.; Hercules, D. *J. Trace Microprobe Tech.***1985**, 3, 149-163.

41. Conzemius, R.; Svec, H. *Anal. Chem.* **1978**, 50, 1854-1860.

42. Fedorowich, J.; Jain, J.; Kerrich, R. *Can. Mineral.* **1995**, 33, 469-480.

43. Van Roy, W.; Struyf, H.; Kennis, P.; Van Vaeck, L.; Grieken, R.; Andrle, C. *Mikrochim. Acta.* **1995**, 120, 121-137.

44. Troendle, F.; Reddick, C.; Yost, R. *J. Am. Soc. Mass Spectrom.* **1999**, 10, 1315-1321.

45. Paul, W.; Steinwedel, H. U.S. Patent 2,939,952 filed June 7, 1960 (German Patent 944,900 filed December 21, 1956).

46. Wuerker, R.; Shelton, H.; Langmuir, R. *J. Appl. Phys.* **1959**, 30, 342-349.

47. Fischer, E. *Z. Phys.* **1959**, 156, 1-26.

48. Rettinghaus, V. *Z. Angew. Phys.* **1967**, 156, 1-26.

49. Dawson, P. H.; Whetten, N. R. *J. Vac. Sci. Tech.* **1967**, 5, 11-18.

50. Stafford, G.; Kelley, P.; Syka, J.; Reynolds, W.; Todd, J. *Int. J. Mass Spectrom. Ion Process.* **1984**, 60, 85-98.

51. Stafford, G. C.; Kelley, P. E.; Bradford, D.C. *Am. Lab.* **1983**, 51-57.

52. Louris, J. N.; Cooks, R. G.; Syka, J. E.; Kelley, P. E.; Stafford, G. C.; Todd, J. F. *Anal. Chem.* **1987**, 59, 1677-1685.

53. Gronowska, J.; Paradisi, C.; Traldi, P.; Vettori, U. *Rapid Commun. Mass Spectrom.* **1990**, 4, 306-313.

54. Weber-Grabau, W.; Kelley, P. E.; Syka, J. E.; Bradshaw, S. C.; Brodbelt, J. S. *Presented at the 35th ASMS Conference on Mass Spectrometry and Allied Topics* **1987**, Denver, CO, 1114-1115.

55. Kaiser, R. E.; Cooks, R. G.; Syka, J. P.; Stafford, G. C. *Rapid Commun. Mass Spectrom.* **1990**, 4, 30-33.

56. Soni, M. H.; Cooks, R. G. *Anal. Chem.* **1994**, 66, 2488-2496.

57. March, R. E.; Londry, F. A. *Practical Aspects of Ion Trap Mass Spectrometry (Vol.1)* March, R.; Todd, J. Eds. CRC Press; Boca Raton, **1995**, 27.

58. Vedel, F.; Vedel, M.; Broadbelt, J. *Practical Aspects of Ion Trap Mass Spectrometry (Vol. 1)* March, R.; Todd, J. Eds. CRC Press; Boca Raton, **1995**, 343-396.

59. Weber-Grabau, M.; Kelly, P.; Bradshaw, S.; Hoekman, D. *Presented at the 36th Conference on Mass Spectrometry and Allied Topics* **1988**, San Francisco, CA, 1106-1107.

60. Stafford, G. C.; Taylor, D. M.; Bradshaw, S. C.; Syka, J. E.; Uhrich, M. *Presented at the 35th ASMS Conference on Mass Spectrometry and Allied Topics* **1987**, Denver, CO, 775-776.

61. Kaiser, R. E.; Louris, J. N.; Amy, J. W.; Cooks, R. G. *Rapid Commun. Mass Spectrom.* **1989**, 3, 225-229.

62. Reddick, C. Ph.D. Dissertation. *The Detection of Pharmaceutical Drug Compounds from Intact Biological Tissue by Matrix-assisted Laser Desorption Ionization (MALDI) Quadrupole Ion Trap Mass Spectrometry.* University of Florida, **1997**.

63. Pedder, R. E.; Yost, R. A. in *Proceedings of the 37th ASMS Conference on Mass Spectrometry and Allied Topics*, **1989**, Miami, Fl., 468.

64. Pedder, R. Ph.D. Dissertation. *Fundamental Studies in a Quadrupole Ion Trap Mass Spectrometer.* University of Florida, **1992**.

65. Sundqvist, B.; Hedin, A.; Hakansson, P.; Kamensky, M.; Salehpour, M.; Sawe, G. *Int. J. Mass Spectrom. Ion Process.* **1985**, 65, 69-89.

66. Chait, B.; Field, F. *Int. J. Mass Spectrom. Ion Process.* **1985**, 65, 169-180.

67. Tanaka, K.; Waki, H.; Ido, Y.; Akita, S.; Yoshida, Y.; Yoshida, T. *Rapid Commun. Mass Spectrom.* **1988**, 8, 151-153.

68. Karas, M.; Hillenkamp, F. *Anal. Chem.* **1988**, 60, 2301-2303.

69. Karas, M.; Bachman, D.; Hillenkamp, F. *Anal. Chem.* **1985**, 57, 2935-2939.

70. Zenobi, R.; Knochenmuss, R. *Mass Spectrom. Rev.* **1998**, 17, 337-366.

71. Johnson, R. *Int. J. Mass Spectrom.* **1994**, 139, 25-39.

72. Vertes, A.; Irinyi, G.; Gijbels, R. *Anal. Chem.* **1993**, 65, 2389-2393.

73. Ens, W.; Mao, Y.; Mayer, F.; Standling, K. *Rapid Commun. Mass Spectrom.* **1991**, 5, 117-123.

74. Vertes, A.; Gijbels, R.; Levine, R. *Rapid Commun. Mass Spectrom.* **1990**, 4, 228-233.

75. Vertes, A.; Levine, R. *Chem. Phys. Let.* **1990**, 171, 284-290.

76. Ehring, H.; Karas, M.; Hillenkamp, F. *Org. Mass Spectrom.* **1992**, 27, 472-480.

77. Allwod, D.; Dyer, P.; Dreyfus, R. *Rapid Commun. Mass Spectrom.* **1997**, 11, 499-503.

78. Knochenmuss, R.; Dubois, F.; Dale, M.; Zenobi, *R. Rapid Comm. Mass Spectrom.* **1996**, 10, 871-877.

79. Ehring, H.; Costa, C.; Demirev, P.; Sundqvist, B. *Rapid Commun. Mass Spectrom.* **1996**, 10, 821-824.

80. Linder, B.; Seydel, U. *Anal. Chem.* **1985**, 57, 895-899.

81. Johnson, R.; Sundqvist, B. *Rapid Commun. Mass Spectrom.* **1991**, 5, 574-578.

82. Cramer, R.; Haglund, R.; Hillenkamp, F. *Int. J. Mass Spectrom. Ion Process.* **1997**, 169/170, 51-67.

83. Scott, C.; Kosmidis, C. Jia, W.; Ledingham, K.; Singhal, R. *Rapid Commun. Mass Spectrom.* **1994**, 8, 829-832.

84. Sunner, J. *Org. Mass Spectrom.* **1993**, 28, 805-823.

85. Van Der Peyl, G.; Isa, K.; Haverkamp, J.; Kistermaker, P. *Nucl. Inst. Methods* **1982**, 198, 125-130.

86. Wani, M. C.; Taylor, H. I.; Wall, M. E. *J. Am. Chem. Soc.* **1971**, 93, 2315-2317.

87. Schiff, P. B.; Horwitz, S. B. *Biochemistry* **1981**, 20(11), 3247-3252.

88. Arbuck, S. G.; Christian, M. C.; Fisherman, J. S.; Cazenave, L. A.; Sarosy, G.; Suffness, M.; Adams, J.; Canetta, R.; Cole, K. E.; Friedman, M. A. *Second National Cancer Institute Workshop on Taxol and Taxus* **1992**, 15, 25-37.

89. Doherty, S.; Busch, K. *Anal. Chim. Acta.* **1989**, 218, 217-229

90. Vertes, A.; Gijbels, R.; Adams, F. *Laser Ionization Mass Analysis.* John Wiley & Sons: New York, **1993**, 7-126.

91. Vastola, F.; Pirone, A. *Adv. Mass Spectrom.* **1968**, 4, 107-111.

92. Vastola, F.; Mumma, R.; Pirone, A. *Org. Mass Spectrom.* **1970**, 3, 101-104.

93. Posthumus, M.; Kistermaker, P.; Meuzelaar, H.; Ten Noever de Brauw, M. *Anal. Chem.* **1978**, 50, 985-991.

94. Van Der Peyl, G.; Haverkamp, J.; Kistermaker, P. *Int. J. Mass Spectrom. Ion Phys.* **1982**, 42, 125-141.

95. Daves, G. *Acc. Chem. Res.* **1979**, 12, 359-365.

96. Hillenkamp. F. *Int. J. Mass Spectrom. Ion Phys.* **1982**, 45, 305-313.

97. Van Der Peyl, G.; Isa, K.; Haverkamp, J.; Kistermaker, P. *Org. Mass Spectrom.* **1981**, 16, 416-420.

98. Linder, B. *Int. J. Mass Spectrom. Ion Process.* **1991**, 103, 203-218.

99. Van Breeman, R.; Snow, M.; Cotter, R. *Int. J. Mass Spectrom. Ion Phys.* **1983**, 49, 35-50.

100. Perchalaski, R. J. Ph.D. Dissertation *Characteristics and Application of a Laser Ionization/Evaporation Source for Tandem Mass Spectrometry.* University of Florida, **1985**.

101. Harrison, A. *Chemical Ionization Mass Spectrometry*, 2nd Ed., CRC Press; Boca Raton, **1992**.

102. Griffin, T. P. Ph.D. Dissertation. *GC/MS/MS on the Quadrupole Ion Trap Mass Spectrometer: Software Development and the Examination of the Effects of Ion Population*. University of Florida, **1995.**

103. Yates, N. A. Ph.D. Dissertation. *Methods for Gas Chromatography-Tandem Mass Spectrometry on the Quadrupole Ion Trap*. University of Florida, **1994.**

104. Escandon, N. A.; Zimmerman, D. C.; McCall, R. B. *J. Pharmacol. Exp. Ther.* **1994**, 268, 441-447.

105. Booth, M. M. Ph.D. Dissertation. *Matrix-Assisted Laser Desorption Ionization (MALDI) Tandem Mass Spectrometry (MS^n) Using a Quadrupole Ion Trap*. University of Florida, **1996.**

106. Vargas, R. Ph.D. Dissertation. *Development of Laser Desorption Ionization on a Quadrupole Ion Trap Mass Spectrometer*. University of Florida, **1993.**

107. Chen, L.; Wang, T. L.; Ricca, T. L.; Marshall, A. G. *Anal. Chem.* **1987**, 59, 449-454.

108. *Finnigan MAT 4500 Series GC/MS Operator's Manual. Revision A.* Finnigan MAT: San Jose, CA, **1982**, 4-3.

109. Stoeckli, M.; Farmer, T.; Caprioli, R. *J. Am. Soc. Mass Spectrom.* **1999**, 10, 67-71.

110. Eckerskorn, C.; Strupat, K.; Schleuder, D.; Hochstrasser, D.; Scanchez, J.; Lottspeich, F.; Hillenkamp, F. *Anal. Chem.* **1997**, 69, 2888-2892.

111. Zhang, W.; Niu, S.; Chait, B. *J. Am. Soc. Mass Spectrom.* **1998**, 9, 879-884.

112. Talrose, V.; Person, M.; Whittal, R.; Walls, F.; Burlingame, A.; Baldwin, M. *Rapid Commun. Mass Spectrom.* **1999**, 13, 2191-2198.

113. Sadeghi, M.; Olumee, Z.; Tang, X.; Vertes, A.; Jiang, Z.; Henderson, A.; Lee, H.; Prasad, C. *Rapid Commun. Mass Spectrom.* **1997**, 11, 393-397.

114. Sheffer, J.; Murray, K. *Rapid Commun. Mass Spectrom.* **1998**, 12, 1685-1690.

115. Kampmeier, J.; Dreiswerd, K.; Schurenberg, M.; Strupat, K. *Int. J. Mass Spectrom. Ion Process.* **1997**, 169/170, 31-41.

116. Overberg, A.; Karas, M.; Hillenkamp, F. *Rapid Commun. Mass Spectrom.* **1991**, 5, 128-132.

117. Menzel, C.; Berkenamp, S.; Hillenkamp, F. *Rapid Commun. Mass Spectrom.* **1999**, 13, 26-32.

118. Niu, S.; Zhang, W.; Chait, B. *J. Am. Soc. Mass Spectrom.* **1998**, 9, 1-7.

119. Berenkamp, S.; Menzel, C.; Karas, M.; Hillenkamp, F. *Rapid Commun. Mass Spectrom.* **1997**, 11, 1399-1406.

120. Williams, P.; Thomas, R.; Nelson, R.; *Rapid Comm. Mass Spectrom.* **1990**, 4, 348-351

121. Feller, A.; Rudman, D. *J. Nutr.* **1988**, 118, 541-547.

122. Briand, G.; Fontaine, M.; Schubert, R.; Ricart, G.; Degand, P.; Vamecq, J. *J. Mass Spectrom.* **1995**, 30, 1731-1741.

BIOGRAPHICAL SKETCH

Frederick Joseph Troendle was born on February 2nd, 1955, in Washington D.C. He lived the first two years of his life in Silver Spring, Maryland, before his family moved to Bethesda, Maryland. He was the second child out of seven (and second son) of Drs. Gloria and Frank Troendle (both were pediatricians). His early childhood dreams were of becoming a rocket scientist like his hero Robert Goddard; however, like several of the Troendle children he suffered from dyslexia (unknown at the time) and the accompanying substandard high school performance.

Rick graduated from Charles W. Woodward high school in 1973 and pursued a career as an automobile mechanic for an Oldsmobile dealership in the Washington D.C. area. In early 1976, he packed up everything he owned and moved to Jacksonville, Florida, and worked as an Oldsmobile mechanic for a local dealership. With the encouragement of a friend, in late 1976 he attended Jones College in Jacksonville, working toward an associate in arts degree in communications. In early 1977, he got a full-time job at a new radio station which went on the air in Green Cove Springs, Florida (just south of Jacksonville) and eventually left college a few credits short of earning his degree. After bouncing around at different radio stations in the Jacksonville

area, Rick landed the afternoon drive job at WIVY radio in 1984. In 1985, he met his future wife Lorraine through a mutual friend and they were married on June 7th, 1986.

In the fall of 1989, Rick was fired from WIVY (the station changed direction and his services were no longer appreciated). Rather than continuing his career in radio, Rick returned to college (first at Florida Community College of Jacksonville and then at the University of North Florida). He graduated from UNF in 1995, summa cum laude with a 4.0 GPA, earning a degree in chemistry. After working for one year as a lab lecturer at UNF, Rick entered the University of Florida to pursue a doctorate in analytical chemistry under the supervision of Dr. Richard A. Yost. In 1997, Rick was awarded the NASA Space Grant Consortium Fellowship and spent his summers while at graduate school working with the Advance Life Support Program group at Kennedy Space Center Florida (back to rockets).

I certify that I have read this study and that in my opinion it conforms to acceptable standards of scholarly presentation and is fully adequate, in scope and quality, as a dissertation for the degree of Doctor of Philosophy.

Richard A. Yost, Chair
Professor of Chemistry

I certify that I have read this study and that in my opinion it conforms to acceptable standards of scholarly presentation and is fully adequate, in scope and quality, as a dissertation for the degree of Doctor of Philosophy.

David H. Powell
Scientist in Chemistry

I certify that I have read this study and that in my opinion it conforms to acceptable standards of scholarly presentation and is fully adequate, in scope and quality, as a dissertation for the degree of Doctor of Philosophy.

Willard W. Harrison
Professor of Chemistry

I certify that I have read this study and that in my opinion it conforms to acceptable standards of scholarly presentation and is fully adequate, in scope and quality, as a dissertation for the degree of Doctor of Philosophy.

Randolph Duran
Associate Professor of Chemistry

I certify that I have read this study and that in my opinion it conforms to acceptable standards of scholarly presentation and is fully adequate, in scope and quality, as a dissertation for the degree of Doctor of Philosophy.

Margaret O. James
Professor of Medicinal Chemistry

This dissertation was submitted to the Graduate Faculty of the Department of Chemistry in the College of Liberal Arts and Sciences and to the Graduate School and was accepted as partial fulfillment of the requirements for the degree of Doctor of Philosophy.

August, 2000

_____

Dean, Graduate School